FUNCTIONAL NUCLEIC ACID NANOPARTICLES AND THEIR DELIVERY
USING EXOSOMES

by

Weina Ke

A dissertation submitted to the faculty of
The University of North Carolina at Charlotte
in partial fulfillment of the requirements
for the degree of Doctor of Philosophy in
Nanoscale Science

Charlotte

2020

Approved by:

_____
Dr. Kirill Afonin

_____
Dr. Didier Dreau

_____
Dr. Joanna Krueger

_____
Dr. Swarnapali Indrasekara

_____
Dr. Faramarz Farahi

ABSTRACT

WEINA KE. Functional Nucleic Acid Nanoparticles and Their Delivery using Exosomes.
(Under the direction of DR. KIRILL AFONIN)

Nucleic acid biopolymers are essential to all living organisms. The chemical makeup of deoxyribonucleic acid (DNA) and ribonucleic acid (RNA) consist of sequences of only four monomers. However, they transmit and express genetic information for various biological functions based on stored blueprints. Along with communicating the flow of genetic information (DNA → RNA→ protein), nucleic acids have also become a preferred material for fabrication of objects and scaffolds at the nanoscale. Nucleic acid-based assemblies that interact with each other and communicate with the cellular machinery represent a new class of reconfigurable nanostructures that enable precise control over their formulation and physicochemical properties and activation of multiple biological functionalities. Therefore, the use of nucleic acids offers a unique platform for development of nanoparticles which consist of nanoscale-size oligonucleotides designed to fold into predicted three-dimentional structures. They can serve as scaffolds capable of carrying numerous functional moieties such as: RNA interference activators for gene silencing, aptamers for specific targeting of selected molecules, immunostimulatory sequences for modulating immune responses, and fluorescent entities for bioimaging. Programmable, controllable, biocompatible, rationally designed, and self-assembled nucleic acid nanoparticles have become attractive candidates for diverse therapeutic options. Despite profound advances in the field of therapeutic nucleic acids, their negative charges decrease membrane permeation capacity, thus hindering their translation from experimental research to clinical application. This dissertation focuses on the development of nucleic acid nanoparticles as therapeutics with defined immunostimulatory properties accompanied by rationally designed systems able to regulate the duration of therapeutic activity. Furthermore, a safe, efficient and stable intracellular delivery system for multi-functional nucleic acid nanoparticle platforms is investigated.

Acknowledgements

transitioning from bench research to clinical experience.

I also acknowledge support from the Department of Chemistry, the Graduate School of UNC Charlotte and the grants I received that supported my research, training and traveling.

Last, but not least, I want to thank my parents who always supported me and believed in me unconditionally even across the Pacific Ocean. I love you, and I hope I make you proud.

Table of Contents

List of Tables

List of Figures

List of abbreviations

3WJ	3-way junction
3D	3 dimension
AB	Assembly buffer
AFM	Atomic force microscopy
AL488	Alexa Fluor 488
AL546	Alexa Fluor 546
ALIX	ALG-2-interacting protein X
AMD	Age-related macular degeneration
APC	Antigen presenting cells
APS	Aminopropyl silatrane
AQP2	Vasopressin-regulated water-channel protein aquaporin-2
AuNP	Gold nanoparticle
BALF	Broncho-alveolar lavage fluid
BBB	Blood brain barrier
BCL2	B-cell lymphoma 2
Bola	Bolaamphiphile
BSA	Bovine serum albumin
cRNA	Coding ribonucleic acid
CARD	Caspase activation recruitment domains
CARPA	Complement activation-related pseudoallergy
CAUTI	Catheter-associated urinary tract infection
CD	Cluster of differentiation
CE-CELEX	Capillary Electrophoresis-system evolution of ligand by exponential enrichment
ceRNA	Competing endogenous RNA
cfu	Colony forming units
cGAS	Cyclic GMP-AMP synthase
CHMP4	Charged multivesicular body protein 4
CNT	Carbon nanotubes
CO2	Carbon dioxide
CpG	Cytosine phosphate guanosine
CPP	Cell-penetrating peptides
CRC	Colorectal cancer
cryo-EM	Cryo-electron microscopy
CTL	Cytotoxic T lymphocyte
DAG	Dialkylglycerol
DAMP	Damage associated molecular pattern
ddH2O	Double deionized water
DC	Dendritic cell
DIS	Dimerization initiation site
DLS	Dynamic light scattering
DMEM	Delbuco's modified eagle medium
DNA	Deoxyribonucleic acid
DS	Dicer substrate
dsRNA	Double-stranded RNA
DTX	Docetaxel
eGFP	Enhanced green fluorescent protein
ELISA	Enzyme linked immunosorbent assay
ER	Endoplasmic reticulum

ESCRT	Endosomal sorting complex required for transport
EVB	Epstein-Barr virus
FBS	Fetal bovine serum
Fc	Fragment crystallizable
FcRn	Fc receptor
FIXa	Factor IXa
FDA	Food and drug administration
EGFR	Epidermal growth factor receptor
EV	Extracellular vehicles
fNTA	fluorescent nanoparticle tracking analysis
FRET	Förster resonance energy transfer
GC	Guanine cytosine
GDV	Gene delivery vector
GDP	Guanosine diphosphate
GFP	Green fluorescent protein
gDNA	Genomic DNA
GNLY	Granulysin
GPI	Glycosylphosphatidylinositol
GTP	Guanosine triphosphate
HARP	High-throughput antibody replacement process
HER2	Human epidermal growth factor receptor 2
hFC	high-resolution flow cytometry
HIV	Human immunodeficiency virus
HRP	Horseradish peroxidase
HRS	Hepatocyte growth factor–regulated tyrosine kinase substrate
HSA	Human serum albumin
Hz	Hertz
IC_{50}	Inhibitory concentration
ICAM	Intercellular adhesion molecules
IFN I	Type one interferon
IFN-α	Interferon alpha
IFN-β	Interferon beta
IL-1B	Interleukin 1B
IL-6	Interleukin 6
IL-8	Interleukin 8
ILV	Intraluminal vesicles
InfA NP	Influenza A nucleoprotein
IP-SELEX	Immunoprecipitation-coupled-system evolution of ligand by exponential enrichment
IVT	In vitro transcription
ISM	In silico maturation
IWB	Iowa black quencher
K-turn	Kick-turn
KARS	Kirsten rat sarcoma
K_d	Dissociation constant
kDa	Kilodaltons
L2K	Lipofectamine 2000
LAMP1	Lysosomal-associated membrane protein 1
LAL	Limulus amoebocyte assay
LBPA	Lysobisphosphatidic acid
LErafAON	Liposome-delivered Raf antisense oligodeoxynucleotide

LFA-1	Lymphocyte function-associated-antigen-1
LGP-2	Laboratory of genomics and physiology 2
LHRH	Luteinizing hormone-releasing hormone
LNA	Locked nucleic acid
lncRNA	Long non-coding ribonucleic acid
LPS	Lipopolysaccharide
LSPR	Localized surface plasmon resonance
MAGE 3	Melanoma antigen 3
MAVS	Mitochondrial antiviral signaling
MDA5	Melanoma differentiation-associated protein 5
miRNA	Micro ribonucleic acid
mRNA	Messenger ribonucleic acid
MPS	Mononuclear phagocyte system
M-SELEX	Microfluidic system-evolution of ligand by exponential enrichment
MSN	Mesoporous silica nanoparticle
mtDNA	Mitochondrial DNA
MV	Microvesicle
MVB	Multivesicular body
MW	Molecular weight
MWCNT	Multi-walled carbon nanotubes
NANP	Nucleic acid nanoparticle
ncRNA	Non-coding ribonucleic acid
NF-κB	Nuclear factor kappa-light-chain-enhancer of activated B cells
NGS	Next generation sequencing
NKG2D	Natural killer group 2 member D
nM	Nanomolar
Nm	Nanometer
NMR	Nuclear magnetic resonance
Nt	nucleotide
NTA	Nanoparticle tracking analysis
ODN	Oligodeoxynucleotide
OMP	Outer membrane proteins
PAGE	Polyacrylamide gel electrophoresis
PAMAM	Poly (β-amino esters), and polyamidoamine
PAMP	Pathogen associated molecular pattern
PBS	Phosphate-buffered saline
PBMC	Peripheral blood mononuclear cell
PCR	Polymerase chain reaction
PDC	Plasmacytoid dendritic cell
PDGFR	Platelet-derived growth factor receptor
pDNA	Plasmid deoxynucleic acid
PEG	Polyethylene glycol
piRNA	p-element-induced wimpy testis (PIWI) interacting ribonucleic acid
PLLeu	Poly-L-leucine
pre-miRNA	precursor micro ribonucleic acid
pri-miRNA	primary micro ribonucleic acid
PgP	Poly (lactide-co-glycolide)-graft-polyethylenimine
PM	Plasma membrane
PPI	Poly (-propylene imine)
PRR	Pattern recognition receptor
PSMA	Prostate-specific membrane antigen

PTK7	protein tyrosine kinase 7
RVG	Rabies viral glycoprotein
QSAR	Quantitative structure activity relationship
RGD	Arginylglycylaspartic acid
RIG	Retinoic inducible gene
RISC	Ribonucleic acid induced silencing complex
RLR	RIG-I like receptor
RNA	Ribonucleic acid
RNA polII	Ribonucleic acid polymerase II
RNAi	Ribonucleic acid interference
rRNA	Ribosomal ribonucleic acid
RT-PCR	Reverse transcriptase polymerase chain reaction
SANS	Small-angle scattering of neutrons
SARS	Severe acute respiratory syndrome
SAXS	Small-angle scattering of X-rays
SBA	Streptavidin-binding aptamer
SD	Standard deviation
SEAP	Secreted embryonic alkaline phosphatase
SELEX	System evolution of ligand by exponential enrichment
SEM	Standard error of the mean
SEM	Scanning electron microscopy
shRNA	Short hairpin ribonucleic acid
SIMPLE	Small integral membrane proteins of lysosomes and late endosome
siRNA	Small interfering ribonucleic acid
SIRPα	Signal regulatory protein α
snRNA	Small nuclear ribonucleic acid
SNARE	Soluble N-ethylmaleimide-sensitive fusion protein attachment protein receptor
sncRNA	Short non-coding ribonucleic acid
SOX	SRY-related HMG-box
SPDB	Succinimidyl-4-(2-pyridyldithio) butyrate
SPP	Succinimidyl-4-(2-pyridyldithio) pentanoate
ssDNA	Single stranded deoxyribonucleic acid
ssRNA	Single stranded ribonucleic acid
STAM	Signal transducing adaptor
STING	Stimulator of interferon genes
SWCNT	Single-walled carbon nanotubes
TAR	Trans-activation-response element
T-ALL	T-cell acute lymphoblastic leukemia
TBA	Thrombin binding aptamers
TdT	Terminal deoxynucleotidyl transferase
TEM	Transmission electron microscopy
TEN	Toxic epidermal necrolysis
TF	Transcription factor
T_h	Helper T cell
TIM-3	T cell immunoglobulin and mucin domain-containing protein-3
TLR	Toll-like receptor
Tm	Melting temperature
TNA	Therapeutic nucleic acid
TNFα	Tumor necrosis factor alpha
Treg	Regulatory T cell

tRNA	Transfer ribonucleic acid
tRPS	tunable resistive pulse sensing
μL	Microliter
μM	Micromolar
UHV	Ultra-high vacuum
UV	Ultraviolet
VEGF	Vascular endothelial growth factor
VEGFR	Vascular endothelial growth factor receptor
Vps4/SKD1	Vacuolar protein sorting 4/suppressor of K+ transport growth defect 1
WC	Watson-Crick

1   Chapter 1: Introduction

1.1   Nucleic acids

1.1.1   Structure and function of nucleic acids

Nucleic acid biopolymers have evolved to preserve and regulate the flow of genetic information across all forms of life. There are two types of nucleic acid: deoxyribonucleic acid (DNA) and ribonucleic acid (RNA). While all living cells contain both, some biological entities carry only one of these molecules. For example, the genome of SARS-CoV-2 is composed of a single-stranded RNA[1]; while the nucleocapsid of hepatitis B only contains viral DNA[2]. DNA and RNA both consist of only four major monomeric subunits, and yet these molecules carry out various functions that determine the inherited characteristics of all known living organisms. Most eukaryotic DNA is located in the nucleus, where it is packaged into sequences called genes from which chromosomes and the entire genome are constructed. In human, the genome consist of approximately 3,200,000,000 bp of DNA arranged into 46 chromosomes.[3] Only 1.5% of the entire DNA library codes for proteins; the vast majority of noncoding DNA carries out numerous functions encompassing small RNA production, transposon reassembly, genome rearrangements, gene expression regulation, etc.[4] Once thought to play ancillary roles, RNAs are now known to be key regulatory players in the cell where they catalyze biological reactions[5, 6], control and modulate gene expression[7, 8], sense and respond to cellular signals[9], serve as targeted delivery of RNA therapeutics[10], etc.

In 1953, James D. Watson and Francis H. C. Crick proposed the double-helical structure of DNA based on analysis of x-ray diffraction patterns. The two strands of sugar-phosphate backbones exist on exterior of the double helix while the nucleobases face towards the interior. These two strands run in opposite directions to each other and are, therefore, anti-parallel. Hydrogen bonds between the nucleotides hold two strands in place. Adjoining nucleobases in each strand lie on top of one another via aromatic pi-pi stacking. Hydrophobic effects and van der Waals interactions between these stacked adjacent base pairs provide stability[11]. Electrostatic interactions

between negatively charged phosphates and positive magnesium ions, cationic proteins, and arginine and lysine residues also contribute to stabilization[12]. All of these forces all support self-assembly of the characteristic DNA double helix. RNA, by contrast, is usually a single-stranded long polynucleotide. However, both DNA and RNA can be double-stranded or single-stranded and possess linear or circular shapes[9]. RNA can also participate in a hybrid helix composed of one RNA and one DNA strand; this hybrid displays a slightly different conformation than the common B-form DNA[11]. Different combination of nucleobases and ribose groups enable various types of RNA to fold into complex conformations which fulfill key biological roles. For example, stem-loop (hairpin) intramolecular base pairing, is a key building block of many RNA secondary structures. When only two regions in the same strand are complementary in nucleotide sequence, a double helix is formed through base pairing with an accompanying unpaired loop. This structure can direct RNA folding, enhance structural stability of messenger RNA (mRNA) and provide recognition sties for RNA binding proteins and enzymatic reactions[13].

The unique chemical configurations of DNA and RNA are widely conserved throughout biology. Their primary structures consist of linear polymers composed of monomers called nucleotides. Nucleobases are heterocyclic compounds with rings containing nitrogen and carbon that attached to the backbones made of sugar and phosphate groups joined by ester bonds. Adenine and guanine are purine bases which contain a pair of fused rings, while cytosine; thymine and uracil are pyrimidines which contain a single ring. Both DNA and RNA possess adenine, guanine and cytosine; thymine is unique to DNA, and uracil is found only in RNA. These nucleobases are responsible for inter-strand hydrogen bonding wherein adenine binds to thymine (DNA) or uracil (RNA) and cytosine binds to guanine. Through these interactions, complementary DNA strands are linked together to create a double helix. DNA has additional interactions known as Hoogsteen base pairs in which a purine's N7 can be held together by hydrogen bonds in the major groove with a C6 amino group, which bind the Watson-Crick (N3-C4) face of the pyrimidine[14]. Nucleotide acidity

is due to the presence of phosphate which dissociates inside cells, leaving behind free hydrogen ions and negatively charged phosphate groups. These charges attract proteins, allowing for protein-nucleic acid interaction[11]. RNA contains a β-D-ribofuranose, whereas DNA has a β-2'-deoxy-D-ribofuranose. The polarity of the 2'-hydroxyl group, which takes part in RNA-mediated enzymatic events, makes RNA more chemically reactive than DNA. As a result of this lability, RNA is cleaved into mononucleotides in alkaline solution, whereas DNA is not[11]. Moreover, the alternating relative orientation of the phosphate backbone, nucleobase and the 2'-hydroxyl group caused by a structural translation, or "sugar pucker", allows the formation of higher order structures.[15] Such differences in shape have important implications for the helix itself. The A-form helix in RNA displays a C3'-endo sugar confirmation, induced by the 2'-hydroxyl group, has a more compact helix due to the shorter distances between the two phosphates in the backbone. On the other hand, the B-form helix in DNA, displays a C2'-endo sugar structure and is less compact. Such helical variations also lead to the differences in length and the number of base pairs required to complete a full helical turn: A-form helices achieve one full turn after 11 bases, whereas 10 bases are required for B-form helices.[16] Although A- and B- form helices are right-handed, a third type of nucleic acid, Z-form, is left-handed with a structure that repeats every other base pair. In addition, it displays a narrower width of helix and requires 12 bases to complete one full helical turn.[17] Alterations in sugar pucker yield structural changes and, consequently, changes nucleic acid functions[18]. For example, A-form helix's C3' endo puckering results in a 19° tilting of the bp away from the normal to the helix, making it less accessible to water molecules than B-form, those facts lead to more favorable action of dehydration seen in A-form[19]. Moreover, the wider and deeper dimension of the major groove in B-form helix makes it play a distinct role in protein recognition[20, 21]. Adoption of specific sugar pucker conformations has also proven vital for polymerization and catalysis reactions of nucleic acids[22, 23]. Cellular RNAs range in length from less than one hundred to many thousands of nucleotides; cellular DNA molecules can be as long as several hundred million nucleotides.[11]

Genetic information stored in an organism's DNA contains the directions required for it to grow, develop, survive and reproduce. Therefore, DNA is known as the blueprint of life. Such information needs to be copied accurately through replication and passed on to progeny. According to the "RNA world hypothesis", early forms of life may have used RNA exclusively to store genetic information and to catalyze chemical reactions. Later, DNA evolved as a more stable storage of genetic information, and RNA emerged as a messenger of this information. According to the Central Dogma of molecular biology, DNA undergoes transcription to make a copy of messenger RNA (mRNA) which is subsequently translated into proteins that support numerous biological functions (Figure 1). During the translation process, mRNA relays genetic codes from DNA to the ribosome, where protein synthesis takes place. Ribosomes are primarily composed of ribosomal RNA (rRNA), whereas transfer RNA (tRNA) decodes mRNA sequence and transfers the corresponding amino acid to the growing polypeptide chain. This process continues until a protein is formed. Approximately 1.2% of human genetic transcripts encode for proteins. The large portion of RNAs that never translated into proteins also perform essential functions and contribute to an organism's complexity[24]. RNA thus can be broadly divided into coding (cRNA) and noncoding RNA (ncRNA) (Figure 1). cRNA simply refers to protein-coding mRNA. ncRNA is further divided into two major categories: short ncRNA (sncRNA) and long ncRNA (IncRNA). sncRNA is defined by an arbitrary threshold of 200 nucleotides (nts) and participates in transcriptional and translational functions. RNAs that fit this category include the aforementioned rRNAs and tRNAs, and small nuclear RNAs (snRNAs). The latter are hypothesized to be primary transcription products of split genes and assist with precise alignment and correct excision of introns[25]. Other sncRNAs involved in regulating gene expression include: microRNA (miRNA), small interfering RNA (siRNA), and P-element-induced wimpy testis (PIWI) interacting RNA (piRNA)[26]. Both siRNA and miRNA are 20-30-nt long and induce either mRNA degradation or translational repression, respectively. Nearly 60% of translated protein-coding genes are negatively regulated by miRNA[27]. SiRNA and miRNA regulate gene expression at the post-transcriptional level, yet, they differ in origin and mechanism of action.
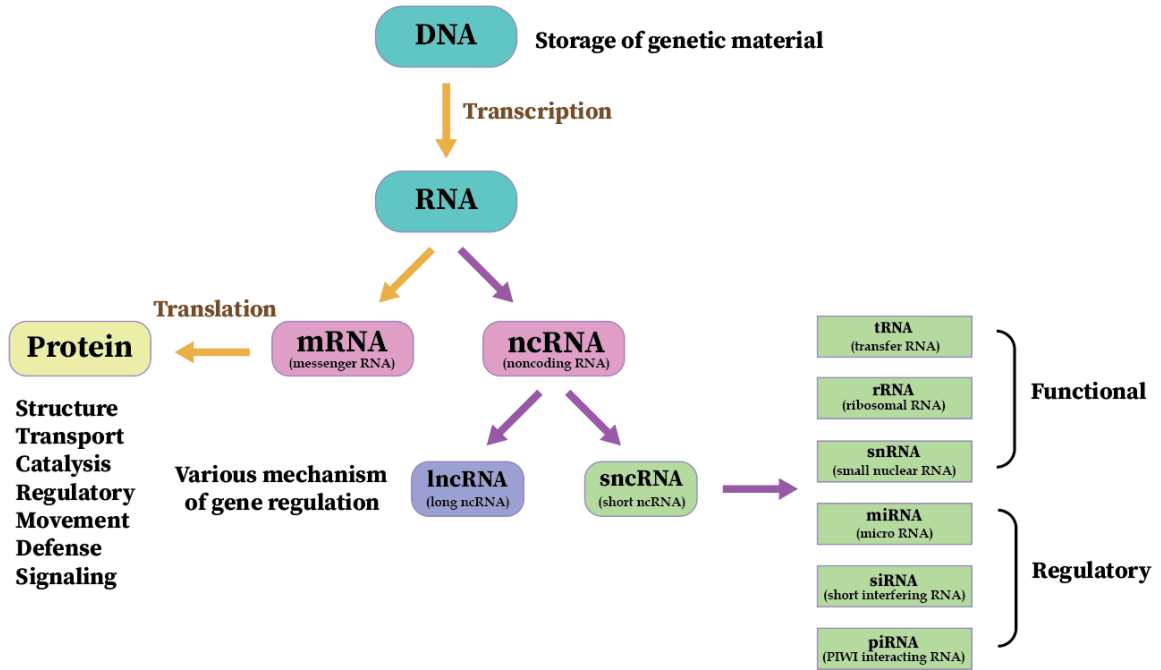
Figure 1. Types of nucleic acids. The yellow arrows illustrate the Central Dogma of molecular biology. The purple arrows show categories of noncoding RNAs.

One major difference between the two is specificity: siRNA is highly specific and targets only one mRNA, while miRNA does not require specific binding and can act on multiple targets. Therefore, some transcripts are regulated by more than one miRNAs[28]. In addition, miRNAs are thought to be endogenously transcribed from DNA by RNA polymerase II (RNA PolII). They are characterized by one or many stem-loop hairpins that contain functional miRNA in their stem through which primary miRNA (pri-miRNA) is formed. This step occurs in eukaryotic nuclei where two nuclear enzymes, Drosha and DiGeorge Syndrome Critical Region 8 (DGCR8), cleave pri-miRNA into double-stranded (ds) hairpin RNA with 2-nt 3' overhang structure, called precursor miRNA (pre-miRNA). Afterwards, the nuclear protein exportin-5 exports the pre-miRNA from the nucleus to the cytoplasm, where it is processed by RNase III endoribonuclease Dicer[29]. Dicer cleaves the hairpin loop, leaving a 20-22-nt long double-stranded miRNA molecule. For siRNA, the maturation of siRNA begins with the transcription from DNA by RNA PolII to form dsRNA, which is then processed by Dicer to create a RNA duplex with 2-nt overhang at 3'end and phosphate groups at
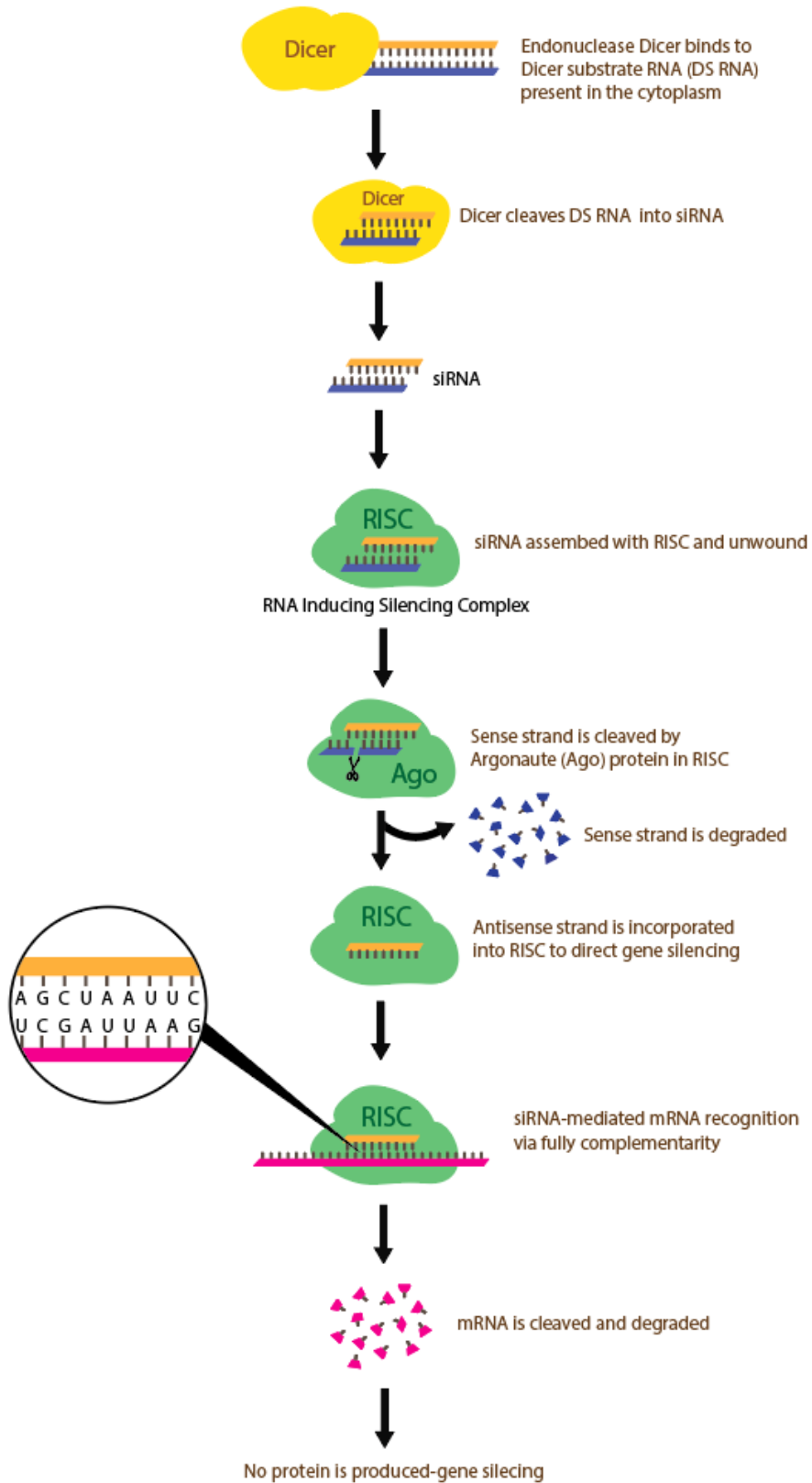
Figure 2. Mechanism of RNA interference.

its 5'end[29]. Only one of the two RNA duplex strands will be used as a guide (antisense) strand and incorporated into RNA-induced silencing complex (RISC) to direct gene silencing. The other strand, also known as the passenger (sense) strand, is degraded. Argonaute protein guides this entire process by selecting the strand having a less thermodynamically stable 5' end[30]. The guide strand serves as a template for recognition of complementary mRNA transcripts by RISC. Next, the guide strand guides RISC to its target mRNA through full complementary binding between the siRNA guide strand and mRNA, resulting in mRNA cleavage at a specific site (Figure 2)[31]. On the other hand, perfect Watson-Crick base-pairing between the miRNA "seed" region and the mRNA target is required, but imperfect binding outside of the "seed" is necessary for miRNA to target multiple mRNAs[32]. The abilities for siRNA and miRNA to silence genes permit them to fill their niche as RNA interference (RNAi) activators. RNAi is a naturally occurring and conserved biological mechanism that regulates the expression of protein-coding genes. This process results in the down-regulation of gene expression via sequence-specific recognition of corresponding mRNAs. Due to their important roles in RNAi activation, siRNA and miRNA have been widely investigated as a novel class of therapeutic agents for the treatment of various diseases including cancers and infections[33]. On August 10, 2018, the Food and Drug Administration (FDA) approved the first siRNA therapeutic, Onpattro (Patisiran), for treatment of polyneuropathies induced by hereditary transthyretin amyloidosis[34]. On November 18, 2019, the FDA approved the second siRNA-based drug Givlaari (givosiran), for treatment of adult patients with acute hepatic porphyria[35]. This paved the way for clinical development of RNAi-induced therapeutics. PiRNA is the largest class of sncRNA molecules expressed in animals[36]. It is thought to be involved in gene silencing[37] via RISC formation, through which piRNA interacts with piwi proteins that are part of the Argonaute family. PiRNAs direct piwi proteins to transposon targets due to their antisense role to transposon sequences[38].

Lnc RNAs are defined as a heterogeneous groups of transcripts with lengths exceeding 200 nts that are not translated into protein[39]. Like mRNAs, lncRNAs are transcribed from DNA by RNA

PolII and undergo post-transcriptional modification such as alternative splicing, 5' capping, polyadenylation and RNA editing[40]. However, unlike mRNA, lncRNAs have fewer and longer exons and carry out diverse regulatory functions[41]. They modulate gene expression at the transcriptional level through chromatin modifying factors at promoters or transcription factors (TFs) at enhancers of their target genes[42]. At the post-transcriptional level, lncRNAs negatively regulate miRNA functions. The short 6-8 nt "seed" sequence within miRNA serves as a transcript binding site; computational models indicate that many lncRNAs contain miRNA binding sites[43]. Thus, the concentration of miRNA available within the cell is limited, and this is referred to as the "competing endogenous RNA (ceRNA)" hypothesis[44]. Additionally, some lncRNAs, (half STAU1-binding site RNAs, for example) bind the Alu element of the 3'-UTR region on the target mRNA and recruit UP-Frameshift-1(UPF1) protein to STAU1, causing target mRNA degradation. This lncRNA mechanism regulates post-transcriptional gene expression by directly targeting and breaking down mRNA. Here, the interaction between miRNA and lncRNA is not involved[45]. LncRNAs also participate in epigenetic regulation through DNA methylation, histone modification and recruitment of chromatin mediator complexes to specific genomic loci in promoter regions. The latter facilitates chromatin conformational changes and targeting by chromatin-modifying enzymes[43, 46].

RNA's diverse set of functions is essential to every living organism. Besides participating in gene regulation and protein synthesis, RNA can take on roles as enzymes in which this function is more commonly carried out by proteins. One well-known example is the ribozyme, an RNA molecule that is able to catalyze biochemical reactions. In addition, RNA can store and replicated genetic information as DNA and some viruses carry only the RNA genome[29]. Besides the aforementioned coronavirus, the genomes of Ebola virus, hepatitis C virus (HCV), poliovirus, human immunodeficiency virus (HIV), and influenza virus all consist of single- or double stranded RNA[47]. Clearly, the importance of RNA cannot be understated and, in one form or another, it participates in nearly all cellular activities. This offers the potential for clinical development of

RNA therapeutics in modern medicine.

Overall, nucleic acids play a vital role in all living organisms, either as transmitters of genetic information or as regulators of various biochemical pathways. The chemical constituents of DNA and RNA provide precise instructions for folding and higher-order assembly of biopolymers [48]. The diversity and complexity of the structures, therefore, carry out a wide range of functions. Structural diversity and complexity of nucleic acid molecules, as well as the proteins they encode, provide a means for enabling all known biological functions. Various naturally existing or experimentally selected nucleic acids may provide multifunctional platforms for numerous applications including diagnostics, therapeutics, nanodevices, and materials[49].

1.1.2 Immune response to nucleic acids

Foreign nucleic acids can initiate a robust and severe immune response. They are capable of stimulating pattern recognition receptors (PRRs) to induce inflammation (Figure 3). Cells expressing PRRs can precisely identify signature motifs called pathogen-associated, or danger-associated, molecular patterns (PAMPs or DAMPs) in locations such as the endosome and cytosol. Binding of PRR to its target, ultimately leads to the production of the type I interferons (IFNs) and/or pro-inflammatory cytokines. Type I IFN's functions include preventing viruses from spreading to nearby cells, promoting the host's innate immune response and assisting in activation of the adaptive immune system[50]. Pro-inflammatory cytokines belong to a specialized intracellular signaling molecule family secreted from immune cells like helper T cells (T_h), macrophages and other cell types that promote inflammation[51]. They play an important role in mediating the innate immune response. In the endosome, membrane proteins, called toll-like receptors (TLR) recognize and bind specific nucleic acid motifs that promote expression of IFNs and/or pro-inflammatory cytokines[52]. Endosomal TLRs such as TLR7 and TLR8 detect single-stranded RNA (ssRNA) and short dsRNAs[53, 54], while TLR3 is more sensitive to longer dsRNA[55]. DNA containing unmethylated CpG can be detected by TLR-9[56]. TLR3 preferentially interacts with 40-50 nt long
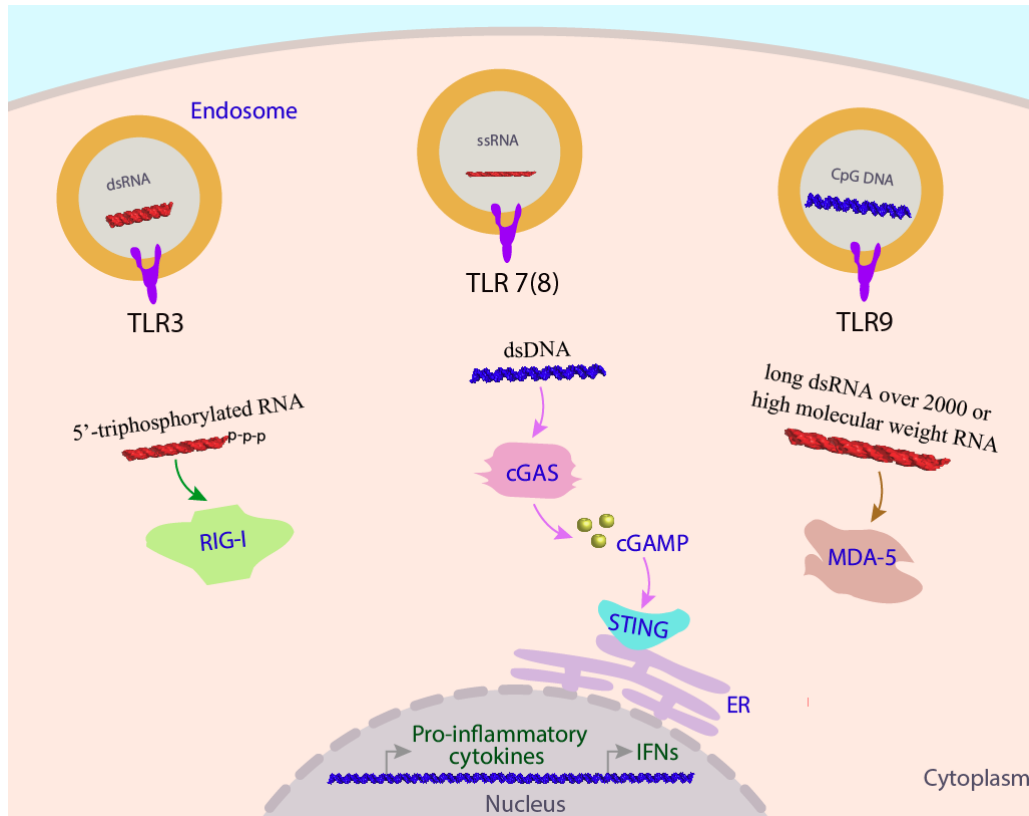
Figure 3. Schematic demonstrating the pathway involving common pattern recognition receptors and proteins inside a cell to coordinate immune responses upon foreign nucleic acid detection. ER: endoplasmic reticulum; TLR: toll-like receptor; RIG-I: retinoic acid–inducible gene I (RIG-I); MDA-5: melanoma differentiation–associated protein 5; cGAS: cyclic GMP-AMP synthase; STING: stimulator of interferon gene; IFN: interferon.

dsRNA dsRNA in acidic conditions[57]. These receptors undergo conformational changes once binding to their ectodomains takes place, producing type I IFNs and proinflammatory cytokines[57]. TLR7-8 prefer to bind on uridine rich sequences of ssRNA[58, 59]. B cells, monocytes and plasmacytoid dendritic cells (pDCs) express TLR7, whereas TLR8 is primarily expressed in myeloid dendritic cells (mDCs) and monocytes[60]. Nucleic acid triggering of TLR-7 or TLR-9 induces plasmacytoid dendritic cells (PDCs) to produce proinflammatory cytokines such as tumor necrosis factor (TNF) and interleukin (IL)-6[61]. TLR-9 is activated by CpG motifs in DNA, leading to the expression of type I IFN and pro-inflammatory cytokines.

In the cytoplasm, the cytosolic RNA receptors retinoic acid–inducible gene I (RIG-I), melanoma differentiation–associated protein 5 (MDA-5) and laboratory of genomics and

Table 1. Intracellular sensors of nucleic acids.

Senors	PRR	Target	Location	Response	Pathway	Ref
Cytosolic DNA sensors	DAI	dsDNAs	cytosol	Type I IFNs; Pro-inflammatory cytokines	STING→TBK1/IKKε/DDX3→β-catenin→IRF3; STING→TBK1/IKKε/DDX3→IRF7; RIP-1/3→NF-κB	69
	AIM2	dsDNAs	cytosol	IL-1β; inflammasome	ASC→Caspase-1	68; 69
	RNA Pol III	AT-rich dsDNAs	cytosol	Type I IFNs; Inflammatory cytokines	RIG-I→MAVS→TBK1/IKKε/DDX3→β-catenin→IRF3; RIG-I→MAVS→TBK1/IKKε/DDX3→IRF7; RIG-I→MAVS→NF-κB	69
	LRRFIP1	dsDNAs	cytosol	Type I IFNs	β-catenin→IRF3	69
	DHX9	CpG dsDNAs	cytosol	Pro-inflammatory cytokines, Type I IFNs	MyD88→NF-κB; MyD88→TBK1/IKKε/DDX3→β-catenin→IRF3; MyD88→TBK1/IKKε/DDX3→IRF7	69
	DHX36	CpG dsDNAs	cytosol	Pro-inflammatory cytokines, Type I IFNs	MyD88→NF-κB; MyD88→TBK1/IKKε/DDX3→β-catenin→IRF3; MyD88→TBK1/IKKε/DDX3→IRF7	69
	Ku70	dsDNAs	cytosol	IFNl 1	IRF7; IRF1	69
	DDX41	dsDNAs	cytosol	Type I IFNs	STING→TBK1/IKKε/DDX3→β-catenin→IRF3; STING→TBK1/IKKε/DDX3→IRF7	69
	DNA-PK	dsDNAs	cytosol	Type I IFNs	STING→TBK1/IKKε/DDX3→β-catenin→IRF3; STING→TBK1/IKKε/DDX3→IRF7	69
	MRE11	dsDNAs	cytosol	Type I IFNs	STING→TBK1/IKKε/DDX3→β-catenin→IRF3; STING→TBK1/IKKε/DDX3→IRF7	69
	cGAS	dsDNAs	cytosol	Type I IFNs	cGAMP→STING→TBK1/IKKε/DDX3→β-catenin→IRF3; cGAMP→STING→TBK1/IKKε/DDX3→IRF7	69

	Rad50	dsDNAs	cytosol	Pro-inflammatory cytokines	CARD9→Bcl-10→NF-κB	69
	IFI16	dsDNAs	nucleus; cytosol	IL-1β; Type I IFNs	ASC→Caspase-1; STING→TBK1/IKKε/DDX3→β-catenin→IRF3; STING→TBK1/IKKε/DDX3→IRF7	69
	LSm14A	dsDNAs	cytosol	Type I IFNs	STING→TBK1/IKKε/DDX3→β-catenin→IRF3	68
	Sox2	dsDNAs	cytosol	Pro-inflammatory cytokines	Tab2/TAK1→NF-κB	68
Endosomal DNA sensors	TLR9	CpG DNA	Endosome	Type I IFNs	MyD88→NF-kB; MyD88→TBK1/IKKε/DDX3→b-catenin→IRF3; MyD88→TBK1/IKKε/DDX3→IRF7	69
Cytosolic RNA sensors	RIG-I	RNA with 5' triphosphate or 5' diphosphate, short dsRNA	Cytosol	Pro-inflammatory cytokines, Type I IFNs	MAVS→TRAF3→TBK1/IKKe→IRF3; MAVS→FADD/TRAF6→IKKs→NF-κB	434
	MDA5	long dsRNA	Cytosol	Pro-inflammatory cytokines, Type I IFNs	MAVS→TRAF3→TBK1/IKKe→IRF3; MAVS→FADD/TRAF6→IKKs→NF-κB	434
	NLRP3	pathogen ssRNA/dsRNA	Cytosol	Pro-inflammatory cytokines	ASC→inflammasome→caspase-1→IL-1; ASC→inflammasome→caspase-1→IL-18	434
	NOD2	virus RNA	Cytosol	Pro-inflammatory cytokines	RIP2→IKKs→NF-κB	434
Endosomal RNA sensors	TLR3	dsRNA	Endosome	Pro-inflammatory cytokines, Type I IFNs	TRIF→RAF6/TRAF3/TBK1/IKKε/IKK→IRF3; TRIF→RAF6/TRAF3/TBK1/IKKε/IKK→IRF7; TRIF→RAF6/TRAF3/TBK1/IKKε/IKK→NF-κB	434
	TLR7/8	ssRNA	Endosome	Pro-inflammatory cytokines, Type I IFNs	MyD88→IRAK4/IRAK1/TRAF6/TRAF3→NF-κB; MyD88→IRAK4/IRAK1/TRAF6/TRAF3→IRF7	434

physiology 2 (LGP-2) are widely expressed across cell types. These three receptors all belong to

the RIG-I–like receptor (RLR) family. RIG-I recognizes 5'-triphosphorylated, uncapped RNA as

well as RNA bearing 5'-diphosphates. MDA-5 recognizes long dsRNA (2000 nts or more in length) and branched, high-molecular weight RNA complexes composed of ssRNA and dsRNA[62]. RIG-I and MDA5 contain N-terminus caspase activation recruitment domains (CARDs). Upon activation, RIG-I and MDA-5 bind to CARDs that in turn, migrate and interact CARD of the mitochondrial antiviral signaling (MAVS) protein, such CARD-CARD interaction initiates a scaffold for stimulation of signaling cascades leads to the production of type I IFNs and other pro-inflammatory genes[63, 64]. LGP-2 is deemed essential for RIG-I and MDA-5-mediated antiviral responses. Since LGP2 lacks CARDs for downstream signaling, it has strong interaction with RIG-I and MDA-5 and acts as both a negative and positive regulator for RIG-I and MDA5 activities[65-67]. Moreover, at least 15 cytosolic DNA sensors have been identified, all of which stimulate production of type I IFNs as well as secretion of inflammasomes and pro-inflammatory cytokines (Table 1)[68, 69]. Binding of dsDNA to cyclic GMP-AMP synthase (cGAS) synthesizes the cyclic dinucleotide 2'-5'- cyclic GMP-AMP (cGAMP) which then binds to the adapter protein stimulator of interferon gene (STING) and concomitant synthesis of IFNβ[64]. Excessive immunostimulation may have deleterious effects and induce necroptosis or apoptosis[70]. Together, these receptors comprise the cellular immune response against foreign nucleic acids. Crosstalk between those receptors is a factor that cannot be neglected in synthetic nucleic acid applications.

1.1.3   Nucleic acid nanotechnology

Nucleic acid-based technologies are an emerging research focus because the ability of DNA and RNA to fold into precise and complex shapes confers unique features that are useful in biology and electronics. In 1982, Nadrian C. Seeman first proposed using DNA as a scaffold to construct ordered arrays[71]. Since then, nucleic acid nanotechnology has experienced an immense growth for nanoscale applications within and outside of biology. DNA and RNA nanotechnologies commonly employ bottom-up molecular self-assembly in which the molecular components organize into stable structures spontaneously[72, 73]. Watson-Crick base pairing rules resulting in

double helical nucleic acids are simple and well understood, and formation of correctly matched base pairs is energetically favorable. These qualities make nucleic acid nanostructure assembly programmable and controllable through rational design in which base pairing interactions yield strand assemblies with desired conformation[74]. This unique property is only seen in nucleic acid material, other materials such as proteins or inorganic nanoparticles face difficulties in design or lack of the capability of self-assembly, respectively[75].

DNA nanotechnology is the use of DNA as building blocks to design, study and apply synthetically created DNA nanostructures[76]. This field has two overlapping subdomains: structural DNA nanotechnology and dynamic DNA nanotechnology. Structural DNA nanotechnology focuses on synthesis and characterization with the finest possible levels of control over spatial and
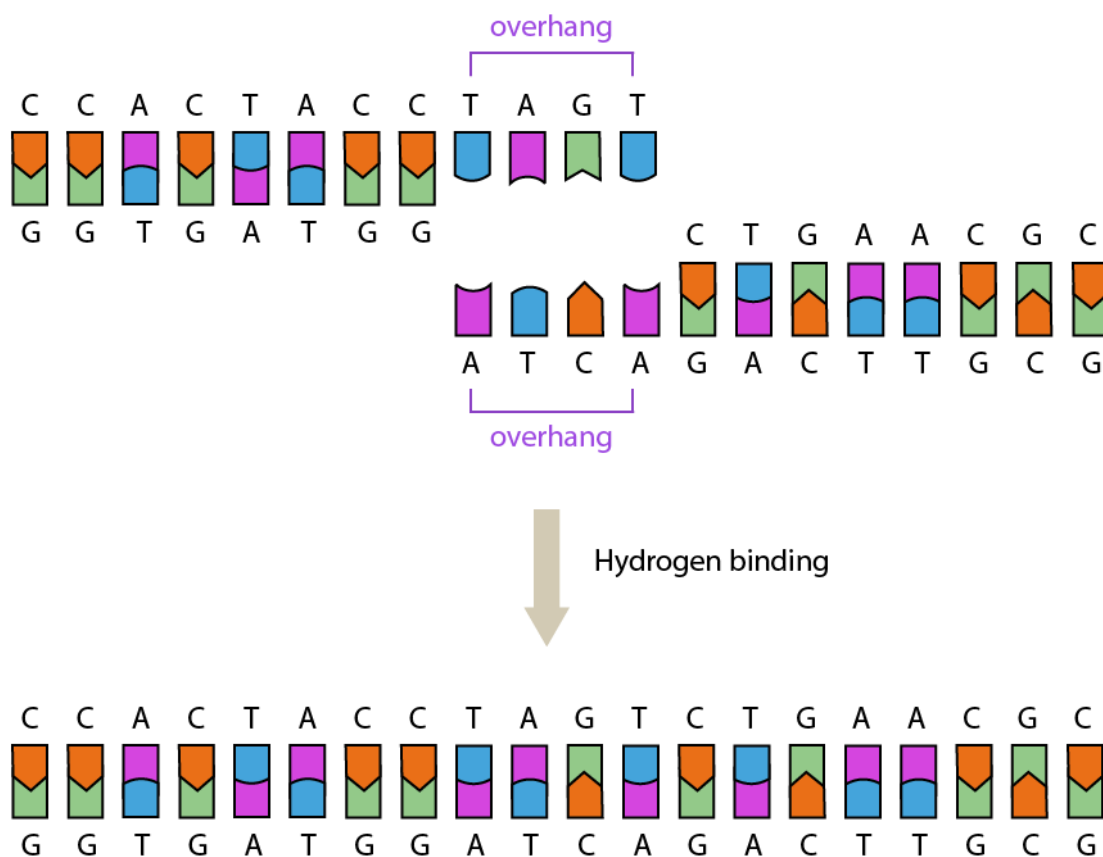
Figure 4. Sticky-Ended Cohesion. The right end of the top molecule and the left end of the bottom molecule have single-stranded extensions ('sticky ends') that are complementary to each other. These two molecules bind to each other via hydrogen bonding.

temporal structure of matter assembly to achieve a static equilibrium end state. Seeman once described the area of structural DNA nanotechnology as "Putting what you want where you want it in three dimensions (3D), when you want it there"[75]. Structural DNA nanotechnology has three fundamental aspects: 1) hybridization, 2) stably branched DNA and 3) convenient synthesis of designed sequences[75]. Hybridization uses sticky-ended cohesion to combine segments of linear duplex DNA; this approach has been a fundamental component of genetic engineering since 1973[77]. Sticky-ended cohesion involves a double helical strand having an overhang complementary to the other helical strand's overhang, and the two strands cohering through hydrogen bonding (Figure 4). Hybridization is critical because almost all sequence-dependent nanomechanical devices and sequentially-fashioned structural motifs are constructed this way[78]. The predictable geometry of sticky-ended cohesion allows for programmable intermolecular features, such as pattern and cavities[79]. 2D arrays have been incorporated in multiple structures including: holiday junction[80], double crossover (DX)[81], triple crossovers[82], and four by four tiles[83]. DNA double-crossovers containing two crossover links between helical domains have become the forerunner of more complex DNA nanostructures such as DNA origami[84]. Probably the most famous illustration of DNA origami "artwork" was the "smiley face" gracing the cover of *Nature* in 2006[85]. Paul Rothemund shifted the focus of DNA nanotechnology from self-assembling short strands motifs to larger structures. Long scaffolds of DNA origami are supported by crossovers built from hundreds of short helper strands called staples which promote folding into specific structures[86]. Staple strands typically bind to adjacent helices. Single-strand four thymidine quadruplets introduced at edges and corners help to avoid aggregation caused by π-π stacking of the folded structure[86]. Since Rothemund's seminal work, more complex structures such as 3D objects (e.g., DNA gear[87] and DNA pod[88]), higher assembled DNA objects (e.g.,nanorobots[89]) and other more sophisticated structures have been synthesized. Branched DNA represents another important player in the realm of DNA nanotechnology. It combines in vitro hybridization and synthetic branched DNA, yielding a highly stable structure[90]. Four copies of a four-arm branched DNA molecule can self-assemble

through their complementary sticky ends to yield a quadrilateral. Because four pairs of the inner sticky ends are used, all other available sticky ends could be used to form an infinite lattice[90]. Because four pairs of inner sticky ends are used, all other available sticky ends could potentially join to form an infinite symmetry[90]. This symmetry, in turn, leads to branch migration that causing branch point relocation[91]. Therefore, minimizing sequence symmetry is critical in sequence design because asymmetrical sequences are rarely seen in nature. Due to these requirements, the third foundation of DNA nanotechnology, already achieved by a number of biotechnology enterprises, is synthesis of arbitrary sequences. These companies not only manufacture pure nucleic acid sequences but also modified products like biotinylated or fluorescent-labeled strands, all of which are readily available.

Dynamic DNA nanotechnology concerns nucleic acid nanostructures equipped with specific and controllable dynamic functionalities. Unlike the static structures formed in structural DNA nanotechnology, dynamic reconfiguration is designed in response to a specific stimulus. Many diverse applications incorporating dynamic nanotechnology have arisen in the past few decades. DNA walkers are a type of nucleic acid nanomachines that achieve translational motion along a DNA "road"[92, 93]. Their range of motion can be linear or extend to two and three dimensions. A linear walker can be used in DNA-templated synthesis as the walker advances along the DNA track without natural enzymes[94]. A 2D walkers can achieve directionality by sensing its environment and carrying out "start", "follow", "turn", and "stop" actions, paving the way for more complex robotic synthesis at the molecular level[95]. Besides their expanded walking space and outstanding DNA amplification capabilities, 3D DNA walkers[96] can exploit DNA-modified nanoparticles to direct their r movement[97]. The "fastest" DNA walker had a reported speed of 300nm/min[98]; common energy sources such as DNA hybridization, ATP, heat, and light power their movement[92, 99]. Another use of dynamic DNA nanotechnology is strand displacement cascades. Unlike traditional nucleic acid assembly which requires a thermal annealing step, strand

displacement reactions permit isothermal assembly operation[100]. The strand displacement reaction

concept relies on the presence of two strands with partial or full complementarity. One domain

displaces another of identical sequence through a series of single nucleotide dissociation and

hybridization processes. Strand displacement can be initiated by short, single-stranded

complementary domains (toeholds). Toehold interaction allows for branch migration, leading to

stand displacement cascades (Figure 5A)[100]. From this disassembly, an entropy gain makes new
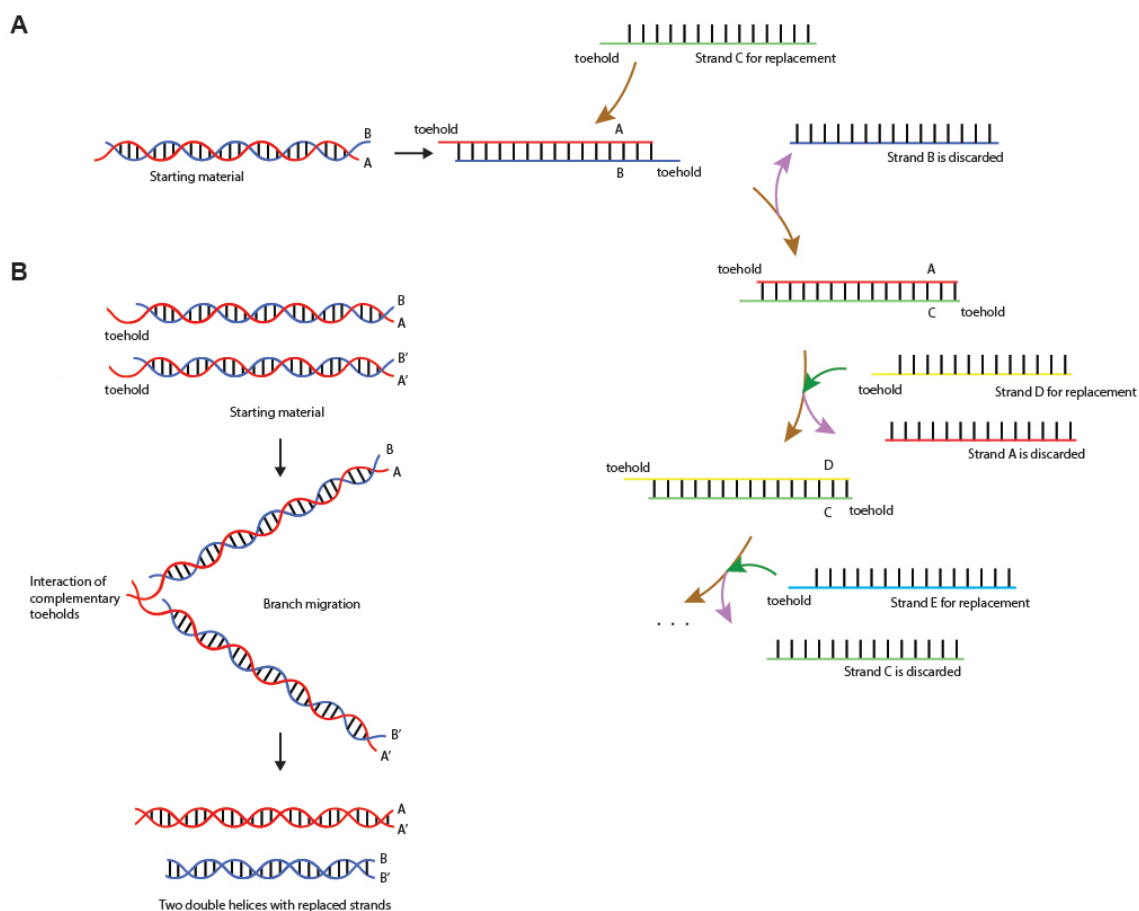
Figure 5. Schematic representation of the strand displacement cascade. A. One strand in a double helix is replaced by a single strand molecule that contains a toehold complementary to the other strand's toehold in the starting material, resulting in a new double helix. This process may be repeated. B. Two double helices with single-stranded toehold overhangs resulting in branch migration. Two double-stranded helices are produced with replacement strands in both.

base pair formation energetically favorable[100]. By changing the toeholds' length, reaction kinetics

can be quantitatively controlled by a power of six factor[101]. These properties allow for the

construction of dynamically assembled structures including hairpins, three- and four-way junctions

(3WJ and Holiday junction), dendrimers[102], as well as computational units like logic gates[103]. RNA nanotechnology is the study, design and application of synthetic architectures whose frame primarily consists of RNA. The core scaffold, functional moieties, and targeting ligand can all be constructed solely from RNA. In 1982, when Seeman demonstrated the principles of rational design of DNA nanostructure, he suggested such advantages could apply to RNA nanostructures as well[75]. Later, in 1996, a synthetic strand of RNA that adopted two topological states, knot and circle, became the first rationally designed RNA architecture. This achievement contributed to discovery of RNA topoisomerase and its associated activity[104]. In the same year, another RNA nanostructure, tectoRNA, was proposed as a mosaic unit for design of RNA motifs with dedicated shapes and properties[105]. Since then, the library of structural and functional RNA motifs hasexpanded dramatically and undergone rapid advances.

While RNA and DNA share numerous similarities, their chemical differences between them lead to distinct behaviors between the two molecules. The 2'-hydroxyl group of the sugar-phosphate backbone on RNA makes it less stable toward base-catalyzed hydrolysis. RNA instability can be overcome via chemical methods including modification of the 2'-OH group with 2'-fluoro[106] or 2'-o-methyl[107], phosphate linkage modification (e.g., boranophosphate)[108], or base alterations like 5BrU and 5IU[109]. In acidic conditions, RNA can maintain its backbone structure. Uracil's substitution for thymine creates additional nonstandard base pairs (uracil-guanine)[110]. RNA helices also display greater mechanical stiffness than DNA helices[111]. Edge-to-edge hydrogen bonding contributes, on average, from -0.4 to -1.6 kcal/mol of available free-energy for folding at 37°C[112]. Moreover, a Leontis/Westhof nomenclature for base pairing classification based on interacting edges of paired bases among Watson–Crick (W), Hoogsteen (H) and Sugar (S) edges yields 12 geometric pairing families which facilitate RNA 3D modeling, sequence alignment and phylogenetic analysis[113]. All of these features make RNA molecules excellent multipurpose building materials for nanoscale engineering[114]. Therefore, various strategies have been explored to design RNA-based scaffolds. Jaeger and Leontis extended the pioneering work of Seeman to

RNA nanodesigns-RNA tectonics. TectoRNAs are constructed of specific, non-Watson-Crick tertiary interactions that promote selective binding of hairpin tetraloops to their receptors. For one-dimensional array self-assembly, each tectoRNA has the potential to interact with two other tectoRNAs via four loop-receptor interactions, culminating in self-assembly of four-way junction molecules[115]. Such structures could be expanded as 2D or 3D models of tectoRNA units[116]. Afonin and Grabow introduced two 3D RNA nanodesigns to synthesize and assemble functionalized nanocubes and nanorings[117]. RNA nanoring design is based on tectoRNA principles and contains a variety of single-stranded stem-loops involved in inter- and intra-molecular interactions, eliminating the need for external linkages during assembly. RNA nanocubes rely solely on canonical Watson-Crick intermolecular interactions among short (26-52 nt) ssRNAs[117]. Guo's group utilized inter-RNA interactions to package RNA assemblies derived from the DNA-packaging motor of bacteriophage phi29 (hand-in-hand, foot-to-foot, arm-on-arm), leading to fabrication of dimers, twins, trimers, triplets, tetramers, quadruplets, pentamers, hexamers, heptamers, other higher-order oligomers, and branched diverse architectures[118]. Some other examples of unique RNA architectures are represented by 3WJ of the pRNA motif[119]; RNA squares with tunable physicochemical properties[120] and RNA triangles with helices and kick-turn (K-turn) motifs for RNA-protein interactions[121]. Everything from individual monomer units containing internal structures to long sequences to more complicated entities can be realized through computational design using programs such as NUPACK[122], MODENA[123], and ERD[124]. NUPACK calculates partition functions over an ensemble while minimizing defects and predicts the target secondary structure at equilibrium[125]. Moreover, it performs thermodynamic analysis of interacting nucleic acid strands[126]. NUPACK's limitation lies in a low overall probability of folding to the desired structure due to its ensemble defect reduction strategy. This method has a low propensity for folding into alternative structures with similar free energies[127]. MODENA, on the other hand, not only produces designed multiples RNA sequences with a wide range of free energies after a single run, but it also permits RNA sequence design based on a non-minimization of free-energy

(MFE) RNA folding algorithms[123]. Unfortunately, MODENA suffers from long computation as it relies on multiple iterations of a direct problem solver[123]. ERD, a novel evolutionary algorithm for RNA structural design, can overcome sequence and energy constraints while outperforming the other two programs in the realms of accuracy, speed, nucleotide distribution, and natural RNA sequence similarity[124]. Experimental assembly methods also display varieties. Simple methods such as one-pot thermal annealing to synthesize split Broccoli fluorets[128]. Co-transcriptional folding for RNA origami structures (e.g., hexagonal lattices[129]) can be used for the production of large nanostructures. The method of co-transcription is also used to produce long RNA-DNA hybrids that permit simultaneous release of multiple split functioanlities[130].

Proper characterization of assembled nucleic acid nanostructures is essential to ensure accurate folding with desired structural or functional capabilities[131]. A wide selection of conventional characterization methods is available. Native-PAGE (non-denaturing PolyAcrylamide Gel Electrophoresis) exploits net charge, size and shape of native assembled structures for separation[132]. Atomic Force Microscopy (AFM) generates a surface profile with atomic resolution[133-143]. Dynamic light scattering (DLS) relies on Brownian diffusion of particles in relation to their equivalent hydrodynamic size[144]. Small-angle scattering of X-rays and neutrons (SAXS and SANS) provide momentary structural information of static or dynamic disordered particles in physiological environments[145]. Scanning and transmission electron microscopy (SEM and TEM) allow analysis of size, size distribution and shape with angstrom resolution[144]. Cryo-electron microscopy (cryo-EM) utilizes single-particle analysis and cryo-electron tomography (ET) for 3D structural determination; these techniques are particularly important for macromolecules that cannot be crystallized[146]. Nuclear magnetic resonance (NMR) quantitatively assesses surface composition of 3D structure in solution at high resolution[147]. Finally, crystallography determines atomic arrangements in crystalline solids[144]. Appropriate combinations of these methods provide information needed to understand numerous physicochemical properties and verify synthesis of a desired target structure.

The disciplines of DNA and RNA nanotechnology have not developed independently; many fundamental principles of DNA nanotechnology apply to RNA nanotechnology as well. For instance, the use of 3WJ and Holiday junction as building blocks to construct more complex structure has been demonstrated in both fields[102]. Mainly, this results from shared structural similarities as well as common goals toward developing libraries of scalable and modular structures. RNA nanotechnology has come a long way since its inception in the 1990's, but only within the last decade has significant progress taken place. A better understanding of structural design principles relying on precise arrangement and controlled functionality may allow for development of nucleic acid nanoparticles (NANPs) with diverse applications in medicine, synthetic biology and nanobiotechnology.

1.1.4   Functionalized nucleic acid nanoparticles and their applications

DNA- and RNA-based therapeutics have potential as nanomedical applications thanks to advancements in nucleic acid nanotechnology. The FDA's approval of the siRNA-based drug, Onpattro, represented a milestone for therapeutic nucleic acids (TNAs). Some emerging classes of TNAs include: the antisense oligonucleotide, Fomivirsen, as a treatment for cytomegalovirus retinitis[148]; mRNA vaccines against the SARS-CoV-2 spike glycoprotein (currently seeking FDA approval); Pegaptanib sodium (Macugen™), a selective RNA aptamer that inhibits vascular endothelial growth factor (VEGF)[149]; and a triple combination vector containing an anti-*tat/rev* short hairpin RNA (shRNA), a nucleolar localizing TAR decoy and an anti-CCR5 ribozyme for autologous peripheral blood stem cell transplantation. The lattermost example has received FDA approval for treatment of AIDS and lymphoma patients in clinical trials[150]. As interest has grown in nanotechnology and TNA development, a new class of TNAs formulated with nanoassemblies — nucleic acid nanoparticles (NANPs) — has become a research focus. NANPs consist of nanoscale-size oligonucleotides (ODNs) designed to fold into unique predicted three-dimensional structures, and serve as scaffold capable of carrying numerous functional moieties [130, 132, 146, 151].

Functionalized NANPs offer a unique and novel platform for various applications including therapeutics, diagnostics, nanodevices, and materials.

Small interfering RNA (siRNA) represents one of the most important therapeutic nucleic acid moieties. It is a key activator of RNAi, a molecule discovered by Andrew Fire and Craig Mello for which they were awarded the Nobel Prize in 2006[152]. Since then, RNAi machinery has been studied extensively because of its ability to modulate genes and treat numerous diseases. Currently, at least 30 different therapeutic siRNAs are undergoing clinical trials, and more candidates are undergoing preclinical study[153]. The biggest hurdle in transitioning siRNA therapy from bench side to bed side is RNA's vulnerability to degradation by plasma and tissue nucleases[154] SiRNAs are thought to be primarily exogenous in origin and usually artificially introduced into cells[155], facilitating programming of NANPs for intracellular Dicer-assisted release of synthetic siRNAs. A recent study showed that 25-30-nt long dsRNAs were more potent effectors of gene silencing than those with 21nts long[156]. Longer lengths provide Dicer with a substrate for cleavage and, in turn, an improvement in loading efficiency of siRNA into RISC was found[157]. Therefore, 25-30 nt long dsRNAs that participate in intracellular release of siRNAs by Dicer are called Dicer Substrate RNAs (DS RNAs). DS RNAs can be packaged into RNA-based scaffolds and delivered into target cells for biomedical applications. For example, computationally designed[158] and experimentally tested[132] RNA nanorings and RNA nanocubes were functionalized with six DS RNAs for RNAi therapeutics; the nanocubes could also be functionalized with malachite green aptamers for fluorescent visualization[159]. In order to obtain a combinatorial RNAi effects, nanorings were functionalized with different DS RNA compositions targeting six different regions of HIV-1: BS-matrix, capsid, protease, reverse transcriptase, envelope, Nef, and Rev-Tat[160]. Despite nanocubes and nanorings having significant advantages, their maximum number of functionalities is limited and advanced computational approaches are required for their design. More importantly, the DS RNAs can be potentially activated in unwanted cells, necessitating additional controls over

simultaneous delivery. One novel technique for conditional activation relies on splitting functionality into cognate pairs of RNA–DNA hybrids (monomers of RNA–DNA fibers) while restoring their original functionalities using intracellular re-association with ssDNA toeholds (Figure 5B)[130], leads to the production of dsDNAs along with DS RNAs. A drawback of this strategy is the length of dsDNA is direct proportional to the number of DS RNAs. These dsDNAs not only represent wasted material, but they may also elicit an immunogenic response in a length dependent manner as a side effect[161]. To offset this immunostimulatory effect, a nuclear factor kappa-light-chain-enhancer of activated B cells (NF-κB) decoy can be functionalized in RNA–DNA fibers that is released as dsDNA. At the meantime, the released DS RNAs target mutated BRAF gene in the treatment of melanoma[139]. Reassociation of complementary hybrid strands can also be achieved without toeholds. For example, the reassociation between the 3D cube and anti-cube with reverse complements at physiological conditions leads to conformational changes and to the swift formation of linear fibers that can further activate multiple functionalities such as transcription initiation via the completion of T7 RNA polymerase promoters, Förster resonance energy transfer (FRET), split RNA aptamers, and specific gene silencing via RNAi pathway[162].

As diagnostics, , miRNAs have emerged as a new generation of biomarkers for disease diagnosis, prognosis, and treatment monitoring[163]. . Ideally, a biomarker should be non-invasive and inexpensive but maintain stability and sensitivity for early stage detection of disease. Blood, urine, saliva, tears, and other bodily secretions are all sources from which miRNAs can be isolated and kept protected within extracellular vesicles[164]. Dysregulation of miRNA expression is seen in neurological disorders[165], muscular dystrophies[166], cardiovascular disease[167], diabetes[168], immunological diseases[169], viral infections[170], and differential expression occurs in cancer migration, invasion and metastasis[171, 172]. As one example, miR-141 is upregulated 105-fold in ovarian cancer cells, whereas miR-370 is down-regulated 100-fold[172]. During progression from Barrett's esophagus to esophageal adenocarcinoma, 4 miRNA families (miR-17, miR-18, miR-19,

and miR-92) are upregulated, while 16 miRNAs are downregulated[173]. Although miRNA has displayed great diagnostic potential, obstacles remain for introduction on the clinical side. One example is the expression of miRNA can be altered in different disease conditions. For example, miR-21 expression level has shown to be altered in cardiovascular diseases, inflammation, and several cancerous conditons[174, 175]. Thus, there exists high demand for new sensitive and accurate detection techniques that generate a specific miRNA signature for a given disease. The advantages of using nanomaterial-based sensors has led to implementation of various DNA-based nanostructures as a means of overcoming limitations associated with miRNA detection and quantification. One of the most commonly used DNA nanoparticles is a self-assembled tetrahedron with six helical edges[176]. DNA tetrahedra have great cellular permeability and rigidity; they also display enzyme resistance. All of these features make them good candidates for aiding miRNA detection. These miRNA-sensing nanodevices are designed such that a DNA tetrahedron is immobilized on a gold electrode surface. Three vertices of the tetrahedron are anchored to the electrode through thiol groups, and the fourth vertex contains a single-stranded extension that is complementary to part of the target miRNA[177]. A biotinylated signal probe complementary to the remaining part of the target miRNA for recruiting avidin-HRP (horseradish peroxidase) conjugates is used for detection. This novel strategy drastically enhances binding recognition, detection sensitivity and reproducibility. Another DNA nanodevice used for miRNA biosensing relies on a DNA origami motif with arbitrary shape[178]. Here, a 2D DNA tile with a single-stranded capture probe complementary to the target mRNA is partly hybridized with a biotinylated reporter strand conjugated with streptavidin-coated quantum dots. Upon target binding, the reporter stand is removed by a toehold-mediated strand displacement reaction, and AFM can be used to visualize the ensuing reduction of quantum dot signals on the AFM[178]. DNA nanodevices that utilize an optical readout for miRNA detection have been employed. Examples include: fluorophore-quencher strategy[179], DNA walker[180], DNA nanoswitch[181], and colorimetric strategy[182].

Diagnostic and therapeutic methods can be combined into a single step. Molecular switches are molecules whose folding and functions shift from their original states in response to ligand binding, pH, light, and other environmental stimuli. Proof of concept two-stranded RNA switches contain an enhanced green fluorescent protein (eGFP) mRNA antitarget strand and an antitrigger strand. After binding to a single-stranded connective tissue growth factor (CTGF), the mRNA target changes its conformation and releases a functional shRNA-like Dicer substrate structure recognized and cleaved by Dicer, ultimately downregulating eGFP expression[183, 184]. Ribozymes are RNA enzymes that catalyze a wide range of chemical reactions. Through enzyme engineering, ribozyme activity can be tailored to respond allosterically to specific effectors that subsequently allow these entities to function as molecular switches, or riboswitch. Generally, ribozymes operating on nucleic acid substrates depend on a specific sequence to form their active structure[185]. By exploiting this feature, two ribozyme fragments specifically bind to the junction sequence of an mRNA encoded by an oncogenic *BCR-ABL* gene. The three-stranded riboswitch not only inhibits oncogene expression, but it also alleviates the anti-apoptotic effect of oncogene production in both normal and leukemic cells[185]. Molecular beacon probes are alternatives to molecular switches and have relevance to biosensing applications. They have a fluorophore and a quencher anchored on opposite ends of an RNA strand that contains a sequence complementary to a specific nucleic acid. A spontaneous conformational change occurs after target binding that forces separation of the fluorophore and quencher. Since the fluorophore no longer lies in close proximity to the quencher, it fluoresces when illuminated by ultraviolet light[186]. Another realm of NANP applications whose progress has been noteworthy is the rapid development of various computational nanodevices such as DNA circuits. Amplification of transmission signals for optimized detection, transport of molecular cargoes by autonomous walking motors and integration of molecular actuators via a series of strand-displacement cascades illustrate just a few uses of these structures[187]. Furthermore, logic-gated nanoassemblies incorporating RNAi machinery as a molecular computing core can implement general Boolean logic gates with AND, OR, YES, and
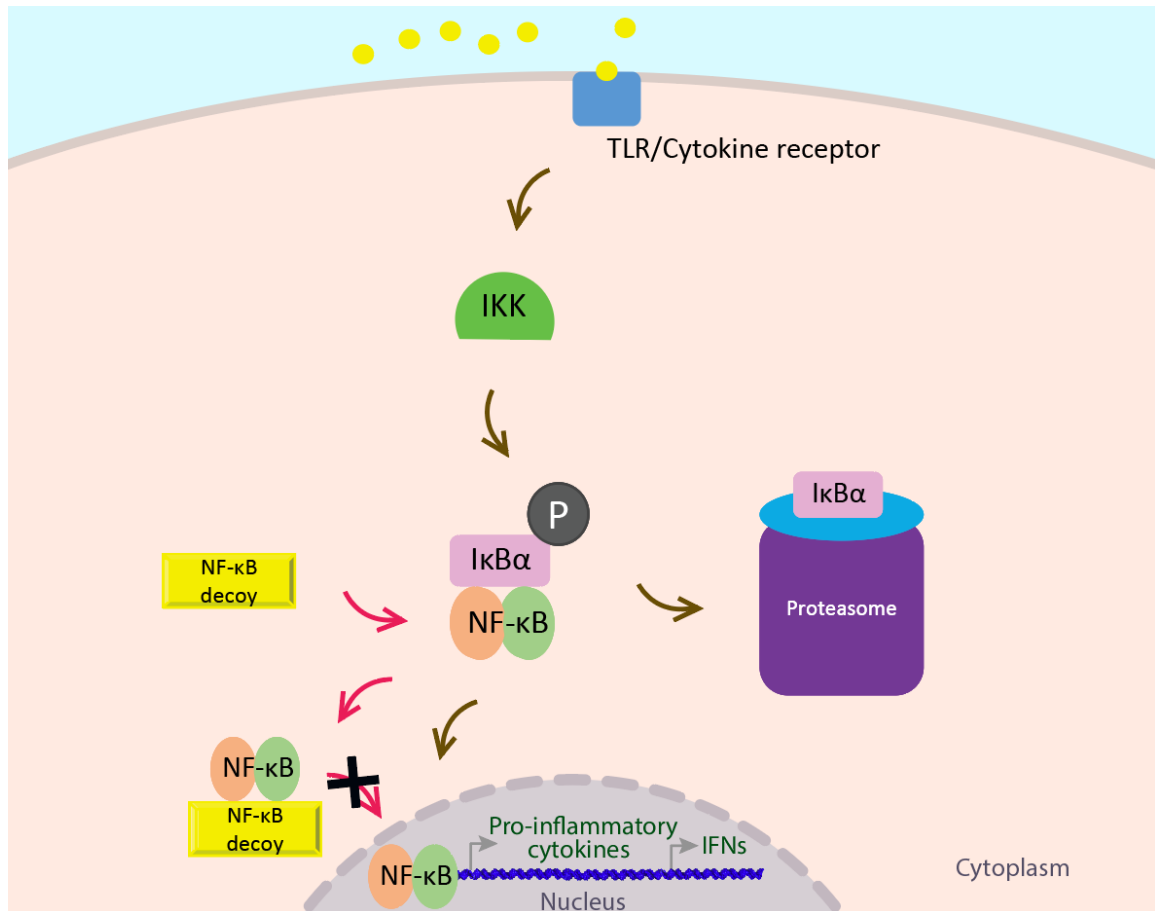
Figure 6. NF-κB activation and hijacking of the NF-κB pathway by NF-κB decoy. In the resting state, NF-κB dimers are located in the cytoplasm in an inactive form, and the inhibitory protein IκBα binds to the dimers. Through external stimuli, TLRs or cytokine receptors recognize these stimuli, resulting in phosphorylation of IκBα by IκB kinase (IKK), and IκBα is subsequently degraded in the proteasome. As a result, NF-κB dimers are free to enter the nucleus and bind to the target gene's promoter region, initiating transcription of pro-inflammatory cytokine and interferon genes. NF-kB decoys are ODNs containing consensus sequences that mimic NF-κB DNA binding sites. They bind to NF-κB dimers and prevent their nuclear translocation, ultimately blocking production of pro-inflammatory cytokines and interferons. NF-κB: nuclear factor kappa light chain enhancer of activated B cells. IκBα: nuclear factor of kappa light chain enhancer in B-cells inhibitor, alpha. IKK: I kappa B kinase. IFN: interferon. TLR: toll like receptor.

NOT arguments based on intracellular molecular circuits. These biological computers can play a role in combined biosensing and gene regulation[188]. The benefits of NANPs open the door to broad applications in therapeutics and biosensing. Also, they can potentially modulate immune behavior through precise design principles of dynamic NANP assembly, providing a controlled and fine-tunable immune response. As discussed earlier, interactions between NANPs and their

immunostimulatory properties must be clearly defined to permit successful and safe translation to the clinic. Pro-inflammatory cytokines and type I IFNs are key players in nucleic acid sensing by immune cells. Quantitative structure-activity relationship (QSAR) modeling uses measured physical and chemical properties as inputs to predict NANPs' potential for generating a pro-inflammatory response[189]. In one study, sixteen NANPs composed of all RNA, RNA with a DNA center, all DNA, and DNA with a RNA center were characterized. Based on the outcome, stability appears to contribute the most to immune response, followed by melting temperature, molecular weight, guanine-cytosine content, dissociation constant and, finally, size. In addition, the first systematic investigation of IFN induction of NANPs with various shapes, connectivities and compositions was performed using primary human peripheral blood mononuclear cells (PBMCs) from more than one hundred healthy donors[190]. It was discovered that linear (1D) NANPs, like RNA fibers, elicit the smallest immune response, planar (2D) structures, such as nanorings, lead to higher immunostimulation and globular NANPs, such as nanocubes, cause the largest immune response. Moreover, DNA- based NANPs exhibit less immunostimulation than RNA-based NANPs, and NANPs functionalized with multiple modalities, such as siRNAs and fluorophores, can be coordinated with minimal immunorecognition. Furthermore, all NANPs used without a delivery carrier in this study were immunoquiescent, while NANPs complexed with Lipofectamine 2000 induced various levels of immunogenicity. A more comprehensive understanding of how NANPs contribute to immune system stimulation allows for accurate prediction and control in various applications. While immunoquiescent NANPs can be used as nanoTNAs and for dynamic NANP constructions, activation of the immune system may be beneficial in cancer treatment. Cancer is a systemic disorder characterized by dysfunction of many immune pathways. The "cancer immunity cycle" refers to a series of stepwise events that must be initiated and expanded iteratively and efficiently in order for an anticancer immune response to effectively terminate cancer cells[191]. Production of type I IFNs and proinflammatory cytokines results from NANPs behaving as stimulatory factors that act on cancer immunity cycles and promote anti-cancer

effect[191]. Immune responses elicited by NANPs may also help restore normal immune function in a host by activating antigen presenting cells (APCs) and functional moieties that regulate expression of immune checkpoint proteins and homing cytokines[192]. This immunostimulatory property may be beneficial as a vaccine adjuvant, avoiding necrosis at the vaccine administration site, as well as an immunotherapy adjuvant that can restore and maintain immune homeostasis[192]. NANPs' efficacy in targeting NF-κB activity has been demonstrated; programming NANPs with NF-κB decoy can reduce NF-κB-dependent pro-inflammatory cytokine and IFN production[139](Figure 6).

1.2 Aptamer as molecular components of therapeutic nucleic acid nanotechnology

1.2.1 Aptamers and its selection process

For a long time, nucleic acids were considered merely carriers of inherited information that culminates in protein production. More recently, studies have confirmed that nucleic acids are essential to a variety of cellular actives including: enzymatic catalysis, gene expression regulation, epigenetic processing[193], etc.

Aptamers are short single-stranded ODNs that bind to their targets by folding into three-dimensional structures. The term "aptamer" is derived from the Latin word, "*aptus*", meaning "to fit" and the Greek word, "*meros*", meaning part[194]. . The idea of using nucleic acids, whether DNA or RNA, as ligands to modulate target activity emerged later as a result of human immunodeficiency virus (HIV) and adenovirus research[194]. These studies demonstrated that a short, structured RNA sequence trans-activation-response element (TAR) regulates gene expression and viral replication via binding of the TAR to viral proteins Cyclin T1 and Tat[195, 196]. Thirty years ago, a TAR RNA-derived aptamer decoy was discovered that bound with high affinity and specificity to Cyclin T1 and Tat proteins, thereby inhibiting viral gene expression and replication[197]. Since then, extensive research has been undertaken to investigate the full potential of aptamers in a variety of fields, especially biosensing, biomedicine and biotechnology.

Over the past decade, numerous approaches were developed to achieve more efficient and reliable aptamer selection. However, all of these strategies depend on modification of a universal process referred to as "systematic evolution of ligands by exponential enrichment" (SELEX). SELEX was first developed by Craig Tuerk and Larry Gold in 1990 as a means of finding two
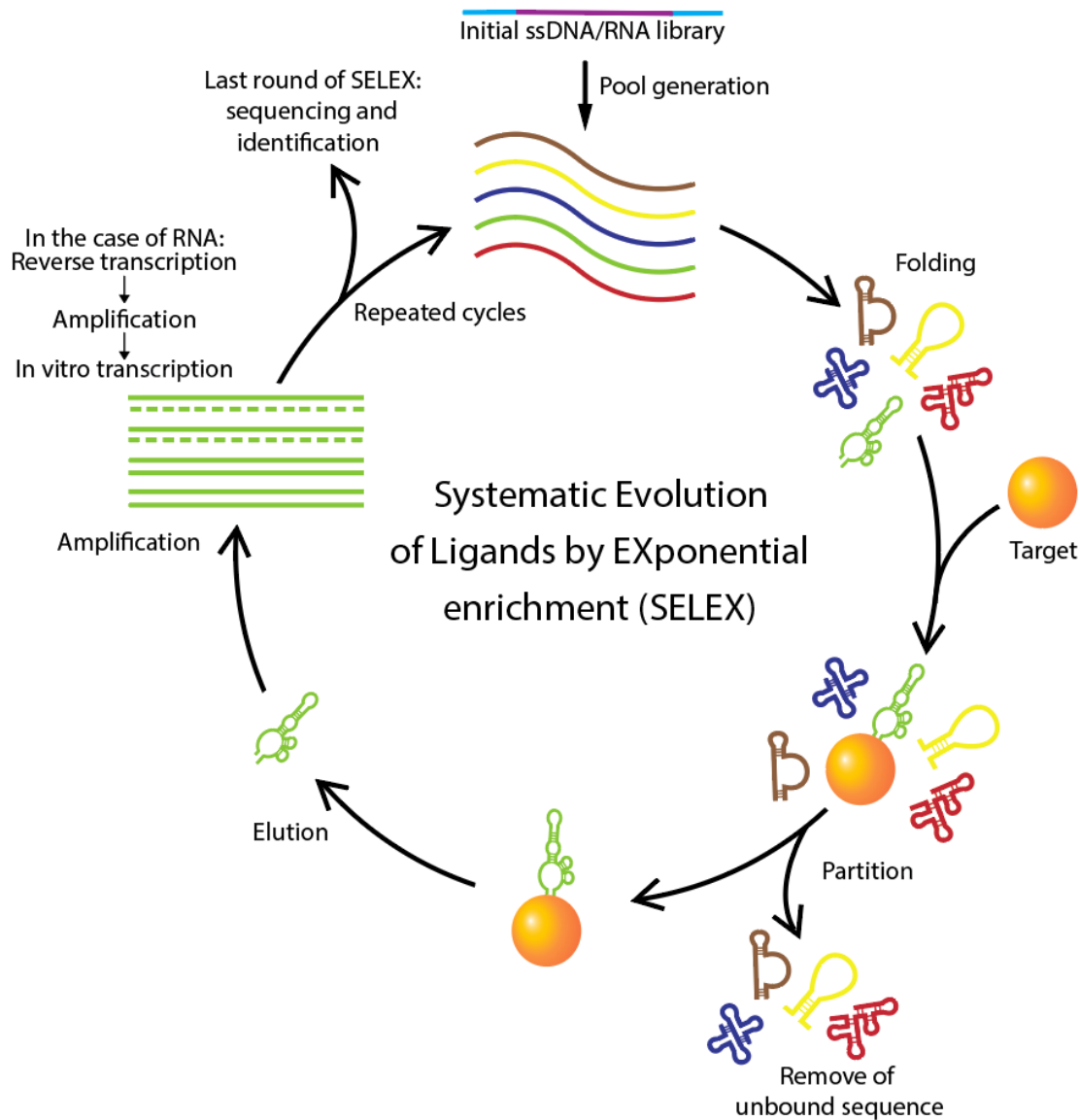
Figure 7. Schematic representation demonstrating the key steps of traditional SELEX. A library containing multiple sequences is generated by in vitro transcription. The library of ODNs is then incubated with the target molecule. The partition step separates the unbound ODNs and the target-bound ones. Finally, the bound ODNs are eluted and amplified by PCR. This cycle is repeated and, at the last cycle, the selected ODNs will undergo sequencing and identification for aptamer selection with high affinity and specificity.

high-affinity RNA ligands for bacteriophage T4 DNA polymerase[198]. In the same year, the SELEX-

selected molecules were named "aptamers" by Andy Ellington and Jack Szostak[199]. The first RNA enzyme carrying both genetic and catalytic properties was screened and identified by Debra Robertson and Gerald Joyce using this technique[200]. SELEX is an iterative process that involves repeated rounds of binding, partitioning and amplification[201]. The process starts with a combinatorial pool of 10^{14}-10^{16} different variants of synthetic single-stranded ODNs. In the SELEX library, ODNs normally contain 40-100 nts, and they harbor a randomized middle region flanked by two known sequence regions at both ends for primer binding (Figure 7). In order to monitor the process in real time, the library is incubated with a target molecule which can be tagged with a fluorophore or radiophore[201]. Partitioning is critical because it separates target-bound ODNs from unbound ones. Because of this step's significance, various strategies have been employed to enhance the specific binding efficiency. At the amplification step, bound ODNs are then eluted and amplified by polymerase chain reaction (PCR). For RNA aptamers, the RNA library is obtained using in vitro transcription of a random DNA pool with T7 RNA polymerase prior to the first round of SELEX selection.[202] Instead of PCR amplification, bound RNAs are amplified by reverse transcription PCR (RT-PCR), and the resulting DNA templates are subsequently transcribed. After a number of selection rounds (usually 10-30), ODNs with high affinity and specificity are isolated and enriched in the library which is then sequenced and characterized for aptamer identification[194]. Finally, Sanger sequencing is used for cloning the library from the last round into vectors and then picking up single clones randomly. Randomness is a blind operation because there is no guarantee that the highest affinity aptamers in the pool will be chosen. Next-generation sequencing (NGS) technology, which has become an attractive tool for deep sequencing of SELEX libraries, represents an alternative and more advantageous approach. It has the capacity for simultaneous deciphering of a large scale of sequences from an amplified library, allowing rapid characterization and real time monitoring. The combination of NGS with bioinformatics enables selection of high affinity aptamers[203]. Post-SELEX analysis of the final sequences includes binding motif identification through examination of primary and predicted secondary structures along with

determination of equilibrium dissociation constants (K_D) from quantitative binding affinity studies motifs[204].

SELEX is a well-established and widely used aptamer selection technique with high affinity and target specificity. Conventional SELEX suffers from certain limitations such as the inability of all molecules to become suitable targets[205]. For example, nucleic acids' negative charges render them difficult to use as targets due to repulsive electrostatic forces. Another drawback is the lack of standardized SELEX protocols in the research community[205]. Since there exist a wide variety of targets with different sizes, environmental stabilities, selection conditions, and immobilization compatibilities, there is no uniform procedure suitable for all targets. Synthesized library quality and subsequently selected pools in each round of SELEX constitute a third problem related to SELEX applications[205]. ODNs in SELEX possess a randomized central region; earlier studies have shown that random DNA library PCR proceeds quite differently in comparison to that of a homogeneous DNA template. Therefore, a marked optimization is needed to reduce selection bias[206]. Over the years, SELEX has evolved and been modified in order to tackle some of the above limitations while simultaneously making the entire selection process more efficient and cost/time/labor-effective. Some examples of novel SELEX strategies include: immunoprecipitation-coupled SELEX[207], capture SELEX[208], cell SELEX[209, 210], microfluidic SELEX[211], capillary electrophoresis SELEX[212], atomic force microscopy SELEX[213], in vivo SELEX[214, 215, 216, 217].

1.2.2 Unique features of aptamer

A salient feature of nucleic acid aptamers is their high affinity and binding specificity to their respective targets. As discussed in the previous section, development of aptamer selection has advanced very quickly, and the demonstrating K_D ranges from nanomolar to picomolar. Aptamer/ligand complexes reveal key interactions that contribute to the specificity of aptamer-ligand association. Unique 3D folding plays a significant role in aptamers' ability to bind targets.

Aptamer secondary structures consist of short helical arms and single stranded loops governed by intramolecular base complementarity[202]. Tertiary aptamer structures result from secondary structures combining with segmental sequence pseudoknotting on bulged[218] interior and multibranched loops via canonical base pairing. As a result, aptamers can bind to their target through precise stacking of flat moieties, hydrogen bonding, Van der Waals forces, electrostatic interactions and shape complementarity[202, 219].

Aptamers possess another extremely important property: they can be isolated against various types of targets ranging from small molecules to peptides and proteins to even larger structures like cells and tissues. Small molecules are important elements of numerous biological processes thanks to their diffusion-mediated cell membrane-crossing capabilities[220]. However, obtaining a suitable affinity ligand for small molecule targets (e. g. antibiotics, toxins and drugs) often poses a challenge. Isolated antibodies against small molecules have poor specificity and affinity[221]. Aptamers offer an alternative method of recognizing small molecules. Due to their flexibility, nucleic acids can fold into proper 3D shapes which fit their targets. A variety of interactions allow aptamers to bind small molecules with high affinity and specificity. Aptamer isolation against small molecule targets without target modification or immobilization is now possible thanks to advances in SELEX technology. A proprietary system named high-throughput antibody replacement process (HARP) can also select for aptamers against small molecules[221]. Traditionally, protein targeting was accomplished by using antibodies. Antibody production against specific proteins must take place in a biological system with intrinsic stochasticity, and the procedure requires a minimum time of six months. Also, batch-to-batch variation may occur, and different antibodies might bind to the same antigen (protein)[216]. Because it is performed in vitro, aptamer selection can remove aptamers which cross-react with unwanted targets via a process called counter-selection, thereby providing precise control of aptamer-target specificity[221]. Hence, discrimination between closely related targets with few differences can be achieved. For example, identifying proteins with and without post-translational modifications, or amino acids of the same

protein with and without a misfolding[221]. Additionally, aptamers' small sizes and flexible

backbones enable an easy fit into protein regions inaccessible to antibodies with large ligands.

Aptamers can be selected against very complex targets such as live or fixed whole cells from

different sources, tissue biopsies or tissue sections[221]. Using IP-SELEX or Animal-SELEX, one

can achieve aptamer isolation under normal physiological conditions; this is advantageous for

selection with cells or tissues. These, in turn, allowing aptamers can be bound to their targets in

"real world" to potentially prevent the inaccessible domains (e.g., transmembrane domains) used

to isolate aptamers[221]. This strategy is not possible with antibodies because a purified form of the

target protein is used and then screened for binding during the selection process[221]. The counter-

selection method is also applied to aptamers isolated from cells and tissues as a means of increasing

specificity[221].

Alongside conformational flexibility and targeting specificity, modifiability is a feature

that enables aptamers to undergo various chemical alterations and carry out diverse functions.

While both aptamers and antibodies can undergo modification, the former are readily modified

without affinity loss, whereas the latter often suffers from reduced activity[216]. Modification of

aptamers' internal surfaces modulates their pharmacokinetic properties. The 2'-hydroxyl position

on RNA nucleobases is susceptible to nuclease degradation. Therefore, a nuclease-stabilized ODN

library including 2'-amino or 2'-fluoropyrimidine modifications is widely used for aptamer

selection. RNA aptamer selection is essential for successful targeting of VEGF, a potent

physiological and pathological angiogenesis stimulator which binds to receptors (VEGFR1 and

VEGFR2) and ultimately activates downstream signaling[202, 222]. Similarly, substitution of a

hydroxyl group with 2'-O-methy at the 2'-hydroxyl site on purine nucleotides confers nuclease

resistance[223]. Replacing the phosphate-sugar backbone with phosphorothioate, or bridging the 2'-

O and 4'-C of ribose, yield locked nucleic acid (LNA) which strengthens aptamer stabilization

against nuclease digestion[224-226]. DNA aptamers that contain 2'-O, 4'-C-methylene-bridged/linked

bicyclic ribonucleotides selected by CE-SELEX have superior nuclease resistance and may bind

human thrombin with high affinity and specificity with K_D less than 30 nanomolar[227]. RNA oligonucleotide base modifications deliver other benefits besides increasing enzymatic stability; they can also enhance catalytic functionality. Incorporation of 5-(3''-Aminopropynyl)-2'-deoxyuridine, a modified nucleoside with a side chain carrying a cationic functional group, into an ODN library pool was reported to enhance catalytic activity[228]. Ligase ribozyme selected from a RNA library containing N^6-aminohexyl-modified adenine residues accelerated ligation about 250-fold compared to those from unmodified library[229]. Modification of aptamer termini was explored as a means of increasing blood stability and in vivo half-life time. Capping the 3'-end of thrombin binding aptamers (TBAs) with bridged nucleotides increased its stability in human serum while leaving the aptamers' binding abilities unaltered[230]. Placement of 2', 4'-bridged nucleotides onto the 3'-end of a DNA aptamer by terminal deoxynucleotidyl transferase (TdT) delivered a 320-fold improvement in nuclease resistance compared to samples tested prior to modification[231].

Besides aptamer residue modifications, a variety of molecules can enhance pharmacokinetic properties through aptamer conjugation. A lipid dialkylglycerol (DAG) phosphoramidite containing a tetraethylene glycol space was introduced at the 5' end of the VEGF aptamer via glycerol ether linkage. Here, the lipid group anchors the aptamer to the liposome bilayer, increasing serum circulation time and vascular permeability[232]. Engagement of human serum albumin (HSA) with cellular recycling neonatal Fc receptor (FcRn) makes HSA an excellent drug delivery platform with its extremely long circulatory half-life of approximately 19 days. Within HSA, domain I contains a single thiol at Cys34 used for selective conjugation to ODN, where aptamer is hybridized[233]. This assembled structure exhibits high stability in blood and extended half-life potential as a combinatorial drug delivery platform[233]. Attachment of polyethylene glycol (PEG) moieties decreases an aptamer's glomerular filtration because their large molecular size that avoiding systemic clearance. A PEGylated anti-VEGF aptamer, NX1838, augmented with several chemical modifications maintained a steady plasma concentration throughout the entire course of one study, exhibiting a prolonged half-life of 9.3 hours[234]. Aptamers

fused with other functional ODN are called chimera aptamers. First described in 2006, these structures have applications ranging from conjugation of diverse functional TNAs, such as siRNA or anti-miRs for gene silencing, to acting as DNAzymes for catalytic purposes[235].

Duration of aptamer activity can be controlled via hybridization with an antidote based on Watson-Crick base pairing, effectively preventing aptamers from binding to their targets (Figure 8). Antidote control is considered the safest method of regulating aptamer-based drug activity[236]. Such control is often extremely difficult or impossible to obtain in antibody- or low-molecular-weight molecule-based applications[237]. Antidote efficiency has been experimentally confirmed in animal models. Once an aptamer is administered into circulation and performs its desired functions, a subsequent injection of the antidote inactivates the aptamer, thereby terminating its action. In one in vitro study, an antidote for a RNA aptamer designed to target prothrombin and thrombin reversed
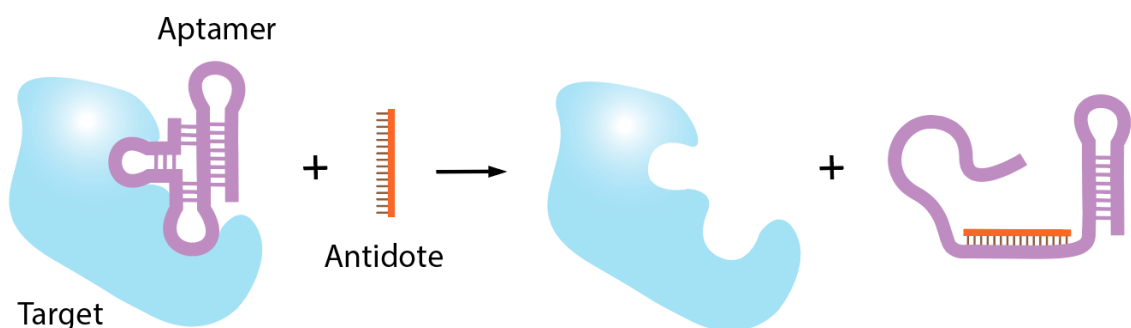
Figure 8. Duration of aptamer activity can be controlled by an antidote. The antidote to an aptamer is usually a single ODN that contains a sequence fully complementary to the aptamer. Consequently, aptamer binds to its antidote with high affinity and is removed from the target binding site, reversing the aptamer's inhibitory properties.

anticoagulation activity within two minutes[238]. Meanwhile, in vivo, an antidote to a cholesterol-modified anticoagulation factor IXa (FIXa) aptamer neutralized its activity within ten minutes after administration[236].

Aptamers are nonimmunogenic and nontoxic. While many monoclonal antibodies suffer from potential immune responses elicited by their fragment crystallizable (Fc) regions, evidence of immunogenicity towards aptamers has yet to be reported[239]. An in vivo study concluded that

aptamers containing 2'-fluoropyrimidines show no toxicity in rats or woodchucks even at high doses (10 mg/kg daily for 90 days via intravenous administration) [240].

Since aptamers are chemically synthesized, their production can be scaled up at moderate cost with high reproducibility and minimal batch-to-batch variability. Moreover, they display excellent stability and renaturation properties. Lyophilized aptamers can be stored for years without loss of activity and, once reconstituted, they can endure multiple freeze-thaw cycles[241].

1.2.3   Applications of aptamer in medicine

With the aforementioned benefits afforded by these materials, aptamers have advanced rapidly as tools of modern medicine, especially as replacements for antibodies. As a result, they have been called chemical antibodies[242]. Although routine use of mono- and polyclonal antibodies for a broad array of applications is common, limitations pointed out earlier are contributing to gradual replacement by aptamers. This is especially true for situations necessitating effective and specific target binding[243].

Prophylaxis is a primary function of antibodies. As their molecular mimics, aptamers also offer a foundation for prophylactic idiotype development based on similar methods. *Proteus mirabilis*, a gram-negative bacterium that causes catheter-associated urinary tract infection (CAUTI) among patients undergoing long-term bladder catheterization. This bacterium often blocks indwelling urethral catheters by forming crystalline biofilms; such blockages often go undetected until onset of complications like pyelonephritis, septicemia, and shock[244]. Unfortunately, no effective means of preventing *Proteus mirabilis* infection currently exists. However, DNA aptamers generated by a combination of CE-SELEX and in silico maturation (ISM) have demonstrated high affinity and specificity for *Proteus mirabilis*[245]. Eventually, they may constitute the basis for novel prophylactic strategies for CAUTI before blockages and complications arise.

Clinical disease diagnosis is another area in which aptamers have flourished as molecular

probes, biosensors, magnetic cell sorters, and components of immunoassays. Because of their high affinity, aptamers can detect very low amounts of diseased or tumor cells. For pathogen recognition, plastic-adherent DNA aptamer-magnetic bead and red quantum dot sandwich assays with detection limits averaging 2.5 colony forming units (cfu) were developed against $MgCl_2$-extracted surface proteins from *Campylobacter jejuni*[246]. A novel high-throughput FRET screening method aided in development of fluorophore-doped DNA aptamers against *Escherichia coli* outer membrane proteins (OMPs)[247]. Instead of bacterial proteins, the whole bacterium-based SELEX technique has successfully detected bacteria such as: *Shigella sonnei*[248], *Vibrio Parahemolyticus*[249], *Staphylococcus aureus*[250], etc. SELEX-based approaches have also generated nucleic acid aptamers as molecular probes for detecting viral and parasitic infections including: severe acute respiratory syndrome (SARS) coronavirus[251], hepatitis B virus[252], HIV[253], human influenza B virus[254], *Leishmania infantum*[255], and Cryptosporidium parvum[256]. More importantly, reliable cancer diagnoses and prognosis evaluations have become the main foci of aptamer-based therapeutic intervention. Thus, aptamers have been developed to detect numerous cancer-related biomarkers. Cell-SELEX technology can be utilized even for cases with unknown surface marker identities on the target protein. In one study, cell-SELEX was used to not only develop an aptamer against T-cell acute lymphoblastic leukemia (T-ALL) without prior knowledge of cell specific binding populations, also identify protein tyrosine kinase 7 (PTK7) as a biomarker for T-ALL[257]. This two-step strategy – selecting cancer cell-specific aptamers and then identifying binding target proteins-has major clinical implications for aptamers as novel cancer-related biomarkers. Accurate identification of tumor cells in peripheral blood is critical for early detection and/or monitoring of post-treatment residual disease[258]. Cancer cell detection also aids in determining whether surgical resection margins are tumor-free. Overexpression of epidermal growth factor receptor (EGFR), the most common oncogene in glioblastoma, has been associated with several tumor types. An immobilized anti-EGFR RNA aptamer was developed on a chemically modified glass surface with the ability to capture human and murine GBM cells overexpressing EGFR[258]. Aptamers can also

be used in flow cytometry to detect a wide variety of cells using cell-type specific probes that have two domains: : a sensing domain which recognizes the target molecule, and a signaling domain which gives feedback via a fluorescent or radionuclide reporter molecule[202]. When integrated with multicolor flow cytometry, such probes can play a role in noninvasive clinical imaging. Fluorescent-labeled RNA aptamer, for example, detected CD30 proteins overexpressed in cultured anaplastic large cell lymphoma and Hodgkin's lymphoma cells at low concentrations (0.3nM)[259]. An emerging application of aptamer biomarkers exploits surface plasmon resonance imaging (SPRI) to sense human thrombin and VEGF protein at picomolar concentration[260]. A surface aptamer-protein-antibody sandwich forms following detection of the target protein on an aptamer microarray, while the SPRI signal is amplified by HRP-conjugated antibodies through localized precipitation or color reactions[260].

Alongside their uses as preventive and diagnostic tools, aptamers hold promise as therapeutic agents due to their merits as cognate molecules[202]. At the present time, a number of aptamer-derived treatments for various diseases are under investigation in clinical and preclinical trials. In 2004, the US Food and Drug Administration (FDA) approved the first aptamer-based drug, pegaptanib sodium (Macugen), for treatment of neovascular age-related macular degeneration (AMD)[261]. This event was considered a milestone for aptamer therapeutics in medicine. Pegaptanib is the first anti-angiogenic therapy for neovascular AMD and one of two anti-VEGF drugs approved for human use[261]. It acts as a VEGF antagonist, reducing blood vessel growth in the eye to bring leakage and swelling under control[262]. At the molecular level, Pegaptanib's chemical modifications (fluorination, methylation and addition of a 5'-poly ethylene glycol moiety) provide nuclease resistance, half-life extension and binding affinity enhancement[261]. Blood coagulation processes are tightly connected to a reaction cascade involving numerous proteins such that activation of one unit generates the next one. Conversion of serum-soluble fibrinogen to insoluble fibrin that forms a clot is the endpoint of this entire process[263]. Hemostatic clot formation is crucial for prevention of excessive blood loss and maintenance of homeostasis[263]. Hemostatic clot formation is crucial for

prevention of excessive blood loss and maintenance of disease [263]. NU172 possesses a half maximal

inhibitory concentration (IC_{50}) of 5-10 μg/ml in plasma[263]. RA36 is another anti-thrombin DNA

aptamer that undergoes intensive investigations. It possesses a bimodular structure in which the

first G-quadruplex binds on thrombin and inhibits its function, whereas the second G-quadruplex

modulates the properties of the first[264]. Another key player in thrombosis is coagulation factor IX

(FIXa), whose activation is the rate-limiting step for thrombin formation[265]. REG1, the first

reversible anti-FIXa aptamer in Phase III clinical trials (ClinicalTrials.gov Identifier:

NCT01848106), may effectively treat patients suffering from percutaneous coronary

intervention[266]. The combined drug consists of pegnivacogin (RB006), a single-stranded 31-nt

aptamer that binds FIXa, and its 15-nt antidote, anivamersen (RB007)[266]. Pegnivacogin is

PEGylated and has a half-life of more than 24 hours, whereas anivamersen is metabolized in a few

minutes[266]. The use of antidote enables the control of the duration action. Cancer therapy represents

yet another area of medicine to which aptamers can contribute. AS1411, a 26-nt G-rich DNA

aptamer against nucleolin, a protein overexpressed in cytoplasm and on cancer cells' plasma

membranes, is in Phase II clinical trials (ClinicalTrials.gov Identifier: NCT01034410) for

treatment of patients with primary refractory acute myeloid leukemia. Another well-established

cancer target is prostate specific membrane antigen (PSMA), whose expression is primarily

prostate-specific[267]. An anti-PSMA RNA aptamer, A9g, has been isolated and studied in preclinical

models[268]. A9g reduces cell migration and invasion in vitro and has demonstrated potent anti-

metastatic activity in vivo[268]. MUC1 is a glycoprotein with O-linked glycosylation at its

extracellular domain[269]. Because MUC1 is overexpressed on epithelial cancer cells but not on

normal cells, it is used for targeting MUC1 cancer cell lines in breast, colon, lung, ovarian, and

pancreatic cancers[270]. DNA aptamers with 5' end modified to conjugate a photodynamic therapy

agent chlorin e6 have been selected to bind MUC1 glycoforms, and subsequently delivered to

epithelial cancer cells. Due to their high affinities and extraordinary targeting specificities, anti-

MUC1 aptamers exhibit a remarkable enhancement (>500-fold increase) in toxicity upon light

activation[270].

Conjugations between photodynamic agents and anti-MUC1 DNA aptamers yield another application: target-specific delivery. Usually, such aptamers are created by Cell-SELEX and in vivo SELEX technologies. A number of "cargos" are carried by aptamers; nucleic acid-based molecules (e.g., siRNA, decoy), nanoparticles (e.g., micelle) and chemotherapeutic drugs are some examples[216]. Different methods can be employed to link aptamers with therapeutic modules. For example, multifunctional conjugate containing the GL21.T aptamer targeting the Axl receptors as the carrier for delivering human let-7g miRNA as a gene-silencing moiety to Axl-expressing cancer cells and subsequently silencing of let-7g target genes via RNAi pathway[271]. The passenger strand of let-7g miRNA is the extension from 3'end of the aptamer sequence and the complementary guide strand is annealed to the template. The conjugate is protected from nuclease with 2'-fluoro pyrimidines modification[271]. As an alternative to the complementary extension strategy, the sticky bridge technique situates a linker on the aptamer to bind and interchange various siRNA motifs[272]. Anti-HIV-1 gp120 aptamer conjugated with a guanine cytosine (GC)-rich-bridge facilitates interchange of three DSRNA (one against HIV-1 tat/rev transcripts and two targeting CD4 and TNPO3, the HIV-1 host-dependency factors) to not only suppress HIV-1 infection but also protect against viral-induced T helper cell ($CD4^+$) depletion[272]. Simply attaching a hydrophobic tail to an aptamer end permits assembly of a highly ordered micelle-like structure, allowing the aptamer to function as the recognition motif of a given target as well as a nanoparticle building block[273]. Through membrane replacement, self-assembled aptamer-micelles can permeate cells and ultimately release their therapeutic payload[273]. Moreover, an elongated anti-transferrin receptor RNA aptamer with a short DNA extension hybridized by its complementary DNA sequence can load several chemotherapeutic drugs (Doxorubicin), and link NF-κB decoys via disulfide bonds[274]. This aptamer-Doxorubicin/NF-κB decoy conjugate performed selective codelivery of chemotherapeutic drugs and inhibited cell-survival factor, thereby increasing Doxorubicin's

therapeutic efficacy in pancreatic tumor cells[274].

1.3 Exosomes as Delivery Vehicles for Drug Delivery

1.3.1 Delivery of TNAs and therapeutic NANPs

Nanomaterials and their properties have made a significant impact in a multitude of areas, and a subset of these materials, namely TNAs and therapeutic NANPs, appear promising as nanomedical applications. Therapeutic NANPs are nanoparticles functionalized with TNAs to treat disease. Examples like DS RNA-carrying RNA–DNA fibers that target mutated *BRAF* gene in the treatment of melanoma[139], high quantum yield malachite green RNA aptamers conjugated with flavin mononucleotide (FMN) or theophylline (TH) that act as sensors for intracellular imaging[275], aptamer-siRNA chimeras that induce apoptosis in cancer cells using target eukaryotic elongation factor 2 (EEF2) gene[276], packaging RNA (pRNA) of bacteriophage phi29 DNA-packaging motors that silence metallothionein-IIa (MT-IIA) and survivin in ovarian cancer[277], and synthetic oligodeoxynucleotides containing unmethylated CpG motifs (CpG DNA) that induce both innate immunity and specific adaptive immune responses as vaccine adjuvant[278] are just a few examples that illustrate their diversity. Because both TNAs and therapeutic NANPs are composed of hydrophilic and negatively charged nucleic acids, they are prohibited from crossing biological membranes. Also, TNAs and NANPs are prone to immune responses and susceptible to nuclease degradation in the blood. These obstacles prevent direct use of nucleic acid-based drugs in medicine without the assistance of appropriate carriers. Lipofectamine 2000 (L2K) is a common reagent that transfects nucleic acids into eukaryotic cells. It provides high transfection efficiency in many cell types and it has a simple operation protocol. Unfortunately, L2K-mediated nucleic acid delivery has been linked to several major problems including: cellular toxicity[279], autophagy induction[280], unfolded protein response[281], type I interferon activation[282], and overproduction of beta-amyloid protein[283]. Therefore, L2K is not suitable for in vivo studies and biomedical applications. These delivery issue significantly slow down therapeutic NANP clinical translation and therefore,

development of new efficient carriers for therapeutic NANPs becomes a top priority for RNA nanotechnology.

Over the last few decades, extensive searches for, and investigations of, stable, efficient and safe carriers for therapeutic NANP delivery have been undertaken. So far, most clinically approved carriers for therapeutics have fallen into lipid-based, polymer-based or inorganic categories. Lipid nanoparticle (LNP), the most widely used and most clinically advanced technique, relies on complexing anionic nucleic acids with cationic lipids via electrostatic interactions[284]. The cell membrane contains a large quantity of lipids and phospholipids which facilitate lipid-cell membrane interactions, thereby enhancing cellular uptake. While non-modified LNPs are effective as in vitro transfection agents, they are rarely used in vivo as they interact with opsonic proteins in the blood to stimulate rapid clearance by mononuclear phagocytes in the reticuloendothelial system (RES). Hence, LNPs used for in vivo studies are usually 100-200 nm in diameter and coated with a neutral polymer such as PEG to prevent uptake by RES cells (particularly Kupfer cells) and improve persistence time in circulation[284]. Cholesterol, which inserts between lipid bilayers to increase their structural rigidity[285], and 2-dioleoyl-sn-glycero-3-phosphoethanolamine (DOPE) both facilitate endosomal escape[285]. Moreover, at their given size range, LNPs may only leave circulation at fenestrated endothelial barriers, particularly in the liver and spleen, and at tumor sites where a high enhanced permeability and retention (EPR) effect is present[284]. The aforementioned first FDA-approved RNAi therapeutic, Onpattro (Patisiran), consisted of a LNP decorated with both cholesterol and PEG_{2000}[286]. Its efficacy in the treatment of hereditary amyloidogenic transthyretin Amyloidosis (hATTR), a progressively incapacitating and often fatal genetic disorder, was demonstrated[286]. LNPs not only protect siRNA from degradation by endogenous nuclease, but they also facilitate its targeted delivery to hepatocytes, the primary sites of transthyretin (TTR) production[287]. Another lipid-based carrier that has garnered much attention is the liposome, and several FDA-approved liposomal formulations have already seen clinical use as cancer therapeutics[288, 289]. Liposomes are spherical-shaped particles composed of a lipid bilayer

surrounding an aqueous core; they are synthesized by dry phospholipid hydration[290]. They can be fabricated with various sizes (20-5000 nm), structures, compositions, and surface modification[291]. Additionally, liposomes may consist of several concentric bilayers separated by aqueous compartments with sizes ranging from 500 nm to 5 μm (multilamellar). These features allow liposomes to carry both hydrophobic molecules dissolved in the lipid membrane and hydrophilic molecules confined to the aqueous interior. Such a structure allows for loading of multiple types of molecules with controllable serial release as layers dissociate from the outer shell to the inner core. In contrast, a unilamellar liposome only contains a single bilayer and usually ranges from 20 nm to 1μm in size[291]. As with LNPs, PEGylation surface modifications are typically used to increase liposome circulation time and improve targeted delivery. More importantly, the liposome's composition makes it prone to cell membrane fusion and concomitant release of its contents into the cytoplasm. The hollow liposome core provides capacity for large volumes of therapeutic molecules. Taken together, these beneficial properties have made liposomes a popular research focus in the context of therapeutic applications. All-*trans*-retinoic acid (ATRA), combined with cationic liposome-mediated delivery of interleukine-12 (IL-12) plasmid DNA (pDNA) stimulated CD4$^+$ cell type I response and activated natural killer (NK) cells, ultimately producing IFN-γ and TNF-α that potentiated antitumor effects in metastatic lung cancers in mice[292]. Preclinical analysis of liposome-delivered Raf antisense oligodeoxynucleotide (LErafAON) showed downregulation of Raf 1 oncogene against human prostate, breast, and pancreatic tumors grown in athymic mice[293].

Polymer-based particles are another promising nanocarrier for therapeutic NANP delivery. Hyperbranched dendrimers possess compartmentalized structures and high monodispersity, which can be fabricated in various sizes by controlling branch number and obtain high entrapment efficiency with high generations[290] Their architecture consists of three domains: a central core, a hyperbranched mantle with internal voids and a corona with many reactive peripheral surface groups that can be readily functionalized via PEGylation, acetylation, hydroxylation, or even conjugation with other biocompatible compounds[294]. Likewise, therapeutic payloads can either be

conjugated with surface functional groups or encapsulated in hydrophobic cavities. Because of such high levels of synthetic control, dendrimers make attractive candidates for delivery vehicles. A diverse set of dendrimers with distinct chemical architectures have been explored[294]. Poly (amidoamine) (PAMAM) is a dendrimer whose amine-terminated surface groups become positively ionized under physiological conditions, promoting complexing with the anionic phosphate backbone of nucleic acids via electrostatic interactions. Over the past two decades, PAMAM has received more attention than any other dendrimer, and it illustrates the biological maxim that structure determines function. Delivery efficiency of PAMAM is highly dependent on the generation of the dendrimer. The number of primary surface amines directly contributes to PAMAM's overall positive charge; too little charge will hinder a stable interaction with nucleic acids. Surface amine group number doubles with each generation, reaching 4096 at the tenth iteration[295]. Achieving a desired transfection efficiency necessitates a minimum amount of G3[296]. A variety of medical applications employ PAMAM to deliver nucleic acid-based therapeutics. Ovarian cancer treatment involves G4 PAMAM-mediated siRNA delivery which targets B-cell lymphoma 2 (BCL2) genes[297]. G7-PAMAM, a carrier of antisense ODNs and antisense mRNA-coding plasmid expression vectors, specifically inhibits luciferase expression at picomolar concentration[295]. Other forms of dendrimers, such as poly (-propylene imine) (PPI) and poly-L-lysine (PLL), transport nucleic acid-based medications as treatments for luteinizing hormone-releasing hormone (LHRH) positive cancer (G5)[298], and gluconeogenesis (G6)[299], respectively.

Micelles are amphiphilic polymers formed by self-assembly in liquid environments. They are characterized by a hydrophilic mantle surface surrounding a hydrophobic core. The hydrophilic portion protects the micelle from nonspecific RES uptake, thereby maintaining its concentration within the body. On the other hand, the hydrophobic portion traps hydrophobic therapeutic agent[290]. Nucleic acids, however, tend to have negatively charged backbones in physiological conditions, making them hydrophilic. As a result, some novel micelle derivatives have been developed for nucleic acid delivery. Inspired by dendrimers, amphiphilic cationic micelles are formed from a

hydrophobic core of poly-L-leucine (PLLeu) which drives self-assembly, a cationic PLL hydrophilic shell that binds ODNs and a neutral PEG corona that provides a protective coating[300]. PEG-PLL-PLLeu polypeptide cationic micelles act as co-deliverers of docetaxel (DTX) and siRNA-Bcl-2[116]. This combination promoted a synergistic anti-cancer effect involving down-regulation of anti-apoptotic Bcl-2 gene alongside enhanced antitumor activity at smaller DTX doses[300]. Like micelles, bolaamphiphile (bola) and poly (lactide-coglycolide)-graft-poly (ethylenimine) (PgP) are amphiphilic polymers that have achieved successful in vitro delivery of TNA into a flank tumor and into the brain[301] as well as in vivo delivery of therapeutic NANPs with different shapes and sizes[302].

Inorganic nanoparticles are another branch of materials possessing a wide variety of physical and structural properties which make them attractive candidates for therapeutic delivery. Mesoporous silica nanoparticles (MSNPs) have large surface areas (>700 m^2/g) with unique porous structures, large pore volumes (>1 cm^3/g) and tunable pore diameters (2-10 nm)[303]. These features enable MSNPs to carry large payloads, increasing local biogenic concentration at a targeted area. In addition, the exterior particle surface and interior pore surfaces readily undergo modification and functionalization with conjugate targeting ligands (antibodies and cell-penetrating peptides (CPP)), bioimaging agents (quantum dots), protective polymer coatings like PEG, or pDNA complexes[136, 303]. MSNP-mediated delivery of three NANPs with different geometries transported a combined functionalities of siRNA targeting BCL2 and the chemotherapeutic drug doxorubicin[136].

Gold nanoparticles (AuNPs) represent another important nanocarrier that plays a role in nucleic acid delivery. As the most stable noble metal, gold confers unique localized surface plasmon resonance (LSPR), low cytotoxicity, versatility, and multifunctionality. AuNPs' versatility makes them ideal for drug delivery and other medical applications. For instance, AuNPs conjugated to siRNA via an acid-sensitive ketal linker group underwent cleavage upon internalization by tumor cells in their acidic extracellular environment. This approach relied on

rapid siRNA release at the target site triggered by the ketal linker's separation[304]. Another study investigated Au-nanobeacons comprised of AuNPs functionalized with fluorophore labeled hairpin DNA for targeting multiple RNAi pathways: downregulation of specific gene silencing via exogenous siRNA and silencing the silencers (e.g., endogenous miRNA), at the same time, yielding a quantifiable fluorescence signal directly proportional to the level of silencing[305]. Also, this approach permitted intracellular tracking of the locations of target recognition and gene silencing[305].

Besides the catalog of materials already discussed, other synthetic carriers like superparamagnetic iron oxide nanoparticles and quantum dots have shown promising outcomes in TNA and therapeutic NANP delivery[306, 307]. Despite their advantages, manufactured nanomaterials often suffer from immunogenicity, cytotoxicity, rapid blood clearance, and poor biodistribution, all of which hinder their clinical translation[308-314]. Development of a new endogenous delivery system to overcome complications associated with synthetic materials is paramount.

1.3.2   Overview of extracellular vesicles

Extracellular vesicles (EVs) are membrane-bound, cytosol-containing particles secreted into the extracellular space by almost all living cells. EVs have been found in bodily fluids including: blood, urine, saliva, breast milk, cerebrospinal fluid, sputum, bile, semen, amniotic fluid, broncho-alveolar lavage fluid (BALF), and ascites[315, 316]. The content, size and membrane composition of EVs depend on their cellular source and physiological conditions. At present, three subgroups of EVs have been broadly classified and generally accepted based on their sizes and biogenetic pathways: apoptotic bodies, microvesicles, and exosomes.

Apoptotic bodies are larger vesicles with 800-5,000 nm diameters that cells release while undergoing programmed cell death[317]. Microvesicles, are generally smaller (50-1,000 nm diameter), membranous vesicles produced via plasma membrane (PM) budding associated with cell shedding[317]. The smallest EVs, exosomes, range from 40-100 nm in diameter and undergo

release during fusion of multivesicular bodies (MVBs) with the PM (Figure 9A). Due to their heterogeneous and dynamic nature, EV subgroup differentiation is challenging. Intercellular communication relies heavily on EVs, and they contribute to numerous physiological and pathological functions. Moreover, cancer cell-derived EVs have shown to promote angiogenesis and coagulation, support tumor progression and generate pre-metastatic niches[318].

A diverse array of quantitative methods is available for vesicle characterization. Assessment of EV sizes and morphologies can be undertaken with transmission electron microscopy (TEM) and cryoelectron microscopy. Nanoparticle tracking analysis (NTA), tunable resistive pulse sensing (tRPS), dynamic light scattering (DLS), and high-resolution flow cytometry (hFC) not only reveal EV size, but also provide information regarding concentration[319]. Traditional methods of EV isolation such as ultracentrifugation[320], density gradient centrifugation[320], size exclusion chromatography[321], ultrafiltration and gel filtration[322]use properties of size and buoyant density. A relatively new method, polymer-based precipitation, exploits PEG to change EV solubility and promot aggregation[323]. Other novel isolation methods that have recently appeared are integrated microfluidic systems with on-chip immunoisolation[324] and lipid-nanoprobe systems that enable spontaneous labelling of EVs with rapid subsequent magnetic enrichment[325]

EVs contain luminal biologically active cargo such as proteins, nucleic acids and lipids that can be taken up by a recipient cell, potentially altering its operation. Based on proteomic studies, EVs are highly abundant in cytoskeletal, cytosolic, heat shock, and PM proteins, as well as proteins associated with intracellular trafficking[326]. EV protein content can be assessed by immunoblotting, immuno-gold labelling with electron microscopy, and antibody-coupled bead flow cytometry analysis[326]. Some transmembrane proteins enriched in EVs are: adhesion molecules such as integrins, tetraspanins (e.g., cluster of differentiation (CD)9, CD81, CD63, and CD82, CD53, CD37), intercellular adhesion molecules (ICAM, also known as CD54), globule-epidermal growth factor-factor VIII (MFGE8, also called lactadherin), antigen presentation proteins such as major

histocompatibility complex (MHC) class I and class II, membrane transport and fusion proteins for intracellular trafficking such as annexins; flotillins and Ras-associated binding (RAB), and ADP-ribosylation factor (ARF) GTPases[326-330]. Cytosolic proteins found in the EV lumen include: cytoskeletal proteins such as actin, cofilin, moesin and tubulin; signal transduction proteins such as heterotrimeric G, syntenin, β-catenin, and 14-3-3; enzymes like elongation factors, glyceraldehyde 3-phosphate dehydrogenase (GAPDH), peroxidases, pyruvate kinase, and enolase; chaperones such as heat shock protein (HSP)70 and HSP90; and biogenesis factors such as programmed cell death 6-interacting protein (Alix), tumor susceptibility gene 101 (Tsg101), syntenin, ubiquitin, clathrin, and vacuolar protein sorting (VPS)4 and VPS36[316, 331]. Certain proteins are commonly considered to be specific markers for EV subgroups. CD9, CD63, CD81, Alix, Tsg101, and HSP70 are exosomal markers; integrins, flotillin-2, CD62, and CD40 are markers for microvesicles; and Annexin V and phosphatidylserine (PS) are used to identify apoptotic bodies[316, 332, 333]. Common EV protein signatures are critical to ensure their correct operation. The post-synaptic density protein, disc-large, zonulin I (PDZ) protein syntenin, is a key component in MVB formation[334] expression of glycosylphosphatidylinositol (GPI)-anchored CD55 and CD59 protect EVs from complement-mediated lysis[335] and surface glycosylation patterns assist EV uptake by recipient cells[336]. Cytokine and chemokine secretions affiliated with EVs (e.g., IL-1α[337], IL-1β[338], CXCL8[339] and CX3CL1)[340] regulate immune response in target cells.

Genetic material, such as DNA and RNA, is present in EVs. RNA pools in EVs have been identified using high-throughput RNA sequencing and verified by RT-qPCR[341]. These RNA populations include: mRNAs, mRNA fragments, lncRNA, miRNAs, snoRNAs, snRNAs, piRNAs, rRNAs, and fragments of tRNAs and rRNAs[316, 341, 342]. EV RNA may regulate gene expression and protein translation in recipient cells. A 3'-untranslated region of mRNAs rich in regulatory sequences is carried by EVs and serves as a binding site for numerous RNA-binding proteins. These "external" mRNAs may compete with the recipient cell's mRNA for miRNA binding and specific

RNA-binding proteins in the recipient cell, potentially leading to downregulation of protein production there[343]. Regarding the RNA sorting mechanism into EVs, growing evidence indicates RNAs are not loaded into cells randomly and passively. Instead, a certain population of RNAs becomes EV-enriched compared to their parental cells, suggesting that cells selectively deliver these RNAs to enhance or modify target cell functioning[344]. Additionally, RNA content of EVs is regulated by cells' physiological states. MiR-150, noted for its participation in hematopoiesis, was preferably packaged into microvesicles (MVs) in lipopolysaccharide (LPS)-treated human blood cells[345]. During immune synapse formation, miR-335 was selectively sorted to EVs derived from T lymphoblasts and unidirectionally transferred to APCs resulting in downregulation of SRY-related HMG-box (SOX)-4 mRNA translation[346] In contrast to RNA, little is known about EV-transported DNA's functions, and its physiological significance in recipient cells remains under investigation[326]. However, genomic DNA (gDNA), oncogenic DNA, mitochondrial DNA (mtDNA), ssDNA, and dsDNA have been detected in EVs[347-350].

Finally, EVs possess a lipid bilayer in which lipid distribution in the outer and inner membranes is expected to resemble the cell membrane due to similar formation mechanisms[351]. Compared to their cells of origin, EVs are enriched in sphingomyelin (SM), PS, cholesterol, and sphingolipids[352]. . However, not all EVs contain high amounts of lipids. Reticulocyte-derived EVs displayed no enrichment of PS or SM, whereas ceramide amounts changed during reticulocyte maturation into red blood cells[353]. Therefore, EVs' lipid composition is dynamic and influenced by the cell's physiological status. Lipids perform essential functions in EVs; cholesterol appears to regulate EV trafficking by selecting membrane rafts and tetraspanin-enriched microdomains for budding[354]. Cholesterol, along with long, saturated sphingolipid fatty acids, provide tight packaging and structural rigidity to EVs[326]. In a cancerous condition, SM stimulates endothelial cell migration and mediates angiogenic activity[355]. PS in platelet-derived EVs contributes to thrombin formation and promotes coagulation[356].

Chemical components are not consistent throughout all EVs. Instead, they are rather specific and dependent on size, the EV's cell of origin and purported functions[357]. Breast cancer cell-derived MVs and exosomes exhibit distinct protein profiles for extracellular matrix degradation, cancer invasion and metastasis, and cell survival[358]. A subpopulation of exosomes, called "exomeres" lack external membranes or spherical shape, and contain different types of proteins based on proteome analysis[359]. Likewise, EVs from diverse origins make up different components of proteins, nucleic acids and lipids that influence various physiological and pathological functions in recipient cells. Renal collecting duct cells excrete EVs that contain vasopressin-regulated water channel aquaporin-2 (AQP2), a protein involved in Na^+ transport and control of water permeability across the nephron[360]. Platelet-derived EVs contain CD154 which stimulates antigen-specific IgG production to modulate inflammation and adaptive immunity at recipient cells distant from the activation site[361]. Saliva-derived EVs carry tissue factor that initiates thrombin formation from the zymogen prothrombin to elicit blood coagulation in target cells[362]. 59 well-characterized, immune-related miRNAs detected and enriched in breast milk-derived EVs are shown to assist with development of the infant immune system[363]. Lipidomic studies reveal a high cholesterol/phospholipid ratio of 2 in prostate gland epithelial cell-derived EVs, namely prostasomes isolated from human semen. Fusion of the sperm plasma membrane with prostasomes contributes to sperm stability, enabling sperm's greater resistance to untimely acrosomal reaction[364].

Compositions of specific cell type-derived EVs also change in response to fluctuations in the extracellular environment as well as different physiological conditions or differentiated cell states. For instance, EVs secreted by vascular endothelial cells under ischemia-induced hypoxia caused cytoskeletal and extracellular matrix rearrangements due to changes in EV protein and mRNA contents[365]. EVs secreted by cells containing mutated Kirsten rat sarcoma (KRAS), which occurs in 30%-40% of colorectal cancer (CRC) cases, dramatically affect proteomic vesicle

composition, such as tumor-promoting proteins KRAS, EGFR, SRC kinase, and integrins[366]. Mature dendritic cell (DC)-derived EVs treated with LPS contain 50-to 100-fold more proteins, with notable enrichment of MHC class II, B7-2 (CD86) and intercellular adhesion molecule 1 (ICAM-1). Compared to EVs from immature DCs, the mature DC-derived EVs displayed greater antigen-specific T cell activation to trigger effector T-cell responses and active naïve T cells to APCs[367].

1.3.3   Exosome biogenesis and trafficking

Exosomes, the smallest members of the EV family, are released by fusion of the endocytic pathway organelle with the PM[368]. At one time, they were considered cellular waste disposed of in the extracellular environment. With exponential growth in exosome research over the past 30 years, their essential roles in healthy and pathological cells, as well as their potential clinical diagnostic and therapeutic applications, have been investigated. In 1987, the term "exosome" was derived from observations of reversed endocytosis activity in which internal cellular contents were externalized through a membrane-bound vesicle released by the same cell[369]. Detailed knowledge of molecular mechanisms behind the biogenesis and transport of exosomes can aid in understanding exosomal functions and further exploration of their medical utility.

Exosome biogenesis starts within the endosomal system. The endocytic pathway consists of distinct membrane compartments which internalize molecules from extracellular components, recycle to the PM, and/or sort for degradation[370]. Early endosomes are the first compartments that receive molecules coming from the cell surface. They primarily function as sorting organelles; at acidic pH, endocytosed ligands dissociate from their receptors[371]. Intraluminal vesicles (ILVs) are formed by inward budding of early endosomal membranes with specifically selected molecules. During maturation of early endosomes to late endosomes, ILVs accumulate in the lumen of transvesicular compartments, such as multivesicular bodies (MVBs), where the sorting process continues preparation for the transcytotic pathway[371]. Generally, lysosomes are the last

compartment of the endocytic pathway, and most MVBs will fuse with lysosomes wherein lysosomal hydrolases will degrade their contents. However, some MVBs, especially those contain high amount of cholesterol, may fuse with the PM, and the released ILVs are denoted exosomes (Figure 9A)[372]. MVB populations are cell-dependent and regulated by various cellular conditions and external factors[368] In addition, cells can host different subpopulations of MVBs. For example, MVBs with lysobisphosphatidic acid (LBPA) negative and LBPA positive coexist in human B lymphocytes, with the latter destined for degration[373].

The process of MVB formation involves more than 20 proteins, most of which belong to the ESCRT (endosomal sorting complex required for transport) system[374]. ESCRT consist of four different protein complexes, ESCRT-0, -I, -II, and -III, along with associated vacuolar protein sorting 4/suppressor of K^+ transport growth defect 1 (Vps4/SKD1) and ALG-2-interacting protein X (ALIX) protein complexes[375]. MVB sorting involves recognition of endocytic cargo subsets that become concentrated in endosomal membrane regions, and this process is conserved throughout eukaryotes[376]. ESCRT-0 complex consists of hepatocyte growth factor–regulated tyrosine kinase substrate (HRS) that sorts monoubiquitinated membrane proteins into MVBs and associates with signal transducing adaptor (STAM). HRS recruits TSG101 of the ESCRT-I complex, whose roles include transferring ubiquitinated proteins between the ESCRT-0 and -II complexes and recruiting the ESCRT-III complex via ESCRT-II or ALIX. ESCRT-I and -II together induce an inward invagination from the endosomal membrane and form a neck structure of the nascent vesicle, while ESCRT-II and -III pinch off the neck and release the vesicle into the MVB lumen[374] Finally, ESCRT-III associates with Vps4/SKD1 ATPase to dissociate and recycle the ESCRT machinery using energy derived from ATPase activity (Figure 10).

In the ESCRT-dependent pathway, ubiquitin is critical for sorting of membrane cargos into the MVB. However, MVB formation also occurs independently of ubiquitination. Heparin sulphate proteoglycans promote exosome biogenesis through syntenin which binds syndecan with ALIX.
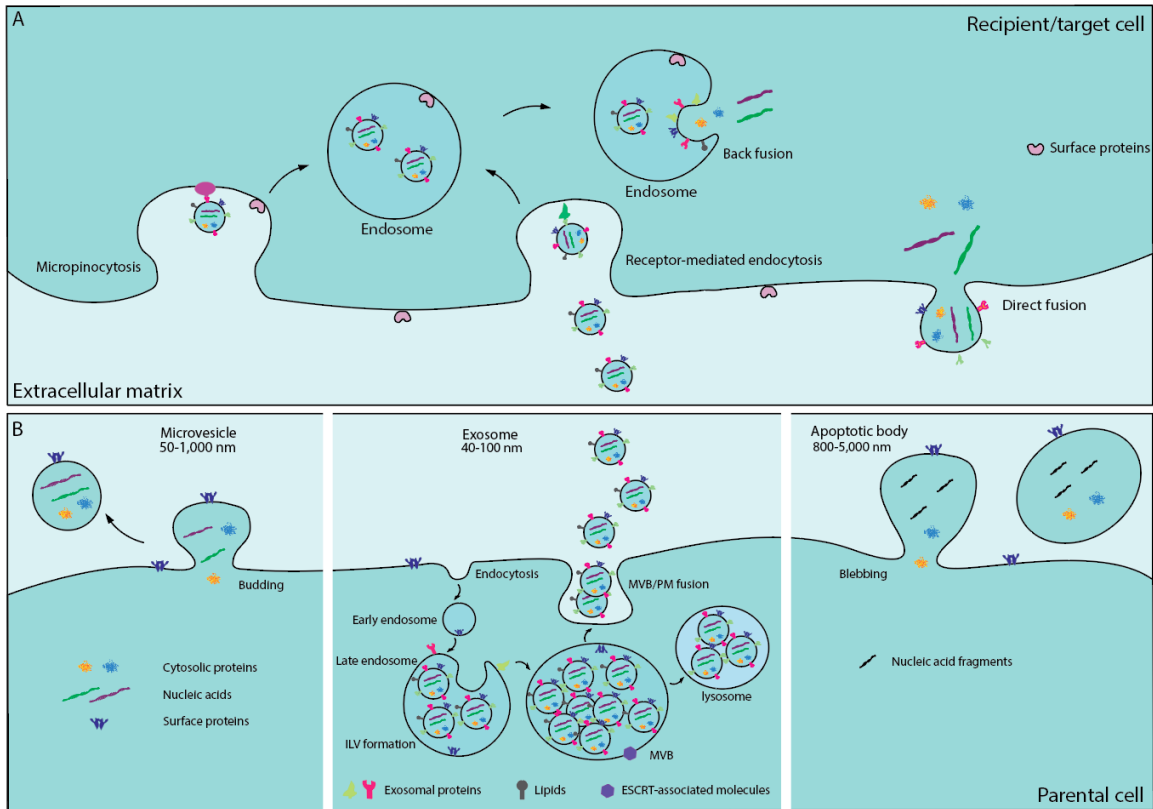
Figure 9. EV biogenesis and trafficking. A. Exosomes are taken up by recipient cells via direct fusion of the exosomal membrane and the PM of the recipient cell, leading to direct release of their contents into the recipient cell's cytoplasm. Alternatively, receptor-mediated endocytosis and micropinocytosis involve exosome uptake into endosomes, but the exosomal contents are released via back fusion of the exosomal membrane and the recipient cell's endosomal membrane. B. Biogenesis of apoptotic body, microvesicle and exosome. From left to right: Microvesicles shed from the cell via budding of the PM. Exosome biogenesis begins with internalization of membrane proteins and lipid complexes via endocytosis and engulfment of cytosolic proteins and nucleic acids into the ILV via inward budding of the endosomal membrane. With endosome maturation, late endosomes enclose numerous ILVs to become MVBs. Some MVBs are degraded in lysosome; exosome secretion occurs when MVB fuses with the PM. During apoptosis, cell disassembly generates apoptotic bodies which are released via blebbing and protrusion.

ALIX then interacts with TSG 101 and charged multivesicular body protein 4 (CHMP4), creating an intermediate between ESCRT-I and ESCRT-III for vesicular budding and scission processes[377].

Additionally, MVB formation can take place without ESCRT complexes and proteins. One alternative pathway involves segregation of cargos associated with raft-based microdomains which possess highly enriched sphingomyelinases. Removal of the phosphocholine moiety from sphingomyelinases via hydrolysis leads to ceramide formation[378]. Ceramides have a cone-shaped

morphology that promotes spontaneous inward curvature of the endosomal membrane and promotes domain-induced budding, facilitating exosomal lipids sorting during exosome biogenesis[379]. In another case, tetraspanin-enriched microdomains serve as ubiquitous specialized membrane platforms for partition of receptors and signaling proteins in the PM, aiding the selection of receptors and intracellular components sorted toward exosomes[380]. Many other molecules and cellular structures, including small integral membrane proteins of lysosomes and late endosomes (SIMPLE) contribute to MVB formation using ESCRT-independent mechanisms[381]. There are two fates following MVB formation: one is fusion with the PM and subsequent release of internal vesicles as exosomes, while the other is lysosomal degradation. Except for the fact that high levels of cholesterol seem to promote PM fusion, the mechanism which controls MVB's route remains unclear[382]. The final fate of MVBs, however, is not immutable but changes under different cellular conditions, such as starvation, rapamycin treatment, ISGylation, etc[383, 384].
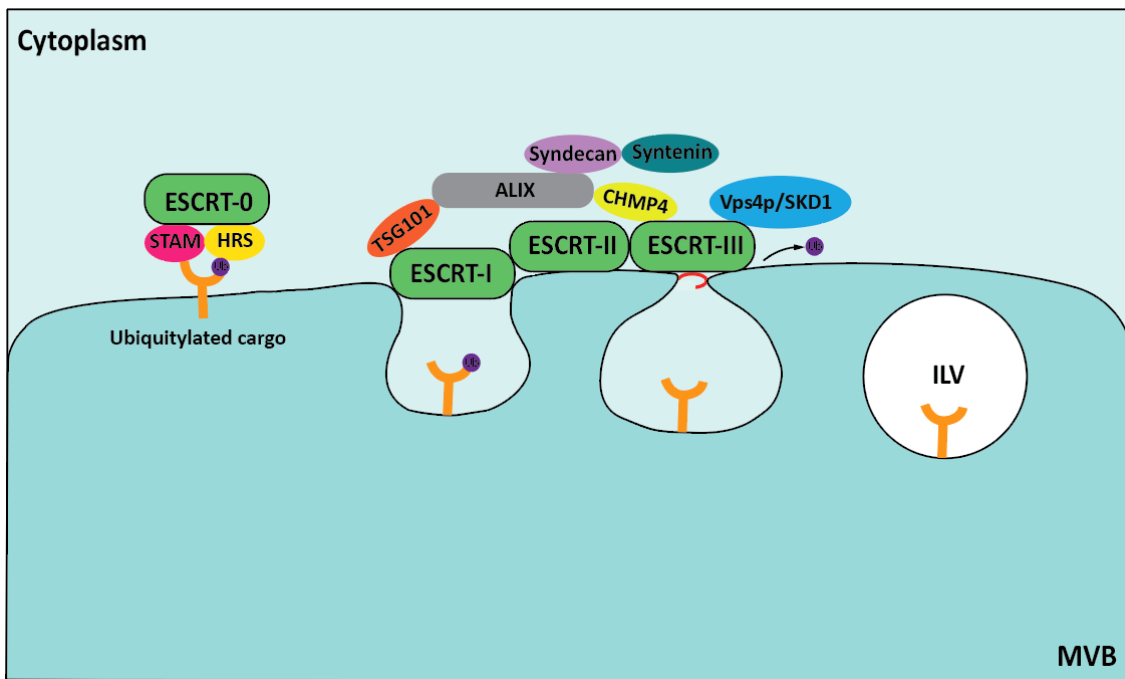
Figure 10. ESCRT pathway for cargo recognition and sorting. ESCRT-0 complex recognizes and sequesters ubiquitylated cargo, whereas the ESCRT-I and -II complexes are responsible for membrane deformation that yields buds with ubiquitylated cargo. ESCRT-III complex subsequently drives vesicle scission, resulting in ILV formation. Various ESCRT-accessory proteins participate in and assist with these processes.

In these cases, MVBs are prone to lysosomal degradation[384]. Exosome release involves contributions from several Rab proteins which act as essential regulators of intracellular vesicle transport. The Rab family is composed of more than 60 GTPases that associate with membranes via geranylgeranylation to regulate cellular trafficking processes like vesicle budding, transport, tethering, as well as fusion mediated by cycling between the active guanosine triphosphate (GTP)-bound state and the inactive guanosine diphosphate (GDP)-bound state[385]. Rab GTPase mechanisms are cell-specific; Rab2b, Rab4, Rab5A, Rab7, Rab9a, Rab11, Rab27a, Rab27b, and Rab35 have been implicated in various stages of exosome release among different cell types[386, 387]. Subcellular MVB location depends on interactions of MVBs with the microtubule cytoskeleton and actin. Cholesterol content partially controls movement of MVBs along the microtubules as well[388]. Once MVBs are docked to the PM, Rab and soluble N-ethylmaleimide-sensitive fusion protein-attachment protein receptor (SNARE) proteins participate in fusion of the MVB membrane with the PM, ultimately releasing exosomes into the extracellular space[389].

As messengers of intercellular communication, exosomes secreted by their cells of origin are assumed to interact with destination cells to deliver information. This exosomal intracellular trafficking and communication takes place through coordination of several steps. First, exosome-cell surface binding is mediated by classical adhesion molecules (integrins and ICAMs) specific to cell-cell interactions. Several classical ligand/receptor pairs such as ICAM-I/lymphocyte function-associated-antigen-1 (LFA-1) are involved in exosome uptake by mature dendritic cells[390]; integrin CD49d and Tspan8 support exosome binding to endothelial cells[391]; and T cell immunoglobulin and mucin domain-containing protein-3 (TIM-3) help mature Th1 lymphocytes capture galectin-9-bearing exosomes[392]. In some situations, exosome binding to a recipient cell PM might be sufficient enough to initiate a signaling cascade. For example, MHC on the surface of APC-derived exosomes presents to antigen-specific T lymphocytes[393]. For most cases, exosomal contents must be delivered inside recipient cells. Internalization occurs via three main pathways: direct fusion[394],

receptor-mediated endocytosis[395], and micropinocytosis[396] (Figure 9B). Exosome-membrane fusion is more likely to occur at acidic endosome sites rather than at the neutral PM[388]. Capabilities for endocytosis or micropinocytosis depend on recipient cells which are typically non-phagocytic. In phagocytic macrophage, neutrophil and monocyte cells, exosomes are internalized via phagocytosis[397].

Once internalized, exosomal contents are then released into the cytoplasm directly or via backfusion with the endosomal membrane. A subsequent effect on the recipient cell may take place[398]. For instance, nucleic acid-induced gene expression modification in recipient cells can be instigated by exosome delivery. Released miRNA and exogenously modified siRNA molecules potentially inhibit mRNA translation and thus silence target genes, or the released mRNA can be translated into a protein using the recipient cell's cellular machinery. Both exosome cargo and functionality solely depend on their cell of origin. Exosome-based intercellular trafficking and communication is a dynamic system, so message modification is feasible and dependent on the physiological and pathological states of the producing cells[399].

1.3.4 Exosome as a natural vehicle for delivery of nucleic acid nanoparticles (NANPs)

In vivo delivery of NANPs remains a significant challenge that precludes their broader biomedical application. Various aforementioned carriers have been investigated and, because most of which are chemically fabricated, they suffer from issues related to immunogenicity, toxicity, rapid blood clearance, and poor biodistribution. Exosomes are natural EVs with endocytic origin, so they possess a multitude of advantages over synthetic materials. They are not immunogenic and not known to induce nonspecific innate immune responses such as activation of the complement system (CARPA)[400]. A benefit of "self-generated" exosomes is the absence of any immune attack against them while they remain in circulation. As a delivery vehicle, the structure of choice should be devoid of any immunologically stimulating activity that could bring forth an inflammatory response. Exosomes' ability to hide from the immune system comes

from an "inheritance" of parental cell surface molecules which protect them from recognition[401]. Such surface molecules, including CD46, CD55, CD59, and CK2, effectively escape detection[401]. Currently, numerous cell types have been exploited as exosome factories, with some seeing more frequent use than others. Human embryonic kidney variant HEK293T cells are one of the most popular sources, and their immunogenicity is well investigated. One study using these cells measured 23 different cytokines in vivo and in detectable ranges. The results revealed no differences in cytokine production between exosomes obtained from HEK293T cells and the phosphate-buffered saline (PBS) control. Therefore, exosomes obtained from HEK293T were concluded to be benign with regard to immune response[402]. As drug delivery systems, exosomes loaded with therapeutic cargoes must also undergo proper immunogenicity assessment. A follow-up study using the same HEK293T cell-derived exosomes loaded with miR-199a-3p, a compound having anti-invasion and anti-migration effects on hepatocellular carcinoma, confirmed slightly higher concentrations of several cytokines compared to free exosome levels, and comparison with PBS control indicated a very limited immuneresponse[403].

Immature DCs bear low levels of MHC II and costimulatory molecules which reduce immune activation by transforming T cells into T helper type 2 (Th2) and regulatory T cells (Treg) or by causing T cell apoptosis, thereby promoting a tolerogenic immune response[404]. Exosomes derived from tumor cells are a source of tumor MHC-I molecules, tetraspanins, HSP70-80, lysosomal-associated membrane protein 1 (LAMP1), tumor rejection antigens, and various immunosuppressive molecules. These molecules can inactivate T lymphocytes or natural killer cells or promote the differentiation of regulatory T lymphocytes to suppress immune response[405, 406]. Mesenchymal stem cell-derived exosomes lack MHC-I, MHC-II and costimulatory molecules such as CD80 and CD86, rendering them less susceptible to immune rejection and suitable for allogeneic therapeutics[407].

Although toxicity is a downside of synthetic formulations, no clear evidence of exosomal

cytotoxic effects exists. The spleen, as the largest lymphoid organ, plays an important role in the immune system, and it is considered a good indicator for initial immunotoxicity screening[310]. Data showed that splenocytes treated with HEK293T cell-derived exosomes loaded with miR-199a-3p had no effect on spleen cell composition, and neither did free exosomes[402]. Furthermore, no significant histopathological changes were reported in harvested spleen, heart, thymus, lung, liver, kidney, adrenal, ovary, uterus, or brain tissues ex vivo, indicating absence of observable organ toxicity. Haematological analysis showed little effect on RBC, WBC, platelet, neutrophil, lymphocyte, and monocyte counts, or on haematocrit and haemoglobin levels between the exosome- (free and loaded) treated group and the untreated control. With a total of 14 markers tested in blood chemistry, no significant difference was observed for all exosome-treated and control groups[402]. Some surface molecules present on exosomes eliminate cytotoxicity. For example, placenta-derived exosomes bear natural killer group 2 member D (NKG2D) ligands and induce down-regulation of the NKG2D receptor on cytotoxic effector cells, leading to reduction of their in vitro cytotoxicity[408]. From benchtop to bedside, exosomes consistently show negligible toxicity. The first exosome Phase I clinical trial used exosomes derived from autologous monocyte derived-DC cultures pulsed with melanoma antigen 3 (MAGE 3) peptides to vaccinate stage III/IV metastatic melanoma patients. Exosomes generated with functional MHC molecules promoted T-cell immune responses including tumor rejection. No grade II toxicity was observed, and no maximal tolerated dose was achieved, demonstrating the safety of exosome administration[409].

As drug carriers, exosomes, along with their behavior in vivo, must be properly understood. This includes detailed analysis of their clearance from systemic circulation. As mentioned earlier, cells of origin determine exosomes' contents, functionality and, consequently, their biological fate. However, exogenously administered exosomes might fail to reach their targets due to very brief half-lives. Recently, a pharmacokinetic profile of intravenously injected exosomes derived from murine melanoma cells showed circulation half-life of approximately 2 minutes with

only minimal retention at 4 hours post-injection. These exosomes were rapidly cleared from circulation by macrophages in the mononuclear phagocyte system (MPS) at a rate comparable to that of synthetic liposomes[395]. Additionally, it has been reported that exosomes derived from bone marrow-dendritic cells[410], splenocytes[411], and rat pancreatic adenocarcinoma[412], and delivered to mice via intravenous injection, ended up being engulfed by macrophages. To compensate for this problem, the exosome's membrane may be engineered using PEGylation to decrease hepatic clearance[413]. As naturally occurring carriers, exosomes have their own strategies to bypass the MPS. They contain transmembrane and membrane-anchored proteins that may enhance endocytosis and promote content delivery. CD47, a widely expressed integrin-associated transmembrane protein, serves as the ligand for signal regulatory protein α (SIRPα) which produces a signal to prevent attack by macrophages. Intranasally administered monocyte- and macrophage-derived exosomes, and intraperitoneally administered primary fibroblast-like mesenchymal cell-derived exosomes, display CD47 on their membranes to shield them from macrophage consumption, resulting in retarded clearance[414, 415].

Development of medications that act on the central nervous system to target neurodegenerative disorders and brain cancers is severely hampered by lack of an efficient drug delivery system to carry therapeutics to the brain. It is well known that only a very small portion (<1%) of injected antibodies enter the brain by passive diffusion, while the rest must be administered by peripheral injection or invasive intra-crania procedures[416]. Studies have shown that exosomes are capable of carrying small molecular drugs across the blood-brain barrier (BBB) with decreased MPS drug clearance[417-419]. Because of this unique ability, exosomes can outcompete most current delivery systems. An understanding of in vivo biodistribution following exosome administration provides a basis for dosage prediction, route of administration, and potential off-target effects. Also, it provides indications for specific therapeutic applications to target tissues. Due to their differing cells of origin, exosomes contain specific proteins on their surfaces that

mediate tissue tropism. For instance, Wnt4-associated exosomes derived from thymic epithelial cells accumulated in the thymus of mice[420]. Tumor-homing exosomes carrying therapeutic agents were employed as delivery vehicles. Hypoxic tumor-derived exosomes loaded with Olaparib increased apoptosis and retarded tumor growth in vivo[421]. Moreover, genetic modification of exosomal surface proteins was reported to increase target-specificity, such as rabies viral glycoprotein (RVG) for brain targeting and human epidermal growth factor receptor 2 (HER2) or TM domain of platelet-derived growth factor receptor (PDGFR) for cancer targeting[422-424].

Among the many diverse vehicle candidates for NANP delivery, both synthetic carriers and exosomes have a "finger in the pie". Synthetic carriers have the advantages of high yield and easy, large-scale manufacturing. Unfortunately, their toxicity, immunogenicity, biological instability, and lack of target specificity obstruct their broad application. These impediments can be overcome by using natural carriers such as exosomes that mediate cell-cell communication as an intrinsic function. Unlike the surface compositions of many other entities, exosomes possess well-defined proteins on their membranes that assist with target cell interactions and conceal them from the immune system. At the same time, exosomes' inherent messenger capabilities allow them to reach their target cells and fulfill their biological fate. As with other carriers, exosome surface engineering may yield greater performance. It is hypothesized that bioengineered surface molecules like arginylglycylaspartic acid (RGD) peptides or other targeting moieties may confer higher binding specificity and affinity when expressed on exosomal membranes as opposed to liposomes[425].

Several studies have been undertaken to examine delivery of a variety of nucleic acid-based payloads. One pioneering work found that use of immunogenicity-reducing DC-derived exosomes with neuron-specific RVG peptide modification successfully delivered exogenous siRNA to the brains of mice[426]. Although the major hurdle for RNAi-based therapeutics constitutes nucleic acid delivery across the cell's PM, exosomes derived from peripheral blood cells[427], HeLa and ascites[428],

aortic endothelial cells[429], and DCs[430] achieved success as gene delivery vectors (GDV) transporting exogenous siRNA into various target cells. Delivery of miRNAs, such as viral miRNA from Epstein-Barr virus (EVB)-infected cells to uninfected ones[431], let-7a miRNA to EGFR-expressing xenograft breast cancer tissue in Rag2−/− mice[432] and miR-335 from the T lymphocyte to APC[346], is possible with exosomes. RNA nucleic acid nanoparticles transferred by exosomes (e.g., 3WJ arrowtail RNA) contain siRNA against survivin and, upon successful delivery, enhance cancer suppression without endosomal trapping[433]. Recently, exosomes were investigated as vehicles for delivering functional NANPs of different shapes, sizes and compositions ranging from globular RNA cubes to planar RNA rings to linear RNA/DNA fibers to target cells with enhanced intracellular uptake, silencing efficiency and low immunostimulatory[135].

Exosomes epigenetically reprogram recipient cells via delivery of functional proteins, lipids, and nucleic acids. These features make exosomes feasible as delivery systems for therapeutic genetic materials including NANPs. In conclusion, exosomal transport mechanisms benefit from safety and efficacy, bioavailability, stability, membrane permeation capacity (including the blood-brain barrier), non-toxicity, low immunogenicity, and low off-target effects. Clearly, they have tremendous potential for further development in personalized medicine.

1.4   Dissertation summary

This dissertation aims to explore dynamic TNAs by programming multifunctional and controllable NANPs, advancing their safe and efficient delivery, and identifying immunostimulatory properties of novel NANP formulations.

Chapter two describes the use of rationally designed RNA–DNA fibers and polygons intended for intacellular use with well-defined immunostimulatory properties. The functional entities are split into two inactive RNA/DNA hybrids. Intracellular reassociation of the cognate hybrids triggers activation of multiple functionalities both in vitro and in vivo. The released siRNA targets mutated *BRAF* genes present in approximately 60% of melanomas with a high relapse rate

due to NF-κB activation. Released DNAs carrying NF-κB decoys hijack the NF-κB pathway to not only counteract the resistance mechanism in patients taking vemurafenib, but also to limit production of pro-inflammatory cytokines. These findings attest to the therapeutic potential of this multipronged approach.

Chapter three further explores RNA–DNA fibers' conjugation with anti-thrombin aptamers and resultant therapeutic potential as anticoagulants in their extracellular action. One key protein involved in the coagulation cascade is thrombin. Anti-thrombin aptamers are a novel class of anticoagulants. However, due to their low molecular weight, they undergo rapid excretion from the circulatory system. Self-assembled RNA–DNA fibers contain sequences of anti-thrombin aptamers formed at strand terminals. Plasma coagulation assays performed on both American and Brazilian blood donor samples show prolonged coagulation times. The anticoagulation abilities of anti-thrombin aptamers can be reversed by kill-switch fibers, and the released short dsRNA and dsDNA result in rapid excretion from the system. Additionally, immunostimutory effects and biodistributions of anti-thrombin fibers are assessed.

Chapter four discusses naturally secreted extracellular vesicle-exosomes as vehicles for the delivery of linear RNA–DNA fibers, planar RNA rings and globular RNA cubes in vitro. Exosomes are proven to successfully deliver NANPs with various dimensions and connectivities while keeping functionality intact. Following uptake, a nuclease protection assay is performed to confirm NANPs are present inside the exosomes rather than attached to the exosomes' surfaces. RNA–DNA fibers, RNA rings and RNA cubes carry DS RNAs against GFP genes, effectively downregulating GFP expression. These NANPs also display limited immunostimutory effects, a precondition for in vivo studies.

Chapter five briefly summarizes major findings regarding the implementation of RNA–DNA fibers as TNAs, as well as the use of exosomes as natural carriers for delivery of NANPs. Evidence from experimental results supports the safety and effectiveness of NANPs as applications

in nanomedicine.

1.5   References

1.	Forster, P.; Forster, L.; Renfrew, C.; Forster, M., Phylogenetic network analysis of SARS-CoV-2 genomes. *Proc Natl Acad Sci U S A* **2020,** *117* (17), 9241-9243.
2.	Valenzuela, P., Hepatitis A, B, C, D and E viruses: structure of their genomes and general properties. *Gastroenterol Jpn* **1990,** *25 Suppl 2*, 62-71.
3.	TA., B., Chapter 1, The Human Genome. *Genomes. 2nd edition* **2002**.
4.	Litwack, G., Chapter 10 - Nucleic Acids and Molecular Genetics. In *Human Biochemistry*, Litwack, G., Ed. Academic Press: Boston, 2018; pp 257-317.
5.	Griffiths AJF, M. J., Suzuki DT, et al, Transcription and RNA polymerase. *An Introduction to Genetic Analysis. 7th edition.* **2000**.
6.	Walter, N. G.; Engelke, D. R., Ribozymes: catalytic RNAs that cut things, make things, and do odd and useful jobs. *Biologist (London)* **2002,** *49* (5), 199-203.
7.	Hawkins, P. G.; Morris, K. V., RNA and transcriptional modulation of gene expression. *Cell Cycle* **2008,** *7* (5), 602-607.
8.	Edwards, A. L. B., R. T., Riboswitches: A Common RNA Regulatory Element. *Nature Education* **2010,** *3(9):9*.
9.	Marcel, E. D.; Timothy, R. M.; John, S. M., RNAs as extracellular signaling molecules. *Journal of Molecular Endocrinology* **2008,** *40* (4), 151-159.
10.	Castanotto, D.; Rossi, J. J., The promises and pitfalls of RNA-interference-based therapeutics. *Nature* **2009,** *457* (7228), 426-433.
11.	Lodish H, B. A., Zipursky SL, et al., Structure of Nucleic Acids. *Molecular Cell Biology. 4th edition* **2000**.
12.	P., S., Interactions That Hold DNA Together. *Life sciences medical news*.
13.	Svoboda, P.; Cara, A. D., Hairpin RNA: a secondary structure of primary importance. *Cellular and Molecular Life Sciences CMLS* **2006,** *63* (7), 901-908.
14.	Nikolova, E. N.; Kim, E.; Wise, A. A.; O'Brien, P. J.; Andricioaei, I.; Al-Hashimi, H. M., Transient Hoogsteen base pairs in canonical duplex DNA. *Nature* **2011,** *470* (7335), 498-502.
15.	Halman, J. R. Immunostimulatory Properties of Nucleic Acid Nanoparticles. Ph.D., The University of North Carolina at Charlotte, Ann Arbor, 2020.
16.	Sinden, R. R., *DNA structure and function*. Elsevier: 2012.
17.	Rich, A.; Nordheim, A.; Wang, A. H. J., The Chemistry and Biology of Left-Handed Z-DNA. **1984,** *53* (1), 791-846.
18.	Huang, M.; Giese, T. J.; Lee, T.-S.; York, D. M., Improvement of DNA and RNA Sugar Pucker Profiles from Semiempirical Quantum Methods. **2014,** *10* (4), 1538-1545.
19.	Berg JM, T. J., Stryer L., DNA Can Assume a Variety of Structural Forms. *Biochemistry. 5th edition.* **2002,** *Section 27.1* (New York: W H Freeman).
20.	Saenger, W., *Principles of nucleic acid structure*. Springer Science & Business Media: 2013.
21.	Leulliot, N.; Varani, G., Current topics in RNA− protein recognition: Control of specificity and biological function through induced fit and conformational capture. *Biochemistry* **2001,** *40* (27), 7947-7956.
22.	Torres, R. A.; Bruice, T. C., The mechanism of phosphodiester hydrolysis: near in-line attack conformations in the hammerhead ribozyme. *Journal of the American Chemical Society* **2000,** *122* (5), 781-791.
23.	Zhang, N.; Zhang, S.; Szostak, J. W., Activated ribonucleotides undergo a sugar pucker switch upon binding to a single-stranded RNA template. *Journal of the American Chemical Society* **2012,** *134* (8), 3691-3694.

24.   Li, J.; Liu, C., Coding or Noncoding, the Converging Concepts of RNAs. *Front Genet* **2019,** *10*, 496-496.

25.   Hull, R., Chapter 8 - Origins and Evolution of Plant Viruses. In *Plant Virology (Fifth Edition)*, Hull, R., Ed. Academic Press: Boston, 2014; pp 423-476.

26.   Srijyothi, L.; Ponne, S.; Prathama, T.; Ashok, C.; Baluchamy, S., Roles of Non-Coding RNAs in Transcriptional Regulation. InTech: 2018.

27.   Lewis, B. P.; Burge, C. B.; Bartel, D. P., Conserved seed pairing, often flanked by adenosines, indicates that thousands of human genes are microRNA targets. *cell* **2005,** *120* (1), 15-20.

28.   Esteller, M., Non-coding RNAs in human disease. *Nature reviews genetics* **2011,** *12* (12), 861-874.

29.   Sun, W.; Julie Li, Y.-S.; Huang, H.-D.; Shyy, J. Y.; Chien, S., microRNA: a master regulator of cellular processes for bioengineering systems. *Annual review of biomedical engineering* **2010,** *12*, 1-27.

30.   Lisowiec-Wąchnicka, J.; Bartyś, N.; Pasternak, A., A systematic study on the influence of thermodynamic asymmetry of 5′ -ends of siRNA duplexes in relation to their silencing potency. *Scientific Reports* **2019,** *9* (1), 2477.

31.   Lam, J. K.; Chow, M. Y.; Zhang, Y.; Leung, S. W., siRNA versus miRNA as therapeutics for gene silencing. *Molecular Therapy-Nucleic Acids* **2015,** *4*, e252.

32.   Bartel, D. P., MicroRNAs: target recognition and regulatory functions. *Cell* **2009,** *136* (2), 215-33.

33.   Lam, J. K. W.; Chow, M. Y. T.; Zhang, Y.; Leung, S. W. S., siRNA Versus miRNA as Therapeutics for Gene Silencing. *Mol Ther Nucleic Acids* **2015,** *4* (9), e252-e252.

34.   Adams, D.; Gonzalez-Duarte, A.; O'Riordan, W. D.; Yang, C.-C.; Ueda, M.; Kristen, A. V.; Tournev, I.; Schmidt, H. H.; Coelho, T.; Berk, J. L., Patisiran, an RNAi therapeutic, for hereditary transthyretin amyloidosis. *New England Journal of Medicine* **2018,** *379* (1), 11-21.

35.   Agarwal, S.; Habtemarium, B.; Goel, V.; Attarwala, H.; Melch, M.; Jiang, X.; Simon, A.; Robbie, G. In *PHARMACOKINETICS AND PHARMACODYNAMICS OF GIVOSIRAN, AN INVESTIGATIONAL RNAI THERAPEUTIC FOR ACUTE INTERMITTENT PORPHYRIA*, CLINICAL PHARMACOLOGY & THERAPEUTICS, WILEY 111 RIVER ST, HOBOKEN 07030-5774, NJ USA: 2019; pp S34-S34.

36.   Seto, A. G.; Kingston, R. E.; Lau, N. C., The coming of age for Piwi proteins. *Mol Cell* **2007,** *26* (5), 603-9.

37.   Molecular Biology Select. *Cell* **2006,** *126* (2), 223-225.

38.   Kelleher, E. S., Reexamining the P-Element Invasion of Drosophila melanogaster Through the Lens of piRNA Silencing. *Genetics* **2016,** *203* (4), 1513-31.

39.   Perkel, J. M., Visiting "noncodarnia". *Biotechniques* **2013,** *54* (6), 301, 303-4.

40.   Derrien, T.; Johnson, R.; Bussotti, G.; Tanzer, A.; Djebali, S.; Tilgner, H.; Guernec, G.; Martin, D.; Merkel, A.; Knowles, D. G., The GENCODE v7 catalog of human long noncoding RNAs: analysis of their gene structure, evolution, and expression. *Genome research* **2012,** *22* (9), 1775-1789.

41.   Cabili, M. N.; Trapnell, C.; Goff, L.; Koziol, M.; Tazon-Vega, B.; Regev, A.; Rinn, J. L., Integrative annotation of human large intergenic noncoding RNAs reveals global properties and specific subclasses. *Genes & development* **2011,** *25* (18), 1915-1927.

42.   Spitz, F.; Furlong, E. E. M., Transcription factors: from enhancer binding to developmental control. *Nature Reviews Genetics* **2012,** *13* (9), 613-626.

43.   Loudu Srijyothi, S. P., Talukdar Prathama, Cheemala Ashok and Sudhakar Baluchamy, Roles of Non-Coding RNAs in Transcriptional Regulation. **2018**.

44.   Salmena, L.; Poliseno, L.; Tay, Y.; Kats, L.; Pandolfi, P. P., A ceRNA hypothesis: the Rosetta Stone of a hidden RNA language? *Cell* **2011,** *146* (3), 353-358.

45.	Gong, C.; Maquat, L. E., lncRNAs transactivate STAU1-mediated mRNA decay by duplexing with 3′ UTRs via Alu elements. *Nature* **2011,** *470* (7333), 284-288.

46.	Tsai, M.-C.; Manor, O.; Wan, Y.; Mosammaparast, N.; Wang, J. K.; Lan, F.; Shi, Y.; Segal, E.; Chang, H. Y., Long noncoding RNA as modular scaffold of histone modification complexes. *Science* **2010,** *329* (5992), 689-693.

47.	Poltronieri, P.; Sun, B.; Mallardo, M., RNA Viruses: RNA Roles in Pathogenesis, Coreplication and Viral Load. *Curr Genomics* **2015,** *16* (5), 327-335.

48.	Panigaj, M.; Johnson, M. B.; Ke, W.; McMillan, J.; Goncharova, E. A.; Chandler, M.; Afonin, K. A., Aptamers as Modular Components of Therapeutic Nucleic Acid Nanotechnology. *ACS Nano* **2019,** *13* (11), 12301-12321.

49.	Halman, J. R.; Afonin, K. A., Editorial for the Special Issue on "Nucleic Acid Architectures for Therapeutics, Diagnostics, Devices and Materials". *Nanomaterials (Basel)* **2019,** *9* (7), 951.

50.	Ivashkiv, L. B.; Donlin, L. T., Regulation of type I interferon responses. *Nat Rev Immunol* **2014,** *14* (1), 36-49.

51.	Zhang, J. M.; An, J., Cytokines, inflammation, and pain. *Int Anesthesiol Clin* **2007,** *45* (2), 27-37.

52.	Majer, O.; Liu, B.; Barton, G. M., Nucleic acid-sensing TLRs: trafficking and regulation. *Curr Opin Immunol* **2017,** *44*, 26-33.

53.	Heil, F.; Hemmi, H.; Hochrein, H.; Ampenberger, F.; Kirschning, C.; Akira, S.; Lipford, G.; Wagner, H.; Bauer, S., Species-specific recognition of single-stranded RNA via toll-like receptor 7 and 8. *Science* **2004,** *303* (5663), 1526-1529.

54.	Cervantes, J. L.; Weinerman, B.; Basole, C.; Salazar, J. C., TLR8: the forgotten relative revindicated. *Cellular & Molecular Immunology* **2012,** *9* (6), 434-438.

55.	Liu, L.; Botos, I.; Wang, Y.; Leonard, J. N.; Shiloach, J.; Segal, D. M.; Davies, D. R., Structural basis of toll-like receptor 3 signaling with double-stranded RNA. *Science* **2008,** *320* (5874), 379-381.

56.	Chandler, M.; Johnson, M. B.; Panigaj, M.; Afonin, K. A., Innate immune responses triggered by nucleic acids inspire the design of immunomodulatory nucleic acid nanoparticles (NANPs). *Curr Opin Biotechnol* **2020,** *63*, 8-15.

57.	Leonard, J. N.; Ghirlando, R.; Askins, J.; Bell, J. K.; Margulies, D. H.; Davies, D. R.; Segal, D. M., The TLR3 signaling complex forms by cooperative receptor dimerization. *Proceedings of the National Academy of Sciences of the United States of America* **2008,** *105* (1), 258-263.

58.	Zhang, Z.; Ohto, U.; Shibata, T.; Taoka, M.; Yamauchi, Y.; Sato, R.; Shukla, N. M.; David, S. A.; Isobe, T.; Miyake, K.; Shimizu, T., Structural Analyses of Toll-like Receptor 7 Reveal Detailed RNA Sequence Specificity and Recognition Mechanism of Agonistic Ligands. *Cell Rep* **2018,** *25* (12), 3371-3381.e5.

59.	Hu, T.; Suter, S. R.; Mumbleau, M. M.; Beal, P. A., TLR8 activation and inhibition by guanosine analogs in RNA: Importance of functional groups and chain length. *Bioorg Med Chem* **2018,** *26* (1), 77-83.

60.	Gorden, K. B.; Gorski, K. S.; Gibson, S. J.; Kedl, R. M.; Kieper, W. C.; Qiu, X.; Tomai, M. A.; Alkan, S. S.; Vasilakos, J. P., Synthetic TLR agonists reveal functional differences between human TLR7 and TLR8. *The Journal of Immunology* **2005,** *174* (3), 1259-1268.

61.	Bekeredjian-Ding, I. B.; Wagner, M.; Hornung, V.; Giese, T.; Schnurr, M.; Endres, S.; Hartmann, G., Plasmacytoid Dendritic Cells Control TLR7 Sensitivity of Naive B Cells via Type I IFN. *The Journal of Immunology* **2005,** *174* (7), 4043-4050.

62.	Pichlmair, A.; Schulz, O.; Tan, C. P.; Rehwinkel, J.; Kato, H.; Takeuchi, O.; Akira, S.; Way, M.; Schiavo, G.; Reis e Sousa, C., Activation of MDA5 requires higher-order RNA structures generated during virus infection. *J Virol* **2009,** *83* (20), 10761-9.

63.   Kell, A. M.; Gale, M., Jr., RIG-I in RNA virus recognition. *Virology* **2015,** *479-480*, 110-21.

64.   Elkon, K. B., Review: Cell Death, Nucleic Acids, and Immunity. *Arthritis & Rheumatology* **2018,** *70* (6), 805-816.

65.   Satoh, T.; Kato, H.; Kumagai, Y.; Yoneyama, M.; Sato, S.; Matsushita, K.; Tsujimura, T.; Fujita, T.; Akira, S.; Takeuchi, O., LGP2 is a positive regulator of RIG-I- and MDA5-mediated antiviral responses. *Proceedings of the National Academy of Sciences* **2010,** *107* (4), 1512-1517.

66.   Komuro, A.; Bamming, D.; Horvath, C. M., Negative regulation of cytoplasmic RNA-mediated antiviral signaling. *Cytokine* **2008,** *43* (3), 350-358.

67.   Kell, A. M.; Gale, M., RIG-I in RNA virus recognition. *Virology* **2015,** *479-480*, 110-121.

68.   Xia, P.; Wang, S.; Gao, P.; Gao, G.; Fan, Z., DNA sensor cGAS-mediated immune recognition. *Protein & Cell* **2016,** *7* (11), 777-791.

69.   Dempsey, A.; Bowie, A. G., Innate immune recognition of DNA: A recent history. *Virology* **2015,** *479-480*, 146-152.

70.   Yang, Y.; Jiang, G.; Zhang, P.; Fan, J., Programmed cell death and its role in inflammation. *Mil Med Res* **2015,** *2*, 12-12.

71.   Seeman, N. C., Nucleic acid junctions and lattices. *Journal of theoretical biology* **1982,** *99* (2), 237-247.

72.   Shu, D.; Moll, W.-D.; Deng, Z.; Mao, C.; Guo, P., Bottom-up Assembly of RNA Arrays and Superstructures as Potential Parts in Nanotechnology. *Nano Letters* **2004,** *4* (9), 1717-1723.

73.   Pelesko, J. A., *Self assembly: the science of things that put themselves together*. CRC Press: 2007.

74.   Seeman, N. C., Nanotechnology and the double helix. *Sci Am* **2004,** *290* (6), 64-9, 72-5.

75.   Seeman, N. C., Nanomaterials Based on DNA. *Annual Review of Biochemistry* **2010,** *79* (1), 65-87.

76.   Arora, A. A.; de Silva, C., Beyond the smiley face: applications of structural DNA nanotechnology. *Nano Reviews & Experiments* **2018,** *9* (1), 1430976.

77.   Cohen, S. N.; Chang, A. C.; Boyer, H. W.; Helling, R. B., Construction of biologically functional bacterial plasmids in vitro. *Proc Natl Acad Sci U S A* **1973,** *70* (11), 3240-3244.

78.   Seeman, N. C., Nanomaterials based on DNA. *Annu Rev Biochem* **2010,** *79*, 65-87.

79.   Constantinou, P. E.; Wang, T.; Kopatsch, J.; Israel, L. B.; Zhang, X.; Ding, B.; Sherman, W. B.; Wang, X.; Zheng, J.; Sha, R.; Seeman, N. C., Double cohesion in structural DNA nanotechnology. *Organic & biomolecular chemistry* **2006,** *4* (18), 3414-3419.

80.   Mao, C.; Sun, W.; Seeman, N. C., Designed Two-Dimensional DNA Holliday Junction Arrays Visualized by Atomic Force Microscopy. *Journal of the American Chemical Society* **1999,** *121* (23), 5437-5443.

81.   Liu, F.; Sha, R.; Seeman, N. C., Modifying the Surface Features of Two-Dimensional DNA Crystals. *Journal of the American Chemical Society* **1999,** *121* (5), 917-922.

82.   LaBean, T. H.; Yan, H.; Kopatsch, J.; Liu, F.; Winfree, E.; Reif, J. H.; Seeman, N. C., Construction, analysis, ligation, and self-assembly of DNA triple crossover complexes. *Journal of the American Chemical Society* **2000,** *122* (9), 1848-1860.

83.   Yan, H.; Park, S. H.; Finkelstein, G.; Reif, J. H.; LaBean, T. H., DNA-templated self-assembly of protein arrays and highly conductive nanowires. *Science* **2003,** *301* (5641), 1882-4.

84.   Hunter, P., Nucleic acid-based nanotechnology: The ability of DNA and RNA to fold into precise and complex shapes can be exploited for applications both in biology and electronics. *EMBO Rep* **2018,** *19* (1), 13-17.

85.   Rothemund, P. W. K., Folding DNA to create nanoscale shapes and patterns. *Nature* **2006,** *440* (7082), 297-302.

86.   Tadakuma, H.; Masubuchi, T.; Ueda, T., Chapter Five - RNA Study Using DNA Nanotechnology. In *Progress in Molecular Biology and Translational Science*, Yoshizawa, S., Ed. Academic Press: 2016; Vol. 139, pp 121-163.

87.   Dietz, H.; Douglas, S. M.; Shih, W. M., Folding DNA into twisted and curved nanoscale shapes. *Science* **2009,** *325* (5941), 725-730.

88.   Han, D.; Pal, S.; Nangreave, J.; Deng, Z.; Liu, Y.; Yan, H., DNA origami with complex curvatures in three-dimensional space. *Science* **2011,** *332* (6027), 342-346.

89.   Gerling, T.; Wagenbauer, K. F.; Neuner, A. M.; Dietz, H., Dynamic DNA devices and assemblies formed by shape-complementary, non–base pairing 3D components. *Science* **2015,** *347* (6229), 1446-1452.

90.   Seeman, N. C., Nucleic acid junctions and lattices. *J Theor Biol* **1982,** *99* (2), 237-47.

91.   Hsieh P., P. I. G., DNA Branch Migration. *Nucleic Acids and Molecular Biology* **1995,** *9*.

92.   Reif, J. H., The design of autonomous DNA nano-mechanical devices: Walking and rolling DNA. *Natural Computing* **2003,** *2* (4), 439-461.

93.   Pan, J.; Li, F.; Cha, T. G.; Chen, H.; Choi, J. H., Recent progress on DNA based walkers. *Curr Opin Biotechnol* **2015,** *34*, 56-64.

94.   He, Y.; Liu, D. R., Autonomous multistep organic synthesis in a single isothermal solution mediated by a DNA walker. *Nature Nanotechnology* **2010,** *5* (11), 778-782.

95.   Lund, K.; Manzo, A. J.; Dabby, N.; Michelotti, N.; Johnson-Buck, A.; Nangreave, J.; Taylor, S.; Pei, R.; Stojanovic, M. N.; Walter, N. G.; Winfree, E.; Yan, H., Molecular robots guided by prescriptive landscapes. *Nature* **2010,** *465* (7295), 206-210.

96.   Xiong, E.; Zhen, D.; Jiang, L.; Zhou, X., Binding-Induced 3D-Bipedal DNA Walker for Cascade Signal Amplification Detection of Thrombin Combined with Catalytic Hairpin Assembly Strategy. *Analytical Chemistry* **2019,** *91* (23), 15317-15324.

97.   Mason, S. D.; Tang, Y.; Li, Y.; Xie, X.; Li, F., Emerging bioanalytical applications of DNA walkers. *TrAC Trends in Analytical Chemistry* **2018,** *107*, 212-221.

98.   Li, J.; Johnson-Buck, A.; Yang, Y. R.; Shih, W. M.; Yan, H.; Walter, N. G., Exploring the speed limit of toehold exchange with a cartwheeling DNA acrobat. *Nature Nanotechnology* **2018,** *13* (8), 723-729.

99.   You, M.; Chen, Y.; Zhang, X.; Liu, H.; Wang, R.; Wang, K.; Williams, K. R.; Tan, W., An autonomous and controllable light-driven DNA walking device. *Angew Chem Int Ed Engl* **2012,** *51* (10), 2457-60.

100.   Zhang, D. Y.; Seelig, G., Dynamic DNA nanotechnology using strand-displacement reactions. *Nat Chem* **2011,** *3* (2), 103-13.

101.   Zhang, D. Y.; Winfree, E., Control of DNA Strand Displacement Kinetics Using Toehold Exchange. *Journal of the American Chemical Society* **2009,** *131* (47), 17303-17314.

102.   Yin, P.; Choi, H. M. T.; Calvert, C. R.; Pierce, N. A., Programming biomolecular self-assembly pathways. *Nature* **2008,** *451* (7176), 318-322.

103.   Seelig, G.; Soloveichik, D.; Zhang, D. Y.; Winfree, E., Enzyme-Free Nucleic Acid Logic Circuits. *Science* **2006,** *314*, 1585 - 1588.

104.   Wang, H.; Di Gate, R. J.; Seeman, N. C., An RNA topoisomerase. **1996,** *93* (18), 9477-9482.

105.   Westhof, E.; Masquida, B.; Jaeger, L., RNA tectonics: towards RNA design. *Folding and Design* **1996,** *1* (4), R78-R88.

106.   Helmling, S.; Moyroud, E.; Schroeder, W.; Roehl, I.; Kleinjung, F.; Stark, S.; Bahrenberg, G.; Gillen, C.; Klussmann, S.; Vonhoff, S., A new class of Spiegelmers containing 2'-fluoro-nucleotides. *Nucleosides Nucleotides Nucleic Acids* **2003,** *22* (5-8), 1035-8.

107.   Boulmé, F.; Freund, F.; Moreau, S.; Nielsen, P. E.; Gryaznov, S.; Toulmé, J. J.; Litvak, S., Modified (PNA, 2'-O-methyl and phosphoramidate) anti-TAR antisense

oligonucleotides as strong and specific inhibitors of in vitro HIV-1 reverse transcription. *Nucleic acids research* **1998,** *26* (23), 5492-5500.

108.   Shaw, B. R.; Moussa, L.; Sharaf, M.; Cheek, M.; Dobrikov, M., Boranophosphate siRNA-aptamer chimeras for tumor-specific downregulation of cancer receptors and modulators. *Nucleic Acids Symp Ser (Oxf)* **2008,** (52), 655-6.

109.   Chawla, M.; Oliva, R.; Bujnicki, J. M.; Cavallo, L., An atlas of RNA base pairs involving modified nucleobases with optimal geometries and accurate energies. *Nucleic acids research* **2015,** *43* (14), 6714-6729.

110.   Leontis, N. B.; Westhof, E., Geometric nomenclature and classification of RNA base pairs. *Rna* **2001,** *7* (4), 499-512.

111.   Kebbekus, P.; Draper, D. E.; Hagerman, P., Persistence length of RNA. *Biochemistry* **1995,** *34* (13), 4354-4357.

112.   Sweeney, B. A.; Roy, P.; Leontis, N. B., An introduction to recurrent nucleotide interactions in RNA. *Wiley Interdisciplinary Reviews: RNA* **2015,** *6* (1), 17-45.

113.   Abu Almakarem, A. S.; Petrov, A. I.; Stombaugh, J.; Zirbel, C. L.; Leontis, N. B., Comprehensive survey and geometric classification of base triples in RNA structures. *Nucleic acids research* **2012,** *40* (4), 1407-1423.

114.   Weizmann, Y.; Andersen, E. S., RNA nanotechnology--The knots and folds of RNA nanoparticle engineering. *Mrs Bulletin* **2017,** *42* (12), 930.

115.   Jaeger, L.; Leontis, N. B., Tecto‐RNA: one‐dimensional self‐assembly through tertiary interactions. *Angewandte Chemie International Edition* **2000,** *39* (14), 2521-2524.

116.   Jaeger, L., TectoRNA: modular assembly units for the construction of RNA nano-objects. *Nucleic Acids Research* **2001,** *29* (2), 455-463.

117.   Afonin, K. A.; Grabow, W. W.; Walker, F. M.; Bindewald, E.; Dobrovolskaia, M. A.; Shapiro, B. A.; Jaeger, L., Design and self-assembly of siRNA-functionalized RNA nanoparticles for use in automated nanomedicine. *Nature protocols* **2011,** *6* (12), 2022.

118.   Shu, Y.; Haque, F.; Shu, D.; Li, W.; Zhu, Z.; Kotb, M.; Lyubchenko, Y.; Guo, P., Fabrication of 14 different RNA nanoparticles for specific tumor targeting without accumulation in normal organs. *RNA (New York, N.Y.)* **2013,** *19* (6), 767-777.

119.   Li, H.; Rychahou, P. G.; Cui, Z.; Pi, F.; Evers, B. M.; Shu, D.; Guo, P.; Luo, W., RNA Nanoparticles Derived from Three-Way Junction of Phi29 Motor pRNA Are Resistant to I-125 and Cs-131 Radiation. *Nucleic Acid Ther* **2015,** *25* (4), 188-197.

120.   Jasinski, D. L.; Khisamutdinov, E. F.; Lyubchenko, Y. L.; Guo, P., Physicochemically tunable polyfunctionalized RNA square architecture with fluorogenic and ribozymatic properties. *ACS Nano* **2014,** *8* (8), 7620-7629.

121.   Ohno, H.; Kobayashi, T.; Kabata, R.; Endo, K.; Iwasa, T.; Yoshimura, S. H.; Takeyasu, K.; Inoue, T.; Saito, H., Synthetic RNA–protein complex shaped like an equilateral triangle. *Nature Nanotechnology* **2011,** *6* (2), 116-120.

122.   Zadeh, J. N.; Steenberg, C. D.; Bois, J. S.; Wolfe, B. R.; Pierce, M. B.; Khan, A. R.; Dirks, R. M.; Pierce, N. A., NUPACK: Analysis and design of nucleic acid systems. *Journal of computational chemistry* **2011,** *32* (1), 170-173.

123.   Taneda, A., MODENA: a multi-objective RNA inverse folding. *Adv Appl Bioinform Chem* **2011,** *4*, 1-12.

124.   Esmaili-Taheri, A.; Ganjtabesh, M., ERD: a fast and reliable tool for RNA design including constraints. *BMC Bioinformatics* **2015,** *16*, 20-20.

125.   Jain, S.; Laederach, A.; Ramos, S. B. V.; Schlick, T., A pipeline for computational design of novel RNA-like topologies. *Nucleic Acids Research* **2018,** *46* (14), 7040-7051.

126.   Zadeh, J. N.; Steenberg, C. D.; Bois, J. S.; Wolfe, B. R.; Pierce, M. B.; Khan, A. R.; Dirks, R. M.; Pierce, N. A., NUPACK: Analysis and design of nucleic acid systems. *J Comput Chem* **2011,** *32* (1), 170-3.

127.   Bellaousov, S.; Kayedkhordeh, M.; Peterson, R. J.; Mathews, D. H., Accelerated RNA secondary structure design using preselected sequences for helices and loops. *RNA (New York, N.Y.)* **2018,** *24* (11), 1555-1567.

128.   Chandler, M.; Lyalina, T.; Halman, J.; Rackley, L.; Lee, L.; Dang, D.; Ke, W.; Sajja, S.; Woods, S.; Acharya, S.; Baumgarten, E.; Christopher, J.; Elshalia, E.; Hrebien, G.; Kublank, K.; Saleh, S.; Stallings, B.; Tafere, M.; Striplin, C.; Afonin, K. A., Broccoli Fluorets: Split Aptamers as a User-Friendly Fluorescent Toolkit for Dynamic RNA Nanotechnology. *Molecules* **2018,** *23* (12).

129.   Geary, C.; Rothemund, P. W. K.; Andersen, E. S., A single-stranded architecture for cotranscriptional folding of RNA nanostructures. *Science* **2014,** *345* (6198), 799-804.

130.   Afonin, K. A.; Desai, R.; Viard, M.; Kireeva, M. L.; Bindewald, E.; Case, C. L.; Maciag, A. E.; Kasprzak, W. K.; Kim, T.; Sappe, A.; Stepler, M.; Kewalramani, V. N.; Kashlev, M.; Blumenthal, R.; Shapiro, B. A., Co-transcriptional production of RNA-DNA hybrids for simultaneous release of multiple split functionalities. *Nucleic acids research* **2014,** *42* (3), 2085-2097.

131.   Oliver, R. C.; Rolband, L. A.; Hutchinson-Lundy, A. M.; Afonin, K. A.; Krueger, J. K., Small-Angle Scattering as a Structural Probe for Nucleic Acid Nanoparticles (NANPs) in a Dynamic Solution Environment. *Nanomaterials (Basel)* **2019,** *9* (5).

132.   Afonin, K. A.; Grabow, W. W.; Walker, F. M.; Bindewald, E.; Dobrovolskaia, M. A.; Shapiro, B. A.; Jaeger, L., Design and self-assembly of siRNA-functionalized RNA nanoparticles for use in automated nanomedicine. *Nature Protocols* **2011,** *6* (12), 2022-2034.

133.   Bald, I.; Keller, A., Molecular Processes Studied at a Single-Molecule Level Using DNA Origami Nanostructures and Atomic Force Microscopy. **2014,** *19* (9), 13803-13823.

134.   Johnson, M. B.; Halman, J. R.; Miller, D. K.; Cooper, J. S.; Khisamutdinov, Emil F.; Marriott, I.; Afonin, K. A., The immunorecognition, subcellular compartmentalization, and physicochemical properties of nucleic acid nanoparticles can be controlled by composition modification. *Nucleic Acids Research* **2020**.

135.   Nordmeier, S.; Ke, W.; Afonin, K. A.; Portnoy, V., Exosome mediated delivery of functional nucleic acid nanoparticles (NANPs). *Nanomedicine: Nanotechnology, Biology and Medicine* **2020,** *30*, 102285.

136.   Juneja, R.; Vadarevu, H.; Halman, J.; Tarannum, M.; Rackley, L.; Dobbs, J.; Marquez, J.; Chandler, M.; Afonin, K.; Vivero-Escoto, J. L., Combination of Nucleic Acid and Mesoporous Silica Nanoparticles: Optimization and Therapeutic Performance In Vitro. *ACS Applied Materials & Interfaces* **2020,** *12* (35), 38873-38886.

137.   Halman, J. R.; Kim, K.-T.; Gwak, S.-J.; Pace, R.; Johnson, M. B.; Chandler, M. R.; Rackley, L.; Viard, M.; Marriott, I.; Lee, J. S.; Afonin, K. A., A cationic amphiphilic co-polymer as a carrier of nucleic acid nanoparticles (Nanps) for controlled gene silencing, immunostimulation, and biodistribution. *Nanomedicine: Nanotechnology, Biology and Medicine* **2020,** *23*, 102094.

138.   Hong, E.; Halman, J. R.; Shah, A.; Cedrone, E.; Truong, N.; Afonin, K. A.; Dobrovolskaia, M. A., Toll-like receptor-mediated recognition of nucleic acid nanoparticles (NANPs) in human primary blood cells. *Molecules* **2019,** *24* (6), 1094.

139.   Ke, W.; Hong, E.; Saito, R. F.; Rangel, M. C.; Wang, J.; Viard, M.; Richardson, M.; Khisamutdinov, E. F.; Panigaj, M.; Dokholyan, N. V.; Chammas, R.; Dobrovolskaia, M. A.; Afonin, K. A., RNA–DNA fibers and polygons with controlled immunorecognition activate RNAi, FRET and transcriptional regulation of NF-κB in human cells. *Nucleic Acids Research* **2018,** *47* (3), 1350-1361.

140.   Rackley, L.; Stewart, J. M.; Salotti, J.; Krokhotin, A.; Shah, A.; Halman, J. R.; Juneja, R.; Smollett, J.; Lee, L.; Roark, K.; Viard, M.; Tarannum, M.; Vivero-Escoto, J.; Johnson, P. F.; Dobrovolskaia, M. A.; Dokholyan, N. V.; Franco, E.; Afonin, K. A., RNA

Fibers as Optimized Nanoscaffolds for siRNA Coordination and Reduced Immunological Recognition. *Advanced Functional Materials* **2018,** *28* (48), 1805959.

141.   Hong, E.; Halman, J. R.; Shah, A. B.; Khisamutdinov, E. F.; Dobrovolskaia, M. A.; Afonin, K. A., Structure and Composition Define Immunorecognition of Nucleic Acid Nanoparticles. *Nano Letters* **2018,** *18* (7), 4309-4321.

142.   Sajja, S.; Chandler, M.; Fedorov, D.; Kasprzak, W. K.; Lushnikov, A.; Viard, M.; Shah, A.; Dang, D.; Dahl, J.; Worku, B.; Dobrovolskaia, M. A.; Krasnoslobodtsev, A.; Shapiro, B. A.; Afonin, K. A., Dynamic Behavior of RNA Nanoparticles Analyzed by AFM on a Mica/Air Interface. *Langmuir* **2018,** *34* (49), 15099-15108.

143.   Halman, J. R.; Satterwhite, E.; Roark, B.; Chandler, M.; Viard, M.; Ivanina, A.; Bindewald, E.; Kasprzak, W. K.; Panigaj, M.; Bui, M. N., Functionally-interdependent shape-switching nanoparticles with controllable properties. *Nucleic acids research* **2017,** *45* (4), 2210-2220.

144.   Berbel Manaia, E.; Paiva Abuçafy, M.; Chiari-Andréo, B. G.; Lallo Silva, B.; Oshiro-Júnior, J. A.; Chiavacci, L., Physicochemical characterization of drug nanocarriers. *International Journal of Nanomedicine* **2017,** *Volume 12*, 4991-5011.

145.   Svergun, D. I.; Koch, M. H. J., Small-angle scattering studies of biological macromolecules in solution. *Reports on Progress in Physics* **2003,** *66* (10), 1735-1782.

146.   Afonin, K. A.; Viard, M.; Koyfman, A. Y.; Martins, A. N.; Kasprzak, W. K.; Panigaj, M.; Desai, R.; Santhanam, A.; Grabow, W. W.; Jaeger, L.; Heldman, E.; Reiser, J.; Chiu, W.; Freed, E. O.; Shapiro, B. A., Multifunctional RNA Nanoparticles. *Nano Letters* **2014,** *14* (10), 5662-5671.

147.   Song, Y.; Chen, S., Janus Nanoparticles: Preparation, Characterization, and Applications. *Chemistry - An Asian Journal* **2014,** *9* (2), 418-430.

148.   Grillone, L. R.; Lanz, R., Fomivirsen. *Drugs Today (Barc)* **2001,** *37* (4), 245-255.

149.   Shukla, D.; Namperumalsamy, P.; Goldbaum, M.; Cunningham, E. T., Jr., Pegaptanib sodium for ocular vascular disease. *Indian J Ophthalmol* **2007,** *55* (6), 427-430.

150.   Rossi, J. J.; June, C. H.; Kohn, D. B., Genetic therapies against HIV. *Nature biotechnology* **2007,** *25* (12), 1444-1454.

151.   Jasinski, D.; Haque, F.; Binzel, D. W.; Guo, P., Advancement of the Emerging Field of RNA Nanotechnology. *ACS Nano* **2017,** *11* (2), 1142-1164.

152.   Fire, A.; Xu, S.; Montgomery, M. K.; Kostas, S. A.; Driver, S. E.; Mello, C. C., Potent and specific genetic interference by double-stranded RNA in Caenorhabditis elegans. *Nature* **1998,** *391* (6669), 806-811.

153.   Hu, B.; Weng, Y.; Xia, X. H.; Liang, X. J.; Huang, Y., Clinical advances of siRNA therapeutics. *The Journal of Gene Medicine* **2019,** *21* (7), e3097.

154.   Petrocca, F.; Lieberman, J., Promise and challenge of RNA interference-based therapy for cancer. *J Clin Oncol* **2011,** *29* (6), 747-54.

155.   Carthew, R. W.; Sontheimer, E. J., Origins and Mechanisms of miRNAs and siRNAs. *Cell* **2009,** *136* (4), 642-655.

156.   Kim, D.-H.; Behlke, M. A.; Rose, S. D.; Chang, M.-S.; Choi, S.; Rossi, J. J., Synthetic dsRNA Dicer substrates enhance RNAi potency and efficacy. *Nature Biotechnology* **2005,** *23* (2), 222-226.

157.   Rose, S. D.; Kim, D.-H.; Amarzguioui, M.; Heidel, J. D.; Collingwood, M. A.; Davis, M. E.; Rossi, J. J.; Behlke, M. A., Functional polarity is introduced by Dicer processing of short substrate RNAs. *Nucleic Acids Research* **2005,** *33* (13), 4140-4156.

158.   Yingling, Y. G.; Shapiro, B. A., Computational Design of an RNA Hexagonal Nanoring and an RNA Nanotube. *Nano Letters* **2007,** *7* (8), 2328-2334.

159.   Afonin, K. A.; Danilov, E. O.; Novikova, I. V.; Leontis, N. B., TokenRNA: A New Type of Sequence-Specific, Label-Free Fluorescent Biosensor for Folded RNA Molecules. *ChemBioChem* **2008,** *9* (12), 1902-1905.

160.	Low, J. T.; Knoepfel, S. A.; Watts, J. M.; ter Brake, O.; Berkhout, B.; Weeks, K. M., SHAPE-directed discovery of potent shRNA inhibitors of HIV-1. *Mol Ther* **2012,** *20* (4), 820-828.

161.	Afonin, K. A.; Desai, R.; Viard, M.; Kireeva, M. L.; Bindewald, E.; Case, C. L.; Maciag, A. E.; Kasprzak, W. K.; Kim, T.; Sappe, A.; Stepler, M.; Kewalramani, V. N.; Kashlev, M.; Blumenthal, R.; Shapiro, B. A., Co-transcriptional production of RNA-DNA hybrids for simultaneous release of multiple split functionalities. *Nucleic Acids Res* **2014,** *42* (3), 2085-97.

162.	Halman, J. R.; Satterwhite, E.; Roark, B.; Chandler, M.; Viard, M.; Ivanina, A.; Bindewald, E.; Kasprzak, W. K.; Panigaj, M.; Bui, M. N.; Lu, J. S.; Miller, J.; Khisamutdinov, E. F.; Shapiro, B. A.; Dobrovolskaia, M. A.; Afonin, K. A., Functionally-interdependent shape-switching nanoparticles with controllable properties. *Nucleic Acids Res* **2017,** *45* (4), 2210-2220.

163.	Chandrasekaran, A. R.; Punnoose, J. A.; Zhou, L.; Dey, P.; Dey, B. K.; Halvorsen, K., DNA nanotechnology approaches for microRNA detection and diagnosis. *Nucleic Acids Research* **2019,** *47* (20), 10489-10505.

164.	Weber, J. A.; Baxter, D. H.; Zhang, S.; Huang, D. Y.; How Huang, K.; Jen Lee, M.; Galas, D. J.; Wang, K., The MicroRNA Spectrum in 12 Body Fluids. *Clinical Chemistry* **2010,** *56* (11), 1733-1741.

165.	Hébert, S. S.; Horré, K.; Nicolaï, L.; Papadopoulou, A. S.; Mandemakers, W.; Silahtaroglu, A. N.; Kauppinen, S.; Delacourte, A.; De Strooper, B., Loss of microRNA cluster miR-29a/b-1 in sporadic Alzheimer's disease correlates with increased BACE1/beta-secretase expression. *Proc Natl Acad Sci U S A* **2008,** *105* (17), 6415-20.

166.	Wu, R.; Li, H.; Zhai, L.; Zou, X.; Meng, J.; Zhong, R.; Li, C.; Wang, H.; Zhang, Y.; Zhu, D., MicroRNA-431 accelerates muscle regeneration and ameliorates muscular dystrophy by targeting Pax7 in mice. *Nat Commun* **2015,** *6*, 7713.

167.	Small, E. M.; Frost, R. J.; Olson, E. N., MicroRNAs add a new dimension to cardiovascular disease. *Circulation* **2010,** *121* (8), 1022-32.

168.	Assmann, T. S.; Recamonde-Mendoza, M.; Puñales, M.; Tschiedel, B.; Canani, L. H.; Crispim, D., MicroRNA expression profile in plasma from type 1 diabetic patients: Case-control study and bioinformatic analysis. *Diabetes Res Clin Pract* **2018,** *141*, 35-46.

169.	Dai, R.; Ahmed, S. A., MicroRNA, a new paradigm for understanding immunoregulation, inflammation, and autoimmune diseases. *Transl Res* **2011,** *157* (4), 163-79.

170.	Girardi, E.; López, P.; Pfeffer, S., On the Importance of Host MicroRNAs During Viral Infection. *Front Genet* **2018,** *9*, 439.

171.	Aghdam, S. G.; Ebrazeh, M.; Hemmatzadeh, M.; Seyfizadeh, N.; Shabgah, A. G.; Azizi, G.; Ebrahimi, N.; Babaie, F.; Mohammadi, H., The role of microRNAs in prostate cancer migration, invasion, and metastasis. *J Cell Physiol* **2019,** *234* (7), 9927-9942.

172.	Kim, Y. W.; Kim, E. Y.; Jeon, D.; Liu, J. L.; Kim, H. S.; Choi, J. W.; Ahn, W. S., Differential microRNA expression signatures and cell type-specific association with Taxol resistance in ovarian cancer cells. *Drug Des Devel Ther* **2014,** *8*, 293-314.

173.	Wu, X.; Ajani, J. A.; Gu, J.; Chang, D. W.; Tan, W.; Hildebrandt, M. A.; Huang, M.; Wang, K. K.; Hawk, E., MicroRNA expression signatures during malignant progression from Barrett's esophagus to esophageal adenocarcinoma. *Cancer Prev Res (Phila)* **2013,** *6* (3), 196-205.

174.	Calin, G. A.; Croce, C. M., MicroRNA signatures in human cancers. *Nat Rev Cancer* **2006,** *6* (11), 857-66.

175.	Kumarswamy, R.; Volkmann, I.; Thum, T., Regulation and function of miRNA-21 in health and disease. *RNA Biol* **2011,** *8* (5), 706-13.

176.   Goodman, R. P.; Schaap, I. A.; Tardin, C. F.; Erben, C. M.; Berry, R. M.; Schmidt, C. F.; Turberfield, A. J., Rapid chiral assembly of rigid DNA building blocks for molecular nanofabrication. *Science* **2005,** *310* (5754), 1661-5.

177.   Wen, Y.; Pei, H.; Shen, Y.; Xi, J.; Lin, M.; Lu, N.; Shen, X.; Li, J.; Fan, C., DNA Nanostructure-based Interfacial engineering for PCR-free ultrasensitive electrochemical analysis of microRNA. *Sci Rep* **2012,** *2*, 867.

178.   Zhu, J.; Feng, X.; Lou, J.; Li, W.; Li, S.; Zhu, H.; Yang, L.; Zhang, A.; He, L.; Li, C., Accurate quantification of microRNA via single strand displacement reaction on DNA origami motif. *PLoS One* **2013,** *8* (8), e69856.

179.   He, X.; Zeng, T.; Li, Z.; Wang, G.; Ma, N., Catalytic Molecular Imaging of MicroRNA in Living Cells by DNA-Programmed Nanoparticle Disassembly. *Angew Chem Int Ed Engl* **2016,** *55* (9), 3073-6.

180.   Wang, L.; Deng, R.; Li, J., Target-fueled DNA walker for highly selective miRNA detection. *Chem Sci* **2015,** *6* (12), 6777-6782.

181.   Halvorsen, K.; Schaak, D.; Wong, W. P., Nanoengineering a single-molecule mechanical switch using DNA self-assembly. *Nanotechnology* **2011,** *22* (49), 494005.

182.   Zhou, W.; Liang, W.; Li, X.; Chai, Y.; Yuan, R.; Xiang, Y., MicroRNA-triggered, cascaded and catalytic self-assembly of functional "DNAzyme ferris wheel" nanostructures for highly sensitive colorimetric detection of cancer cells. *Nanoscale* **2015,** *7* (19), 9055-61.

183.   Bindewald, E.; Afonin, K. A.; Viard, M.; Zakrevsky, P.; Kim, T.; Shapiro, B. A., Multistrand Structure Prediction of Nucleic Acid Assemblies and Design of RNA Switches. *Nano Letters* **2016,** *16* (3), 1726-1735.

184.   Zakrevsky, P.; Parlea, L.; Viard, M.; Bindewald, E.; Afonin, K. A.; Shapiro, B. A., Preparation of a Conditional RNA Switch. *Methods Mol Biol* **2017,** *1632*, 303-324.

185.   Soukup, G., Nucleic acid molecular switches. *Trends in Biotechnology* **1999,** *17* (12), 469-476.

186.   Tyagi, S.; Kramer, F. R., Molecular Beacons: Probes that Fluoresce upon Hybridization. *Nature Biotechnology* **1996,** *14* (3), 303-308.

187.   Zhang, D. Y.; Seelig, G., Dynamic DNA nanotechnology using strand-displacement reactions. *Nature Chemistry* **2011,** *3* (2), 103-113.

188.   Rinaudo, K.; Bleris, L.; Maddamsetti, R.; Subramanian, S.; Weiss, R.; Benenson, Y., A universal RNAi-based logic evaluator that operates in mammalian cells. *Nature Biotechnology* **2007,** *25* (7), 795-801.

189.   Johnson, M. B.; Halman, J. R.; Satterwhite, E.; Zakharov, A. V.; Bui, M. N.; Benkato, K.; Goldsworthy, V.; Kim, T.; Hong, E.; Dobrovolskaia, M. A.; Khisamutdinov, E. F.; Marriott, I.; Afonin, K. A., Programmable Nucleic Acid Based Polygons with Controlled Neuroimmunomodulatory Properties for Predictive QSAR Modeling. *Small* **2017,** *13* (42).

190.   Hong, E.; Halman, J. R.; Shah, A. B.; Khisamutdinov, E. F.; Dobrovolskaia, M. A.; Afonin, K. A., Structure and Composition Define Immunorecognition of Nucleic Acid Nanoparticles. *Nano Lett* **2018,** *18* (7), 4309-4321.

191.   Chen, D. S.; Mellman, I., Oncology meets immunology: the cancer-immunity cycle. *Immunity* **2013,** *39* (1), 1-10.

192.   Dobrovolskaia, M. A., Nucleic Acid Nanoparticles at a Crossroads of Vaccines and Immunotherapies. *Molecules (Basel, Switzerland)* **2019,** *24* (24), 4620.

193.   Latronico, A. C.; Silveira, L. F., Genetic and Epigenetic Control of Puberty. In *Encyclopedia of Endocrine Diseases (Second Edition)*, Huhtaniemi, I.; Martini, L., Eds. Academic Press: Oxford, 2019; pp 126-136.

194.   Nimjee, S. M.; White, R. R.; Becker, R. C.; Sullenger, B. A., Aptamers as therapeutics. *Annual review of pharmacology and toxicology* **2017,** *57*, 61-79.

195.   Cullen, B. R.; Greene, W. C., Regulatory pathways governing HIV-1 replication. *Cell* **1989,** *58* (3), 423-6.

196.   Marciniak, R. A.; Garcia-Blanco, M. A.; Sharp, P. A., Identification and characterization of a HeLa nuclear protein that specifically binds to the trans-activation-response (TAR) element of human immunodeficiency virus. *Proc Natl Acad Sci U S A* **1990,** *87* (9), 3624-8.

197.   Sullenger, B. A.; Gallardo, H. F.; Ungers, G. E.; Gilboa, E., Overexpression of TAR sequences renders cells resistant to human immunodeficiency virus replication. *Cell* **1990,** *63* (3), 601-608.

198.   Tuerk, C.; Gold, L., Systematic evolution of ligands by exponential enrichment: RNA ligands to bacteriophage T4 DNA polymerase. *Science* **1990,** *249* (4968), 505-510.

199.   Ellington, A. D.; Szostak, J. W., In vitro selection of RNA molecules that bind specific ligands. *Nature* **1990,** *346* (6287), 818-22.

200.   Robertson, D. L.; Joyce, G. F., Selection in vitro of an RNA enzyme that specifically cleaves single-stranded DNA. *Nature* **1990,** *344* (6265), 467-468.

201.   Kaur, H., Recent developments in cell-SELEX technology for aptamer selection. *Biochimica et Biophysica Acta (BBA) - General Subjects* **2018,** *1862* (10), 2323-2329.

202.   Santosh, B.; Yadava, P. K., Nucleic Acid Aptamers: Research Tools in Disease Diagnostics and Therapeutics. *BioMed Research International* **2014,** *2014*, 540451.

203.   Tolle, F.; Mayer, G., Preparation of SELEX Samples for Next-Generation Sequencing. *Methods Mol Biol* **2016,** *1380*, 77-84.

204.   Hoinka, J.; Zotenko, E.; Friedman, A.; Sauna, Z. E.; Przytycka, T. M., Identification of sequence-structure RNA binding motifs for SELEX-derived aptamers. *Bioinformatics* **2012,** *28* (12), i215-i223.

205.   III, R. S. S., EXPANDING QUANTITATIVE TOOLS FOR SECONDARY STRUCTURE ANALYSIS OF DNA APTAMER CANDIDATES SELECTED VIA COMPELS. *Georgia Institute of Technology* **2017**.

206.   Musheev, M. U.; Krylov, S. N., Selection of aptamers by systematic evolution of ligands by exponential enrichment: Addressing the polymerase chain reaction issue. *Analytica Chimica Acta* **2006,** *564* (1), 91-96.

207.   Wang, C. W.; Chung, W. H.; Cheng, Y. F.; Ying, N. W.; Peck, K.; Chen, Y. T.; Hung, S. I., A new nucleic acid-based agent inhibits cytotoxic T lymphocyte-mediated immune disorders. *J Allergy Clin Immunol* **2013,** *132* (3), 713-722.e11.

208.   Stoltenburg, R.; Nikolaus, N.; Strehlitz, B., Capture-SELEX: Selection of DNA Aptamers for Aminoglycoside Antibiotics. *Journal of Analytical Methods in Chemistry* **2012,** *2012*, 415697.

209.   Graham, J. C.; Zarbl, H., Use of cell-SELEX to generate DNA aptamers as molecular probes of HPV-associated cervical cancer cells. *PLoS One* **2012,** *7* (4), e36103.

210.   Zhong, Y.; Zhao, J.; Li, J.; Liao, X.; Chen, F., Advances of aptamers screened by Cell-SELEX in selection procedure, cancer diagnostics and therapeutics. *Analytical Biochemistry* **2020,** *598*, 113620.

211.   Lou, X.; Qian, J.; Xiao, Y.; Viel, L.; Gerdon, A. E.; Lagally, E. T.; Atzberger, P.; Tarasow, T. M.; Heeger, A. J.; Soh, H. T., Micromagnetic selection of aptamers in microfluidic channels. *Proceedings of the National Academy of Sciences* **2009,** *106* (9), 2989-2994.

212.   Luo, Z.; Zhou, H.; Jiang, H.; Ou, H.; Li, X.; Zhang, L., Development of a fraction collection approach in capillary electrophoresis SELEX for aptamer selection. *The Analyst* **2015,** *140* (8), 2664-2670.

213.   Miyachi, Y.; Shimizu, N.; Ogino, C.; Kondo, A., Selection of DNA aptamers using atomic force microscopy. *Nucleic Acids Res* **2010,** *38* (4), e21.

214.   Cheng, C.; Chen, Y. H.; Lennox, K. A.; Behlke, M. A.; Davidson, B. L., In vivo SELEX for Identification of Brain-penetrating Aptamers. *Mol Ther Nucleic Acids* **2013,** *2* (1), e67-e67.

215.   Fernández, G.; Moraga, A.; Cuartero, M. I.; García-Culebras, A.; Peña-Martínez, C.; Pradillo, J. M.; Hernández-Jiménez, M.; Sacristán, S.; Ayuso, M. I.; Gonzalo-Gobernado, R.; Fernández-López, D.; Martín, M. E.; Moro, M. A.; González, V. M.; Lizasoain, I., TLR4-Binding DNA Aptamers Show a Protective Effect against Acute Stroke in Animal Models. *Mol Ther* **2018,** *26* (8), 2047-2059.

216.   Zhang, Y.; Lai, B. S.; Juhas, M., Recent Advances in Aptamer Discovery and Applications. *Molecules* **2019,** *24* (5).

217.   Ali, M. H.; Elsherbiny, M. E.; Emara, M., Updates on Aptamer Research. *Int J Mol Sci* **2019,** *20* (10).

218.   Sullivan, R.; Adams, M. C.; Naik, R. R.; Milam, V. T., Analyzing Secondary Structure Patterns in DNA Aptamers Identified via CompELS. *Molecules (Basel, Switzerland)* **2019,** *24* (8), 1572.

219.   Hermann, T., Adaptive Recognition by Nucleic Acid Aptamers. *Science* **2000,** *287* (5454), 820-825.

220.   McKeague, M.; DeRosa, M. C., Challenges and Opportunities for Small Molecule Aptamer Development. *Journal of Nucleic Acids* **2012,** *2012*, 748913.

221.   group, A., Targets of aptamers. *aptamer group*.

222.   Willis, M. C.; Collins, B.; Zhang, T.; Green, L. S.; Sebesta, D. P.; Bell, C.; Kellogg, E.; Gill, S. C.; Magallanez, A.; Knauer, S.; Bendele, R. A.; Gill, P. S.; Janjić, N., Liposome-Anchored Vascular Endothelial Growth Factor Aptamers. *Bioconjugate Chemistry* **1998,** *9* (5), 573-582.

223.   Burmeister, P. E.; Lewis, S. D.; Silva, R. F.; Preiss, J. R.; Horwitz, L. R.; Pendergrast, P. S.; McCauley, T. G.; Kurz, J. C.; Epstein, D. M.; Wilson, C.; Keefe, A. D., Direct In Vitro Selection of a 2′-O-Methyl Aptamer to VEGF. *Chemistry & Biology* **2005,** *12* (1), 25-33.

224.   Zon, G.; Geiser, T. G., Phosphorothioate oligonucleotides: chemistry, purification, analysis, scale-up and future directions. *Anticancer Drug Des* **1991,** *6* (6), 539-68.

225.   Veedu, R. N.; Wengel, J., Locked nucleic acids: promising nucleic acid analogs for therapeutic applications. *Chem Biodivers* **2010,** *7* (3), 536-42.

226.   Knudsen, S. M.; Robertson, M. P.; Ellington, A. D., In vitro selection using modified or unnatural nucleotides. *Curr Protoc Nucleic Acid Chem* **2002,** *Chapter 9*, Unit 9.6.

227.   Kasahara, Y.; Irisawa, Y.; Ozaki, H.; Obika, S.; Kuwahara, M., 2′,4′-BNA/LNA aptamers: CE-SELEX using a DNA-based library of full-length 2′-O,4′-C-methylene-bridged/linked bicyclic ribonucleotides. *Bioorganic & Medicinal Chemistry Letters* **2013,** *23* (5), 1288-1292.

228.   Battersby, T. R.; Ang, D. N.; Burgstaller, P.; Jurczyk, S. C.; Bowser, M. T.; Buchanan, D. D.; Kennedy, R. T.; Benner, S. A., Quantitative Analysis of Receptors for Adenosine Nucleotides Obtained via In Vitro Selection from a Library Incorporating a Cationic Nucleotide Analog. *Journal of the American Chemical Society* **1999,** *121* (42), 9781-9789.

229.   Teramoto, N.; Imanishi, Y.; Ito, Y., In Vitro Selection of a Ligase Ribozyme Carrying Alkylamino Groups in the Side Chains. *Bioconjugate Chemistry* **2000,** *11* (6), 744-748.

230.   Kasahara, Y.; Kitadume, S.; Morihiro, K.; Kuwahara, M.; Ozaki, H.; Sawai, H.; Imanishi, T.; Obika, S., Effect of 3′-end capping of aptamer with various 2′,4′-bridged nucleotides: Enzymatic post-modification toward a practical use of polyclonal aptamers. *Bioorganic & Medicinal Chemistry Letters* **2010,** *20* (5), 1626-1629.

231.   Kuwahara, M.; Obika, S.; Takeshima, H.; Hagiwara, Y.; Nagashima, J.-I.; Ozaki, H.; Sawai, H.; Imanishi, T., Smart conferring of nuclease resistance to DNA by 3′-end protection using 2′,4′-bridged nucleoside-5′-triphosphates. *Bioorganic & Medicinal Chemistry Letters* **2009,** *19* (11), 2941-2943.

232.   Willis, M. C.; Collins, B. D.; Zhang, T.; Green, L. S.; Sebesta, D. P.; Bell, C.; Kellogg, E.; Gill, S. C.; Magallanez, A.; Knauer, S.; Bendele, R. A.; Gill, P. S.; Janjić, N., Liposome-anchored vascular endothelial growth factor aptamers. *Bioconjug Chem* **1998,** *9* (5), 573-82.

233.   Matthias Kuhlmann, J. B. R. H., Anders Voldum, Georgia Tsakiridou, Maja T. Larsen, Julie S. Schmøkel, Emil Sohn, Konrad Bienk, David Schaffert, Esben S. Sørensen, Jesper Wengel, Daniel M. Dupont, Kenneth A. Howard, An Albumin-Oligonucleotide Assembly for Potential Combinatorial Drug Delivery and Half-Life Extension Applications. *Molecular Biology Nucleic Acids* **2017,** *9*, 284-293.

234.   Tucker, C. E.; Chen, L.-S.; Judkins, M. B.; Farmer, J. A.; Gill, S. C.; Drolet, D. W., Detection and plasma pharmacokinetics of an anti-vascular endothelial growth factor oligonucleotide-aptamer (NX1838) in rhesus monkeys. *Journal of Chromatography B: Biomedical Sciences and Applications* **1999,** *732* (1), 203-212.

235.   Martin, P.; Jakob, R., Aptamer guided delivery of nucleic acid-based nanoparticles. *DNA and RNA Nanotechnology* **2016,** (1), 42-52.

236.   Rusconi, C. P.; Roberts, J. D.; Pitoc, G. A.; Nimjee, S. M.; White, R. R.; Quick, G.; Scardino, E.; Fay, W. P.; Sullenger, B. A., Antidote-mediated control of an anticoagulant aptamer in vivo. *Nature Biotechnology* **2004,** *22* (11), 1423-1428.

237.   Lakhin, A. V.; Tarantul, V. Z.; Gening, L. V., Aptamers: problems, solutions and prospects. *Acta Naturae* **2013,** *5* (4), 34-43.

238.   Nimjee, S. M.; Keys, J. R.; Pitoc, G. A.; Quick, G.; Rusconi, C. P.; Sullenger, B. A., A Novel Antidote-Controlled Anticoagulant Reduces Thrombin Generation and Inflammation and Improves Cardiac Function in Cardiopulmonary Bypass Surgery. *Molecular Therapy* **2006,** *14* (3), 408-415.

239.   Hidding, J., A therapeutic battle: Antibodies vs. Aptamers. *NS109 - Research pape*.

240.   Richardson, F. C.; Tennant, B. C.; Meyer, D. J.; Richardson, K. A.; Mann, P. C.; McGinty, G. R.; Wolf, J. L.; Zack, P. M.; Bendele, R. A., An evaluation of the toxicities of 2'-fluorouridine and 2'-fluorocytidine-HCl in F344 rats and woodchucks (Marmota monax). *Toxicol Pathol* **1999,** *27* (6), 607-17.

241.   Pendergrast, P. S.; Marsh, H. N.; Grate, D.; Healy, J. M.; Stanton, M., Nucleic acid aptamers for target validation and therapeutic applications. *J Biomol Tech* **2005,** *16* (3), 224-34.

242.   Zhu, G.; Niu, G.; Chen, X., Aptamer-Drug Conjugates. *Bioconjugate chemistry* **2015,** *26* (11), 2186-2197.

243.   Kim, M. Y.; Jeong, S., In vitro selection of RNA aptamer and specific targeting of ErbB2 in breast cancer cells. *Nucleic Acid Ther* **2011,** *21* (3), 173-178.

244.   Jones, B. V.; Young, R.; Mahenthiralingam, E.; Stickler, D. J., Ultrastructure of Proteus mirabilis swarmer cell rafts and role of swarming in catheter-associated urinary tract infection. *Infect Immun* **2004,** *72* (7), 3941-3950.

245.   Savory, N.; Lednor, D.; Tsukakoshi, K.; Abe, K.; Yoshida, W.; Ferri, S.; Jones, B. V.; Ikebukuro, K., In silico maturation of binding-specificity of DNA aptamers againstProteus mirabilis. *Biotechnology and Bioengineering* **2013,** *110* (10), 2573-2580.

246.   Bruno, J. G.; Phillips, T.; Carrillo, M. P.; Crowell, R., Plastic-adherent DNA aptamer-magnetic bead and quantum dot sandwich assay for Campylobacter detection. *J Fluoresc* **2009,** *19* (3), 427-35.

247.   Bruno, J. G.; Carrillo, M. P.; Phillips, T.; Andrews, C. J., A Novel Screening Method for Competitive FRET-Aptamers Applied to E. coli Assay Development. *Journal of Fluorescence* **2010,** *20* (6), 1211-1223.

248.   Chen, F.; Zhou, J.; Luo, F.; Mohammed, A. B.; Zhang, X. L., Aptamer from whole-bacterium SELEX as new therapeutic reagent against virulent Mycobacterium tuberculosis. *Biochem Biophys Res Commun* **2007,** *357* (3), 743-8.

249.   Duan, N.; Wu, S.; Chen, X.; Huang, Y.; Wang, Z., Selection and identification of a DNA aptamer targeted to Vibrio parahemolyticus. *J Agric Food Chem* **2012**, *60* (16), 4034-8.

250.   Cao, X.; Li, S.; Chen, L.; Ding, H.; Xu, H.; Huang, Y.; Li, J.; Liu, N.; Cao, W.; Zhu, Y.; Shen, B.; Shao, N., Combining use of a panel of ssDNA aptamers in the detection of Staphylococcus aureus. *Nucleic Acids Res* **2009**, *37* (14), 4621-8.

251.   Jang, K. J.; Lee, N. R.; Yeo, W. S.; Jeong, Y. J.; Kim, D. E., Isolation of inhibitory RNA aptamers against severe acute respiratory syndrome (SARS) coronavirus NTPase/Helicase. *Biochem Biophys Res Commun* **2008,** *366* (3), 738-44.

252.   Fukuda, K.; Vishinuvardhan, D.; Sekiya, S.; Kakiuchi, N.; Shimotohno, K.; Kumar, P. K.; Nishikawa, S., Specific RNA aptamers to NS3 protease domain of hepatitis C virus. *Nucleic Acids Symp Ser* **1997,** (37), 237-8.

253.   Boiziau, C.; Dausse, E.; Yurchenko, L.; Toulmé, J. J., DNA aptamers selected against the HIV-1 trans-activation-responsive RNA element form RNA-DNA kissing complexes. *J Biol Chem* **1999,** *274* (18), 12730-7.

254.   Gopinath, S. C.; Kawasaki, K.; Kumar, P. K., Selection of RNA-aptamer against human influenza B virus. *Nucleic Acids Symp Ser (Oxf)* **2005,** (49), 85-6.

255.   Guerra-Pérez, N.; Ramos, E.; García-Hernández, M.; Pinto, C.; Soto, M.; Martín, M. E.; González, V. M., Molecular and Functional Characterization of ssDNA Aptamers that Specifically Bind Leishmania infantum PABP. *PLoS One* **2015,** *10* (10), e0140048.

256.   Iqbal, A.; Labib, M.; Muharemagic, D.; Sattar, S.; Dixon, B. R.; Berezovski, M. V., Detection of Cryptosporidium parvum Oocysts on Fresh Produce Using DNA Aptamers. *PLoS One* **2015,** *10* (9), e0137455.

257.   Shangguan, D.; Cao, Z.; Meng, L.; Mallikaratchy, P.; Sefah, K.; Wang, H.; Li, Y.; Tan, W., Cell-specific aptamer probes for membrane protein elucidation in cancer cells. *J Proteome Res* **2008,** *7* (5), 2133-9.

258.   Wan, Y.; Kim, Y. T.; Li, N.; Cho, S. K.; Bachoo, R.; Ellington, A. D.; Iqbal, S. M., Surface-immobilized aptamers for cancer cell isolation and microscopic cytology. *Cancer Res* **2010,** *70* (22), 9371-80.

259.   Zhang, P.; Zhao, N.; Zeng, Z.; Feng, Y.; Tung, C. H.; Chang, C. C.; Zu, Y., Using an RNA aptamer probe for flow cytometry detection of CD30-expressing lymphoma cells. *Lab Invest* **2009,** *89* (12), 1423-32.

260.   Li, Y.; Lee, H. J.; Corn, R. M., Detection of Protein Biomarkers Using RNA Aptamer Microarrays and Enzymatically Amplified Surface Plasmon Resonance Imaging. *Analytical Chemistry* **2007,** *79* (3), 1082-1088.

261.   Ng, E. W. M.; Shima, D. T.; Calias, P.; Cunningham, E. T.; Guyer, D. R.; Adamis, A. P., Pegaptanib, a targeted anti-VEGF aptamer for ocular vascular disease. *Nature Reviews Drug Discovery* **2006,** *5* (2), 123-132.

262.   Macugen (pegaptanib). *European Medicines Agency* **2010**.

263.   Roxo, C.; Kotkowiak, W.; Pasternak, A., G-Quadruplex-Forming Aptamers-Characteristics, Applications, and Perspectives. *Molecules (Basel, Switzerland)* **2019,** *24* (20), 3781.

264.   Zavyalova, E.; Samoylenkova, N.; Revishchin, A.; Turashev, A.; Gordeychuk, I.; Golovin, A.; Kopylov, A.; Pavlova, G., The Evaluation of Pharmacodynamics and Pharmacokinetics of Anti-thrombin DNA Aptamer RA-36. *Frontiers in Pharmacology* **2017,** *8* (922).

265.   Plautz, W. E.; Sekhar Pilli, V. S.; Cooley, B. C.; Chattopadhyay, R.; Westmark, P. R.; Getz, T.; Paul, D.; Bergmeier, W.; Sheehan, J. P.; Majumder, R., Anticoagulant Protein S Targets the Factor IXa Heparin-Binding Exosite to Prevent Thrombosis. *Arterioscler Thromb Vasc Biol* **2018,** *38* (4), 816-828.

266.   Sinha, G., Regado's aptamer lines up against anticoagulants. *Nature Biotechnology* **2013,** *31* (12), 1060-1060.

267.	Correction: Identification and Characterization of Nuclease-Stabilized RNA Molecules That Bind Human Prostate Cancer Cells via the Prostate-Specific Membrane Antigen. *Cancer Research* **2012,** *72* (15), 3887-3887.

268.	Dassie, J. P.; Hernandez, L. I.; Thomas, G. S.; Long, M. E.; Rockey, W. M.; Howell, C. A.; Chen, Y.; Hernandez, F. J.; Liu, X. Y.; Wilson, M. E.; Allen, L.-A.; Vaena, D. A.; Meyerholz, D. K.; Giangrande, P. H., Targeted Inhibition of Prostate Cancer Metastases with an RNA Aptamer to Prostate-specific Membrane Antigen. *Molecular Therapy* **2014,** *22* (11), 1910-1922.

269.	Hollingsworth, M. A.; Swanson, B. J., Mucins in cancer: protection and control of the cell surface. *Nat Rev Cancer* **2004,** *4* (1), 45-60.

270.	Ferreira, C. S. M.; Cheung, M. C.; Missailidis, S.; Bisland, S.; Gariépy, J., Phototoxic aptamers selectively enter and kill epithelial cancer cells. *Nucleic acids research* **2009,** *37* (3), 866-876.

271.	Esposito, C. L.; Cerchia, L.; Catuogno, S.; De Vita, G.; Dassie, J. P.; Santamaria, G.; Swiderski, P.; Condorelli, G.; Giangrande, P. H.; de Franciscis, V., Multifunctional aptamer-miRNA conjugates for targeted cancer therapy. *Mol Ther* **2014,** *22* (6), 1151-1163.

272.	Zhou, J.; Neff, C. P.; Swiderski, P.; Li, H.; Smith, D. D.; Aboellail, T.; Remling-Mulder, L.; Akkina, R.; Rossi, J. J., Functional In Vivo Delivery of Multiplexed Anti-HIV-1 siRNAs via a Chemically Synthesized Aptamer With a Sticky Bridge. *Molecular Therapy* **2013,** *21* (1), 192-200.

273.	Wu, Y.; Sefah, K.; Liu, H.; Wang, R.; Tan, W., DNA aptamer-micelle as an efficient detection/delivery vehicle toward cancer cells. *Proceedings of the National Academy of Sciences of the United States of America* **2010,** *107* (1), 5-10.

274.	Porciani, D.; Tedeschi, L.; Marchetti, L.; Citti, L.; Piazza, V.; Beltram, F.; Signore, G., Aptamer-Mediated Codelivery of Doxorubicin and NF-κB Decoy Enhances Chemosensitivity of Pancreatic Tumor Cells. *Mol Ther Nucleic Acids* **2015,** *4* (4), e235.

275.	Stojanovic, M. N.; Kolpashchikov, D. M., Modular Aptameric Sensors. *Journal of the American Chemical Society* **2004,** *126* (30), 9266-9270.

276.	An Aptamer–siRNA Chimera Silences the Eukaryotic Elongation Factor 2 Gene and Induces Apoptosis in Cancers Expressing αvβ3 Integrin. *Nucleic Acid Ther* **2013,** *23* (3), 203-212.

277.	Tarapore, P.; Shu, Y.; Guo, P.; Ho, S. M., Application of phi29 motor pRNA for targeted therapeutic delivery of siRNA silencing metallothionein-IIA and survivin in ovarian cancers. *Mol Ther* **2011,** *19* (2), 386-94.

278.	Dalpke, A. H.; Zimmermann, S.; Albrecht, I.; Heeg, K., Phosphodiester CpG oligonucleotides as adjuvants: polyguanosine runs enhance cellular uptake and improve immunostimulative activity of phosphodiester CpG oligonucleotides in vitro and in vivo. *Immunology* **2002,** *106* (1), 102-112.

279.	Arbab, A.; Yocum, G. T.; Wilson, L. B.; Parwana, A.; Jordan, E.; Kalish, H.; Frank, J., Comparison of Transfection Agents in Forming Complexes with Ferumoxides, Cell Labeling Efficiency, and Cellular Viability. *Molecular Imaging* **2004,** *3*.

280.	Mo, R. H.; Zaro, J.; Ou, J.; Shen, W., Effects of Lipofectamine 2000/siRNA Complexes on Autophagy in Hepatoma Cells. *Molecular Biotechnology* **2011,** *51*, 1-8.

281.	Li, Z.; Zhang, C.; Wang, Z.; Shen, J.; Xiang, P.; Chen, X.; Nan, J.; Lin, Y., Lipofectamine 2000/siRNA complexes cause endoplasmic reticulum unfolded protein response in human endothelial cells. *Journal of Cellular Physiology* **2019,** *234*, 21166 - 21181.

282.	Guo, X.; Wang, H.; Li, Y.; Leng, X.; Huang, W.; Ma, Y.; Xu, T.; Qi, X., Transfection reagent Lipofectamine triggers type I interferon signaling activation in macrophages. *Immunology and Cell Biology* **2019,** *97*.

283.	Urmoneit, B.; Turner, J.; Dyrks, T., Cationic lipids (lipofectamine) and disturbance of cellular cholesterol and sphingomyelin distribution modulates gamma-secretase activity within amyloid precursor protein in vitro. *Prostaglandins & other lipid mediators* **1998,** *55 5-6,* 331-43.

284.	Juliano, R. L., The delivery of therapeutic oligonucleotides. *Nucleic acids research* **2016,** *44* (14), 6518-6548.

285.	Shim, G.; Kim, M.-G.; Park, J. Y.; Oh, Y.-K., Application of cationic liposomes for delivery of nucleic acids. *Asian Journal of Pharmaceutical Sciences* **2013,** *8* (2), 72-80.

286.	Zhang, X.; Goel, V.; Robbie, G. J., Pharmacokinetics of Patisiran, the First Approved RNA Interference Therapy in Patients With Hereditary Transthyretin-Mediated Amyloidosis. *The Journal of Clinical Pharmacology* **2020,** *60* (5), 573-585.

287.	Cullis, P. R.; Hope, M. J., Lipid Nanoparticle Systems for Enabling Gene Therapies. *Molecular Therapy* **2017,** *25* (7), 1467-1475.

288.	Barenholz, Y., Doxil®--the first FDA-approved nano-drug: lessons learned. *J Control Release* **2012,** *160* (2), 117-34.

289.	Kaposi's sarcoma: DaunoXome approved. *AIDS Treat News* **1996,** (no 246), 3-4.

290.	Yetisgin, A. A.; Cetinel, S.; Zuvin, M.; Kosar, A.; Kutlu, O., Therapeutic Nanoparticles and Their Targeted Delivery Applications. *Molecules* **2020,** *25* (9).

291.	Barba, A. A.; Bochicchio, S.; Dalmoro, A.; Lamberti, G., Lipid Delivery Systems for Nucleic-Acid-Based-Drugs: From Production to Clinical Applications. *Pharmaceutics* **2019,** *11* (8), 360.

292.	Charoensit, P.; Kawakami, S.; Higuchi, Y.; Yamashita, F.; Hashida, M., Enhanced growth inhibition of metastatic lung tumors by intravenous injection of ATRA-cationic liposome/IL-12 pDNA complexes in mice. *Cancer Gene Therapy* **2010,** *17* (7), 512-522.

293.	Zhang, C.; Pei, J.; Kumar, D.; Sakabe, I.; Boudreau, H. E.; Gokhale, P. C.; Kasid, U. N., Antisense oligonucleotides: target validation and development of systemically delivered therapeutic nanoparticles. *Methods Mol Biol* **2007,** *361,* 163-85.

294.	Jain, V.; Bharatam, P. V., Pharmacoinformatic approaches to understand complexation of dendrimeric nanoparticles with drugs. **2014,** *6* (5), 2476.

295.	Bielinska, A., Regulation of in vitro gene expression using antisense oligonucleotides or antisense expression plasmids transfected using starburst PAMAM dendrimers. *Nucleic Acids Research* **1996,** *24* (11), 2176-2182.

296.	Palmerston Mendes, L.; Pan, J.; Torchilin, V., Dendrimers as Nanocarriers for Nucleic Acid and Drug Delivery in Cancer Therapy. *Molecules* **2017,** *22* (9), 1401.

297.	Patil, M. L.; Zhang, M.; Taratula, O.; Garbuzenko, O. B.; He, H.; Minko, T., Internally cationic polyamidoamine PAMAM-OH dendrimers for siRNA delivery: effect of the degree of quaternization and cancer targeting. *Biomacromolecules* **2009,** *10* (2), 258-66.

298.	Taratula, O.; Garbuzenko, O. B.; Kirkpatrick, P.; Pandya, I.; Savla, R.; Pozharov, V. P.; He, H.; Minko, T., Surface-engineered targeted PPI dendrimer for efficient intracellular and intratumoral siRNA delivery. *J Control Release* **2009,** *140* (3), 284-93.

299.	Inoue, Y.; Kurihara, R.; Tsuchida, A.; Hasegawa, M.; Nagashima, T.; Mori, T.; Niidome, T.; Katayama, Y.; Okitsu, O., Efficient delivery of siRNA using dendritic poly(L-lysine) for loss-of-function analysis. *J Control Release* **2008,** *126* (1), 59-66.

300.	Zheng, C.; Zheng, M.; Gong, P.; Deng, J.; Yi, H.; Zhang, P.; Zhang, Y.; Liu, P.; Ma, Y.; Cai, L., Polypeptide cationic micelles mediated co-delivery of docetaxel and siRNA for synergistic tumor therapy. *Biomaterials* **2013,** *34* (13), 3431-3438.

301.	Kim, T.; Viard, M.; Afonin, K. A.; Gupta, K.; Popov, M.; Salotti, J.; Johnson, P. F.; Linder, C.; Heldman, E.; Shapiro, B. A., Characterization of Cationic Bolaamphiphile Vesicles for siRNA Delivery into Tumors and Brain. *Molecular Therapy - Nucleic Acids* **2020,** *20,* 359-372.

302.	Halman, J. R.; Kim, K. T.; Gwak, S. J.; Pace, R.; Johnson, M. B.; Chandler, M. R.; Rackley, L.; Viard, M.; Marriott, I.; Lee, J. S.; Afonin, K. A., A cationic amphiphilic co-

polymer as a carrier of nucleic acid nanoparticles (Nanps) for controlled gene silencing, immunostimulation, and biodistribution. *Nanomedicine* **2020,** *23*, 102094.

303.   Vivero-Escoto, J. L.; Slowing, I. I.; Trewyn, B. G.; Lin, V. S. Y., Mesoporous Silica Nanoparticles for Intracellular Controlled Drug Delivery. *Small* **2010,** *6* (18), 1952-1967.

304.   Shim, M. S.; Kim, C. S.; Ahn, Y.-C.; Chen, Z.; Kwon, Y. J., Combined Multimodal Optical Imaging and Targeted Gene Silencing Using Stimuli-Transforming Nanotheragnostics. *Journal of the American Chemical Society* **2010,** *132* (24), 8316-8324.

305.   Conde, J.; Rosa, J.; de la Fuente, J. M.; Baptista, P. V., Gold-nanobeacons for simultaneous gene specific silencing and intracellular tracking of the silencing events. *Biomaterials* **2013,** *34* (10), 2516-2523.

306.   Dey, S.; Maiti, T. K., Superparamagnetic Nanoparticles and RNAi-Mediated Gene Silencing: Evolving Class of Cancer Diagnostics and Therapeutics. *Journal of Nanomaterials* **2012,** *2012*, 129107.

307.   Lin, G.; Chen, T.; Zou, J.; Wang, Y.; Wang, X.; Li, J.; Huang, Q.; Fu, Z.; Zhao, Y.; Lin, M. C.; Xu, G.; Yong, K. T., Quantum Dots-siRNA Nanoplexes for Gene Silencing in Central Nervous System Tumor Cells. *Front Pharmacol* **2017,** *8*, 182.

308.   Shah, V.; Taratula, O.; Garbuzenko, O. B.; Patil, M. L.; Savla, R.; Zhang, M.; Minko, T., Genotoxicity of different nanocarriers: possible modifications for the delivery of nucleic acids. *Curr Drug Discov Technol* **2013,** *10* (1), 8-15.

309.   Szebeni, J., Complement activation-related pseudoallergy: A new class of drug-induced acute immune toxicity. *Toxicology* **2005,** *216* (2), 106-121.

310.   Syama, S.; Gayathri, V.; Mohanan, P. V., Assessment of Immunotoxicity of Dextran Coated Ferrite Nanoparticles in Albino Mice. *Molecular Biology International* **2015,** *2015*, 518527.

311.   Szebeni, J.; Moghimi, S. M., Liposome triggering of innate immune responses: a perspective on benefits and adverse reactions. *J Liposome Res* **2009,** *19* (2), 85-90.

312.   Knudsen, K. B.; Northeved, H.; Kumar, P. E.; Permin, A.; Gjetting, T.; Andresen, T. L.; Larsen, S.; Wegener, K. M.; Lykkesfeldt, J.; Jantzen, K.; Loft, S.; Møller, P.; Roursgaard, M., In vivo toxicity of cationic micelles and liposomes. *Nanomedicine* **2015,** *11* (2), 467-77.

313.   Dams, E. T.; Laverman, P.; Oyen, W. J.; Storm, G.; Scherphof, G. L.; van Der Meer, J. W.; Corstens, F. H.; Boerman, O. C., Accelerated blood clearance and altered biodistribution of repeated injections of sterically stabilized liposomes. *J Pharmacol Exp Ther* **2000,** *292* (3), 1071-9.

314.   Kobayashi, N.; Izumi, H.; Morimoto, Y., Review of toxicity studies of carbon nanotubes. *J Occup Health* **2017,** *59* (5), 394-407.

315.   Carnino, J. M.; Lee, H.; Jin, Y., Isolation and characterization of extracellular vesicles from Broncho-alveolar lavage fluid: a review and comparison of different methods. *Respiratory Research* **2019,** *20* (1), 240.

316.   Colombo, M.; Raposo, G.; Théry, C., Biogenesis, secretion, and intercellular interactions of exosomes and other extracellular vesicles. *Annu Rev Cell Dev Biol* **2014,** *30*, 255-89.

317.   Crescitelli, R.; Lässer, C.; Szabó, T. G.; Kittel, A.; Eldh, M.; Dianzani, I.; Buzás, E. I.; Lötvall, J., Distinct RNA profiles in subpopulations of extracellular vesicles: apoptotic bodies, microvesicles and exosomes. *Journal of Extracellular Vesicles* **2013,** *2* (1), 20677.

318.   Becker, A.; Thakur, B. K.; Weiss, J. M.; Kim, H. S.; Peinado, H.; Lyden, D., Extracellular Vesicles in Cancer: Cell-to-Cell Mediators of Metastasis. *Cancer Cell* **2016,** *30* (6), 836-848.

319.   Konoshenko, M. Y.; Lekchnov, E. A.; Vlassov, A. V.; Laktionov, P. P., Isolation of Extracellular Vesicles: General Methodologies and Latest Trends. *BioMed Research International* **2018,** *2018*, 1-27.

320.   Tauro, B. J.; Greening, D. W.; Mathias, R. A.; Ji, H.; Mathivanan, S.; Scott, A. M.; Simpson, R. J., Comparison of ultracentrifugation, density gradient separation, and immunoaffinity capture methods for isolating human colon cancer cell line LIM1863-derived exosomes. *Methods* **2012,** *56* (2), 293-304.

321.   Böing, A. N.; Van Der Pol, E.; Grootemaat, A. E.; Coumans, F. A.; Sturk, A.; Nieuwland, R., Single-step isolation of extracellular vesicles by size-exclusion chromatography. *Journal of extracellular vesicles* **2014,** *3* (1), 23430.

322.   Taylor, D. D.; Shah, S., Methods of isolating extracellular vesicles impact down-stream analyses of their cargoes. *Methods* **2015,** *87*, 3-10.

323.   Andreu, Z.; Rivas, E.; Sanguino-Pascual, A.; Lamana, A.; Marazuela, M.; González-Alvaro, I.; Sánchez-Madrid, F.; de la Fuente, H.; Yáñez-Mó, M., Comparative analysis of EV isolation procedures for miRNAs detection in serum samples. *Journal of extracellular vesicles* **2016,** *5* (1), 31655.

324.   He, M.; Crow, J.; Roth, M.; Zeng, Y.; Godwin, A. K., Integrated immunoisolation and protein analysis of circulating exosomes using microfluidic technology. *Lab on a Chip* **2014,** *14* (19), 3773.

325.   Wan, Y.; Cheng, G.; Liu, X.; Hao, S.-J.; Nisic, M.; Zhu, C.-D.; Xia, Y.-Q.; Li, W.-Q.; Wang, Z.-G.; Zhang, W.-L., Rapid magnetic isolation of extracellular vesicles via lipid-based nanoprobes. *Nature biomedical engineering* **2017,** *1* (4), 1-11.

326.   Yáñez-Mó, M.; Siljander, P. R. M.; Andreu, Z.; Bedina Zavec, A.; Borràs, F. E.; Buzas, E. I.; Buzas, K.; Casal, E.; Cappello, F.; Carvalho, J.; Colás, E.; Cordeiro-Da Silva, A.; Fais, S.; Falcon-Perez, J. M.; Ghobrial, I. M.; Giebel, B.; Gimona, M.; Graner, M.; Gursel, I.; Gursel, M.; Heegaard, N. H. H.; Hendrix, A.; Kierulf, P.; Kokubun, K.; Kosanovic, M.; Kralj-Iglic, V.; Krämer-Albers, E.-M.; Laitinen, S.; Lässer, C.; Lener, T.; Ligeti, E.; Linē, A.; Lipps, G.; Llorente, A.; Lötvall, J.; Manček-Keber, M.; Marcilla, A.; Mittelbrunn, M.; Nazarenko, I.; Nolte-'T Hoen, E. N. M.; Nyman, T. A.; O'Driscoll, L.; Olivan, M.; Oliveira, C.; Pállinger, É.; Del Portillo, H. A.; Reventós, J.; Rigau, M.; Rohde, E.; Sammar, M.; Sánchez-Madrid, F.; Santarém, N.; Schallmoser, K.; Stampe Ostenfeld, M.; Stoorvogel, W.; Stukelj, R.; Van Der Grein, S. G.; Helena Vasconcelos, M.; Wauben, M. H. M.; De Wever, O., Biological properties of extracellular vesicles and their physiological functions. *Journal of Extracellular Vesicles* **2015,** *4* (1), 27066.

327.   Sugano, G.; Bernard-Pierrot, I.; Laé, M.; Battail, C.; Allory, Y.; Stransky, N.; Krumeich, S.; Lepage, M. L.; Maille, P.; Donnadieu, M. H.; Abbou, C. C.; Benhamou, S.; Lebret, T.; Sastre-Garau, X.; Amigorena, S.; Radvanyi, F.; Théry, C., Milk fat globule—epidermal growth factor—factor VIII (MFGE8)/lactadherin promotes bladder tumor development. *Oncogene* **2011,** *30* (6), 642-653.

328.   Hosseinkhani, B.; Kuypers, S.; van den Akker, N. M. S.; Molin, D. G. M.; Michiels, L., Extracellular Vesicles Work as a Functional Inflammatory Mediator Between Vascular Endothelial Cells and Immune Cells. *Front Immunol* **2018,** *9*, 1789-1789.

329.   D'Souza-Schorey, C.; Chavrier, P., ARF proteins: roles in membrane traffic and beyond. *Nature Reviews Molecular Cell Biology* **2006,** *7* (5), 347-358.

330.   Raposo, G.; Stoorvogel, W., Extracellular vesicles: Exosomes, microvesicles, and friends. *Journal of Cell Biology* **2013,** *200* (4), 373-383.

331.   Zhao, K.; Bleackley, M.; Chisanga, D.; Gangoda, L.; Fonseka, P.; Liem, M.; Kalra, H.; Al Saffar, H.; Keerthikumar, S.; Ang, C.-S.; Adda, C. G.; Jiang, L.; Yap, K.; Poon, I. K.; Lock, P.; Bulone, V.; Anderson, M.; Mathivanan, S., Extracellular vesicles secreted by Saccharomyces cerevisiae are involved in cell wall remodelling. *Commun Biol* **2019,** *2*, 305-305.

332.   Borges, F. T.; Reis, L. A.; Schor, N., Extracellular vesicles: structure, function, and potential clinical uses in renal diseases. *Brazilian Journal of Medical and Biological Research* **2013,** *46* (10), 824-830.

333.   Shlomovitz, I.; Speir, M.; Gerlic, M., Flipping the dogma – phosphatidylserine in non-apoptotic cell death. *Cell Communication and Signaling* **2019,** *17* (1), 139.

334.   Baietti, M. F.; Zhang, Z.; Mortier, E.; Melchior, A.; Degeest, G.; Geeraerts, A.; Ivarsson, Y.; Depoortere, F.; Coomans, C.; Vermeiren, E., Syndecan–syntenin–ALIX regulates the biogenesis of exosomes. *Nature cell biology* **2012,** *14* (7), 677-685.

335.   Clayton, A.; Harris, C. L.; Court, J.; Mason, M. D.; Morgan, B. P., Antigen‐presenting cell exosomes are protected from complement‐mediated lysis by expression of CD55 and CD59. *European journal of immunology* **2003,** *33* (2), 522-531.

336.   Barrès, C.; Blanc, L.; Bette-Bobillo, P.; André, S.; Mamoun, R.; Gabius, H.-J.; Vidal, M., Galectin-5 is bound onto the surface of rat reticulocyte exosomes and modulates vesicle uptake by macrophages. *Blood* **2010,** *115* (3), 696-705.

337.   Berda-Haddad, Y.; Robert, S.; Salers, P.; Zekraoui, L.; Farnarier, C.; Dinarello, C. A.; Dignat-George, F.; Kaplanski, G., Sterile inflammation of endothelial cell-derived apoptotic bodies is mediated by interleukin-1α. *Proceedings of the National Academy of Sciences* **2011,** *108* (51), 20684-20689.

338.   MacKenzie, A.; Wilson, H. L.; Kiss-Toth, E.; Dower, S. K.; North, R. A.; Surprenant, A., Rapid secretion of interleukin-1β by microvesicle shedding. *Immunity* **2001,** *15* (5), 825-835.

339.   Baj-Krzyworzeka, M.; WĘGLARCZYK, K.; MYTAR, B.; SZATANEK, R.; BARAN, J.; Zembala, M., Tumour-derived microvesicles contain interleukin-8 and modulate production of chemokines by human monocytes. *Anticancer research* **2011,** *31* (4), 1329-1335.

340.   Truman, L. A.; Ford, C. A.; Pasikowska, M.; Pound, J. D.; Wilkinson, S. J.; Dumitriu, I. E.; Melville, L.; Melrose, L. A.; Ogden, C. A.; Nibbs, R., CX3CL1/fractalkine is released from apoptotic lymphocytes to stimulate macrophage chemotaxis. *Blood, The Journal of the American Society of Hematology* **2008,** *112* (13), 5026-5036.

341.   Kim, K. M.; Abdelmohsen, K.; Mustapic, M.; Kapogiannis, D.; Gorospe, M., RNA in extracellular vesicles. *Wiley Interdisciplinary Reviews: RNA* **2017,** *8* (4), e1413.

342.   Jenjaroenpun, P.; Kremenska, Y.; Nair, V. M.; Kremenskoy, M.; Joseph, B.; Kurochkin, I. V., Characterization of RNA in exosomes secreted by human breast cancer cell lines using next-generation sequencing. *PeerJ* **2013,** *1*, e201.

343.   Batagov, A. O.; Kurochkin, I. V., Exosomes secreted by human cells transport largely mRNA fragments that are enriched in the 3′-untranslated regions. *Biology Direct* **2013,** *8* (1), 12.

344.   Nolte-'t Hoen, E. N. M.; Buermans, H. P. J.; Waasdorp, M.; Stoorvogel, W.; Wauben, M. H. M.; t Hoen, P. A. C., Deep sequencing of RNA from immune cell-derived vesicles uncovers the selective incorporation of small non-coding RNA biotypes with potential regulatory functions. *Nucleic acids research* **2012,** *40* (18), 9272-9285.

345.   Zhang, Y.; Liu, D.; Chen, X.; Li, J.; Li, L.; Bian, Z.; Sun, F.; Lu, J.; Yin, Y.; Cai, X.; Sun, Q.; Wang, K.; Ba, Y.; Wang, Q.; Wang, D.; Yang, J.; Liu, P.; Xu, T.; Yan, Q.; Zhang, J.; Zen, K.; Zhang, C.-Y., Secreted Monocytic miR-150 Enhances Targeted Endothelial Cell Migration. *Molecular Cell* **2010,** *39* (1), 133-144.

346.   Mittelbrunn, M.; Gutiérrez-Vázquez, C.; Villarroya-Beltri, C.; González, S.; Sánchez-Cabo, F.; González, M. Á.; Bernad, A.; Sánchez-Madrid, F., Unidirectional transfer of microRNA-loaded exosomes from T cells to antigen-presenting cells. *Nature Communications* **2011,** *2* (1), 282.

347.   Balaj, L.; Lessard, R.; Dai, L.; Cho, Y.-J.; Pomeroy, S. L.; Breakefield, X. O.; Skog, J., Tumour microvesicles contain retrotransposon elements and amplified oncogene sequences. *Nature Communications* **2011,** *2* (1), 180.

348.   Thakur, B. K.; Zhang, H.; Becker, A.; Matei, I.; Huang, Y.; Costa-Silva, B.; Zheng, Y.; Hoshino, A.; Brazier, H.; Xiang, J.; Williams, C.; Rodriguez-Barrueco, R.; Silva, J. M.; Zhang, W.; Hearn, S.; Elemento, O.; Paknejad, N.; Manova-Todorova, K.; Welte, K.;

Bromberg, J.; Peinado, H.; Lyden, D., Double-stranded DNA in exosomes: a novel biomarker in cancer detection. *Cell Research* **2014,** *24* (6), 766-769.

349.   Guescini, M.; Genedani, S.; Stocchi, V.; Agnati, L. F., Astrocytes and Glioblastoma cells release exosomes carrying mtDNA. *Journal of Neural Transmission* **2010,** *117* (1), 1-4.

350.   Cai, J.; Han, Y.; Ren, H.; Chen, C.; He, D.; Zhou, L.; Eisner, G. M.; Asico, L. D.; Jose, P. A.; Zeng, C., Extracellular vesicle-mediated transfer of donor genomic DNA to recipient cells is a novel mechanism for genetic influence between cells. *J Mol Cell Biol* **2013,** *5* (4), 227-38.

351.   Skotland, T.; Sagini, K.; Sandvig, K.; Llorente, A., An emerging focus on lipids in extracellular vesicles. *Advanced Drug Delivery Reviews* **2020**.

352.   Record, M.; Carayon, K.; Poirot, M.; Silvente-Poirot, S., Exosomes as new vesicular lipid transporters involved in cell-cell communication and various pathophysiologies. *Biochim Biophys Acta* **2014,** *1841* (1), 108-20.

353.   Carayon, K.; Chaoui, K.; Ronzier, E.; Lazar, I.; Bertrand-Michel, J.; Roques, V.; Balor, S.; Terce, F.; Lopez, A.; Salomé, L.; Joly, E., Proteolipidic Composition of Exosomes Changes during Reticulocyte Maturation. *Journal of Biological Chemistry* **2011,** *286* (39), 34426-34439.

354.   Helms, J. B.; Zurzolo, C., Lipids as Targeting Signals: Lipid Rafts and Intracellular Trafficking. *Traffic* **2004,** *5* (4), 247-254.

355.   Kim, C. W.; Lee, H. M.; Lee, T. H.; Kang, C.; Kleinman, H. K.; Gho, Y. S., Extracellular Membrane Vesicles from Tumor Cells Promote Angiogenesis via Sphingomyelin. *Cancer Research* **2002,** *62* (21), 6312-6317.

356.   Tripisciano, C.; Weiss, R.; Eichhorn, T.; Spittler, A.; Heuser, T.; Fischer, M. B.; Weber, V., Different Potential of Extracellular Vesicles to Support Thrombin Generation: Contributions of Phosphatidylserine, Tissue Factor, and Cellular Origin. *Scientific Reports* **2017,** *7* (1), 6522.

357.   Théry, C.; Witwer, K. W.; Aikawa, E.; Alcaraz, M. J.; Anderson, J. D.; Andriantsitohaina, R.; Antoniou, A.; Arab, T.; Archer, F.; Atkin-Smith, G. K.; Ayre, D. C.; Bach, J.-M.; Bachurski, D.; Baharvand, H.; Balaj, L.; Baldacchino, S.; Bauer, N. N.; Baxter, A. A.; Bebawy, M.; Beckham, C.; Bedina Zavec, A.; Benmoussa, A.; Berardi, A. C.; Bergese, P.; Bielska, E.; Blenkiron, C.; Bobis-Wozowicz, S.; Boilard, E.; Boireau, W.; Bongiovanni, A.; Borràs, F. E.; Bosch, S.; Boulanger, C. M.; Breakefield, X.; Breglio, A. M.; Brennan, M. Á.; Brigstock, D. R.; Brisson, A.; Broekman, M. L.; Bromberg, J. F.; Bryl-Górecka, P.; Buch, S.; Buck, A. H.; Burger, D.; Busatto, S.; Buschmann, D.; Bussolati, B.; Buzás, E. I.; Byrd, J. B.; Camussi, G.; Carter, D. R.; Caruso, S.; Chamley, L. W.; Chang, Y.-T.; Chen, C.; Chen, S.; Cheng, L.; Chin, A. R.; Clayton, A.; Clerici, S. P.; Cocks, A.; Cocucci, E.; Coffey, R. J.; Cordeiro-Da-Silva, A.; Couch, Y.; Coumans, F. A.; Coyle, B.; Crescitelli, R.; Criado, M. F.; D'Souza-Schorey, C.; Das, S.; Datta Chaudhuri, A.; De Candia, P.; De Santana, E. F.; De Wever, O.; Del Portillo, H. A.; Demaret, T.; Deville, S.; Devitt, A.; Dhondt, B.; Di Vizio, D.; Dieterich, L. C.; Dolo, V.; Dominguez Rubio, A. P.; Dominici, M.; Dourado, M. R.; Driedonks, T. A.; Duarte, F. V.; Duncan, H. M.; Eichenberger, R. M.; Ekström, K.; El Andaloussi, S.; Elie-Caille, C.; Erdbrügger, U.; Falcón-Pérez, J. M.; Fatima, F.; Fish, J. E.; Flores-Bellver, M.; Försönits, A.; Frelet-Barrand, A.; Fricke, F.; Fuhrmann, G.; Gabrielsson, S.; Gámez-Valero, A.; Gardiner, C.; Gärtner, K.; Gaudin, R.; Gho, Y. S.; Giebel, B.; Gilbert, C.; Gimona, M.; Giusti, I.; Goberdhan, D. C.; Görgens, A.; Gorski, S. M.; Greening, D. W.; Gross, J. C.; Gualerzi, A.; Gupta, G. N.; Gustafson, D.; Handberg, A.; Haraszti, R. A.; Harrison, P.; Hegyesi, H.; Hendrix, A.; Hill, A. F.; Hochberg, F. H.; Hoffmann, K. F.; Holder, B.; Holthofer, H.; Hosseinkhani, B.; Hu, G.; Huang, Y.; Huber, V.; Hunt, S.; Ibrahim, A. G.-E.; Ikezu, T.; Inal, J. M.; Isin, M.; Ivanova, A.; Jackson, H. K.; Jacobsen, S.; Jay, S. M.; Jayachandran, M.; Jenster, G.; Jiang, L.; Johnson, S. M.; Jones, J. C.; Jong, A.; Jovanovic-Talisman, T.; Jung, S.; Kalluri, R.; Kano, S.-I.; Kaur, S.; Kawamura, Y.; Keller, E. T.;

Khamari, D.; Khomyakova, E.; Khvorova, A.; Kierulf, P.; Kim, K. P.; Kislinger, T.; Klingeborn, M.; Klinke, D. J.; Kornek, M.; Kosanović, M. M.; Kovács, Á. F.; Krämer-Albers, E.-M.; Krasemann, S.; Krause, M.; Kurochkin, I. V.; Kusuma, G. D.; Kuypers, S.; Laitinen, S.; Langevin, S. M.; Languino, L. R.; Lannigan, J.; Lässer, C.; Laurent, L. C.; Lavieu, G.; Lázaro-Ibáñez, E.; Le Lay, S.; Lee, M.-S.; Lee, Y. X. F.; Lemos, D. S.; Lenassi, M.; Leszczynska, A.; Li, I. T.; Liao, K.; Libregts, S. F.; Ligeti, E.; Lim, R.; Lim, S. K.; Linē, A.; Linnemannstöns, K.; Llorente, A.; Lombard, C. A.; Lorenowicz, M. J.; Lörincz, Á. M.; Lötvall, J.; Lovett, J.; Lowry, M. C.; Loyer, X.; Lu, Q.; Lukomska, B.; Lunavat, T. R.; Maas, S. L.; Malhi, H.; Marcilla, A.; Mariani, J.; Mariscal, J.; Martens-Uzunova, E. S.; Martin-Jaular, L.; Martinez, M. C.; Martins, V. R.; Mathieu, M.; Mathivanan, S.; Maugeri, M.; McGinnis, L. K.; McVey, M. J.; Meckes, D. G.; Meehan, K. L.; Mertens, I.; Minciacchi, V. R.; Möller, A.; Møller Jørgensen, M.; Morales-Kastresana, A.; Morhayim, J.; Mullier, F.; Muraca, M.; Musante, L.; Mussack, V.; Muth, D. C.; Myburgh, K. H.; Najrana, T.; Nawaz, M.; Nazarenko, I.; Nejsum, P.; Neri, C.; Neri, T.; Nieuwland, R.; Nimrichter, L.; Nolan, J. P.; Nolte-'T Hoen, E. N.; Noren Hooten, N.; O'Driscoll, L.; O'Grady, T.; O'Loghlen, A.; Ochiya, T.; Olivier, M.; Ortiz, A.; Ortiz, L. A.; Osteikoetxea, X.; Østergaard, O.; Ostrowski, M.; Park, J.; Pegtel, D. M.; Peinado, H.; Perut, F.; Pfaffl, M. W.; Phinney, D. G.; Pieters, B. C.; Pink, R. C.; Pisetsky, D. S.; Pogge Von Strandmann, E.; Polakovicova, I.; Poon, I. K.; Powell, B. H.; Prada, I.; Pulliam, L.; Quesenberry, P.; Radeghieri, A.; Raffai, R. L.; Raimondo, S.; Rak, J.; Ramirez, M. I.; Raposo, G.; Rayyan, M. S.; Regev-Rudzki, N.; Ricklefs, F. L.; Robbins, P. D.; Roberts, D. D.; Rodrigues, S. C.; Rohde, E.; Rome, S.; Rouschop, K. M.; Rughetti, A.; Russell, A. E.; Saá, P.; Sahoo, S.; Salas-Huenuleo, E.; Sánchez, C.; Saugstad, J. A.; Saul, M. J.; Schiffelers, R. M.; Schneider, R.; Schøyen, T. H.; Scott, A.; Shahaj, E.; Sharma, S.; Shatnyeva, O.; Shekari, F.; Shelke, G. V.; Shetty, A. K.; Shiba, K.; Siljander, P. R. M.; Silva, A. M.; Skowronek, A.; Snyder, O. L.; Soares, R. P.; Sódar, B. W.; Soekmadji, C.; Sotillo, J.; Stahl, P. D.; Stoorvogel, W.; Stott, S. L.; Strasser, E. F.; Swift, S.; Tahara, H.; Tewari, M.; Timms, K.; Tiwari, S.; Tixeira, R.; Tkach, M.; Toh, W. S.; Tomasini, R.; Torrecilhas, A. C.; Tosar, J. P.; Toxavidis, V.; Urbanelli, L.; Vader, P.; Van Balkom, B. W.; Van Der Grein, S. G.; Van Deun, J.; Van Herwijnen, M. J.; Van Keuren-Jensen, K.; Van Niel, G.; Van Royen, M. E.; Van Wijnen, A. J.; Vasconcelos, M. H.; Vechetti, I. J.; Veit, T. D.; Vella, L. J.; Velot, É.; Verweij, F. J.; Vestad, B.; Viñas, J. L.; Visnovitz, T.; Vukman, K. V.; Wahlgren, J.; Watson, D. C.; Wauben, M. H.; Weaver, A.; Webber, J. P.; Weber, V.; Wehman, A. M.; Weiss, D. J.; Welsh, J. A.; Wendt, S.; Wheelock, A. M.; Wiener, Z.; Witte, L.; Wolfram, J.; Xagorari, A.; Xander, P.; Xu, J.; Yan, X.; Yáñez-Mó, M.; Yin, H.; Yuana, Y.; Zappulli, V.; Zarubova, J.; Žėkas, V.; Zhang, J.-Y.; Zhao, Z.; Zheng, L.; Zheutlin, A. R.; Zickler, A. M.; Zimmermann, P.; Zivkovic, A. M.; Zocco, D.; Zuba-Surma, E. K., Minimal information for studies of extracellular vesicles 2018 (MISEV2018): a position statement of the International Society for Extracellular Vesicles and update of the MISEV2014 guidelines. *Journal of Extracellular Vesicles* **2018,** *7* (1), 1535750.
358.   Green, T. M.; Alpaugh, M. L.; Barsky, S. H.; Rappa, G.; Lorico, A., Breast cancer-derived extracellular vesicles: characterization and contribution to the metastatic phenotype. *BioMed research international* **2015,** *2015*.
359.   Zhang, H.; Freitas, D.; Kim, H. S.; Fabijanic, K.; Li, Z.; Chen, H.; Mark, M. T.; Molina, H.; Martin, A. B.; Bojmar, L.; Fang, J.; Rampersaud, S.; Hoshino, A.; Matei, I.; Kenific, C. M.; Nakajima, M.; Mutvei, A. P.; Sansone, P.; Buehring, W.; Wang, H.; Jimenez, J. P.; Cohen-Gould, L.; Paknejad, N.; Brendel, M.; Manova-Todorova, K.; Magalhães, A.; Ferreira, J. A.; Osório, H.; Silva, A. M.; Massey, A.; Cubillos-Ruiz, J. R.; Galletti, G.; Giannakakou, P.; Cuervo, A. M.; Blenis, J.; Schwartz, R.; Brady, M. S.; Peinado, H.; Bromberg, J.; Matsui, H.; Reis, C. A.; Lyden, D., Identification of distinct nanoparticles and subsets of extracellular vesicles by asymmetric flow field-flow fractionation. *Nature Cell Biology* **2018,** *20* (3), 332-343.

360.	Kanno, K.; Sasaki, S.; Hirata, Y.; Ishikawa, S.-e.; Fushimi, K.; Nakanishi, S.; Bichet, D. G.; Marumo, F., Urinary Excretion of Aquaporin-2 in Patients with Diabetes Insipidus. *New England Journal of Medicine* **1995,** *332* (23), 1540-1545.

361.	Sprague, D. L.; Elzey, B. D.; Crist, S. A.; Waldschmidt, T. J.; Jensen, R. J.; Ratliff, T. L., Platelet-mediated modulation of adaptive immunity: unique delivery of CD154 signal by platelet-derived membrane vesicles. *Blood* **2008,** *111* (10), 5028-36.

362.	Berckmans, R. J.; Sturk, A.; Van Tienen, L. M.; Schaap, M. C. L.; Nieuwland, R., Cell-derived vesicles exposing coagulant tissue factor in saliva. *Blood* **2011,** *117* (11), 3172-3180.

363.	Zhou, Q.; Li, M.; Wang, X.; Li, Q.; Wang, T.; Zhu, Q.; Zhou, X.; Wang, X.; Gao, X.; Li, X., Immune-related microRNAs are abundant in breast milk exosomes. *Int J Biol Sci* **2012,** *8* (1), 118-123.

364.	Arienti, G.; Carlini, E.; Polci, A.; Cosmi, E. V.; Palmerini, C. A., Fatty Acid Pattern of Human Prostasome Lipid. *Archives of Biochemistry and Biophysics* **1998,** *358* (2), 391-395.

365.	de Jong, O. G.; Verhaar, M. C.; Chen, Y.; Vader, P.; Gremmels, H.; Posthuma, G.; Schiffelers, R. M.; Gucek, M.; van Balkom, B. W. M., Cellular stress conditions are reflected in the protein and RNA content of endothelial cell-derived exosomes. *Journal of extracellular vesicles* **2012,** *1*, 10.3402/jev.v1i0.18396.

366.	Demory Beckler, M.; Higginbotham, J. N.; Franklin, J. L.; Ham, A.-J.; Halvey, P. J.; Imasuen, I. E.; Whitwell, C.; Li, M.; Liebler, D. C.; Coffey, R. J., Proteomic analysis of exosomes from mutant KRAS colon cancer cells identifies intercellular transfer of mutant KRAS. *Mol Cell Proteomics* **2013,** *12* (2), 343-355.

367.	Segura, E.; Nicco, C.; Lombard, B. R. R.; VéRon, P.; Raposo, G. A.; Batteux, F. D. R.; Amigorena, S.; ThéRy, C., ICAM-1 on exosomes from mature dendritic cells is critical for efficient naive T-cell priming. *Blood* **2005,** *106* (1), 216-223.

368.	Hessvik, N. P.; Llorente, A., Current knowledge on exosome biogenesis and release. *Cellular and Molecular Life Sciences* **2018,** *75* (2), 193-208.

369.	Johnstone, R. M.; Adam, M.; Hammond, J.; Orr, L.; Turbide, C., Vesicle formation during reticulocyte maturation. Association of plasma membrane activities with released vesicles (exosomes). *Journal of Biological Chemistry* **1987,** *262* (19), 9412-9420.

370.	Marsh, M., Endocytosis. *Oxford University Press* **2001**.

371.	Mellman, I., Endocytosis and molecular sorting. *Annu Rev Cell Dev Biol* **1996,** *12*, 575-625.

372.	Möbius, W.; Ohno-Iwashita, Y.; van Donselaar, E. G.; Oorschot, V. M.; Shimada, Y.; Fujimoto, T.; Heijnen, H. F.; Geuze, H. J.; Slot, J. W., Immunoelectron microscopic localization of cholesterol using biotinylated and non-cytolytic perfringolysin O. *J Histochem Cytochem* **2002,** *50* (1), 43-55.

373.	Wubbolts, R.; Leckie, R. S.; Veenhuizen, P. T. M.; Schwarzmann, G.; Mobius, W.; Hoernschemeyer, J.; Slot, J. W.; Geuze, H. J.; Stoorvogel, W., Proteomic and biochemical analyses of human B cell-derived exosomes - Potential implications for their function and multivesicular body formation. *Journal of Biological Chemistry* **2003,** *278* (13), 10963-10972.

374.	Chandler, M.; Ke, W.; Halman, J. R.; Panigaj, M.; Afonin, K. A., Reconfigurable nucleic acid materials for cancer therapy. In *Nanooncology*, Springer: 2018; pp 365-385.

375.	Colombo, M.; Moita, C.; Van Niel, G.; Kowal, J.; Vigneron, J.; Benaroch, P.; Manel, N.; Moita, L. F.; Théry, C.; Raposo, G., Analysis of ESCRT functions in exosome biogenesis, composition and secretion highlights the heterogeneity of extracellular vesicles. *Journal of Cell Science* **2013,** *126* (24), 5553-5565.

376.	Davies, B. A.; Lee, J. R. E.; Oestreich, A. J.; Katzmann, D. J., Membrane protein targeting to the MVB/lysosome. *Chem Rev* **2009,** *109* (4), 1575-1586.

377.	Baietti, M. F.; Zhang, Z.; Mortier, E.; Melchior, A.; Degeest, G.; Geeraerts, A.; Ivarsson, Y.; Depoortere, F.; Coomans, C.; Vermeiren, E.; Zimmermann, P.; David, G.,

Syndecan-syntenin-ALIX regulates the biogenesis of exosomes. *Nat Cell Biol* **2012,** *14* (7), 677-85.

378.   Airola, M. V.; Hannun, Y. A., Sphingolipid Metabolism and Neutral Sphingomyelinases. In *Sphingolipids: Basic Science and Drug Development*, Gulbins, E.; Petrache, I., Eds. Springer Vienna: Vienna, 2013; pp 57-76.

379.   Castro, B. M.; Prieto, M.; Silva, L. C., Ceramide: A simple sphingolipid with unique biophysical properties. *Progress in Lipid Research* **2014,** *54*, 53-67.

380.   Perez-Hernandez, D.; Gutiérrez-Vázquez, C.; Jorge, I.; López-Martín, S.; Ursa, A.; Sánchez-Madrid, F.; Vázquez, J.; Yáñez-Mó, M., The Intracellular Interactome of Tetraspanin-enriched Microdomains Reveals Their Function as Sorting Machineries toward Exosomes. *Journal of Biological Chemistry* **2013,** *288* (17), 11649-11661.

381.   Zhu, H.; Guariglia, S.; Yu, R. Y.; Li, W.; Brancho, D.; Peinado, H.; Lyden, D.; Salzer, J.; Bennett, C.; Chow, C. W., Mutation of SIMPLE in Charcot-Marie-Tooth 1C alters production of exosomes. *Mol Biol Cell* **2013,** *24* (11), 1619-37, s1-3.

382.   Villarroya-Beltri, C.; Baixauli, F.; Gutiérrez-Vázquez, C.; Sánchez-Madrid, F.; Mittelbrunn, M., Sorting it out: Regulation of exosome loading. *Seminars in Cancer Biology* **2014,** *28*, 3-13.

383.   Fader, C. M.; Sánchez, D.; Furlán, M.; Colombo, M. I., Induction of autophagy promotes fusion of multivesicular bodies with autophagic vacuoles in k562 cells. *Traffic* **2008,** *9* (2), 230-250.

384.   Villarroya-Beltri, C.; Baixauli, F.; Mittelbrunn, M.; Fernández-Delgado, I.; Torralba, D.; Moreno-Gonzalo, O.; Baldanta, S.; Enrich, C.; Guerra, S.; Sánchez-Madrid, F., ISGylation controls exosome secretion by promoting lysosomal degradation of MVB proteins. *Nature communications* **2016,** *7* (1), 1-11.

385.   Sönnichsen, B.; De Renzis, S.; Nielsen, E.; Rietdorf, J.; Zerial, M., Distinct Membrane Domains on Endosomes in the Recycling Pathway Visualized by Multicolor Imaging of Rab4, Rab5, and Rab11. *Journal of Cell Biology* **2000,** *149* (4), 901-914.

386.   Hsu, C.; Morohashi, Y.; Yoshimura, S.-i.; Manrique-Hoyos, N.; Jung, S.; Lauterbach, M. A.; Bakhti, M.; Grønborg, M.; Möbius, W.; Rhee, J.; Barr, F. A.; Simons, M., Regulation of exosome secretion by Rab35 and its GTPase-activating proteins TBC1D10A–C. *Journal of Cell Biology* **2010,** *189* (2), 223-232.

387.   Ostrowski, M.; Carmo, N. B.; Krumeich, S.; Fanget, I.; Raposo, G.; Savina, A.; Moita, C. F.; Schauer, K.; Hume, A. N.; Freitas, R. P.; Goud, B.; Benaroch, P.; Hacohen, N.; Fukuda, M.; Desnos, C.; Seabra, M. C.; Darchen, F.; Amigorena, S.; Moita, L. F.; Thery, C., Rab27a and Rab27b control different steps of the exosome secretion pathway. *Nature Cell Biology* **2010,** *12* (1), 19-30.

388.   Record, M.; Carayon, K.; Poirot, M.; Silvente-Poirot, S., Exosomes as new vesicular lipid transporters involved in cell–cell communication and various pathophysiologies. *Biochimica et Biophysica Acta (BBA) - Molecular and Cell Biology of Lipids* **2014,** *1841* (1), 108-120.

389.   Fader, C. M.; Sánchez, D. G.; Mestre, M. B.; Colombo, M. I., TI-VAMP/VAMP7 and VAMP3/cellubrevin: two v-SNARE proteins involved in specific steps of the autophagy/multivesicular body pathways. *Biochimica et Biophysica Acta (BBA) - Molecular Cell Research* **2009,** *1793* (12), 1901-1916.

390.   Segura, E.; Nicco, C.; Lombard, B.; Véron, P.; Raposo, G.; Batteux, F.; Amigorena, S.; Théry, C., ICAM-1 on exosomes from mature dendritic cells is critical for efficient naive T-cell priming. *Blood* **2005,** *106* (1), 216-223.

391.   Nazarenko, I.; Rana, S.; Baumann, A.; McAlear, J.; Hellwig, A.; Trendelenburg, M.; Lochnit, G.; Preissner, K. T.; Zöller, M., Cell Surface Tetraspanin Tspan8 Contributes to Molecular Pathways of Exosome-Induced Endothelial Cell Activation. *Cancer Research* **2010,** *70* (4), 1668-1678.

392.	Klibi, J.; Niki, T.; Riedel, A.; Pioche-Durieu, C.; Souquere, S.; Rubinstein, E.; Le Moulec, S.; Guigay, J.; Hirashima, M.; Guemira, F.; Adhikary, D.; Mautner, J.; Busson, P., Blood diffusion and Th1-suppressive effects of galectin-9-containing exosomes released by Epstein-Barr virus-infected nasopharyngeal carcinoma cells. *Blood* **2009,** *113* (9), 1957-66.

393.	Denzer, K.; van Eijk, M.; Kleijmeer, M. J.; Jakobson, E.; de Groot, C.; Geuze, H. J., Follicular dendritic cells carry MHC class II-expressing microvesicles at their surface. *The Journal of Immunology* **2000,** *165* (3), 1259-1265.

394.	Parolini, I.; Federici, C.; Raggi, C.; Lugini, L.; Palleschi, S.; De Milito, A.; Coscia, C.; Iessi, E.; Logozzi, M.; Molinari, A.; Colone, M.; Tatti, M.; Sargiacomo, M.; Fais, S., Microenvironmental pH is a key factor for exosome traffic in tumor cells. *The Journal of biological chemistry* **2009,** *284* (49), 34211-34222.

395.	Tian, T.; Wang, Y.; Wang, H.; Zhu, Z.; Xiao, Z., Visualizing of the cellular uptake and intracellular trafficking of exosomes by live‐cell microscopy. *Journal of cellular biochemistry* **2010,** *111* (2), 488-496.

396.	Saeedi, S.; Israel, S.; Nagy, C.; Turecki, G., The emerging role of exosomes in mental disorders. *Translational Psychiatry* **2019,** *9* (1), 122.

397.	Feng, D.; Zhao, W. L.; Ye, Y. Y.; Bai, X. C.; Liu, R. Q.; Chang, L. F.; Zhou, Q.; Sui, S. F., Cellular internalization of exosomes occurs through phagocytosis. *Traffic* **2010,** *11* (5), 675-87.

398.	Marcus, M. E.; Leonard, J. N., FedExosomes: Engineering Therapeutic Biological Nanoparticles that Truly Deliver. *Pharmaceuticals (Basel)* **2013,** *6* (5), 659-680.

399.	De Jong, O. G.; Van Balkom, B. W. M.; Schiffelers, R. M.; Bouten, C. V. C.; Verhaar, M. C., Extracellular Vesicles: Potential Roles in Regenerative Medicine. *Front Immunol* **2014,** *5*.

400.	Milosevits, G.; Szebeni, J.; Krol, S., Exosomes: potential model for complement-stealth delivery systems. *European Journal of Nanomedicine* **2015,** *7* (3), 207.

401.	Milosevits, G.; Szebeni, J.; Krol, S., Exosomes: potential model for complement-stealth delivery systems. *European Journal of Nanomedicine* **2015,** *7* (3).

402.	Zhu, X.; Badawi, M.; Pomeroy, S.; Sutaria, D. S.; Xie, Z.; Baek, A.; Jiang, J.; Elgamal, O. A.; Mo, X.; Perle, K. L.; Chalmers, J.; Schmittgen, T. D.; Phelps, M. A., Comprehensive toxicity and immunogenicity studies reveal minimal effects in mice following sustained dosing of extracellular vesicles derived from HEK293T cells. *Journal of extracellular vesicles* **2017,** *6* (1), 1324730-1324730.

403.	Zhu, X.; Badawi, M.; Pomeroy, S.; Sutaria, D. S.; Xie, Z.; Baek, A.; Jiang, J.; Elgamal, O. A.; Mo, X.; Perle, K. L.; Chalmers, J.; Schmittgen, T. D.; Phelps, M. A., Comprehensive toxicity and immunogenicity studies reveal minimal effects in mice following sustained dosing of extracellular vesicles derived from HEK293T cells. *Journal of Extracellular Vesicles* **2017,** *6* (1), 1324730.

404.	Yin, W.; Ouyang, S.; Li, Y.; Xiao, B.; Yang, H., Immature dendritic cell-derived exosomes: a promise subcellular vaccine for autoimmunity. *Inflammation* **2013,** *36* (1), 232-40.

405.	Théry, C.; Zitvogel, L.; Amigorena, S., Exosomes: composition, biogenesis and function. *Nature Reviews Immunology* **2002,** *2* (8), 569-579.

406.	Théry, C., Exosomes: secreted vesicles and intercellular communications. *F1000 Biol Rep* **2011,** *3*, 15-15.

407.	Zhang, B.; Yeo, R. W. Y.; Lai, R. C.; Sim, E. W. K.; Chin, K. C.; Lim, S. K., Mesenchymal stromal cell exosome-enhanced regulatory T-cell production through an antigen-presenting cell-mediated pathway. *Cytotherapy* **2018,** *20* (5), 687-696.

408.	Hedlund, M.; Stenqvist, A. C.; Nagaeva, O.; Kjellberg, L.; Wulff, M.; Baranov, V.; Mincheva-Nilsson, L., Human placenta expresses and secretes NKG2D ligands via exosomes that down-modulate the cognate receptor expression: evidence for immunosuppressive function. *J Immunol* **2009,** *183* (1), 340-51.

409.	Escudier, B.; Dorval, T.; Chaput, N.; André, F.; Caby, M.-P.; Novault, S.; Flament, C.; Leboulaire, C.; Borg, C.; Amigorena, S.; Boccaccio, C.; Bonnerot, C.; Dhellin, O.; Movassagh, M.; Piperno, S.; Robert, C.; Serra, V.; Valente, N.; Le Pecq, J.-B.; Spatz, A.; Lantz, O.; Tursz, T.; Angevin, E.; Zitvogel, L., Vaccination of metastatic melanoma patients with autologous dendritic cell (DC) derived-exosomes: results of thefirst phase I clinical trial. *Journal of Translational Medicine* **2005,** *3* (1), 10.

410.	Morelli, A. E.; Larregina, A. T.; Shufesky, W. J.; Sullivan, M. L. G.; Stolz, D. B.; Papworth, G. D.; Zahorchak, A. F.; Logar, A. J.; Wang, Z.; Watkins, S. C.; Falo, L. D.; Thomson, A. W., Endocytosis, intracellular sorting, and processing of exosomes by dendritic cells. *Blood* **2004,** *104* (10), 3257-3266.

411.	Saunderson, S. C.; Dunn, A. C.; Crocker, P. R.; McLellan, A. D., CD169 mediates the capture of exosomes in spleen and lymph node. *Blood* **2014,** *123* (2), 208-16.

412.	Zech, D.; Rana, S.; Büchler, M. W.; Zöller, M., Tumor-exosomes and leukocyte activation: an ambivalent crosstalk. *Cell Commun Signal* **2012,** *10* (1), 37.

413.	Murphy, D. E.; de Jong, O. G.; Brouwer, M.; Wood, M. J.; Lavieu, G.; Schiffelers, R. M.; Vader, P., Extracellular vesicle-based therapeutics: natural versus engineered targeting and trafficking. *Experimental & Molecular Medicine* **2019,** *51* (3), 1-12.

414.	Koh, E.; Lee, E. J.; Nam, G. H.; Hong, Y.; Cho, E.; Yang, Y.; Kim, I. S., Exosome-SIRPα, a CD47 blockade increases cancer cell phagocytosis. *Biomaterials* **2017,** *121*, 121-129.

415.	Kamerkar, S.; LeBleu, V. S.; Sugimoto, H.; Yang, S.; Ruivo, C. F.; Melo, S. A.; Lee, J. J.; Kalluri, R., Exosomes facilitate therapeutic targeting of oncogenic KRAS in pancreatic cancer. *Nature* **2017,** *546* (7659), 498-503.

416.	Agrawal, M.; Ajazuddin; Tripathi, D. K.; Saraf, S.; Saraf, S.; Antimisiaris, S. G.; Mourtas, S.; Hammarlund-Udenaes, M.; Alexander, A., Recent advancements in liposomes targeting strategies to cross blood-brain barrier (BBB) for the treatment of Alzheimer's disease. *J Control Release* **2017,** *260*, 61-77.

417.	Ha, D.; Yang, N.; Nadithe, V., Exosomes as therapeutic drug carriers and delivery vehicles across biological membranes: current perspectives and future challenges. *Acta Pharm Sin B* **2016,** *6* (4), 287-296.

418.	Lai, C. P.; Mardini, O.; Ericsson, M.; Prabhakar, S.; Maguire, C.; Chen, J. W.; Tannous, B. A.; Breakefield, X. O., Dynamic biodistribution of extracellular vesicles in vivo using a multimodal imaging reporter. *ACS Nano* **2014,** *8* (1), 483-494.

419.	Rashid, M. H.; Borin, T. F.; Ara, R.; Angara, K.; Cai, J.; Achyut, B. R.; Liu, Y.; Arbab, A. S., Differential in vivo biodistribution of (131)I-labeled exosomes from diverse cellular origins and its implication for theranostic application. *Nanomedicine* **2019,** *21*, 102072.

420.	Banfai, K.; Garai, K.; Ernszt, D.; Pongracz, J. E.; Kvell, K., Transgenic Exosomes for Thymus Regeneration. *Front Immunol* **2019,** *10*, 862-862.

421.	Jung, K. O.; Jo, H.; Yu, J. H.; Gambhir, S. S.; Pratx, G., Development and MPI tracking of novel hypoxia-targeted theranostic exosomes. *Biomaterials* **2018,** *177*, 139-148.

422.	Cui, G. H.; Guo, H. D.; Li, H.; Zhai, Y.; Gong, Z. B.; Wu, J.; Liu, J. S.; Dong, Y. R.; Hou, S. X.; Liu, J. R., RVG-modified exosomes derived from mesenchymal stem cells rescue memory deficits by regulating inflammatory responses in a mouse model of Alzheimer's disease. *Immun Ageing* **2019,** *16*, 10.

423.	Liang, G.; Zhu, Y.; Ali, D. J.; Tian, T.; Xu, H.; Si, K.; Sun, B.; Chen, B.; Xiao, Z., Engineered exosomes for targeted co-delivery of miR-21 inhibitor and chemotherapeutics to reverse drug resistance in colon cancer. *J Nanobiotechnology* **2020,** *18* (1), 10.

424.	Barile, L.; Vassalli, G., Exosomes: Therapy delivery tools and biomarkers of diseases. *Pharmacol Ther* **2017,** *174*, 63-78.

425.	Kibria, G.; Ramos, E. K.; Wan, Y.; Gius, D. R.; Liu, H., Exosomes as a Drug Delivery System in Cancer Therapy: Potential and Challenges. *Mol Pharm* **2018,** *15* (9), 3625-3633.

426.   Alvarez-Erviti, L.; Seow, Y.; Yin, H.; Betts, C.; Lakhal, S.; Wood, M. J., Delivery of siRNA to the mouse brain by systemic injection of targeted exosomes. *Nat Biotechnol* **2011,** *29* (4), 341-5.

427.   Wahlgren, J.; Karlson, T. D. L.; Brisslert, M.; Vaziri Sani, F.; Telemo, E.; Sunnerhagen, P.; Valadi, H., Plasma exosomes can deliver exogenous short interfering RNA to monocytes and lymphocytes. *Nucleic Acids Research* **2012,** *40* (17), e130-e130.

428.   Shtam, T. A.; Kovalev, R. A.; Varfolomeeva, E.; Makarov, E. M.; Kil, Y. V.; Filatov, M. V., Exosomes are natural carriers of exogenous siRNA to human cells in vitro. *Cell Communication and Signaling* **2013,** *11* (1), 88.

429.   Banizs, A. B.; Huang, T.; Dryden, K.; Berr, S. S.; Stone, J. R.; Nakamoto, R. K.; Shi, W.; He, J., In vitro evaluation of endothelial exosomes as carriers for small interfering ribonucleic acid delivery. *International journal of nanomedicine* **2014,** *9*, 4223-4230.

430.   El-Andaloussi, S.; Lee, Y.; Lakhal-Littleton, S.; Li, J.; Seow, Y.; Gardiner, C.; Alvarez-Erviti, L.; Sargent, I. L.; Wood, M. J. A., Exosome-mediated delivery of siRNA in vitro and in vivo. *Nature Protocols* **2012,** *7* (12), 2112-2126.

431.   Pegtel, D. M.; Cosmopoulos, K.; Thorley-Lawson, D. A.; Van Eijndhoven, M. A. J.; Hopmans, E. S.; Lindenberg, J. L.; De Gruijl, T. D.; Wurdinger, T.; Middeldorp, J. M., Functional delivery of viral miRNAs via exosomes. *Proceedings of the National Academy of Sciences* **2010,** *107* (14), 6328-6333.

432.   Ohno, S.-i.; Takanashi, M.; Sudo, K.; Ueda, S.; Ishikawa, A.; Matsuyama, N.; Fujita, K.; Mizutani, T.; Ohgi, T.; Ochiya, T.; Gotoh, N.; Kuroda, M., Systemically injected exosomes targeted to EGFR deliver antitumor microRNA to breast cancer cells. *Mol Ther* **2013,** *21* (1), 185-191.

433.   Pi, F.; Binzel, D. W.; Lee, T. J.; Li, Z.; Sun, M.; Rychahou, P.; Li, H.; Haque, F.; Wang, S.; Croce, C. M.; Guo, B.; Evers, B. M.; Guo, P., Nanoparticle orientation to control RNA loading and ligand display on extracellular vesicles for cancer regression. *Nature nanotechnology* **2018,** *13* (1), 82-89.

434.   Chen, N.; Xia, P.; Li, S.; Zhang, T.; Wang, T. T.; Zhu, J., RNA sensors of the innate immune system and their detection of pathogens. *IUBMB Life* **2017**, 69 (5), 297-304.

2   Chapter 2: RNA–DNA fibers and polygons with controlled immunrecognition activate RNAi, FRET and transcriptional regulation of NF-κB human cells

2.1   Introduction

Various nucleic acids that are natural, rationally designed, or selected by directed evolution can be used to manipulate biological systems and therapeutically utilized to downregulate gene expression (e.g. siRNAs), target receptors (e.g. aptamers), cleave RNAs (e.g. ribozymes), or antagonize transcription (e.g. DNA decoys)[1-3]. The potential of therapeutic nucleic acids (TNAs) becomes apparent from a recent inspiring example of the very first RNA interference therapeutic agent approved by FDA[4] and from many studies showing versatility, programmability, and modularity of TNAs[5-7]. In addition, TNAs have intrinsic immunomodulatory properties based on the ability of human cells to discriminate self from non-self oligonucleotides and trigger innate immune responses. The size, sequence and composition of TNAs contribute to their immunorecognition[8]. While the level of immune response can adversely affect the therapeutic benefit of applied TNAs, the controlled immunostimulation by nucleic acids can be used synergistically as an adjuvant[9, 10]. Due to the programmability of RNA and DNA, we can design their nanoassemblies with controllable physicochemical and immunogenic potential[11-18]. Recently, we demonstrated that the composition of nucleic acid nanoparticles (NANPs) affects the outcome of their immune response[11, 12], and while RNA NANPs stimulate the production of interferons and some pro-inflammatory cytokines, we found that DNA analogs, in most cases, stay immunoquiescent[11-13].

NANPs that can respond to temperature, pH changes, light, small molecules, or the presence of oligonucleotides represent an additional level of functional control[19-22] by performing preprogrammed logical operations. For example, the potential therapeutic application of rationally designed RNA logic gates was exemplified by two-stranded RNA switches. These switches were designed to bind an intracellular mRNA (disease marker), initiate conformational changes, and release therapeutically relevant short hairpin RNAs,

further activating an RNAi pathway[23]. Cell-specific delivery and conditional release of therapeutic cargo was demonstrated by DNA 'nanorobots' activated by simultaneous recognition of key proteins; interactions of aptamers with specific cell-surface receptors dissociated the locking duplexes, exposing the cargo otherwise hidden inside the nanorobot[24]. In a similar manner, a DNA robotic device was recently shown to expose a thrombin after interaction with nucleolin on the surface of the tumor vessels in vivo[25].

Another strategy for the conditional activation of multiple functionalities is demonstrated by nucleic acid–based assemblies that communicate with each other through sequence complementarity[11, 14, 15, 26-33]. The strategy is based on cognate pairs of RNA–DNA hybrids that trigger the activation of different functionalities both in vitro and in vivo. The central idea is to split the functional entities (e.g. RNA aptamers, a Förster resonance energy transfer (FRET) pair of dyes, DNA templates for in vitro transcription, siRNAs, etc.) into two inactive RNA–DNA hybrids. The cognate pair of hybrids is equipped with complementary ssDNA or ssRNA toeholds designed to promote the reassociation of the inactive hybrids via preprogrammed isothermal strand displacements, which restores the intended function. Although up to seven active siRNAs can be released from a single pair of hybrids, the resulting byproduct - long dsDNAs - becomes immunostimulatory[14]. We could avoid the formation of long dsDNAs while still maintaining a higher number of split functionalities by embedding up to six hybrids in various RNA and DNA nanoparticles and mixing them with cognate hybrids[15, 28, 29, 31]. This technique, however, requires the simultaneous presence of seven assemblies and may be inefficient due to potential problems with intracellular compartmentalization. Recently, we introduced a strategy that relies on interdependent complementary NANPs that require the presence of only one cognate partner for intracellular activation of multiple functionalities[11]. However, combining the simple design of conditionally activated NANPs with the maximal capacity for split functionalities, minimal immunotoxicity and removal of byproduct dsDNAs remained a major challenge.

Here, we introduce a simplified and user-friendly approach that allows for conditional activation of RNAi while blocking the transcription of pro-inflammatory genes forming intracellular dsDNAs. Our system is based on a pair of rationally designed RNA–DNA hybrid constructs that, upon mutual recognition in the cytoplasm, give a fluorescent response and release a large number of Dicer substrate (DS) RNAs[34] and short dsDNAs with embedded NF-κB decoys[35-38]. NF-κB (nuclear factor kappa-light-chain-enhancer of activated B cells) is expressed in most mammalian cells and remains inactive in the cytoplasm when bound to inhibitory proteins (IκB). There are two classes of NF-κB proteins, and both classes contain the N-terminal DNA-binding domain, which serves as a dimerization interface to other transcription factors as well as the binding site of IκB[39, 40]. NF-κB can be activated by various stimuli that lead to phosphorylation and subsequent degradation of the IκB, followed by translocation of NF-κB to the nucleus, where it binds to a consensus sequence in the promoter regions of target genes. NF-κB activation can be altered through either IκB overexpression or the introduction of synthetic DNA decoys with a high binding affinity for NF-κB. The NF-κB bound to decoys cannot translocate to the nucleus; consequently, production of pro-inflammatory cytokines becomes limited.

Our system offers multiple advantages, including: (i) very simple design and assembly protocols that significantly lower the production costs and shorten the experimental time; (ii) released dsDNAs that are no longer nonfunctional byproducts, as well as embedded NF-κB decoys that restrain the immunostimulatory responses; (iii) the ability to change the shapes of the hybrids from long fibers to closed polygons by simply changing the orientation of DNA–DNA interacting parts, which in turn leads to distinguished physiochemical and immunological properties. In addition, such a novel strategy increases the control over the precise knockdown of a specific protein and allows the activation of other functionalities, such as FRET, that can be used for real-time intracellular tracking of reassociation.

2.2 Methods

2.2.1 Design of RNA–DNA fibers and polygons

The schematic explanation of the main design principles used for constructing RNA–

DNA fibers and polygons is shown in Figure 11. The correct base pairing was confirmed with

NUPACK.

2.2.2 Assemblies of hybrid RNA–DNA fibers and polygons and their analysis by native-PAGE

All individual oligonucleotides were purchased from Integrated DNA Technologies, Inc.

Fibers and polygons were assembled by combining individual monomers at equimolar
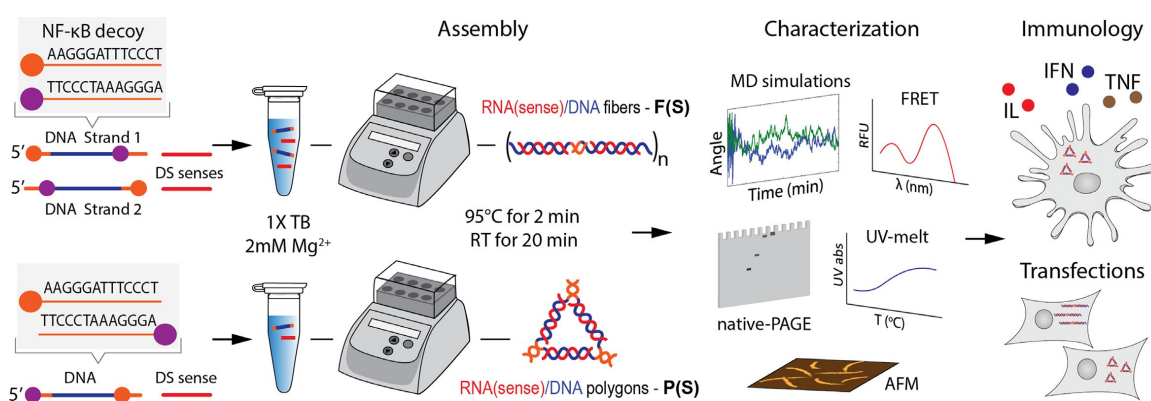
Figure 11. Design principles of RNA–DNA fibers and polygons carring DS RNA sense strands. DNA pieces in blue are reverse complements for DS sense, and pieces in orange are NF-kB decoy-based toeholds (colored balls indicate orientations of the DNA-DNA interactions). Fibers and polygons with antisense strands are designed as their reverse complements.

concentrations. Assemblies and their reassociations were analyzed on 8% non-denaturing native

polyacrylamide (19:1) gel electrophoresis (native-PAGE). A Bio-Rad ChemiDoc MP Imager was

used to visualize gels stained with ethidium bromide and view the fluorescence of labeled RNAs.

All assemblies were further tested for the presence of bacterial endotoxins by kinetic turbidity

limulus amoebocyte lysate (LAL) assay, as detailed in our previous work[42] (Table 1).

2.2.3 Ultraviolet melting experiments

Temperature-dependent absorption spectra were recorded at 260 nm on an Agilent

spectrophotometer (Agilent, Inc.) equipped with a thermoelectrically controlled cell holder.

2.2.4 Kinetics of reassociation

To determine the kinetics, fluorescently labeled fibers (polygons) were mixed with equimolar cognate partners and aliquoted at set time points. Results were analyzed by native-PAGE using the ChemiDoc MP System.

Table 2: Physicochemical parameters measured for fibers and polygons tested in this work. Endotoxin was measured by kinetic turbidity LAL assay using a Pyros Kinetix Flex instrument (Associates of Cape Cod, East Falmouth, MA). Acceptance criteria was endotoxin < 0.05 EU/mL in 1 μM stocks of assemblies. According to the United States Pharmacopoeia, the results of endotoxin testing by LAL are valid if endotoxin spike recover is between 50 and 200%.

Assembly	T_{m1}, T_{m2} (°C)	Endotoxin,(EU/ml)	Endotoxin Spike Recovery (%)
P(A)	43.8±3; 81.5±2	<0.05	109
P(S)	44±5; 84±2	<0.05	122
F(A)	45.5±4; 80.2±2.5	<0.05	153
F(S)	48.2±3; 78.3±3.5	<0.05	162

2.2.5 Blood stability

Fibers (polygons) containing Alexa® 546-labeled RNAs were mixed with 10% (v/v) human blood serum. The mixtures were analyzed by 8% native-PAGE. The bands of treated samples were visualized with the ChemiDoc MP System and analyzed using the complementary Image Lab™ Software.

2.2.6 Atomic force microscopy (AFM) imaging

A freshly cleaved mica surface was modified with APS (1- (3-aminopropyl) silatrane) according to the established protocol[11,12,43] and used for AFM imaging performed on the MultiMode AFM NanoScope IV system (Bruker Instruments, Santa Barbara, CA) in tapping mode. Images were processed by the FemtoScan Online software package (Advanced Technologies Center, Moscow, Russia) [44, 45].

2.2.7 Primary human peripheral blood mononuclear cells (PBMCs) and whole-blood culture for analysis of interferon and cytokine secretion

The blood was used within 2 h of collection. Whole-blood cultures were performed to analyze the induction of chemokines and cytokines, while PBMC cultures were used for the analysis of type I interferons. Supernatants were analyzed using a chemiluminescence-based multiplex system (Quansys, Logan, UT, USA). Two independent repeats were prepared for each

sample and tested in at least three different donors.

2.2.8 Reporter cell-based assay

HEK-Blue hTLR4 cells (Invivogen, San Diego, CA, USA) were used to assess the functionality of NF-κB decoy oligonucleotides. These cells are engineered to express both human Toll-like receptor (TLR) 4 and, under NF-κB promoter, secreted alkaline phosphatase (SEAP).

2.2.9 Activation of FRET

To determine the reassociation of RNA–DNA assemblies in vitro, FRET measurements were performed using a FluoroMax-3 (Jobin Yvon, Horiba). The excitation wavelength was set at 460 nm and the excitation and emission slit widths were set at 5 nm. To track the reassociation of RNA–DNA assemblies in cells, FRET measurements were performed using an LSM 710 confocal microscope (Carl Zeiss) with a 63×, 1.4 NA magnification lens.

2.2.10 Transfection of human breast cancer cells expressing green fluorescent protein (MDA-MB-231/GFP

MDA-MB-231/GFP cells were used to assay the delivery of functional fibers and polygons. All transfections were performed using Lipofectamine® 2000 (L2K).

2.2.11 Analysis of cell death and cell cycle by propidium iodide staining and flow cytometry

A375 melanoma cells were incubated with transfection complexes prepared in Opti-MEM serum-free medium (Gibco) with Lipofectamine RNAiMAX (Thermo Fisher Scientific) and fibers. Transfected cells were incubated with propidium iodide solution (200 μg/ml RNase A, 0.1% v:v Triton X-100, 20 μg/ml P), and fluorescence was measured by flow cytometry using the Attune NxT cytometer (Life Technologies) to determine the percentage of hypodiploid cells (cell death, subG1 phase) and the cell cycle (G0/G1 and S/G2/M phases)..

2.2.12 Western blot

After the transfection of A375 melanoma cells with fibers, the cells were trypsinized and centrifuged. The cell pellet was dispersed in cell lysis buffer, the homogenate was centrifuged, and the protein content of supernatant was analyzed using primary anti-*BRAF* antibody (SantaCruz)

and peroxidase-conjugated secondary antibody.

2.2.13 Immunofluorescence analysis for detection of NF-κB

Transfected A375 melanoma cells were treated with lipopolysaccharide (LPS); incubated

overnight with an anti-NF-κB, p65 subunit (MAB3026, Millipore, 1:100) antibody; then incubated

with an Alexa Fluor® 488- conjugated secondary antibody (Molecular Probes, 1:1000) and Hoechst

(Sigma-Aldrich, 25 µg/ml). The fluorescence microscope EVOS FL Auto Imaging System

(Thermo Fisher Scientific) was used for visualization.

2.2.14 Statistical analysis

All results were presented as mean SD of at least three independent experiments.

Statistical analyses were performed using one-way analysis of variance (ANOVA) conducted with

the GraphPad Prism software. Differences were considered statistically significant with a P-value

of <0.05.

2.3 Results and Discussion

Recently, we reported a new concept of interdependent self- recognizing nucleic acid-based

NANPs that can conditionally activate multiple functionalities in human cancer cells11. Here, we

offer a new, simplified technology by designing a set of dynamic RNA–DNA fibers and polygons

that can interact inside the cells to release a large number of DS RNAs, give a fluorescent response,

and activate NF-kB decoys. The design rationale was based on separating DS RNAs and

substituting each strand with complementary DNAs. The DNA–NF-kB decoy duplex was also

separated, and the individual sequences were added to both ends of complementary DNAs and used

as toeholds for assemblies (Figure 11). We found that a simple change in the orientation of one

sequence by 180∘ promotes the formation of either fibers or polygon structures (Figure 12). When

complementary hybrid structures are introduced in close proximity inside the cells, the

thermodynamically driven isothermal reassociation initiates the release of DS RNAs and NF-κB
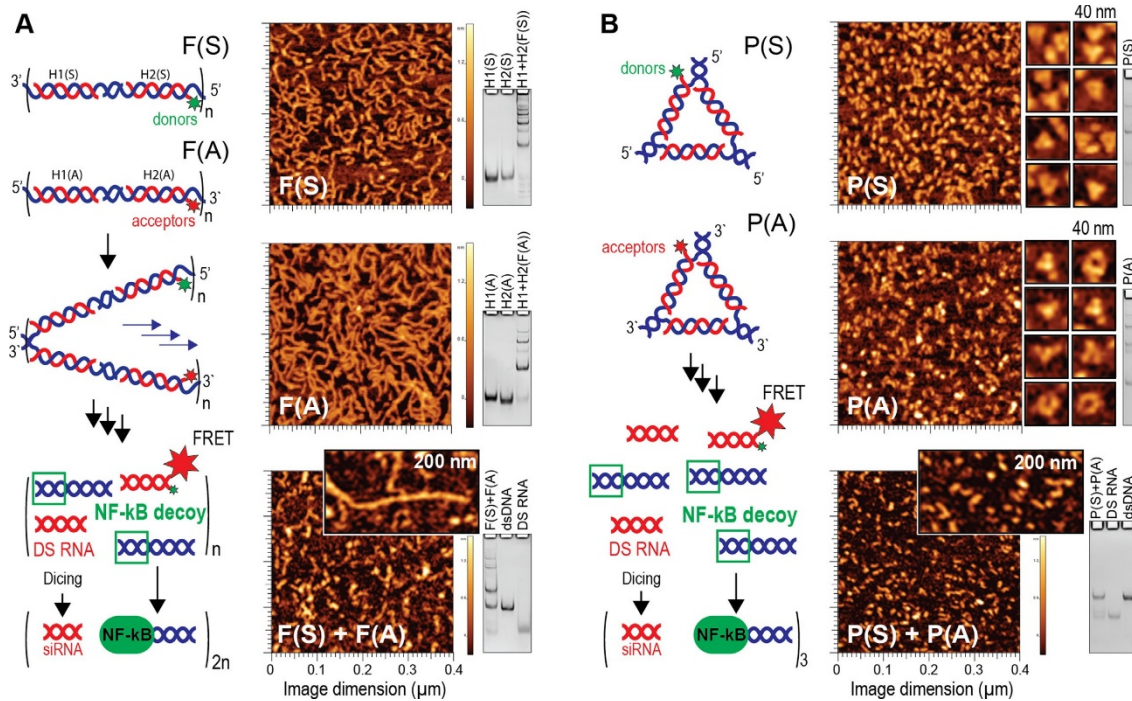
Figure 12. Schematic representation and experimentally verified formation of RNA–DNA hybrid fibers (A) and polygons (B) and their reassociation that results in release of NF-κB decoys and DS RNAs. NF-κB decoys must fit the groove of NF-κB in order to bind it[77]; consequently, the reassociation is needed to release the decoys from the bulky structures of the assemblies. Native-PAGE and AFM confirm the formation of fibers and polygons and their reassociation products.

decoys and activates FRET. The formation of fibers and polygons, along with their further reassociation, was confirmed by native-PAGE and visualized by AFM (Figure 12 and 13). The AFM images showed distinct structures of either fibers or polygons, with polygons being present primarily in a triangle shape. Both AFM and native-PAGE confirmed the release of DS RNAs and DNA duplexes when cognate assemblies were incubated together. Aside from the difference in their morphology, fibers and polygons possessed different physicochemical properties and reassociation times (Figure 14). A kinetics study showed that polygons re-associated much faster than fibers: polygons required <30 min to complete the reassociation, while fibers required up to 5h of incubation (Figure 14A). Importantly, preincubation of individual fibers with Lipofectamine 2000 (L2K), that would mimic later described transfection experiments, prevented fibers' re-association (Figure 14B). These results are consistent with previously reported studies[33, 46]. The blood stability assays also showed a longer retention time for fibers

compared to polygons and both RNA/DNA hybrid constructs being more stable for digestion

when compared to RNA (Figure 14C).
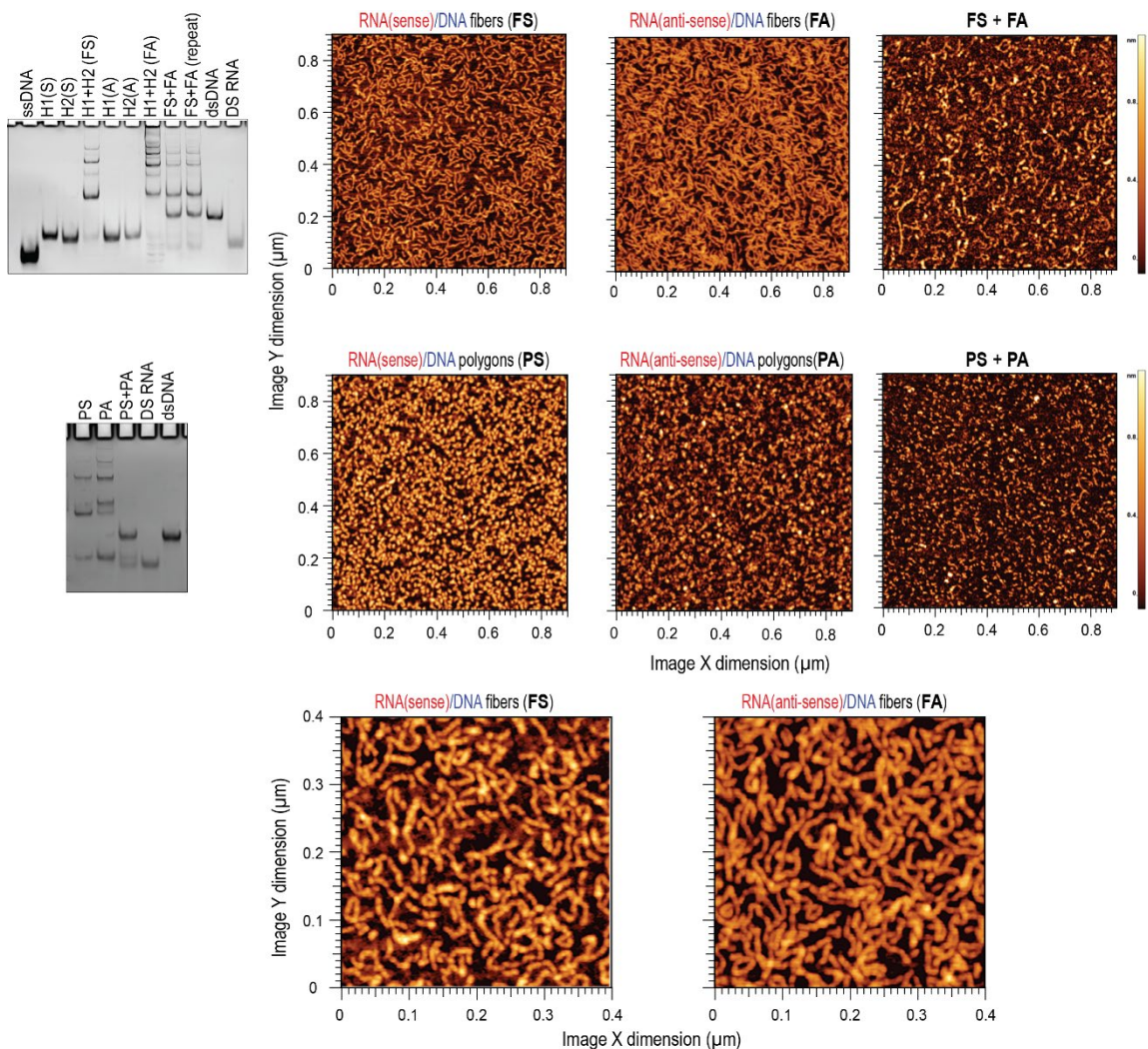
Figure 13. Experimentally verified fiber and polygon formation and release of DNA duplex and DS RNA through native-PAGE and AFM. For native-PAGE, ssDNA, preformed individual hybrids, DNA duplexes and DS RNAs are used as controls. Zoomed AFM images of fibers are shown below. Average length of the fibers was calculated in ImageJ software using particle analysis function. The sum of area of all counted particles is divided by the number of particles. Average sizes for F(S) and F(A) were calculated to be 328.9 a.u. and 938.1 a.u., respectively.

Absorbance versus temperature profiles were measured to determine the melting

transitions of individual polygons and fibers as well as their reassociation products after 5 h of

incubation (Figure 14D). In polygons P(A) and P(S) and fibers F(A) and F(S), two melting

transitions were observed; the first was only a minor melting transition at T_{m1} ~45°C, and the

second transition was distinct at T_{m2} ~80°C. Considering the complexity of multi-strand

nucleic acid assemblies, our assumption was that T_{m1} is the result of dissociation of the

dsDNAs in both fibers and polygons. The T_{m2} then resulted from the dissociation of hybrid

RNA–DNA parts of the assemblies. The experimentally measured values were consistent with

Tms measured for corresponding DNA duplex (T_m ~ 43.4°C for 1 μM, 5'-

AGGGAAATCCCTT-3'/5'-AAGGGATTTCCCT-3') and matched the value calculated (T_m

$_{calc}$=43.4°C) using the Mfold program[47]. The UV melting profile for the reassociated complexes

exhibited only one strong transition at 80°C that is in agreement with the computed T_ms for the

resulting 25-bp RNA duplex ($T_{m\ calc}$ = 80°C) and the 53-bp dsDNA ($T_{m\ calc}$ = 90°C).

We then computationally analyzed the formation of fibers in silico. There were four

different and repetitive regions (Figure 15A) that connected the RNA and DNA fragments in

the F(S) and the F(A) fibers. These interconnected regions had two distinct conformations. We

used iFoldRNA[48] and discrete molecular dynamics[49, 50] to reconstruct the tertiary structures of

regions 1 and 5, which were the two representative regions of the two conformations. Region 1 had

a large gap between the RNA fragment and the DNA fragment, while region 5 resembled a double

helix and nearly all the adjacent bases were stacked. We then used Gromacs[51] to perform molecular

dynamics for the two regions. The simulation results (Figure 15B) showed that the base pairs near

the gap in the F(S) opened rapidly, while the base pairs at the same position in F(A) were maintained

during the whole simulation. It suggested that the existence of the gap made the sense fibers more

flexible than the antisense fibers. Theoretically, there is the possibility that only one extremely long

fiber exists in the solution, which is composed of all the RNA and DNA fragments joined by the

regions shown in Figure 15A. The reason why the ideal one single fiber is not maintained is because

these connected regions are constantly undergoing thermodynamic changes, which increase the

likelihood that some of the connected regions may be broken. Apparently, the average length of

fibers in the solution is inversely proportional to the number of connected regions that are broken.

Therefore, the more stable the connected regions, the less the connected regions break, and the
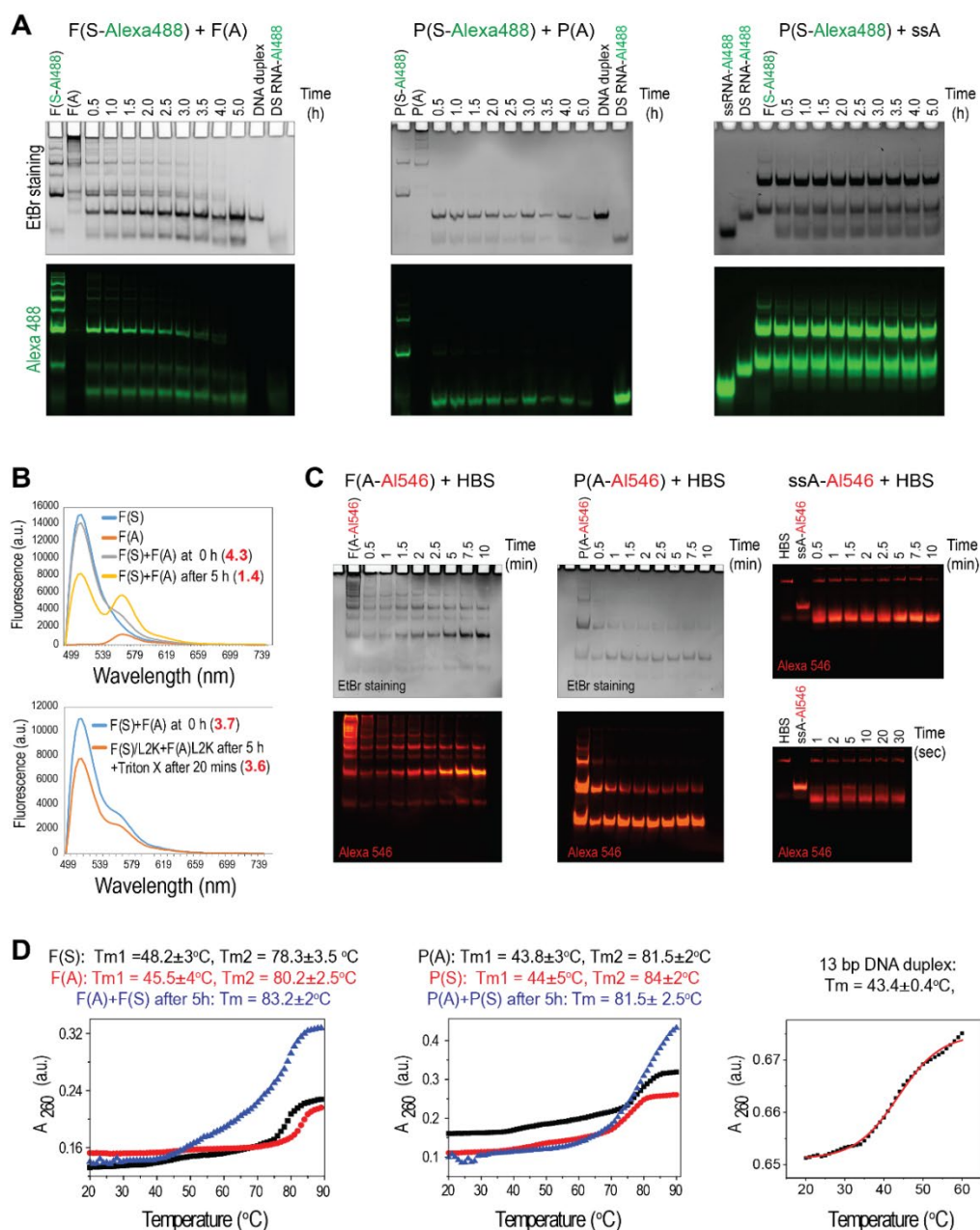
Figure 14. Re-association kinetics, influence of transfection agent on re-association, blood stability studies, and melting temperatures of fibers and polygons. (A) Re-association extent of Alexa® 488 labeled fiber (polygon) sense and non-labeled fiber (polygon) antisense though a set of time points, verified with native-PAGE stained with EtBr. Also, Alexa® 488 labeled fiber sense and non-labeled ssRNA antisense were tested for re-association. (B) Complexation with Lipofectamine 2000 prevents re-association as can be seen from FRET experiments. Numbers in red are calculated Donor/acceptor fluorescence ratios. (C) Blood stability assessment of Alexa® 546 labeled ssRNA antisense, fiber antisense, and polygon antisense in human blood serum at through set of time points. (D) Melting temperatures of individual fibers and polygons before and after their re-association assessed by UV-melt experiments. As a control, 13 bp DNA duplexes required for formation of fibers and polygons are tested.

longer the average length of the fibers. Thus, the fibers assessed by AFM and native-PAGE (Figure 12A and Figure 13) showed that the average lengths of F(S) were shorter than F(A) because the higher flexibility made them more easily broken. The opened base pair near the gap would cause more base pairs to open since it gave the fibers higher flexibility. All base pairs in F(S) would finally open, resulting in the formation of more stable helices with F(A). We then utilized the nucleic acid
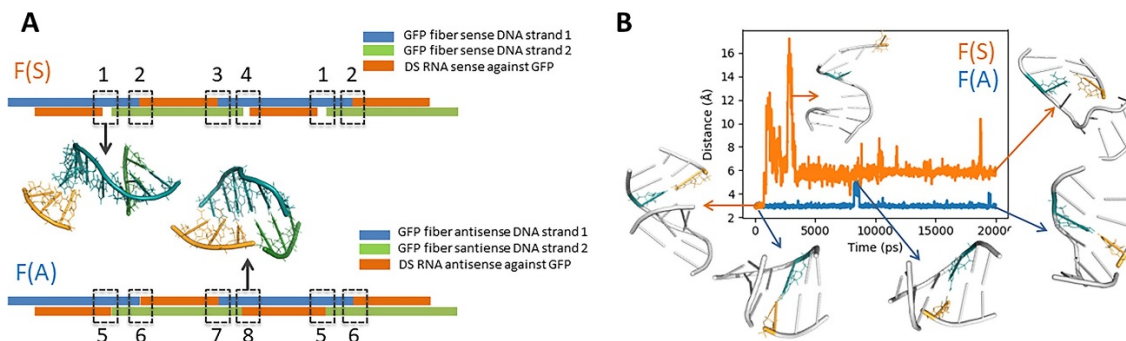
Figure 15. Molecular dynamics simulation of the interconnected region of the sense and antisense fibers. In the fibers, there are four different and repetitive interconnected regions that connect the DNA and RNA fragments. The eight boxes labeled from 1–8 in (A) represent the interconnected regions in the sense fibers and the antisense fibers, respectively. Regions 1 and 4 are nearly the same, while regions 2, 3 and 5–8 are the same. Molecular dynamics simulations are performed for regions 1 and 5. Results (B) show that the distance between the base pair near the gap in the sense fiber undergoes remarkable changes, while the distance between the base pair near the gap in the antisense fiber is relatively stable during the simulation.

simulation tool (NAST)[52] to perform a coarse-grained molecular dynamics simulation for a triangle and a rectangle, respectively. The results (Figure 16) showed that the triangle shape is relatively stable, whereas the rectangle shape was very hard to maintain during the simulation. That explained why triangle shapes are the most common among polygon structures observed by AFM (Figure 12B).

The fibers were programmed to activate multiple split functionalities upon their intracellular activation (FRET, RNAi and formation of functional NF-B decoys). FRET activation allowed direct visualization of the reassociation process in vitro (Figure 17A–B) and in cells (Figure 17C and Figure 18), evidencing the differences in the kinetics of the process. To experimentally examine the functionality of released DS RNAs, we transfected human breast cancer cells expressing the

enhanced green fluorescent protein (MDA-MB-231/GFP) with cognate fibers and polygons. The GFP can be used as a visual tag for confirming the activation of RNAi, which directly results in the released DS RNAs from the reassociation. The extent of GFP gene silencing was assessed by fluorescence microscopy and flow cytometry (Figure 17D–E and Figures 19-21). Individual sense or antisense fibers and polygons did not alter fluorescence intensity (Figures 19-20). Co-delivery of sense and antisense strands containing fibers (polygons) at different concentrations resulted in a concentration-dependent shift of fluorescence intensity. Interestingly, the co-delivery of individual fibers with cognate ssRNAs resulted in some GFP silencing (Figure 21B), thus allowing to specifically activate only an RNAi functionality pre-programmed to fibers. However, due to chemical instability of ssRNA (Figure 14C), requirements for a large number of ssRNAs to be present in the same intracellular location with fibers, and inability to activate preprogrammed DNA functionalities, this approach may not be optimal. However, it potentially opens the avenue of research for the delivery of RNA within fiber that will interact with endogenous RNAs (e.g. similar to antimiR oligos[53].

The reassociation process was also designed to activate decoys designed to bind NF-κB and prevent its translocation to the nucleus upon cell activation. In agreement with previous observations[36], immunofluorescence analysis revealed a perinuclear accumulation of NF-κB upon LPS treatment when the cognate fibers were co-transfected, suggesting that the reassociation of fibers impairs NF-κB nuclear translocation induced by LPS (Figure 17F). To further demonstrate the functional consequences of NF-κB decoy during the intracellular reassociation of fibers (polygons), human PBMCs were treated with constructs (Figure 22 and Figure 23). We chose PBMCs as a model system because they are known to be more reliable and predictive of the cytokine storm toxicity than common preclinical animal models such as rodents and nonhuman primates. The significance of this model comes from the tragic experience of a pharmaceutical company (TeGenero Immuno Therapeutics, AG) with a biotechnology product, TGN1412, which
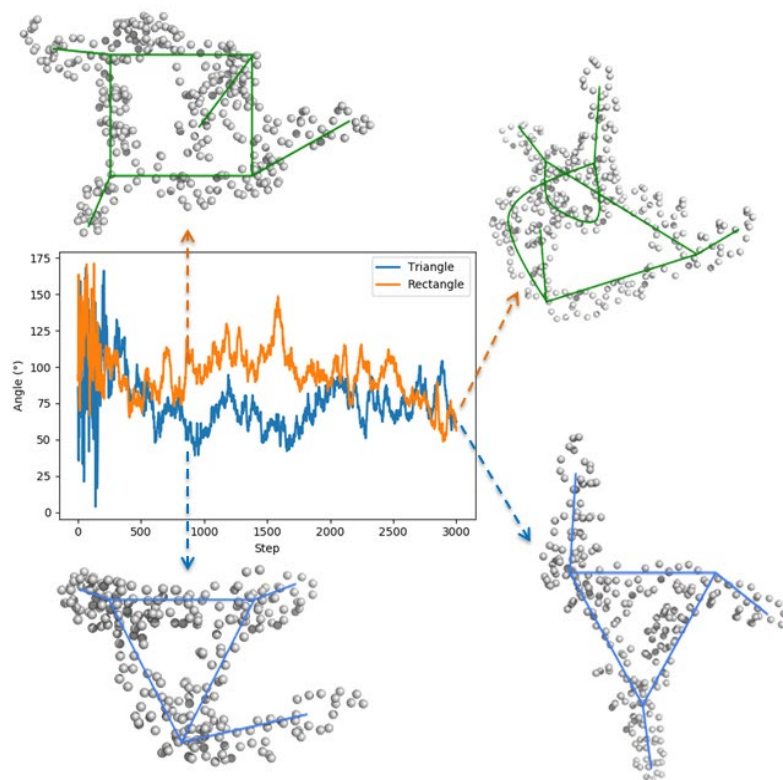
Figure 16: Molecular dynamics simulation of the triangle and the rectangle, respectively. The simulation is performed by using the NAST software[78], and the model is coarse grained by using the "C3'" atom to represent each atom in the molecule. The triangle shape is always preserved during the simulation, while the rectangle shape is unstable. The angle between two edges in the triangle remains stable after the triangle shape is formed, while the angle between two edges in the rectangle decreases steadily after the rectangle shape is formed.

resulted in severe toxicity in human patients after successfully passing preclinical safety studies in rats and monkeys; its cytokine storm toxicity was predicted by in vitro tests using human PBMCs[54]. With PBMC experiments, we used two experimental scenarios for RNA–DNA hybrid complexation with the delivery carrier, L2K, used in all transfections. In the first scenario, fibers and polygons, as well as their complementary structures, were mixed together, then complexed with L2K prior to their addition to the cells (see (F(S) + F(A))-L2K and (P(S) + P(A))- L2K in Figure 22). This scenario guaranteed co-delivery of complementary constructs into the same cell. In the second scenario, fibers and polygons, as well as their complementary structures, were pre-incubated

with L2K as two separate samples, after that, these complexes were mixed together for co-delivery (see (F(S)-L2K) + (F(A)-L2K) and (P(S)-L2K + (P(A)-L2K) in Figure 22). This scenario was more challenging to the system than the first scenario because there was no guarantee for the co-delivery into the same cell. For the purpose of this study, we call fibers prepared using these scenarios 'co-complexed/delivered' and 'complexed/co-delivered,' respectively. Fibers and polygons complexed with L2K and added to cultures as separate samples were used as controls (see F(S)-L2K, F(A)-L2K, P(S)-L2K, and P(A)-L2K in Figure 22). Twenty-four hours after transfection, the PBMCs were challenged with LPS for an additional 24 h. Supernatants were then collected and analyzed for the presence of interleukin-6 (IL-6) and tumor necrosis factor alpha (TNFα). These cytokines are known biomarkers of LPS-mediated activation of PBMCs, and their induction by LPS depends on NF-κB[55]. Therefore, if our NF-κB decoy fibers were functional, we would have expected that only the simultaneous presence of fibers and complementary fibers in the same culture would inhibit LPS-induced cytokines. The LPS-only control, represent- ing cells treated with phosphate-buffered saline (PBS) for the first 24 h and LPS alone for the second 24 h, demonstrated that PBMCs still functioned and produced both cytokines in response to LPS after 48 h of total cell culture (compare PBS and PBS/LPS samples in Figure 22B and C). When complementary fibers were delivered separately prior to LPS stimulation, no inhibition in the LPS- induced IL-6 and TNFα was observed. A higher level of both cytokines was noticed and was consistent with the known phenomenon of an increase in the LPS-mediated inflammation by certain types of nanomaterials (compare samples F(S)-L2K and F(A)-L2K to LPS-only in Figure 22B–C)[56-59]. In contrast, co-complexed/delivered and complexed/co-delivered fibers resulted in the inhibition of LPS-induced IL-6 and TNFα (compare samples (F(S)+F(A))-L2K and (F(S)-L2K) + (F(A)-L2K) to individual fibers and LPS-only control). These data were consis- tent with the expected inhibition of NF-κB due to the formation of an NF-κB decoy functional oligonucleotide system following the delivery of both components into the cell. The complete inhibition could not be achieved, likely due to the remaining
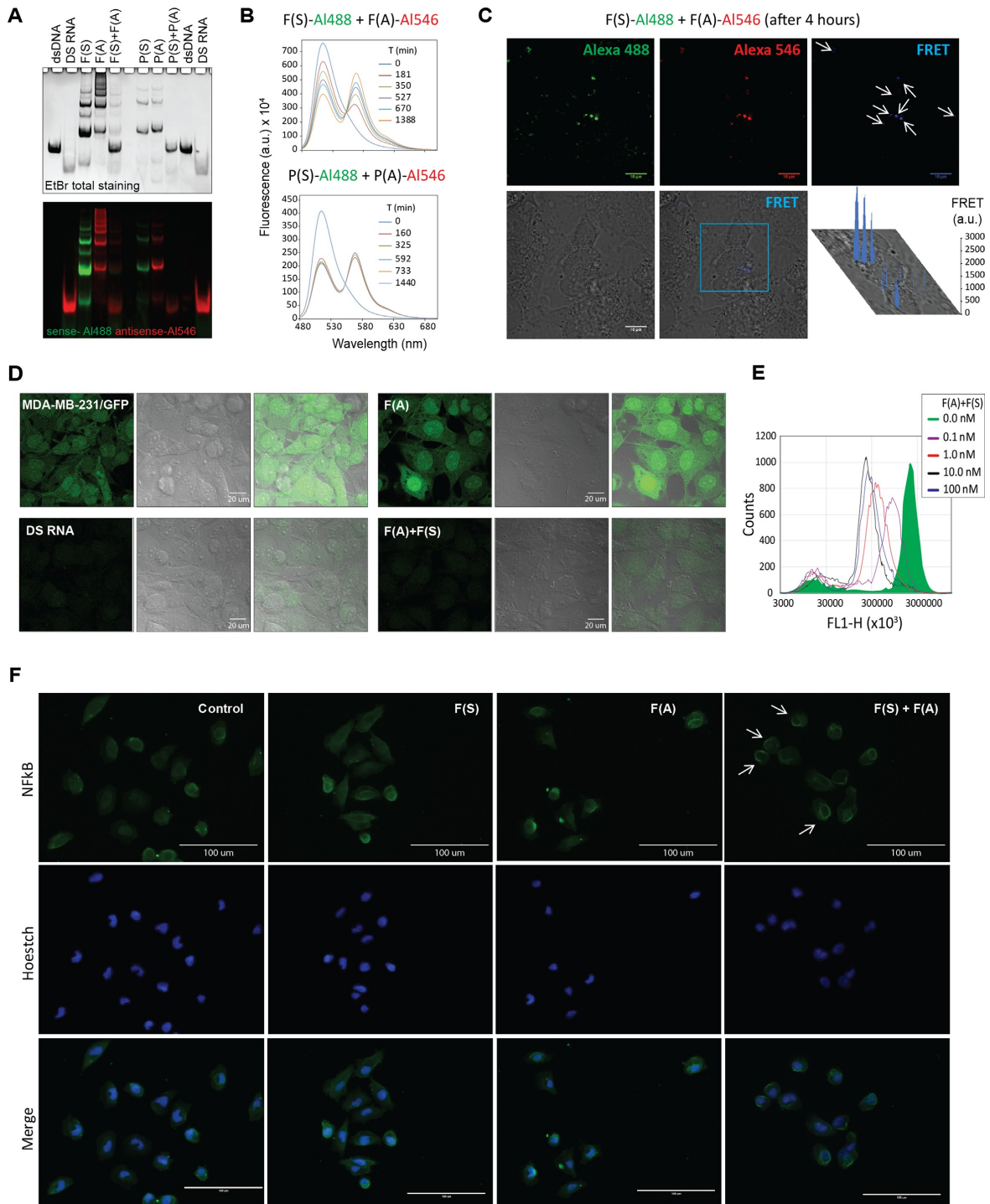
Figure 17. Intracellular reassociation of fibers followed with FRET, gene silencing, and perinuclear NF-κB accumulation upon LPS treatment. (A, B) Reassociation of fluorescently labeled fibers and polygons confirmed by native-PAGE and FRET measurements. (C) FRET (indicated with arrows) observed upon reassociation of fibers in human breast cancer cells (MDA-MB-231). (D, E) Reassociation of fibers promotes the release of DS RNAs specifically designed to target GFP. Three days after the transfection of cells (MDA-MB-231/GFP), GFP

silencing was confirmed by fluorescence microscopy and flow cytometry. (F) Cells transfected with fibers were treated with LPS for 4 h. After fixation and permeabilization, cells were processed for immunofluorescence staining with NF-κB (p65) using Alexa Fluor 488-conjugated secondary antibodies (green) and Hoechst (blue). Panel F(S) + F(A) reveals perinuclear accumulation of NF-κB (arrows), suggesting that reassociated fibers impair NF-κB nuclear translocation induced by LPS (scale bar: 100 μm).

effect of co-treatment between the LPS and the fibers. There was no statistically significant difference between co-complexed/delivered and complexed/co-delivered fibers, although the decrease in cytokine production observed with co-complexed/co- delivered fibers was more pronounced ((F(S) + F(FA))-L2K versus (F(S)- L2K) + (F(A)-L2K) in Figure 22B and C). Altogether these data demonstrate the robustness of the system and suggest that co-delivery can be considered to further ensure the efficiency of the system across cells from different individuals and various types. The same trends were observed in polygons (compare P(S)-L2K and P(A)-L2K as single treatments to (P(S) + P(A))-L2K and (P(S)-L2K) + (P(A)-L2K) in Figure 22B and C).

Human PBMCs were a complex system because they contained multiple cell types that expressed various receptors and transcription factors contributing differently to the LPS-triggered inflammatory response. Moreover, there are several factors such as (i) known polymorphisms of genes encoding proteins involved in the LPS response; (ii) the induction of IFN by fibers, which, among other mechanisms, may contribute to the greater induction of the pro-inflammatory cytokines by the LPS and (iii) challenges with the delivery of nucleic acid nanoparticles into primary cell cultures in vitro, which collectively may complicate the verification of NF-κB specificity in the primary cultures of blood cells from individual human donors. Therefore, to further verify the specificity of the response to NF-κB, we conducted a follow-up study using the reporter cell line HEK-Blue hTLR4. These cells express SEAP under the NF-κB promoter, which can be activated only through one pathway that is triggered by bacterial LPS. When RNA–DNA fibers were co-transfected, and the cells were stimulated with LPS, the NF-κB-dependent SEAP production was inhibited regardless of the scenario used for fiber complexation with L2K (Figure 22D, compare (F(S) + F(A))-L2K and (F(S)-L2K) + (F(A)-L2K) to PBS/LPS and L2K/LPS

controls). The same trend was observed in polygons (Figure 20D, compare (P(S) + P(A))-L2K and

(P(S)-L2K) + (P(A)-L2K) to PBS/LPS and L2K/LPS controls). These findings are consistent with

the intended mechanism of action. When only individual fibers or polygons were delivered to the

cells, no such inhibition was observed, further confirming the specificity of the mechanism of action
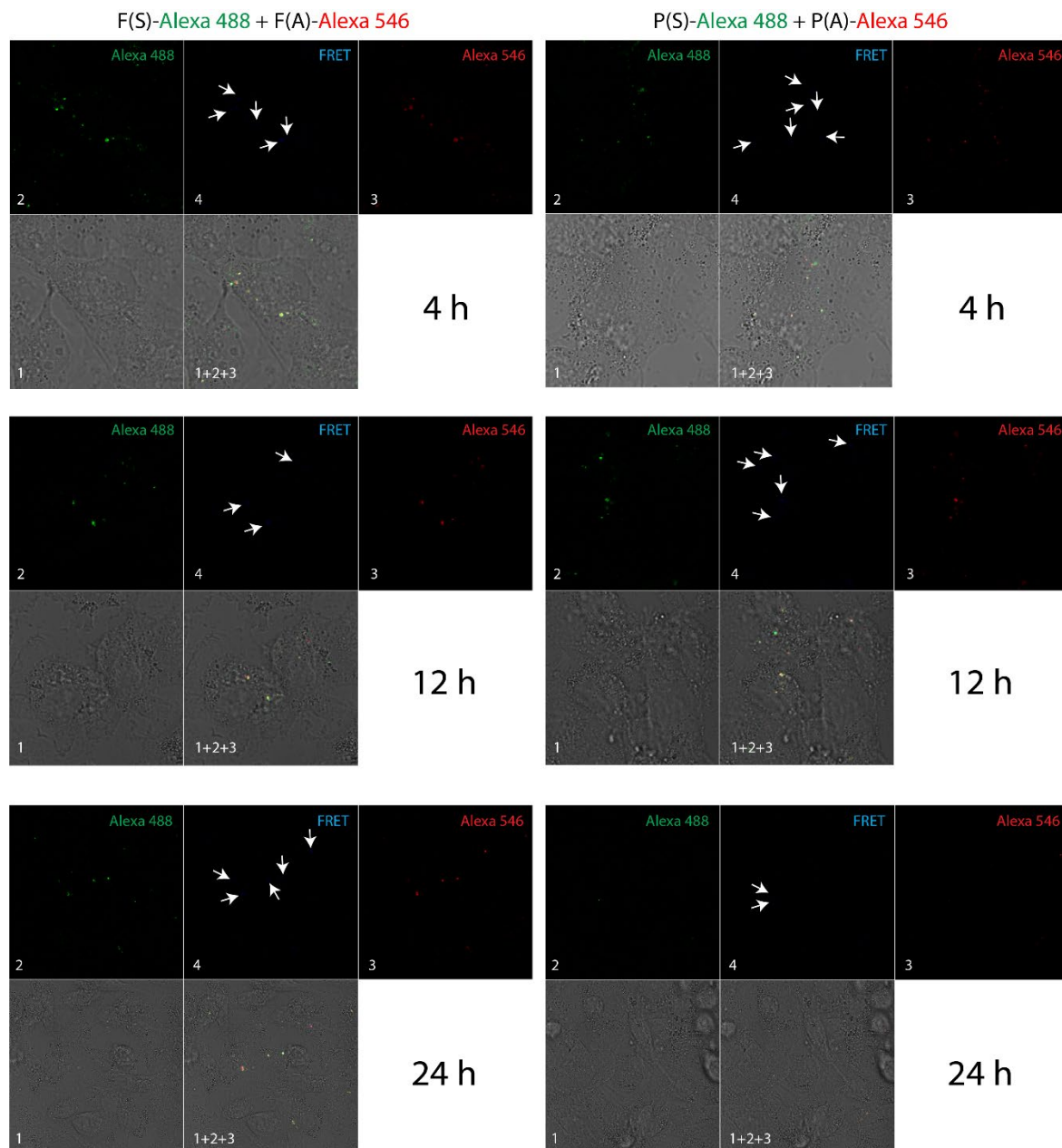
Figure 18. Intracellular re-association of fibers and polygons can be followed with FRET. FRET (indicated with arrows) is observed upon re-association of fibers in human breast cancer cells (MDA-MB-231). All measurements were done in triplicates.
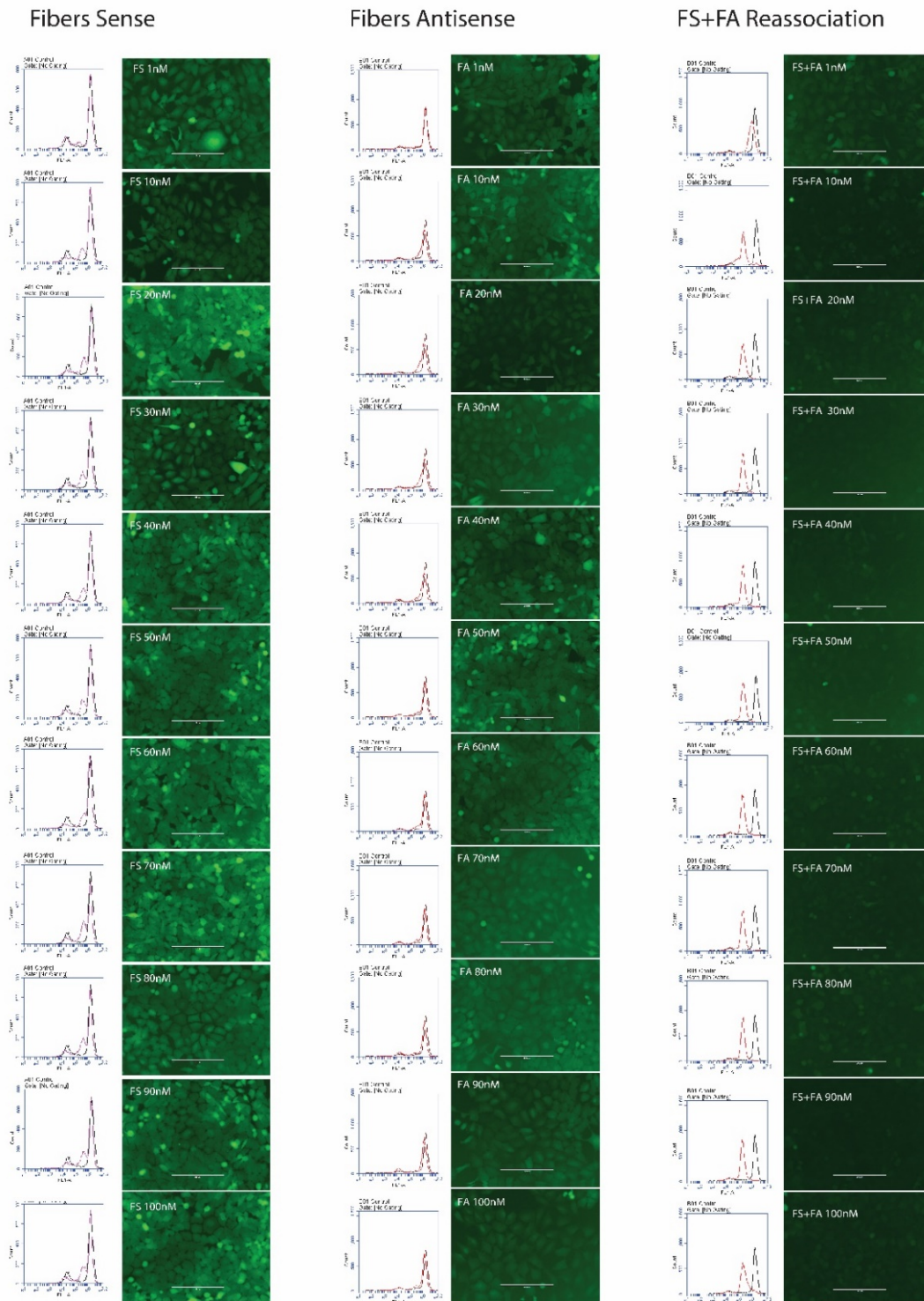
Figure 19. GFP silencing experiments carried out for different concentrations of RNA–DNA fibers. The silencing efficiencies were assessed by fluorescent microscopy and flow cytometry. In flow cytometry, black and red curves represent control and transfected cells, respectively. Note that the individual fibers have minimal effect on gene silencing.
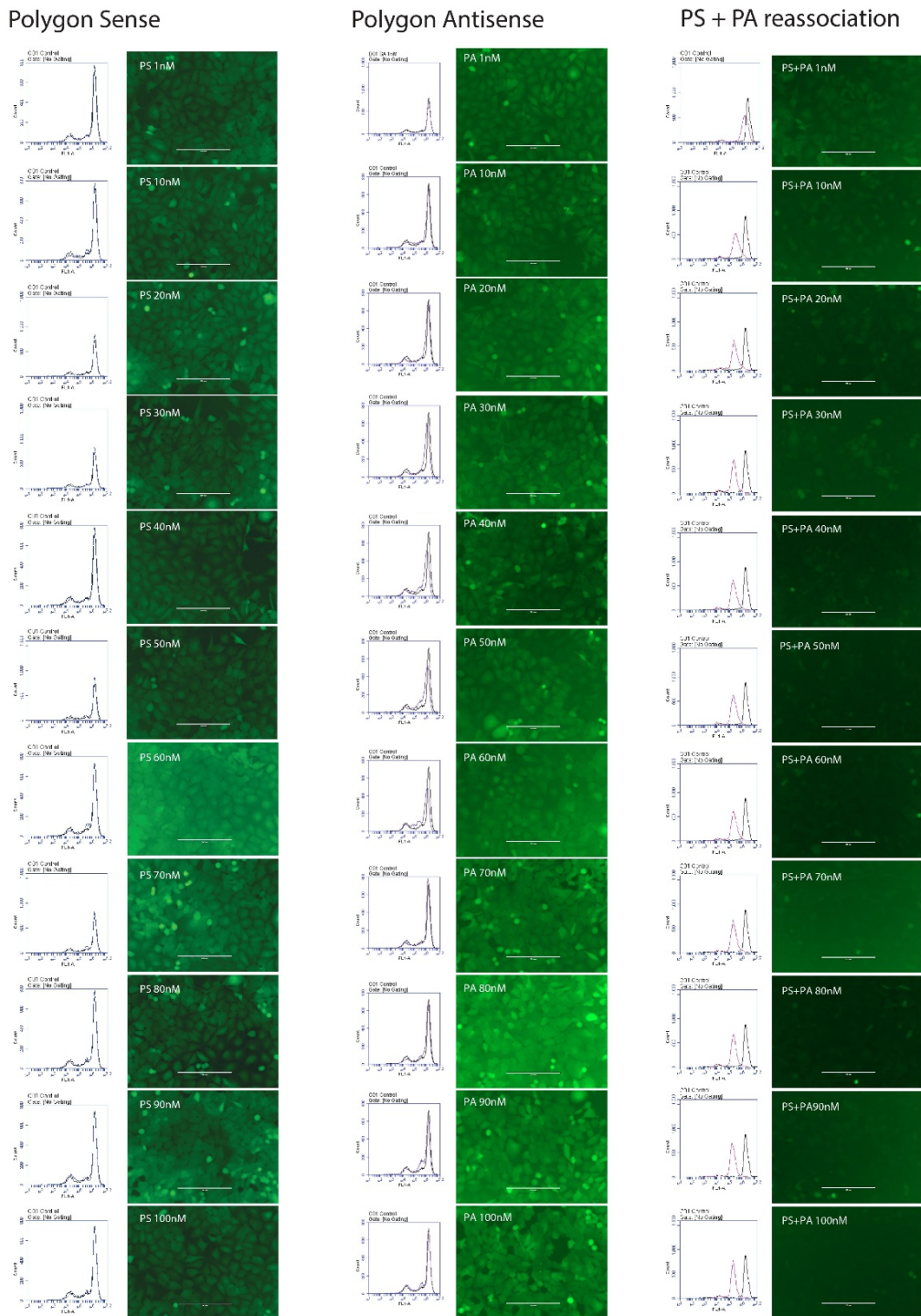
Figure 20. GFP silencing experiments carried out for different concentrations of RNA–DNA polygons. The silencing efficiencies were assessed by fluorescent microscopy and flow cytometry. In flow cytometry, black and red curves represent control and transfected cells, respectively. Note that the individual polygons have minimal effect on gene silencing.

A

B
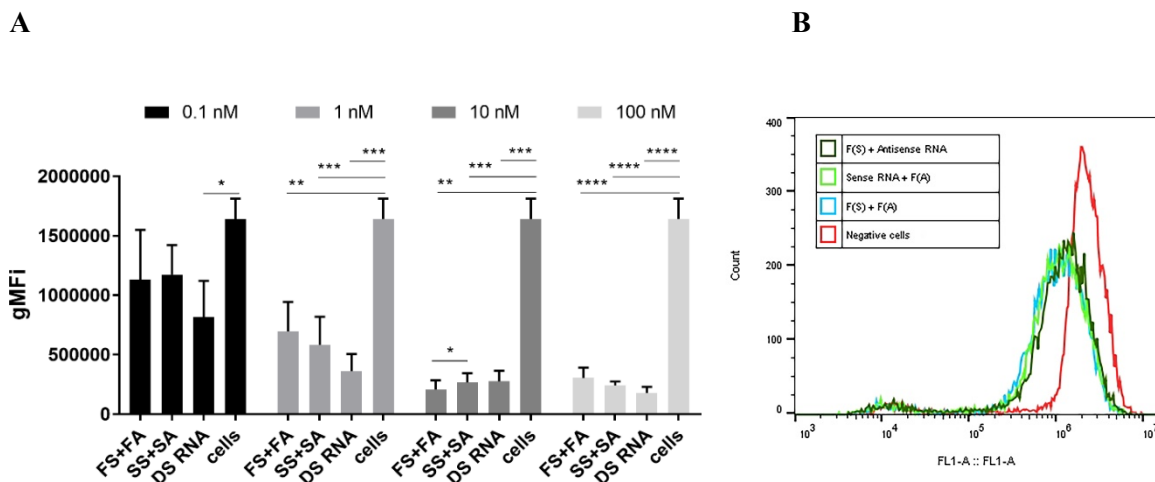
Figure 21. (A) GFP silencing experiments carried out for different concentrations of RNA/DNA fibers, RNA/DNA polygons, and control DS RNA. The silencing efficiencies were assessed by flow cytometry. Statistical analysis was performed by one-way ANOVA (* $p < 0.05$, ** $p < 0.01$, *** < 0.001, **** $p < 0.0001$). (B) GFP silencing can be observed for RNA/DNA fibers co-transfected with cognate ssRNAs (final concentration of 10 nM was used for all constructs).

to NF-κB (Figure 22D, compare F(S)-L2K, F(A)-L2K, P(S)-L2K, and P(A)-L2K to PBS/LPS and L2K/LPS controls). These data confirmed that fibers' and polygons' reassociation is specific to NF-κB decoy formation.

The induction of pro-inflammatory cytokines and interferons (IFNs) in human immune cells is a tool commonly used for vaccines and immunotherapies when activation of the immune system is desirable[60]. However, excessive production of the cytokines, particularly TNFα, may cause tissue necrosis at the site of injection[61]. Decreasing the injection site reactions in patients is therefore considered an essential safety goal for vaccines and immunotherapies[62-65]. TLR agonists are commonly used as adjuvants for their ability to induce cytokines and interferons[66]. Some current approaches for immune system stimulation include using nanoparticles to deliver a TLR ligand or combining different TLR agonists to achieve both cytokine and interferon induction[67, 68]. For example, TLR4 adjuvants, which are more potent at inducing cytokines, can be combined with TLR9 adjuvants, which are more potent at inducing interferons[66]. In the traditional approach, such a combination is associated with a higher risk of injection-site reactions in sensitive

individuals. Therefore, we hypothesized that the fibers and polygons described in our study could provide a desirable tool for vaccine and immunotherapy adjuvant production by regulating the amounts of pro-inflammatory cytokines triggered by NF-κB-dependent TLR4 co-adjuvants while inducing interferons via an NF-nB-independent mechanism. To verify that designed fibers and polygons are capable of inducing type I IFNs and that such induction is not affected by the NF-κB decoy function, we tested supernatants collected from PBMC cultures for the presence of type I interferons. We confirmed that fibers and polygons stimulate interferons and that this property is not affected when sense and antisense fibers or polygons are combined to inhibit NF-κB (Figure
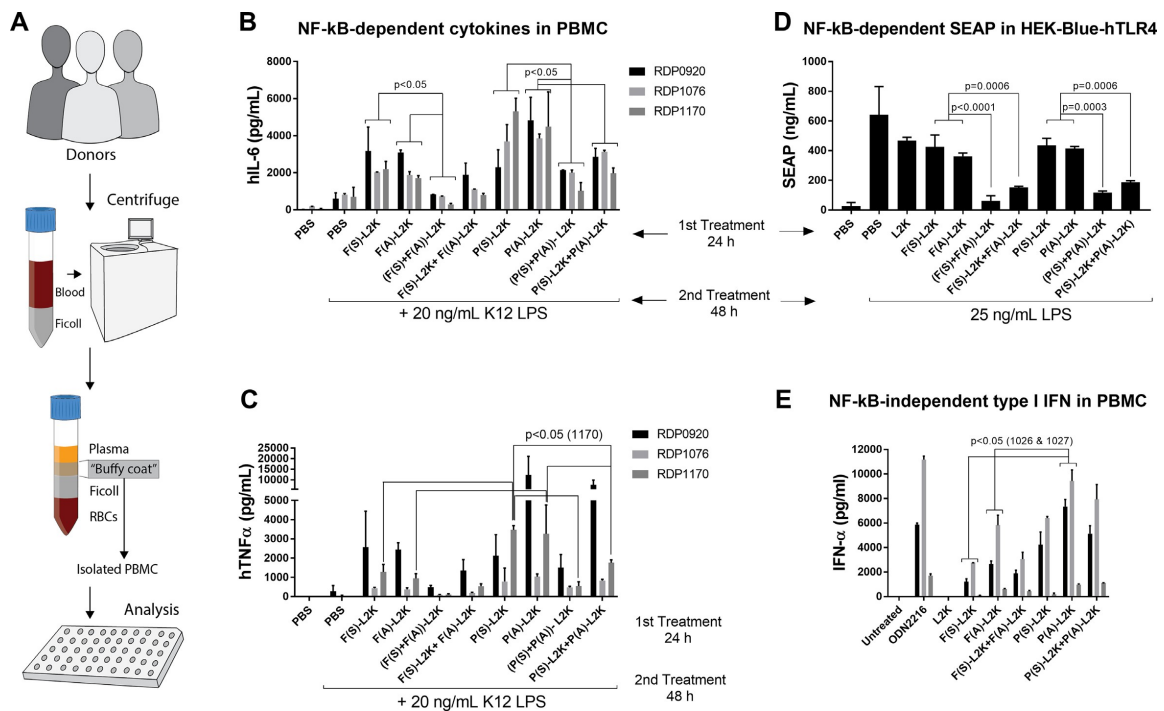
Figure 22. Functional effects of RNA–DNA fibers on NF-κB-dependent and -independent expression of pro-inflammatory markers. Human peripheral blood mononuclear cells from at least three donor volunteers and the reporter cell line HEK-Blue hTLR4 were studied. (A) Schematics explaining PBMC isolation and further analysis. (B, C) PBMCs were treated for the first 24 h with controls or fibers and then stimulated with 20 ng/mL of ultrapure bacterial K12 LPS. Levels of IL-6 (B) and TNFα (C) were measured in the supernatants by multiplex ELISA. (D) Reporter cell line HEK-Blue hTLR4 was transfected with fibers and, 24 h later, stimulated with ultrapure K12 LPS. The cells were incubated for an additional 24 h, and the levels of NF-κB-dependent SEAP were measured in supernatants. (E) PBMCs were treated with positive control (ODN2216), negative control (L2K alone), or fibers for 24 h, and the levels of type I interferon (IFNα) were assessed by multiplex ELISA. PBS: phospate-buffered saline; L2K: Lipofectamine 2000; LPS: E. coli K12 lipopolysacharide; ODN2216: CpG oligonucleotide known to induce IFNα.
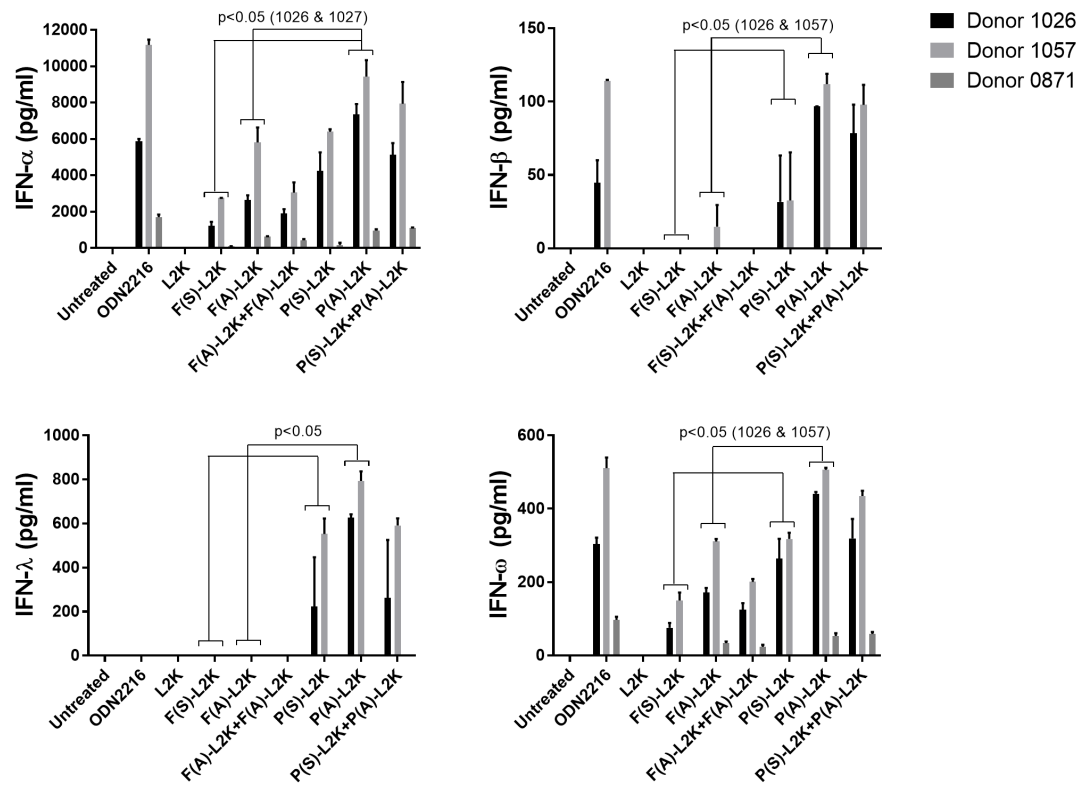
Figure 23. Induction of type I interferons by RNA–DNA fibers and polygons. Human peripheral blood mononuclear cells from at least three donor volunteers were studied. The cells were treated with positive control (ODN2216), negative control (L2K alone), fibers or polygons complexed with L2K for 24 hours and the levels of type I interferons (alpha, beta, lambda and omega) were assessed by multiplex ELISA. PBS – phospate buffered saline; L2K – Lipofectamine 2000; ODN2216 – CpG oligonucleotide known to induce IFNα; F(S)-L2K and F(A)-L2K sense- and antisense fibers complexed with L2K; (F(S)+F(A))-L2K – fibers mixed together then complexed with L2K; F(S)-L2K+F(A)-L2K – fibers complexed with L2K and then mixed together for co-delivery; P1-L2K and P2-L2K sense- and antisense polygons complexed with L2K; (P(S)+P(A))-L2K – polygons mixed together then complexed with L2K; P(S)-L2K+(A)-L2K) – polygons complexed with L2K and then mixed together for co-delivery.

22E). An inter-donor variability in IFN response was observed, in that a stronger IFN induction was detected in cultures of one out of three donors in response to the antisense fiber (Figure 20E and Figure 23). This variability as well as a difference in the potency of IFN induction between fibers and polygons are consistent with the current knowledge of the IFN induction by RNA nanopar- ticles in primary human cells[69]. While the scope of our project did not include establishing the relation of this property to a decrease in injection-site reactions in humans, the data presented

in this study are very promising and warrant further, more focused investigation. Interestingly enough, polygons were more potent inducers of type I IFNs in some donors (Figure 22E and Figure 23), suggesting that the shape of the assemblies was an important pre-requisite to their adjuvanticity.

To show the therapeutic potential of this multipronged approach, we treated human melanoma cell line with RNA–DNA fibers designed to release the NF-κB decoy along with DS RNAs targeting the mutated *BRAF* gene[70–72] (Figure 24). Melanoma is a form of skin cancer with
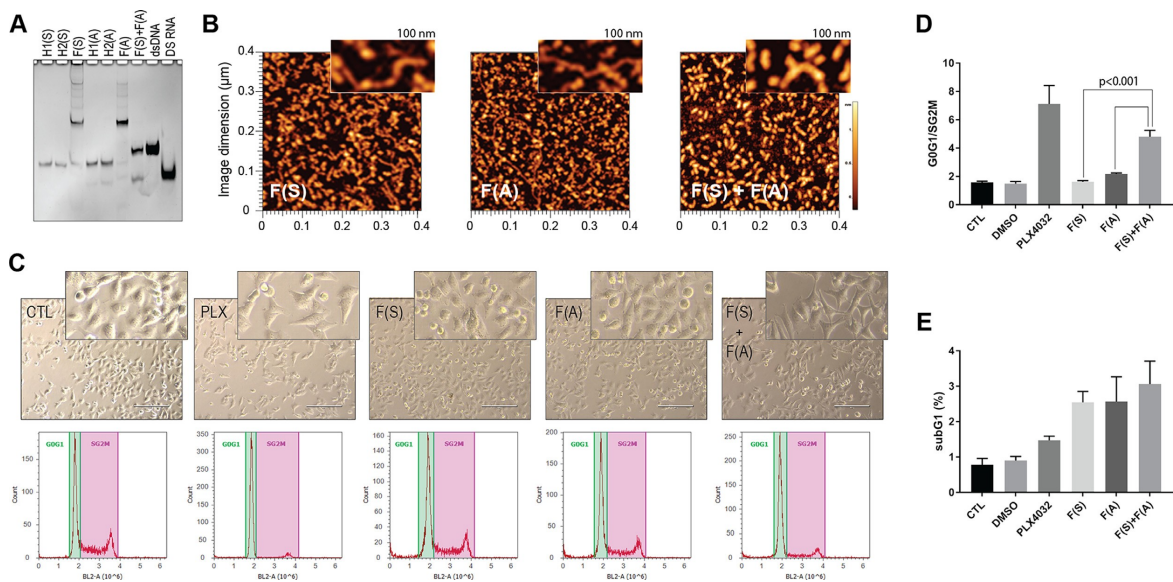
Figure 24. Growth-inhibition effects and morphological alterations upon complementary intracellular reassociation of fibers. (A) Native-PAGE shows the formation of sense F(S) and antisense F(A) fibers and their reassociation products F(S) + F(A). (B) AFM images of F(S), F(A), and the reassociated F(S) + F(A) that release NF-κB decoys and DS RNAs. A375 melanoma cells were transfected with nanofibers and stained with the fluorescent intercalating agent propidium iodide 48 h post-transfection. Flow cytometry analysis was performed to evaluate cell viability and DNA content in the cell cycle. (C) Upper panel: Pictures taken at 48 h post-transfection show melanoma cells' morphological changes to a fusiform phenotype upon intracellular association of fibers, similar to cells under treatment with PLX4032 (magnification: 20×, scale bar: 200 µm). Lower panel: Histograms representing the number of cells in G0/G1 (quiescence/checkpoint 1) and S/G2/M (checkpoint 2/mitosis) phases of the cell cycle. (D) Analysis of cell cycle arrest, characterized by the ratio of G0/G1 over S/G2/M, showing significant accumulation of cells in G0/G1 phases when fibers were associated F(S) + F(A). (E) Analysis of cell death, observed by the accumulation of haplodiploid cells in the subG1 phase, indicating the process of nuclear DNA fragmentation. CTL –control cells without treatment; PLX: PLX4032 (vemurafenib).

poor prognosis, and because conventional therapies are consistently ineffective and the disease often recurs, melanomas are one of the prime candidates for the development of novel

combinatorial treatment strategies. The discovery that missense mutations in the *BRAF* gene were present in approximately 60% of melanomas encouraged the development of RAF inhibitors to block the constitutive activation of this gene, an essential regulator of MAPK cell proliferation and survival pathways. In 2011, the U.S. Food and Drug Administration approved vemurafenib for the treatment of metastatic melanomas harboring the *BRAF*[V600E] mutation. Despite the high response rates of patients to vemurafenib, relapse still occurs within months of initiating the treatment in most cases[73]. Activation of the NF-κB pathway is among the multiple mechanisms of acquired resistance to vemurafenib in melanomas, and the inhibition of this transcription factor increases cell death of vemurafenib- resistant cells[74, 75]. In this scenario, melanoma cells represent an attractive model to evaluate the therapeutic potential of fibers designed to release DS RNAs targeting mutated *BRAF* and DS DNA as an NF-κB decoy. We treated A375 melanoma cells, which carry the *BRAF*[V600E] mutation, with fibers F(S), F(A) and F(S) + F(A) (Figure 24D and Figure 25). Cell cycle analysis by propidium iodide intercalation revealed that, after association, the fibers induced an accumulation of cells in the G0G1 phase, similar to the cells treated with vemurafenib (PLX4032) (Figure 24D). Histograms illustrating the distribution of melanoma cells throughout the cell cycle (G0/G1 and S/G2/M) (Figure 24E) showed a similar cell cycle arrest profile between an accumulation of cells in the G0G1 phase, similar to the cells treated with vemurafenib (PLX4032) (Figure 24D). Histograms illustrating the distribution of melanoma cells
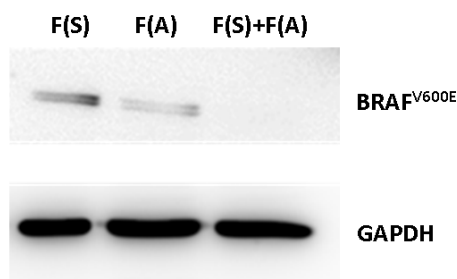
Figure 25. Specific gene silencing triggered by intracellular re-association of RNA/DNA fibers in human melanoma cells A375. Relative *BRAF* silencing is compared to the house keeping gene GAPDH.

throughout the cell cycle (G0/G1 and S/G2/M) (Figure 24E) showed a similar cell cycle arrest profile between associated nanofibers and PLX4032. Therefore, the cytostatic effect observed in melanoma cells upon treatment with fibers was similar to the effects of treatment with PLX4032. Fibers also induced cell-shape alterations similar to PLX4032, as observed by the presence of fusiform cells among epithelial cells after treatment, which was more evident with F-actin staining and the apparent microtubule polarization for the maintenance of NF-κB in an inactive state[76] (Figure 26). These data suggested that the DS RNAs released by nanofibers to target the mutated *BRAF* gene in melanoma cells resulted in a similar cellular response as observed with PLX4032. A drawback of the PLX4032 treatment is the emergence of a resistance mechanism through the activation of the NF-κB pathway, as displayed by the A375 melanoma cells. Beyond the silencing of mutated *BRAF*, reassociation of the fibers releases an NF-κB decoy that induces the retention of NF-κB in the cytoplasm of the cells, which could thereby revert the resistance mechanism. These results suggest the promising use of RNA–DNA nanofibers as a strategy to overcome the resistance of melanoma cells to PLX4032 treatment. Combinaorial approaches are emerging as being critical for successful therapies, and the development of smart nanoparticles capable of releasing multiple functionalities in a controlled fashion can represent a significant advantage in that direction.

In conclusion, the responsive behaviors of this novel system are determined by the specific design principles of individual constructs, the type of their assembly, and physicochemical properties. The innovative use of dynamic systems presents multiple advantages: (i) fibers and polygons can be programmed to gather multiple different functionalities for their simultaneous delivery to cells, thus allowing simultaneous targeting of various biological pathways with higher synergistic effects; (ii) the relatively inexpensive cost of the materials and simple assembly protocols of fibers and polygons enable their economic industrial-scale production; (iii) thermal and chemical stabilities of constructs can be fine-tuned, and other functionalities can be programmed into constructs (e.g. fluorophores) to induce multi-responsive behavior; (iv) naked
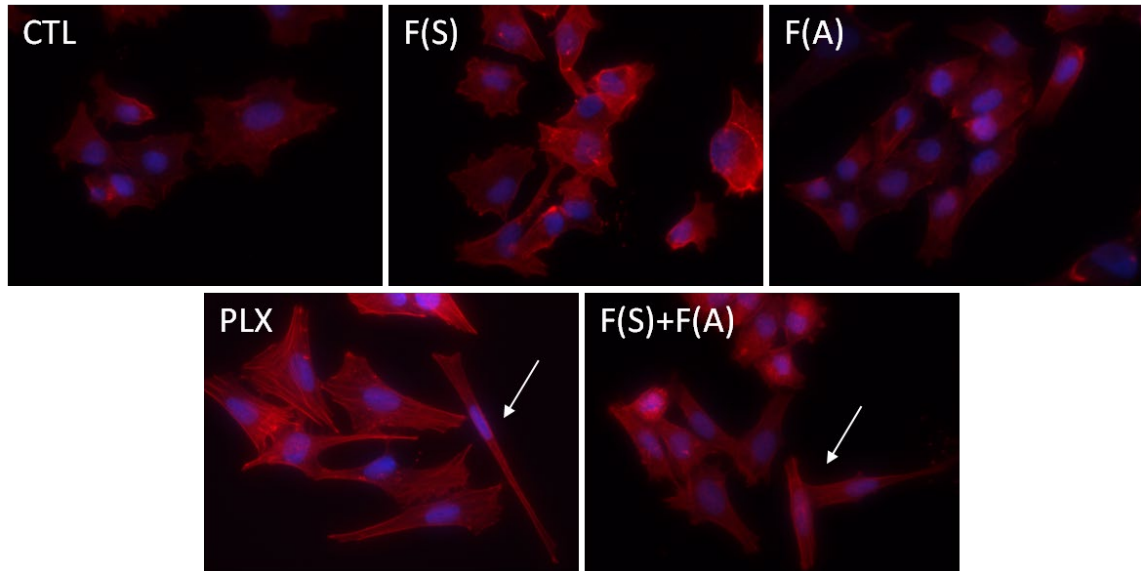
Figure 26. Morphological alterations in melanoma cells transfected with sense/antisense RNA/DNA fibers. A375 melanoma cells were transfected with either *BRAF*/NF-κB nanofiber sense, *BRAF*/NF-κB nanofiber antisense, or both nanofibers together. Cells were fixed 48 hours post-transfection and processed for F-actin immunofluorescence staining with Rhodamine-conjugated phalloidin (red); nuclei were stained with Hoechst (blue). Arrows in lower panel demonstrates the influence of re-associated fibers on the morphology of melanoma cells, producing more elongated cells. Magnification is 60×.

constructs avoid non-specific cell penetration due to their negative charge and (v) the

immunological properties of fibers and polygons are tunable and can potentially be predicted.

This work expands our understanding of different parameters in design principles and

formulation protocols of RNA–DNA nanoassemblies, and it allows us to identify the best settings

and techniques for possible pipeline production of dynamic, functionally interdependent systems

that can be used for a broad spectrum of biological applications.

2.4   Sequence used in this project

Fibers and polygons with split Dicer Substrate (DS) RNAs against GFP:

To assemble fibers carrying sense (antisense) strands, mix GFP fiber sense (antisense) DNA strand 1 with GFP fiber sense (antisense) DNA strand 2 with DS RNA sense (antisense) against GFP in 1 to 1 to 2 ratio.

GFP fiber sense DNA strand 1:

5' – AAGGGATTTCCCTCGGTGGTGCAGATGAACTTCAGGGTcaTTCCCTAAAGGGA

GFP fiber sense DNA strand 2:

5' – AGGGAAATCCCTTCGGTGGTGCAGATGAACTTCAGGGTcaTCCCTTTAGGGAA

GFP fiber antisense DNA strand 1:

5' –TCCCTTTAGGGAATGACCCTGAAGTTCATCTGCACCACCGAGGGAAATCCCTT

GFP fiber antisense DNA strand 2:

5' – TTCCCTAAAGGGATGACCCTGAAGTTCATCTGCACCACCGAAGGGATTTCCCT

DS RNA sense against GFP:

5' –ACCCUGAAGUUCAUCUGCACCACCG

DS RNA antisense against GFP:

5' –CGGUGGUGCAGAUGAACUUCAGGGUCA

DS RNA sense labeled with Alexa 488:

5' –ACCCUGAAGUUCAUCUGCACCACCG-Alexa488

DS RNA antisense labeled with Alexa 546:

5' –Alexa 546-CGGUGGUGCAGAUGAACUUCAGGGUCA

Polygons with split Dicer Substrate (DS) RNAs against GFP gene:

To assemble polygons carrying sense (antisense) strands, mix GFP polygon sense (antisense) DNA with DS RNA sense (antisense) against GFP in 1 to 1 ratio.

GFP polygon sense DNA:

5' – AAGGGATTTCCCTCGGTGGTGCAGATGAACTTCAGGGTcaAGGGAAATCCCTT

GFP polygon antisense DNA:

5' –AAGGGATTTCCCTTGACCCTGAAGTTCATCTGCACCACCGAGGGAAATCCCTT

DS RNA sense against GFP:

5' –ACCCUGAAGUUCAUCUGCACCACCG

DS RNA antisense against GFP:

5' –CGGUGGUGCAGAUGAACUUCAGGGUCA

DS RNA sense labeled with Alexa 488:

5' –ACCCUGAAGUUCAUCUGCACCACCG-Alexa488

DS RNA antisense labeled with Alexa 546:

5' –Alexa 546-CGGUGGUGCAGAUGAACUUCAGGGUCA

Fibers and polygons with split Dicer Substrate (DS) RNAs against *BRAF*[V600E] gene (4):

To assemble fibers carrying sense (antisense) strands, mix *BRAF* fiber sense (antisense) DNA strand 1 with *BRAF* fiber sense (antisense) DNA strand 2 with *BRAF* DS RNA sense (antisense) in 1 to 1 to 2 ratio.

BRAF fiber sense DNA strand 1:

5' –AAGGGATTTCCCTAAATCGAGATTTCTCTGTAGCTAGACTTCCCTAAAGGGA

BRAF fiber sense DNA strand 2:

5' –AGGGAAATCCCTTAAATCGAGATTTCTCTGTAGCTAGACTCCCTTTAGGGAA

BRAF fiber antisense DNA strand 1

5' –TCCCTTTAGGGAAGTCTAGCTACAGAGAAATCTCGATTTAGGGAAATCCCTT

BRAF fiber antisense DNA strand 2:

5' –TTCCCTAAAGGGAGTCTAGCTACAGAGAAATCTCGATTTAAGGGATTTCCCT

BRAF DS RNA sense:

5' –/5Phos/GCUACAGAGAAAUCUCGAUGGAGUG

BRAF DS RNA antisense:

5' –CACUCCAUCGAGAUUUCUCUGUAGCUU

13 bp DNA duplex used for Tm studies:

5'-AAGGGATTTCCCT

5- AGGGAAATCCCTT

2.5   References

1.   Vogel,A.B., Lambert,L., Kinnear,E., Busse,D., Erbar,S., Reuter,K.C., Wicke,L., Perkovic,M., Beissert,T., Haas,H. *et al.* (2018) Self-Amplifying RNA vaccines give equivalent protection against influenza to mRNA vaccines but at much lower doses. *Mol. Ther.*, **26**, 446–455.
2.   Chakraborty,C., Sharma,A.R., Sharma,G., Doss,C.G.P. and Lee,S.S. (2017) Therapeutic miRNA and siRNA: Moving from bench to clinic as next generation medicine. *Mol. Ther. Nucleic Acids*, **8**, 132–143.
3.   Sun,H. and Zu,Y. (2015) Aptamers and their applications in nanomedicine. *Small*, **11**, 2352–2364.
4.   Adams,D., Gonzalez-Duarte,A., O'Riordan,W.D., Yang,C.C., Ueda,M., Kristen,A.V., Tournev,I., Schmidt,H.H., Coelho,T., Berk,J.L. *et al.* (2018) Patisiran, an RNAi therapeutic, for hereditary transthyretin amyloidosis. *N. Engl. J. Med.*, **379**, 11–21
5.   Grijalvo,S., Alagia,A., Jorge,A.F. and Eritja,R. (2018) Covalent strategies for targeting messenger and Non-Coding RNAs: An updated review on siRNA, miRNA and antimiR conjugates. *Genes (Basel)*, **9**, E74.
6.   Sasaki,S. and Guo,S. (2018) Nucleic acid therapies for cystic fibrosis. *Nucleic Acid Ther.*, **28**, 1–9.
7.   Nimjee,S.M., White,R.R., Becker,R.C. and Sullenger,B.A. (2017) Aptamers as therapeutics. *Annu. Rev. Pharmacol. Toxicol.*, **57**, 61–79.
8.   Barbalat,R., Ewald,S.E., Mouchess,M.L. and Barton,G.M. (2011) Nucleic acid recognition by the innate immune system. *Annu. Rev. Immunol.*, **29**, 185–214.
9.   Junt,T. and Barchet,W. (2015) Translating nucleic acid-sensing pathways into therapies. *Nat. Rev. Immunol.*, **15**, 529–544.
10.   Radovic-Moreno,A.F., Chernyak,N., Mader,C.C., Nallagatla,S., Kang,R.S., Hao,L., Walker,D.A., Halo,T.L., Merkel,T.J., Rische,C.H. *et al.* (2015) Immunomodulatory spherical nucleic acids. *Proc. Natl. Acad. Sci. U.S.A.*, **112**, 3892–3897.
11.   Halman,J.R., Satterwhite,E., Roark,B., Chandler,M., Viard,M., Ivanina,A., Bindewald,E., Kasprzak,W.K., Panigaj,M., Bui,M.N. et al. (2017) Functionally-interdependent shape-switching nanoparticles with controllable properties. Nucleic Acids Res., 45, 2210–2220.
12.   Johnson,M.B., Halman,J.R., Satterwhite,E., Zakharov,A.V., Bui,M.N., Benkato,K., Goldsworthy,V., Kim,T., Hong,E., Dobrovolskaia,M.A. et al. (2017)

Programmable Nucleic Acid Based polygons with controlled neuroimmunomodulatory properties for predictive QSAR modeling. Small, 13, doi:10.1002/smll.201701255.

13. Bui,M.N., Brittany Johnson,M., Viard,M., Satterwhite,E., Martins,A.N., Li,Z, Marriott,I., Afonin,K.A. and Khisamutdinov,E.F. (2017) Versatile RNA tetra-U helix linking motif as a toolkit for nucleic acid nanotechnology. Nanomedicine, 13, 1137–1146

14. Afonin,K.A., Desai,R., Viard,M., Kireeva,M.L., Bindewald,E., Case,C.L., Maciag,A.E., Kasprzak,W.K., Kim,T., Sappe,A. et al. (2014) Co-transcriptional production of RNA-DNA hybrids for simultaneous release of multiple split functionalities. Nucleic Acids Res., 42, 2085–2097.

15. Afonin,K.A., Viard,M., Kagiampakis,I., Case,C.L., Dobrovolskaia,M.A., Hofmann,J., Vrzak,A., Kireeva,M., Kasprzak,W.K., KewalRamani,V.N. et al. (2015) Triggering of RNA interference with RNA-RNA, RNA-DNA, and DNA-RNA nanoparticles. ACS Nano, 9, 251–259.

16. Khisamutdinov,E.F., Li,H., Jasinski,D.L., Chen,J., Fu,J. and Guo,P. (2014) Enhancing immunomodulation on innate immunity by shape transition among RNA triangle, square and pentagon nanovehicles. Nucleic Acids Res., 42, 9996–10004.

17. Li,H., Lee,T., Dziubla,T., Pi,F., Guo,S., Xu,J., Li,C., Haque,F., Liang,X.J. and Guo,P. (2015) RNA as a stable polymer to build controllable and defined nanostructures for material and biomedical applications. Nano Today, 10, 631–655.

18. Khisamutdinov,E.F., Jasinski,D.L. and Guo,P. (2014) RNA as a boiling-resistant anionic polymer material to build robust structures with defined shape and stoichiometry. *ACS Nano*, **8**, 4771–4781.

19. Saragliadis,A., Krajewski,S.S., Rehm,C., Narberhaus,F. and Hartig,J.S. (2013) Thermozymes: Synthetic RNA thermometers based on ribozyme activity. *RNA Biol.*, **10**, 1010–1016.

20. Modi,S., Nizak,C., Surana,S., Halder,S. and Krishnan,Y. (2013) Two DNA nanomachines map pH changes along intersecting endocytic pathways inside the same cell. *Nat. Nanotechnol.*, **8**, 459–467.

21. Morse,D.P., Nevins,C.E., Aggrey-Fynn,J., Bravo,R.J., Pfaeffle,H.O.I. and Laney,J.E. (2018) Sensitive and specific detection of ligands using engineered riboswitches. *J. Biotechnol.*, **272–273**, 22–32.

22. Andersen,E.S., Dong,M., Nielsen,M.M., Jahn,K., Subramani,R., Mamdouh,W., Golas,M.M., Sander,B., Stark,H., Oliveira,C.L. *et al.* (2009) Self-assembly of a nanoscale DNA box with a controllable lid. *Nature*, **459**, 73–76.

23. Bindewald,E., Afonin,K.A., Viard,M., Zakrevsky,P., Kim,T. and Shapiro,B.A. (2016) Multistrand structure prediction of Nucleic Acid Assemblies and design of RNA switches. *Nano Lett.*, **16**, 1726–1735.

24. Douglas,S.M., Bachelet,I. and Church,G.M. (2012) A logic-gated nanorobot for targeted transport of molecular payloads. *Science*, **335**, 831–834.

25. Li,S., Jiang,Q., Liu,S., Zhang,Y., Tian,Y., Song,C., Wang,J., Zou,Y., Anderson,G.J., Han,J.Y. *et al.* (2018) A DNA nanorobot functions as a cancer therapeutic in response to a molecular trigger in vivo. *Nat. Biotechnol.*, **36**, 258–264.

26. Afonin,K.A., Viard,M., Martins,A.N., Lockett,S.J., Maciag,A.E., Freed,E.O., Heldman,E., Jaeger,L., Blumenthal,R. and Shapiro,B.A. (2013) Activation of different split functionalities on re-association of RNA-DNA hybrids. *Nat. Nanotechnol.*, **8**, 296–304.

27. Afonin,K.A., Kasprzak,W.K., Bindewald,E., Kireeva,M., Viard,M., Kashlev,M. and Shapiro,B.A. (2014) In silico design and enzymatic synthesis of functional RNA nanoparticles. *Acc. Chem. Res.*, **47**, 1731–1741.

28. Afonin,K.A., Viard,M., Koyfman,A.Y., Martins,A.N., Kasprzak,W.K., Panigaj,M., Desai,R., Santhanam,A., Grabow,W.W., Jaeger,L. *et al.* (2014) Multifunctional RNA nanoparticles. *Nano Lett.*, **14**, 5662–5671.

29. Dao,B.N., Viard,M., Martins,A.N., Kasprzak,W.K., Shapiro,B.A. and Afonin,K.A. (2015) Triggering RNAi with multifunctional RNA nanoparticles and their delivery. *DNA RNA Nanotechnol.*, **1**, 27–38.

30. Martins,A.N., Ke,W., Jawahar,V., Striplin,M., Striplin,C., Freed,E.O. and Afonin,K.A. (2017) Intracellular reassociation of RNA-DNA hybrids that activates RNAi in HIV-Infected cells. *Methods Mol. Biol.*, **1632**, 269–283.

31. Afonin,K.A., Viard,M., Tedbury,P., Bindewald,E., Parlea,L., Howington,M., Valdman,M., Johns-Boehme,A., Brainerd,C., Freed,E.O. *et al.* (2016) The use of minimal RNA toeholds to trigger the activation of multiple functionalities. *Nano Lett.*, **16**, 1746–1753.

32. Rogers,T.A., Andrews,G.E., Jaeger,L. and Grabow,W.W. (2015) Fluorescent monitoring of RNA assembly and processing using the split-spinach aptamer. *ACS Synth. Biol.*, **4**, 162–166.

33. Groves,B., Chen,Y.J., Zurla,C., Pochekailov,S., Kirschman,J.L., Santangelo,P.J. and Seelig,G. (2016) Computing in mammalian cells with nucleic acid strand exchange. *Nat. Nanotechnol.*, **11**, 287–294.

34. Rose,S.D., Kim,D.H., Amarzguioui,M., Heidel,J.D., Collingwood,M.A., Davis,M.E., Rossi,J.J. and Behlke,M.A. (2005) Functional polarity is introduced by Dicer processing of short substrate RNAs. *Nucleic Acids Res.*, **33**, 4140–4156.

35. Mitchell,S., Vargas,J. and Hoffmann,A. (2016) Signaling via the NFnB system. *Wiley Interdiscip. Rev. Syst. Biol. Med.*, **8**, 227–241.

36. Porciani,D., Tedeschi,L., Marchetti,L., Citti,L., Piazza,V., Beltram,F. and Signore,G. (2015) Aptamer-Mediated codelivery of doxorubicin and NF-kappaB decoy enhances chemosensitivity of pancreatic tumor cells. *Mol. Ther. Nucleic Acids*, **4**, e235.

37. Griesenbach,U., Scheid,P., Hillery,E., de Martin,R., Huang,L., Geddes,D.M. and Alton,E.W. (2000) Anti-inflammatory gene therapy directed at the airway epithelium. *Gene Ther.*, **7**, 306–313.

38. Kim,K.H., Lee,E.S., Cha,S.H., Park,J.H., Park,J.S., Chang,Y.C. and Park,K.K. (2009) Transcriptional regulation of NF-kappaB by ring type decoy oligodeoxynucleotide in an animal model of nephropathy. *Exp. Mol. Pathol.*, **86**, 114–120.

39. Brasier,A.R. (2006) The NF-kappaB regulatory network. *Cardiovasc. Toxicol.*, **6**, 111–130.

40. Gilmore,T.D. (2006) Introduction to NF-kappaB: players, pathways, perspectives. *Oncogene*, **25**, 6680–6684.

41. Zadeh,J.N., Steenberg,C.D., Bois,J.S., Wolfe,B.R., Pierce,M.B., Khan,A.R., Dirks,R.M. and Pierce,N.A. (2011) NUPACK: Analysis and design of nucleic acid systems. *J. Comput. Chem.*, **32**, 170–173.

42. Afonin,K.A., Grabow,W.W., Walker,F.M., Bindewald,E., Dobrovolskaia,M.A., Shapiro,B.A. and Jaeger,L. (2011) Design and self-assembly of siRNA-functionalized RNA nanoparticles for use in automated nanomedicine. *Nat. Protoc.*, **6**, 2022–2034.

43. Alibakhshi,M.A., Halman,J.R., Wilson,J., Aksimentiev,A., Afonin,K.A. and Wanunu,M. (2017) Picomolar fingerprinting of nucleic acid nanoparticles using solid-state nanopores. *ACS Nano*, **11**, 9701–9710.

44. Shlyakhtenko,L.S., Gall,A.A. and Lyubchenko,Y.L. (2013) Mica functionalization for imaging of DNA and protein-DNA complexes with atomic force microscopy. *Methods Mol. Biol.*, **931**, 295–312.

45. Shlyakhtenko,L.S., Gall,A.A., Filonov,A., Cerovac,Z., Lushnikov,A. and Lyubchenko,Y.L. (2003) Silatrane-based surface chemistry for immobilization of DNA, protein-DNA complexes and other biological materials. *Ultramicroscopy*, **97**, 279–287.

46. Afonin,K.A., Viard,M., Martins,A.N., Lockett,S.J., Maciag,A.E., Freed,E.O., Heldman,E., Jaeger,L., Blumenthal,R. and Shapiro,B.A. (2013) Activation of different split

functionalities upon re-association of RNA-DNA hybrids. *Nat. Nanotechnol.*, **8**, 296–304.

47. Markham,N.R. and Zuker,M. (2005) DINAMelt web server for nucleic acid melting prediction. *Nucleic Acids Res.*, **33**, W577–W581.

48. Sharma,S., Ding,F. and Dokholyan,N.V. (2008) iFoldRNA: three-dimensional RNA structure prediction and folding. *Bioinformatics*, **24**, 1951–1952.

49. Shirvanyants,D., Ding,F., Tsao,D., Ramachandran,S. and Dokholyan,N.V. (2012) Discrete molecular dynamics: an efficient and versatile simulation method for fine protein characterization. *J. Phys. Chem. B*, **116**, 8375–8382.

50. Ding,F., Sharma,S., Chalasani,P., Demidov,V.V., Broude,N.E. and Dokholyan,N.V. (2008) Ab initio RNA folding by discrete molecular dynamics: from structure prediction to folding mechanisms. *RNA*, **14**, 1164–1173.

51. Berendsen,H.J.C., van der Spoel,D. and van Drunen,R. (1995) GROMACS: a message-passing parallel molecular dynamics implementation. *Comput. Phys. Commun.*, **91**, 43–56.

52. Jonikas,M.A., Radmer,R.J., Laederach,A., Das,R., Pearlman,S., Herschlag,D. and Altman,R.B. (2009) Coarse-grained modeling of large RNA molecules with knowledge-based potentials and structural filters. *RNA*, **15**, 189–199.

53. Stenvang,J., Petri,A., Lindow,M., Obad,S. and Kauppinen,S. (2012) Inhibition of microRNA function by antimiR oligonucleotides. *Silence*, **3**, 1.

54. Vessillier,S., Eastwood,D., Fox,B., Sathish,J., Sethu,S., Dougall,T., Thorpe,S.J., Thorpe,R. and Stebbings,R. (2015) Cytokine release assays for the prediction of therapeutic mAb safety in first-in man trials–Whole blood cytokine release assays are poorly predictive for TGN1412 cytokine storm. *J. Immunol. Methods*, **424**, 43–52.

55. Zuckerman,S.H., Evans,G.F. and Guthrie,L. (1991) Transcriptional and post-transcriptional mechanisms involved in the differential expression of LPS-induced IL-1 and TNF mRNA. *Immunology*, **73**, 460–465.

56. Dobrovolskaia,M.A. (2015) Pre-clinical immunotoxicity studies of nanotechnology-formulated drugs: challenges, considerations and strategy. *J. Control. Release*, **220**, 571–583.

57. Inoue,K. (2011) Promoting effects of nanoparticles/materials on sensitive lung inflammatory diseases. *Environ. Health Prev. Med.*, **16**, 139–143.

58. Inoue,K. and Takano,H. (2011) Aggravating impact of nanoparticles on immune-mediated pulmonary inflammation. *ScientificWorldJournal*, **11**, 382–390.

59. Inoue,K., Takano,H., Yanagisawa,R., Hirano,S., Sakurai,M., Shimada,A. and Yoshikawa,T. (2006) Effects of airway exposure to nanoparticles on lung inflammation induced by bacterial endotoxin in mice. *Environ. Health Perspect.*, **114**, 1325–1330.

60. Hong,E. and Dobrovolskaia,M.A. (2018) Addressing barriers to effective cancer immunotherapy with nanotechnology: achievements, challenges, and roadmap to the next generation of nanoimmunotherapeutics. *Adv. Drug. Deliv. Rev.*, doi:10.1016/j.addr.2018.01.005.

61. Kondo,S. and Sauder,D.N. (1997) Tumor necrosis factor (TNF) receptor type 1 (p55) is a main mediator for TNF-alpha-induced skin inflammation. *Eur. J. Immunol.*, **27**, 1713–1718.

62. Phillips,A., Patel,C., Pillsbury,A., Brotherton,J. and Macartney,K. (2018) Safety of human papillomavirus vaccines: an updated review. *Drug Saf.*, **41**, 329–346.

63. Miller,E.R., Lewis,P., Shimabukuro,T.T., Su,J., Moro,P., Woo,E.J., Jankosky,C. and Cano,M. (2018) Post-licensure safety surveillance of zoster vaccine live (Zostavax(R)) in the United States, Vaccine Adverse Event Reporting System (VAERS), 2006–2015. *Hum Vaccin Immunother*, **14**, 1963–1969.

64. Woo,E.J., Moro,P.L., Cano,M. and Jankosky,C. (2017) Postmarketing safety surveillance of trivalent recombinant influenza vaccine: reports to the vaccine adverse event

reporting system. *Vaccine*, **35**, 5618–5621.

65.　　Gause,K.T., Wheatley,A.K., Cui,J., Yan,Y., Kent,S.J. and Caruso,F. (2017) Immunological principles guiding the rational design of particles for vaccine delivery. *ACS Nano*, **11**, 54–68.

66.　　De Gregorio,E. (2015) The path forward. *Vaccine*, **33**(Suppl. 2), B60–B63.

67.　　Reed,S.G., Hsu,F.C., Carter,D. and Orr,M.T. (2016) The science of vaccine adjuvants: advances in TLR4 ligand adjuvants. *Curr. Opin. Immunol.*, **41**, 85–90.

68.　　Hanagata,N. (2017) CpG oligodeoxynucleotide nanomedicines for the prophylaxis or treatment of cancers, infectious diseases, and allergies. *Int. J. Nanomed.*, **12**, 515–531.

69.　　Hong,E., Halman,J.R., Shah,A.B., Khisamutdinov,E.F., Dobrovolskaia,M.A. and Afonin,K.A. (2018) Structure and composition define immunorecognition of Nucleic Acid Nanoparticles. *Nano Lett.*, **18**, 4309–4321.

70.　　Davies,H., Bignell,G.R., Cox,C., Stephens,P., Edkins,S., Clegg,S., Teague,J., Woffendin,H., Garnett,M.J., Bottomley,W. *et al.* (2002) Mutations of the BRAF gene in human cancer. *Nature*, **417**, 949–954.

71.　　Hingorani,S.R., Jacobetz,M.A., Robertson,G.P., Herlyn,M. and Tuveson,D.A. (2003) Suppression of BRAF(V599E) in human melanoma abrogates transformation. *Cancer Res.*, **63**, 5198–5202.

72.　　Rackley,L., Stewart,J.M., Salotti,J., Krokhotin,A., Shah,A., Halman,J., Juneja,R., Smollett,J., Roark,B., Viard,M. *et al.* (2018) RNA fibers as optimized nanoscaffolds for siRNA coordination and reduced immunological recognition. *Adv. Funct. Mater.*, **28**, 1805959.

73.　　Sosman,J.A., Kim,K.B., Schuchter,L., Gonzalez,R., Pavlick,A.C., Weber,J.S., McArthur,G.A., Hutson,T.E., Moschos,S.J., Flaherty,K.T. *et al.* (2012) Survival in BRAF V600-mutant advanced melanoma treated with vemurafenib. *N. Engl. J. Med.*, **366**, 707–74.

74.　　Lehraiki,A., Cerezo,M., Rouaud,F., Abbe,P., Allegra,M., Kluza,J., Marchetti,P., Imbert,V., Cheli,Y., Bertolotto,C. *et al.* (2015) Increased CD271 expression by the NF-kB pathway promotes melanoma cell survival and drives acquired resistance to BRAF inhibitor vemurafenib. *Cell Discov.*, **1**, 15030.

75.　　Liu,J., Suresh Kumar,K.G., Yu,D., Molton,S.A., McMahon,M., Herlyn,M., Thomas-Tikhonenko,A. and Fuchs,S.Y. (2007) Oncogenic BRAF regulates beta-Trcp expression and NF-kappaB activity in human melanoma cells. *Oncogene*, **26**, 1954–1958.

76.　　Rosette,C. and Karin,M. (1995) Cytoskeletal control of gene expression: depolymerization of microtubules activates NF-kappa B. *J. Cell Biol.*, **128**, 1111–1119.

77.　　Ghosh,G., Huang,D. and Huxford,T. (2011) Recognition of nucleic acids by transcription factor NF-kB. In: Williams,M.C. and Maher,LJ III (eds). *Biological System*. Springer-Verlag, pp. 85–106.

78.　　Jonikas, M.A., Radmer, R.J., Laederach, A., Das, R., Pearlman, S., Herschlag, D. and Altman, R.B. (2009) Coarse-grained modeling of large RNA molecules with knowledge-based potentials and structural filters. *RNA*, **15**, 189-199.

3   Chapter 3: Effective lock and unlock thrombin functionality by nucleic acid nano-device

3.1   Introduction

Blood clotting, or coagulation, is a critical mechanism that prevents excessive bleeding when a blood vessel is damaged. The coagulation cascade involves many proteins which are activated one after another, ultimately leading to the formation of fibrin strands that strengthen the platelet plug. There are three pathways that contribute to the blood coagulation process. Modern time-based in vitro coagulation tests provide a reasonable model to measure time elapsed from coagulation cascade activation at different points to the generation of fibrin[1]. Thrombin is one of the most important proteins in the coagulation cascade. It has multiple functional roles including activating platelets and coagulation factors V, VIII and XI, and cleaving fibrinogen to fibrin as a procoagulant. On the other hand, it also acts as an anticoagulant by binding to thrombomodulin which, in turn, causes fibrinolysis[2]. Thrombin has a globular shape with three functional binding sites: the protease catalytic site, the anionic fibrinogen recognition site (exosite I), and the anionic heparin binding site (exosite II) [3]. Exosite I and II are on opposite sides of the protein, and they mediate its interactions with cofactors and substrates. The catalytic site enables thrombin as a serine protease, it is negatively charged and located on the β-chain of thrombin[4].

The blood coagulation process begins with the exposure of tissue factor, together with factor VIIa, generating small quantities of factor Xa and IXa[5]. Subsequently, the minute concentration of Xa activates factor XI and cofactors VIII and V. When sufficient quantities of Xa are produced, the prothrombinase complex composed of factors Va, Xa, $Ca2^+$, and phospholipids is formed. At that point, a large amount of thrombin will be generated from prothrombin[6].

Sometimes, clots can form inside of vessels even in the absence of injury. These situations can be life threatening, requiring accurate diagnosis and timely treatment. Deep vein thrombosis (DVT) is a type of clot that forms in a major vein, often in the lower leg or thigh. The clot may break loose and detach from its origin. If it travels through the heart to the lungs and becomes

trapped, a life-threatening pulmonary embolism (PE) may occur. Clotting in arteries is often associated with atherosclerosis - a condition characterized by plaque deposits which narrow the arterial canal. High arterial pressure may cause the plaques to rupture. Molecules released during this process form an arterial clot, potentially precipitating a heart attack or stroke. Compared to the general population, cancer patients have a 5- to 6-fold increased risk of venous thromboembolism (VTE) characterized by DVT and PE as well as major bleeding episodes[7].

Anticoagulants are a vital class of drugs that reduce and prevent blood clots from forming inside the body; they are often called blood thinners. These medications are used in short-term surgical procedures as well as long-term treatment and prevention of thrombosis in high risk groups. In short-term surgery, anticoagulation is essential for safely performing invasive procedures. There are several types of anticoagulants on the market including: Warfarin (Coumadin), low molecular weight heparins (Dalteparin, Tinzaparin and Enoxaparin)[8], and factor Xa inhibitors (Rivaroxaban, Apixaban and Edoxaban)[9]. These drugs are known for inducing excessive bleeding (haemorrhage) as a side effect leading to further complications such as passage of blood in urine, severe bruising, bleeding gums, prolonged nosebleeds, and heavy bleeding during menstruation[10]. Therefore, a novel, effective, and safe treatment of thrombotic diseases with easy, rapid, and reversible control of the coagulation process is in high demand.

Nucleic acid aptamers are single-stranded DNA or RNA with lengths ranging from 20 to 100 nucleotides[11]. They readily undergo adaptive conformational changes, resulting in a unique binding conformation corresponding to a specific target[12]. Their high specificity and selectivity, low cost, biocompatibility, biodegradability, high affinity, low toxicity, and efficiency as protein-based drugs make nucleic acid aptamers a promising class of novel pharmaceuticals[13, 14]. A particular group of guanine-rich aptamers stand out due to their ability to fold into stable G-quadruplex structures consisting of four guanines assembled in a planar shape through Hoogsteen hydrogen bonding and stabilizing stacking interactions of G-quartets[15]. G-quadruplex structures are thermodynamically

and chemically stable, immunoquiescent, and resistant to serum nucleases[16]. Aptamers containing G-quadruplex structures been extensively studied for anti-HIV[17], anti-proliferative[18], anti-tumor[19], and anti-thrombin applications [20-22], as well as nanodevices[23] and aptasensors[24].

The anti-thrombin aptamer offers several potential clinical advantages over traditional drugs used for anticoagulation. Aptamers' high specificity effectively decreases the possibility of unintended effects[24]. For the past two decades, a variety of DNA aptamers targeting human thrombin have been developed using SELEX[25]. Among them, the first and most well-known anti-thrombin aptamer was discovered in 1992 by Bock who successfully identified thrombin-binding aptamer (TBA). TBA is a 15-mer DNA G-quadruplex with the sequence d (GGTTGGTGTGGTTGG) that possesses anti-thrombin activity[26]. Characterization of the thrombin-aptamer interaction using X-ray crystallography and NMR showed that binding activity was taking place at exosite-I rather than the thrombin active site. Thus, the anti-thrombin aptamer can inhibit both free and clot-bound thrombin[27, 28]. Because TBA is highly susceptible to nuclease degradation in a biological environment, its therapeutic usage is limited[28]. As a result, more efficient anti-thrombin aptamers with high affinity and biostability are required. Numerous modifications of anti-thrombin TBA, such as RA-36 (31-mer) and NU172 (20-mer), have been developed[26]. RA-36's structure is based on TBA's sequence, but it augments the underlying structure with two covalently linked pharmacophore G-quadruplexes. Pharmacophore is defined as "an ensemble of steric and electronic features that is necessary to ensure the optimal supramolecular interactions with a specific biological target and to trigger (or block) its biological response" by the IUPAC[30]. The first pharmacophore targets and inhibits thrombin activity, whereas the second one is an aptamer modulator that varies the properties of the pharmacophore module[13]. RA-36 exerts its anti-coagulant effect by binding to exosite-I on thrombin, preventing fibrinogen from binding to the thrombin molecule[31]. NU172 is another potent anti-thrombin aptamer that folds into a duplex/G-quadruplex complex. Such a structure possesses an intramolecular compactness that provides a

boundary surface for interaction with thrombin exosite-I[32]. Also, NU172 is able to bind to both prothrombin and thrombin, thereby enhancing its anticoagulant properties[33]. Clinical trials using NU172 for the treatment of heart disease have been conducted (NCT00808964)[34]. Both RA-36 and NU172 anti-thrombin aptamers are effective anticoagulants. Unfortunately, they often suffer from rapid degradation and renal clearance, yielding a short half-life which hampers further clinical use[36, 36].

In this work, we develop a robust and dynamic platform based on rationally designed RNA–DNA fibers decorated with anti-thrombin aptamers for efficient and reversible control of blood coagulation. We have developed a RNA–DNA hybrid fiber that was featured in a recent publication from our group[14]. This molecular device assembles multiple aptamers and substantially increases their molecular weight, prolonging their blood stability and increasing their retention time. Another unique benefit of this RNA–DNA fiber anti-thrombin aptamer system is its ability to be regulated therapeutically via kill-switch fibers that reverse its anticoagulant function. These kill-switch fibers can rapidly reverse anti-thrombin activity by recognizing and binding to the aptamer's primary sequence through complete Watson-Crick base pairing. The disrupted aptamer structure is no longer able to bind, leaving the target thrombin intact and functional[37]. Essentially, when the kill-switch fibers are applied, thrombin functionality is retrieved and the coagulation cascade can resume. We successfully assembled RNA–DNA fibers with NU172 and RA 36 aptamers and characterized the assembly using Native-PAGE along with AFM. We demonstrated effective inhibition of human plasma coagulation using the constructs and reversal of this effect through introduction of the kill-switch fibers in vitro. The reassociation process described in our previous paper[14] resulted in a rapid disassembly of anti-thrombin fiber devices and promoted the excretion of aptamers from the human body. We investigated the biodistribution and retention time of anti-thrombin fibers compared with free aptamers in vivo. Moreover, cytokine production induced by the anti-thrombin fibers was evaluated during this study, and our results show our constructs have

minimal immunogenicity. Overall, our system has the following advantages: 1) Simple design and assembly leading to lower costs and shorter experimental time. 2) Anti-thrombin aptamer successfully prolongs blood coagulation time. 3) Attaching fibers to the aptamer and increasing its molecular weight stabilized the aptamer and extended its blood circulation time. 4) Kill-switch fibers successfully restore thrombin activity. 5) The kill-switch fibers rapidly disassemble the device and promote aptamer excretion.

3.2   Methods

3.2.1   Assembly and characterizaion of anti-thrombin aptamer fibers and kill-switch fibers

All individual ssDNAs, ssRNAs, and fluorescently labeled oligos were purchased from Integrated DNA Technologies, Inc. The sequence of NU172 DNA aptamer was obtained from Zavyalova et al, Current Medicinal Chemistry 2013, and the aptamer sequence was embedded to either one end or both ends of DNA oligonucleotides. Similarly, the sequence of RA-36 was obtained from Zavyalova et al, Frontiers in Pharmacology, 2017, the aptamer is attached to either one end or both ends of DNA oligonucleotides. Kill-switch fibers are reverse complementary sequence. Anti-thrombin aptamer fibers and their kill-switch fibers were assembled by combining individual monomers at equimolar concentrations in hybridization buffer (89 mM Tris, 80 mM Boric Acid (pH 8.3), 2 mM magnesium acetate) and was heated to 95°C for 5 minutes followed by snap-cooling to room temperature and further incubation for 20 minutes. Assemblies and their reassociations were analyzed at 4°C on 8% non-denaturing native polyacrylamide (19:1) gel electrophoresis (native-PAGE) in the presence of hybridization buffer. A Bio-Rad ChemiDoc MP Imager was used to visualize gels stained with ethidium bromide and view the fluorescence of labeled RNAs. All assemblies for in vivo study were further tested for the presence of bacterial endotoxins by kinetic turbidity limulus amoebocyte lysate (LAL) assay, as detailed in our previous work[1].

3.2.2   Blood Stability

Freshly drawn human blood serum (blood was allowed to coagulate, then spun down and

supernatant was collected) was immediately aliquoted and frozen at -80 °C. Antithrombin aptamer fibers (1 µM final) and the kill-switch fibers (1 µM final) were mixed with 10% human blood serum respectively at 37°C and aliquoted 2µl at each time points with 2ul Native PAGE loading buffer. The mixtures were placed on dry ice and were loaded in reverse time order and analyzed by 8% native-PAGE at 4°C. The bands of treated samples were visualized with a Bio-Rad ChemiDoc MP System and analyzed using Image Lab™ Software and compared to the bands of corresponding untreated nanoparticles to determine the relative degradation. Ethidium bromide staining was used to assist the visualization.

3.2.3   Kinetics of Reassociation

To determine the kinetics, Alexa 546 labeled antithrombin aptamer fibers were mixed with equimolar ss and aliquoted at set time points. 2µl of the antithrombin aptamer with its kill-switch fiber was aliquoted at each time points with 2ul Native PAGE loading buffer. The mixtures were placed on dry ice and were loaded in reverse time order and analyzed by 8% native-PAGE at 4°C. The bands of treated samples were visualized with a Bio-Rad ChemiDoc MP System and analyzed using Image Lab™ Software and compared to the bands of corresponding untreated nanoparticles to determine the relative degradation. Ethidium bromide staining was used to assist the visualization. Images with and without Ethidium bromide staining were performed.

3.2.4   Atomic Force Microscopy (AFM) imaging

A freshly cleaved mica surface was modified with APS (1-(3-Aminopropyl) silatrane) according to established protocol[1-3]. 5 µL of 1 µM sample solution were deposited onto APS modified mica for 2 min. The unbound assemblies and excess of salts were washed twice with 50 µL of DI water and the mica surface was dried under a stream of argon gas. AFM imaging was performed on MultiMode AFM Nanoscope IV system (Bruker Instruments, Santa Barbara, CA) in tapping mode. The images were recorded with 1.5 Hz scanning rate using a TESPA-300 probe from Bruker with a resonance frequency of 320 kHz and spring constant about 40 N/m. Images were processed by the FemtoScan Online software package (Advanced Technologies Center, Moscow,

Russia).

3.2.5 Prothrombin, Activated Partial Thromboplastin and Thrombin Time Assessment

Blood was obtained under NCI-at-Frederick Protocol OH9-C-N046. The blood was collected from least three healthy donors and anti-coagulated with sodium citrate. A plasma pool was prepared by spinning down the blood in a centrifuge for 10 min at 2500g and was used within 8h after collection. 50 µL antithrombin fibers or kill-switch fibers with concentration of 5µM were added to 450 µLof human plasma in a 1.5mL eppendorf tube. The tubes were incubated in 37°C incubator for 30 mins. Following manufacture's protocol, the respective reagents were added to induce the coagulation cascade, the Diagnostica Stago ST4 Coagulation Analyzer was used to determine the PT, aPTT and TT.

3.2.6 Complement Activation Determined by iC3b EIA kit

Complement activation was determined by the cleavage of the C3 factor by enzyme immunoassay for the presence of iC3b. The antibodies specific to iC3b were immobilized on 96 well plates and were obtained from MicroVue by Quidel. Blood was obtained under NCI-at-Frederick Protocol OH9-C-N046. The blood was collected from least three healthy donors and anti-coagulated with EDTA. A plasma pool was prepared by spinning down the blood in a centrifuge for 10 min at 2500g and was used within 8h after collection. The samples were prepared at a concentration three times higher than the tested concentration (500nM). Cobra venom factor (CVF) (Quidel Corporation, San Diego, USA) was used as a positive control. 50µL (1.0-1.2 mg/ml) of CVF solution was used. PEGylated liposomal doxorubicin (Doxil) was also used as a positive control which is a prescription medication available from a licensed pharmacy (20 mg of Doxorubicin HCl in 10 mL of vehicle). 50µL of Doxil solution was used and 50µL PBS was used as a negative control. In a 1.5mL eppendorf tube, combined 50µL veronal buffer, 50µL human plasma, and 50µL CVF, Doxil, PBS and anti-thrombin fibers or kill-switch fibers. Plasma samples were prepared in complement specimen diluent reagent (provided with each kit). Use the following

dilution guide: iC3b—1:500 for CVF; 1:10 for negative control and other test samples. Two replicates of each sample were prepared. Vortex and centrifuge then incubate in a 37 °C incubator for 30 mins. 100μL aliquots was used in EIA for each replicates. Following the manufacturer's instruction to reconstitute complement standard, buffers, and controls as well as for plate loading volumes, incubation time, and plate washing. Read the optical density at 405nm and analyze the assay results using a semi-log curve fit.

3.2.7 Primary Human Peripheral Blood Mononuclear Cell (PBMC) Isolation and Treatment with NANPs

Blood was obtained under NCI-at-Frederick Protocol OH9-C-N046. The blood was collected from at least three healthy donors and anti-coagulated with Lithium-heparin. It was mixed 1:1 with PBS at room temperature and layered on top of the Ficoll-Paque Plus, then centrifuged at 900 g with low acceleration and no brake for 30 mins at room temperature. The mononuclear layer was collected and 3 times the volume of 1X HBSS was added and centrifuged at 400g for 15 mins at room temperature. This wash step was repeated one more time then resuspended in complete RPMI medium (RPMI 1640 with 10% FBS, 2mM L-glutamine, and penicillin/streptomycin). Live cells were enumerated by AO/PI and used in subsequent experiments. To stimulate PBMCs with antithrombin fibers or kill-switch fibers for cytokine induction assessment, the cells were seeded at 1.25×10^6 cells/mL in 96 well U-bottomed plates, 200 μL per well. Antithrombin fibers or kill-switch fiber at 1μM stock solution were complexed to Lipofectamine 2000 at a 5:1 v/v ratio. After 30 min incubation at room temperature, OptiMEM was added which brought the final concentration of antithrombin fibers or kill-switch fibers to 50nM. Afterwards, 40μL of prepared controls and antithrombin fibers or kill-switch fibers were added to PBMC, for a final stimulation concentration of 10 nM. After 20 h incubation at 37 °C, supernatants were collected and analyzed for cytokines by multiplexed ELISA (Q-Plex™ Multiplex Array from Quansys Biosciences).

3.2.8 Animal study

Prior to the animal study, anti-thrombin fibers and their kill-switch fibers were screened for

endotoxin contamination in order to minimize toxicity risk resulting from presence of bacterial structural components that might elicit a lethal pyrogenic response. Eight-week-old male Balb/C mice were purchased from Jackson Laboratory. All animal experiments were carried out in compliance with institutional guidelines (Protocol #: 18-007). The oligos were assembled in vitro in the Afonin lab just prior to in vivo experiment. In all sample preparation, endotoxin-free HyClone Cell Culture-Grade Water was used to avoid endotoxin contamination. Total 50 mice were used in this study. Anti-thrombin fibers were injected via R.O. with 100 µl of 500 nM solutions. For the groups with kill-switch fibers, one injection each in alternating eyes with 100 ul of 500 nM of anti-thrombin fibers and with 100 ul of 500 nM kill-switch fibers was performed, respectively. Experimental and control groups (N=5/group) were imaged at 15 minutes, 30 minutes, 1 hour and 2 hours using IVIS. At the 2-hour time point, animals were enthanized (isoflurance 1-3% followed by cervical dislocation) and the organs (lungs, heart, kidneys and liver) were extracted and imaged for fluorescence. A portion of liver and kidneys were later weighted and lysed, their fluorescence amount were determined by IVIS. Lab sand was purchased from Datesand and were used in all cages for urine collection after the injection. The urine was collected from all animals and the relative amounts of fluorescence were determined by IVIS. A standard curve was used to normalize the fluorophore concentration of the constructs.

3.2.9 Limulus Amoebocyte Lysate (LAL) assay

The LAL assay was utilized to assess preparation contamination with the bacterial endotoxin, lipopolysaccharide. The anti-thrombin fibers and the kill-switch fibers were tested at several dilutions according to a standardized procedure described in NCL method (https://ncl.cancer.gov/sites/default/files/protocols/NCL_Method_STE-1.2.pdf)[41].Controls contain the addition of known quantities of an endotoxin standard to nanoparticle samples to eliminate potential nanoparticle interference with the assay. Reported values were from dilutions that demonstrated acceptable spike recovery and did not interfere with the assay.

3.2.10 Statistics
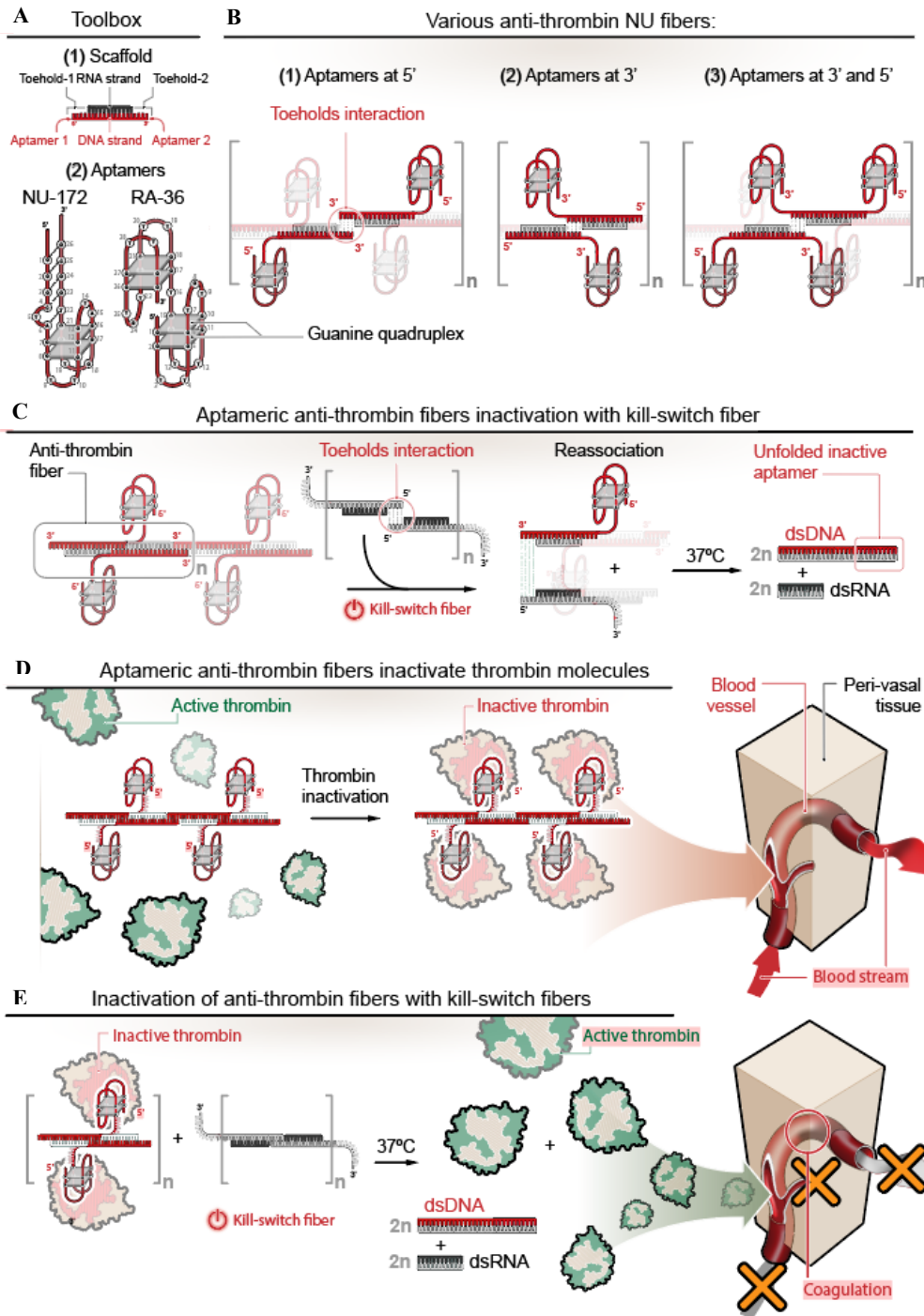
Figure 27. Schematic of anti-thrombin fibers inhibiting thrombin functionality and kill-switch fibers restoring thrombin functionality. (A) The design of anti-thrombin fiber and the structure of NU172 and RA-36 aptamers. (B) 3 possible aptamer locations on RNA–DNA fibers. (C) Kill-switch fibers inactivate anti-thrombin fibers causing reassociation which produces dsDNA and dsRNA. (D) Anti-thrombin fibers bind to thrombin, inactivating thrombin functionality, and in turn, preventing the blood clotting cascade. (E) Kill-switch fibers bind to anti-thrombin fibers with full complementary sequence, causing anti-thrombin fiber detachment, retrieval of thrombin function, and thrombosis reactivation.

The results of the different assays were presented as mean ± standard deviation (SD). Each experiment was performed at least three times (n ≥ 3) and a t-test was carried out to determinate significant differences. In all cases, differences were considered significant when $p < 0.05$.

3.3 Results and discussion
Design, Assembly and Characterization of anti-thrombin fibers

In a previous communication, we reported a novel assembly of dynamic RNA–DNA fibers with a simple design and fabrication protocol that displayed high stability in human blood serum[14]. Here, we combined the advantages of this system with incorporation of anti-thrombin aptamers to interrupt the coagulation cascade. The effectiveness of this approach relies on thrombin inactivation as well as prolonged aptamer retention time due to increased molecular weight. We designated these RNA–DNA/aptamer complexes as anti-thrombin fibers. The anti-thrombin aptamer was attached either at the 5' end or the 3' end, or both ends of the RNA–DNA fibers. To exert even greater control over thrombin activity, we designed kill-switch fibers that possess high affinity due to full complementarity with anti-thrombin (Figure 27). Kill-switch fiber binding results in the detachment of anti-thrombin fibers from thrombin, ultimately retrieving full thrombin functionality. When anti-thrombin fibers and kill-switch fibers are introduced in close proximity inside a cell, the thermodynamically driven isothermal reassociation process leads to release of double stranded (ds) RNAs and dsDNAs. The short duplexes increase the excretion rate and accelerate fiber clearance. Formation of anti-thrombin and kill-switch fibers, along with their reassociation, was confirmed by native-PAGE and visualized by AFM (Figure 28). The AFM images illustrate the fiber shapes of both anti-thrombin fibers and the associated kill-switch fibers (Figure 28A). Anti-thrombin fibers were fluorescently labeled and incubated together with their kill-switch fibers. The reassociation process was monitored every half hour over a five-hour period and incubation was continued at 37°C up to 24 hours. Native-PAGE analysis confirmed the release of dsDNA and dsRNA as reassociation products (Figure 28B). The three anti-thrombin fibers and their corresponding kill-switch fibers showed different reassociation times. A kinetics study
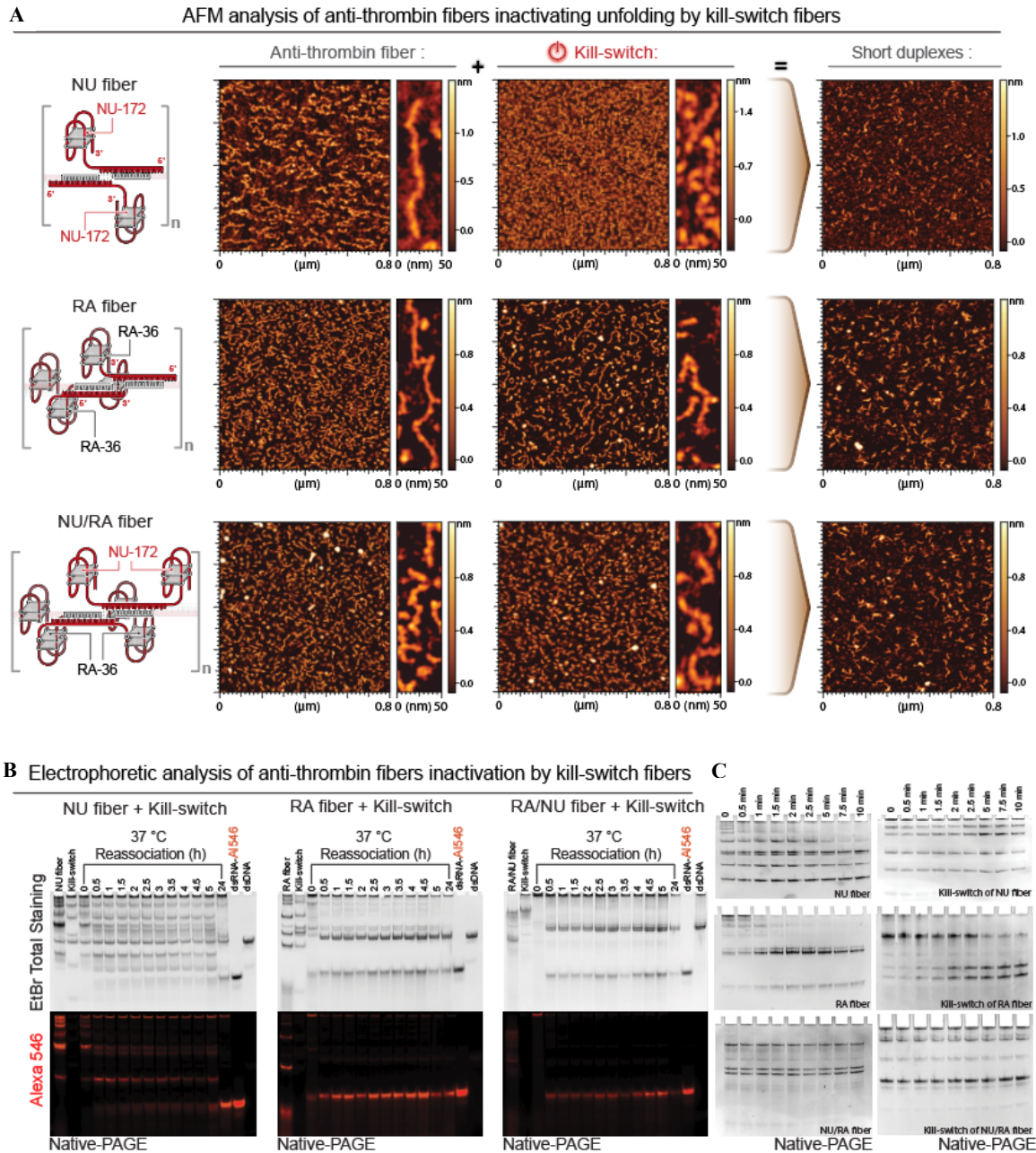
Figure 28. In vitro characterization of antithrombin and kill-switch fibers. (A) AFM images showing antithrombin and kill-switch fibers as well as their reassociation products. (B) The reassociation of antithrombin fibers and corresponding kill-switch fibers at various timepoints analyzed by native-PAGE gel. (C) Blood stability of anti-thrombin aptamers and kill-switch fibers at different timepoints. NU fiber: NU172 aptamer attached on 3' of DNA1 and 3' of DNA2. RA fiber: RA-36 aptamer attached on 3' of DNA1 and 5' of DNA2. RA/NU fiber: NU172 aptamer attached on both 5' and 3' of DNA1, and RA-36 aptamer on both 5' and 3' of DNA2. Kill switch of NU fiber: complements of NU fiber. Kill switch of RA fiber: complements of RA fiber. Kill switch of RA/NU fiber: complements of RA/NU fiber.

showed that RA fibers and NU/RA fibers reassociated much faster than NU fibers: RA fibers and

NU/RA fibers needed less than 30 minutes for complete reassociation, whereas NU fibers required up to 24h of incubation to complete this process. (Figure 28B). To investigate durability of both anti-thrombin fibers and their kill-switch fibers in blood, a blood stability assay was performed (Figure 28C). Within 10 minutes, this experiment showed the presence of various anti-thrombin fibers of different designs. NU, RA and RA anti fiber underwent slow digestion by human blood serum, whereas NU/RA, anti NU, and anti NU/RA fibers failed to undergo any noticeable changes. After 24 hours elapsed, the assay indicated that all structures were broken down.

To study the faster reassociation rate of RA and NU/RA fibers, we analyzed the structure of NU, RA and RA/NU fibers computationally. The three-dimensional structures of NU172 and RA-36 aptamers show the presence of two symmetric G quadruplexes in the RA-36 aptamer and one G-quadruplex in the NU aptamer (Figure 29A). Next, we performed molecular dynamics simulations using DMD and calculated the RMSF (root mean square fluctuation). RA/NU fibers have higher RMSF (3.65 Å) than RA fibers (3.37 Å) and NU fibers (3.21 Å) (Figure 29B). The high RMSF regions mostly consist of the 5' and 3' ends of the DNA strands, the G-quadruplex regions, and the single stranded regions that connect G-quadruplex and duplex regions of the DNA strands. The number of G-quadruplexes is directly related to the flexibility and length of the fibers. RA/NU fibers contain 6 G-quadruplex regions, RA fibers contain 4 G-quadruplex regions and NU fibers contain 2 G-quadruplex regions. Thus, RA/NU fibers have greater flexibility and shorter length than RA fibers, while RA fibers are more flexible and shorter than NU fibers. Due to their high degree of flexibility, RA/NU fibers are most prone to disassociation. The interaction between NU fiber and thrombin is indicated in Figure 30D.

Immunorecognition of anti-thrombin fibers

To determine whether antithrombin fibers can be recognized by the immune system and the magnitude of associated production of type I interferons (IFNs), human peripheral blood mononuclear cells (PBMC) were treated with constructs (Figure 30). Type I interferon production

is usually triggered by pathogen-associated molecular patterns which recognize nucleic acid nanoparticles (NANPs) and lipopolysaccharides[38]. In this experiment, we studied NU, RA and RA/NU fibers as well as NU fiber with three different concentrations in PBMC cultures derived from the blood of three healthy donor volunteers. PBMCs were chosen as a model system because they provide a more accurate prediction of cytokine storm toxicity in humans as compared to other preclinical in vivo studies in non-human primates and rodents. Thus, PBMCs, and their responses to cytokine- mediated toxicities, represent an ideal model for studies of novel therapeutics.
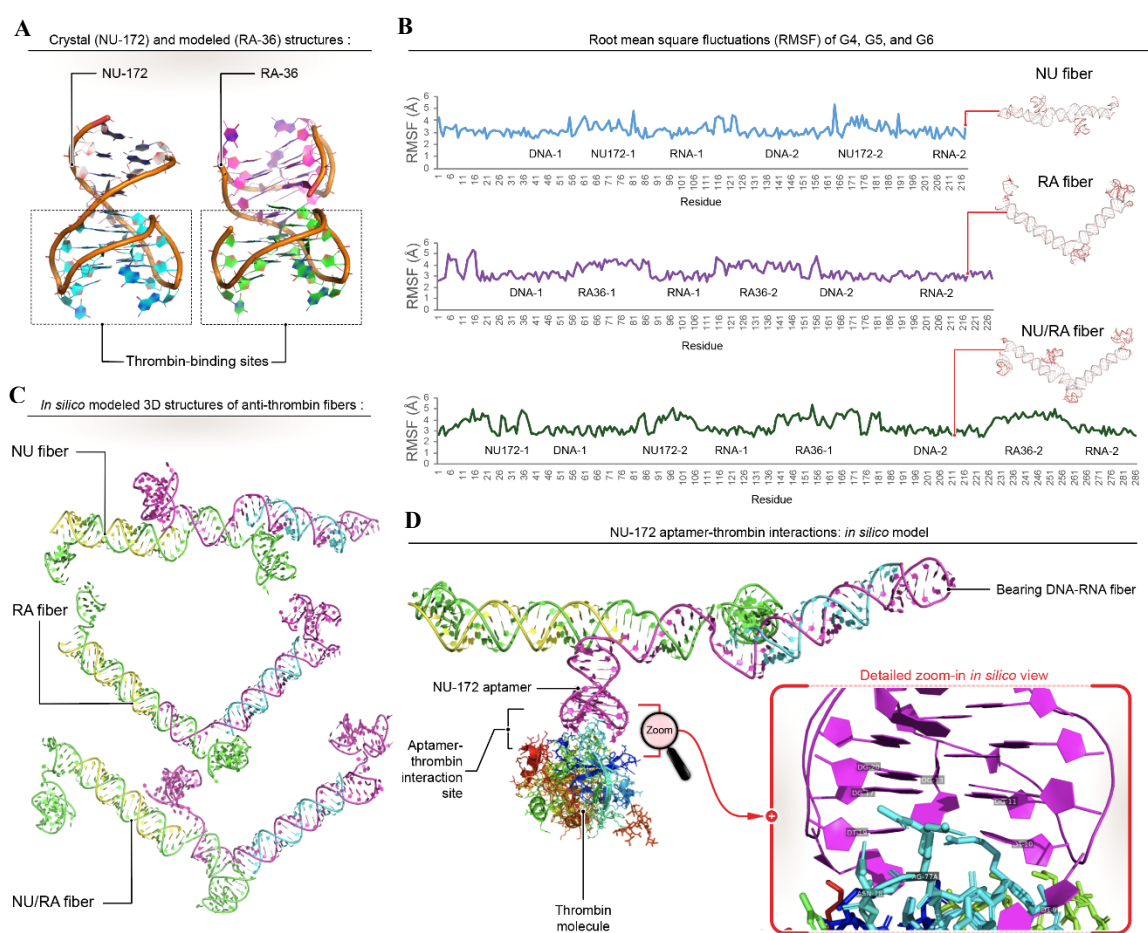
Figure 29. Molecular dynamics stimulation of the aptamers and anti-thrombin fibers. (A) Comparison of the 3D structures of NU172 and RA36. Left: crystal structure of NU172 (PDB ID: 6GN7). The G-quadruplex region is colored by cyan. Right: modeled structure of RA36. The structure is composed of two g-quadruplex regions (green and magenta). Both regions are identical to the region in NU172. (B) Root mean square fluctuation (RMSF) of NU fibers (top), RA fibers (middle), and RA/NU fibers (bottom). (C) 3D structure of NU fibers (top), RA fibers (middle), and RA/NU fibers (bottom). (D) 3D structure of the interaction of NU fiber and thrombin. The labeled residues indicate where the interaction occurs.

The complement system plays an essential role in innate immunity[40]. This system is composed of over 30 plasma proteins that trigger a proteolytic cascade upon activation, resulting in the production of opsonins and anaphylatoxins. Ultimately, this process leads to the formation of a membrane attack complex whose purpose is to destroy invading pathogens[41]. There are three pathways of complement activation: lectin, classical and alternative. Activation of any of these pathways involves a series of cleavage reactions that culminate in the formation of C3 convertase[42]. C3 convertase cleaves its complement component, C3, to generate large amounts of C3b, the main effector molecule of the complement system[42]. Therefore, production of C3b serves to indicate which complement system is activated. Here, we used an immunoassay to detect the presence of C3b (Figure 30B). The same experiment was performed to detect C3b in plasma treated with Cobra venom factor (CVF), a known complement-activating protein from cobra venom that functionally resembles C3b[43]. Our data show activation by any of the constructs is less than that seen with administration of Doxil (Pegylated liposomal doxorubicin) medications that are used extensively in various cancer treatments. Hence, no significant activation was observed under the given experimental conditions. Although these results do not completely rule out potential complement activation at higher concentrations or in particularly sensitive individuals, the outcomes seem promising and suggest negligible stimulation of the complement system by antithrombin fibers.

Further more, NU fiber with 3 concentrations (10nM, 100nM and 500nM) are tested in PBMC (Figure 30C), we didn't observe the cytokine responses were related to concentration but rather displayed a donor specific manner, eg. IL-15. IL-7, IL-17 and hIFNλ showed more potent stimulation among three donor than other cytokines. The other cytokines displayed negligible responses compared to individual negative controls.

Lock and unlock thrombin activity by anti-thrombin and kill-switch fibers

There are three pathways that lead toward the coagulation cascade. The contact activation, or intrinsic, pathway is activated by trauma within the vascular system. The tissue factor, or extrinsic
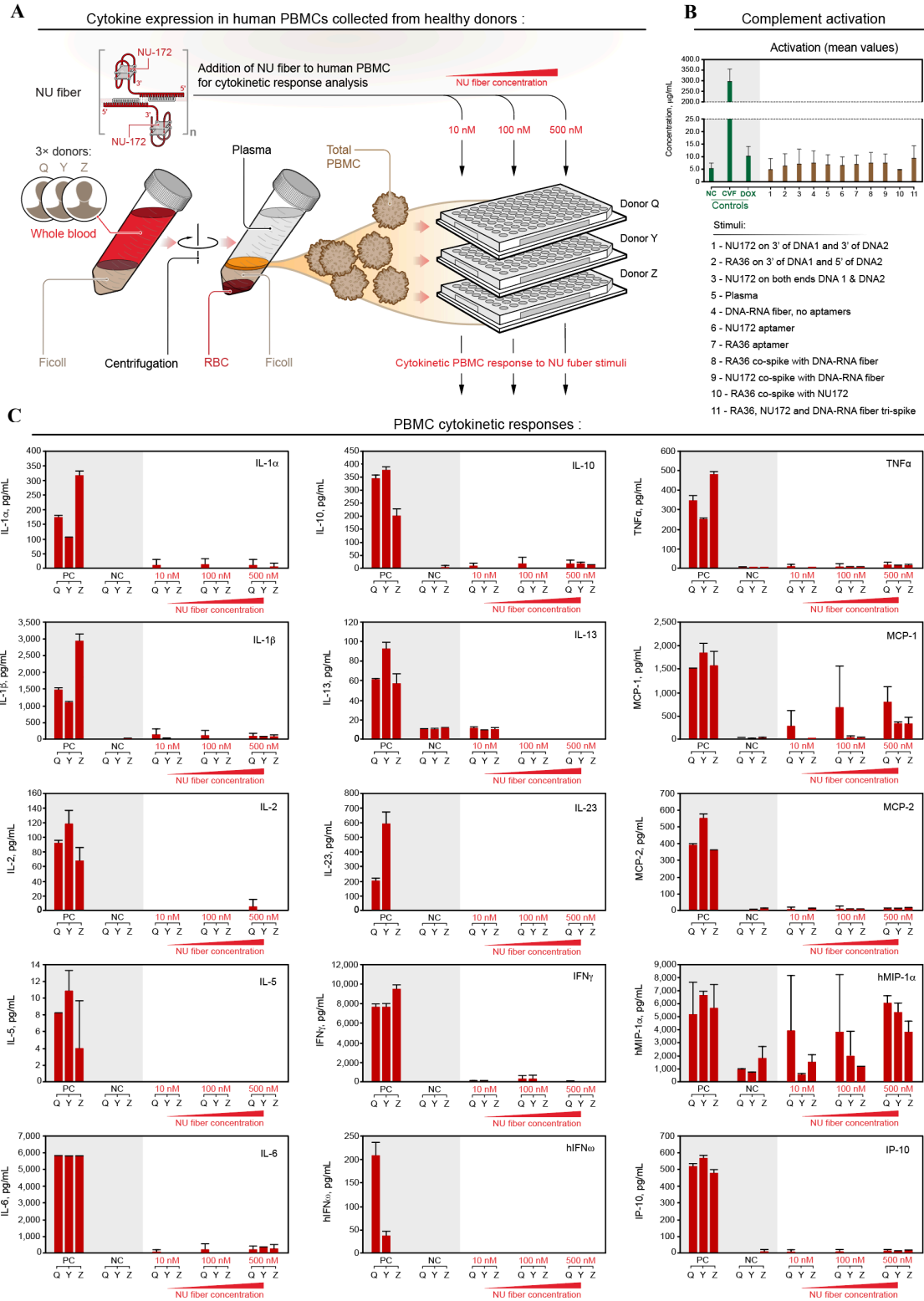
Figure 30. The immune response of antithrombin fibers. (A) Schematic representation. (B) Complement activation of antithrombin fibers and aptamers. (C) Cytokine stimulation of NU fibers at different concentrations.

A

B

Sample	US Data	Brazil Data	US Data	Brazil Data	US Data	Brazil Data
	PT Mean (s) 13.4s	PT Mean (s) 13.4s	APTT Mean (s) 34.1s	APTT Mean (s) 34.1s	TT Mean (s) 21s	TT Mean (s) 21s
NU fiber	17.33±0.23	16.55±0.25	120.00±0	89.40±1.40	60.00±0	26.75±0.15
RA fiber	16.60±0.41	19.70±0.20	70.90±5.01	104.65±1.85	60.00±0	31.55±0.55
RA/NU fiber	16.78±0.37	17.70±0	81.30±4.26	100.35±1.45	60.00±0	28.60±0
DNA-RNA fiber	11.84±0.33	13.50±0.20	36.68±0.75	40.20±0.10	15.76±0.71	19.30±0.10
plasma	10.76±0.17	13.60±0.20	33.37±1.20	28.60±0.30	16.28±0.34	19.40±0.10
Aptamer NU172	10.90±0.23	14.05±0.15	37.98±1.46	39.50±0.10	15.32±0.75	18.95±0.15
Aptamer RA36	11.32±0.38	15.30±0.50	41.50±3.15	45.52±0.80	16.55±0.77	26.45±0.45

C

Sample	PT Mean (s) 13.4s	APTT Mean (s) 34.1s	TT Mean (s) 21s
Control (Normal)	12.65±0.15	36.80±1.50	21.35±0.55
Control (Abnormal)	20.65±0.35	71.75±1.35	41.30±1.40
Plasma	9.65±0.03	29.38±0.15	16.13±0.276
NU172 Aptamer	16.07±0.50	37.93±0.70	25.32±1.79
RA36 Aptamer	17.27±0.33	44.18±0.62	45.00±1.42
NU Fiber	18.56±1.65	101.68±2.01	59.52±0.48
NU Fiber + kill-switch	10.92±0.13	36.73±0.16	17.53±0.43
RA fiber	20.83±0.09	89.93±1.11	60.00±0.00
RA fiber + kill-switch	13.67±0.09	42.90±0.26	44.70±0.06
RA/NU Fiber	16.80±0.94	95.25±2.95	60.00±0
RA/NU Fiber + kill-switch	10.58±0.32	38.52±0.38	18.40±0.59

Figure 31. Plasma coagulation assessment. (A) Schematic presentation of the process of the experiment: whole blood was collected from 3 healthy donors and centrifuged to isolate the "buffy coat", which is then incubated with constructs and assayed for coagulation time using a coagulometer. (B) Results of prothrombin time (PT), activated partial thromboplastin time (APTT) and thrombin time (TT) of anti-thrombin fibers for their abilities in delaying the coagulation between the donors from the United States and Brail, displayed regional variations. (C) Results of prothrombin time (PT), activated partial thromboplastin time (APTT) and thrombin time (TT) of anti-thrombin fibers with their kill-switch fibers. The addition of kill-swtich fibers restored the

normal coagulation time. In this study, whole blood were collected from donors from the United States only.

pathway is activated by trauma-induced blood loss outside of the vascular system and is always more rapid than the intrinsic system. The common pathway is the final step in the cascade to which both intrinsic and extrinsic pathways lead and which results in fibrin formation[44].

Coagulation assays allowed direct measurement of the overall speed of blood clot formation (Figure 31). Activated partial thromboplastin time (APTT) measures the overall speed of intrinsic and common pathways. Prothrombin time (PT) measures the quality of the extrinsic and common pathways. Thrombin time (TT) assesses the speed of the common pathway. APTT, PT and TT tests all evaluate thrombin functionality because thrombin is the key protein in the common coagulation pathway. When anti-thrombin fibers bind to thrombin at its exosite-I location, fibrinogen is unable to bind to thrombin. Therefore, anti-thrombin fibers play a key role in thrombin deactivation. In order to evaluate the effectiveness of antithrombin fibers with regard to thrombin inhibition, we performed APTT, PT and TT tests on blood samples donated by volunteers from the United States and Brazil (Figure 31B). APTT tests showed significantly prolonged APTT time (cf. 34.1s for normal APTT) of all three antithrombin fibers compared to free NU172 and RA aptamers. Also, we observed variation of APTT performance between the American and Brazilian donors. PT tests showed a slightly delayed coagulation process among all three antithrombin fibers (cf.13.4s for normal PT) compared to free NU172 and RA aptamers. Donor variation between American and Brazilian subjects was not significant among the fibers, but there exist clear differences among the controls. Finally, TT tests showed that the three antithrombin fibers tested on US donors dramatically prolonged the coagulation process compared to free NU172 aptamers, RA36 aptamers and fibers tested on the Brazilian donors. Clearly, antithrombin fiber performance differs by nationality, especially for the APTT and TT tests. Furthermore, we added kill-switch fibers to retrieve thrombin functionality and assess their efficacy. After equimolar amounts of kill-switch fibers were added to the samples, APTT, PT and TT values returned to normal (Figure 31C).

A Removal of anti-thrombin fibers from mouse blood circulation system with kill-switch fiber

B Removal of anti-thrombin fibers from mouse blood circulation system with kill-switch fiber

C *Post mortem* NANP organ accumulation analysis:
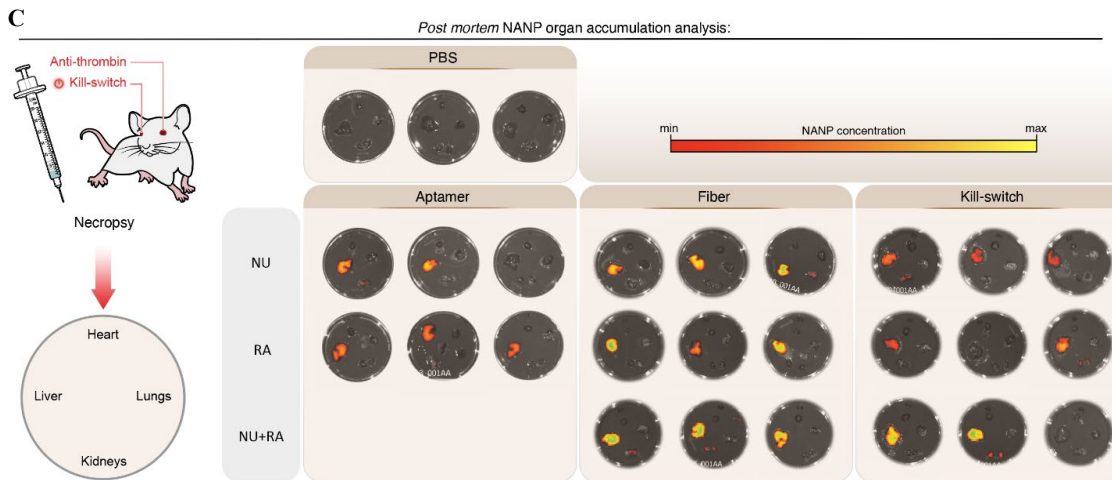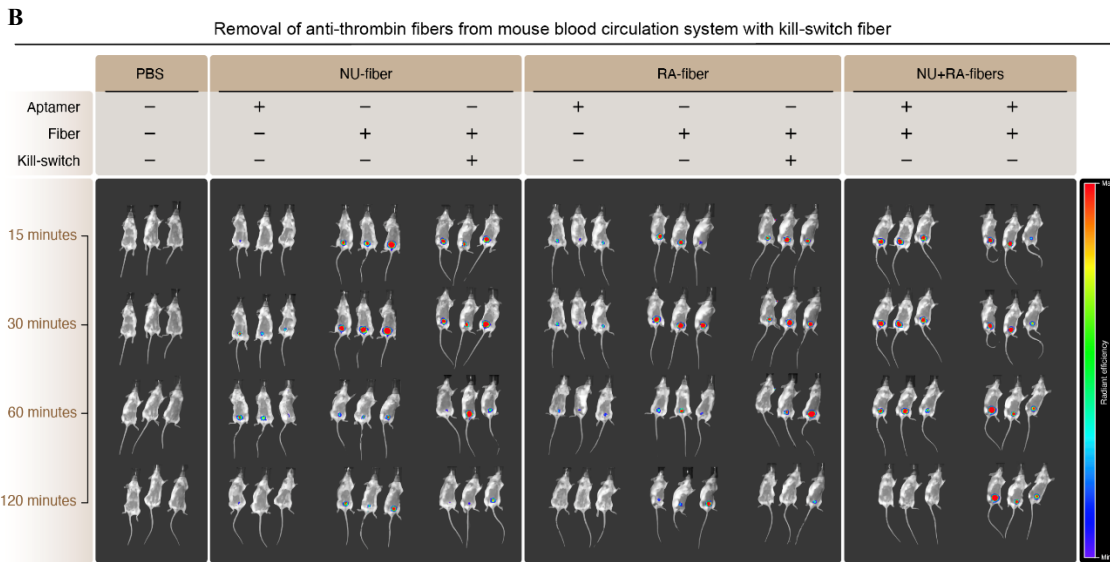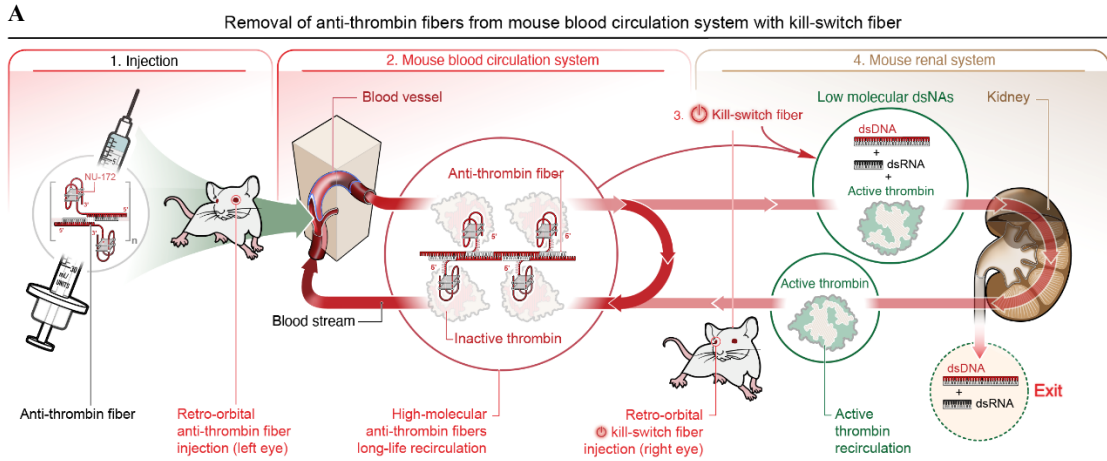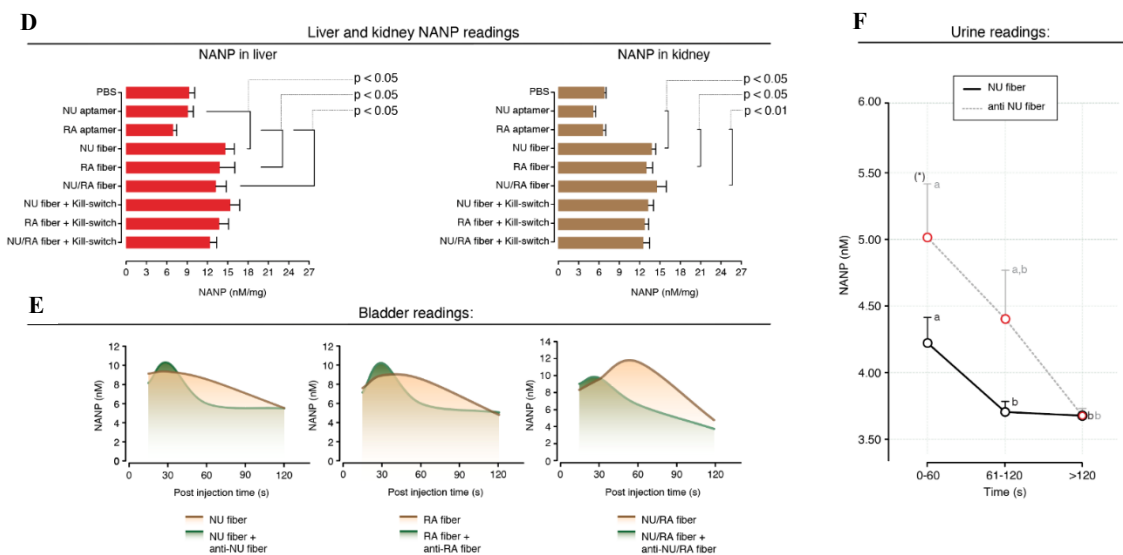
Figure 32. In vivo biodistribution and ex vivo organ lysate experiment. (A) Schematic presentation of the process of the experiment. (B) Mice images at different timepoints post injection. (C) Ex vivo organ imaging 2 hours post injection. (D) Constructs concentration in lysed kidneys, constructs concentration in lysed liver. (E) constructs concentration in bladder at different timepoints after injection. (F) constructs concentration in urine at different timepoints after injection.

These results suggest the kill-switch fibers successfully inactivated anti-thrombin fibers, thereby allowing us to conditionally control thrombin functionality. APTT, PT and TT from other constructs tested in this work are listed in Table 2.

In vivo biodistribution

To further examine in vivo behavior of anti-thrombin fibers and their associated kill-switch fibers, fluorescent-labeled anti-thrombin and kill-switch fibers were administered to BALB/c mice via retro-orbital injection. Biodistribution of both entities was evaluated using an in vivo optical imaging system (IVIS) at various timepoints post-injection (Figure 32). Whole-body fluorescence analysis revealed a strong signal in the bladder region (Fig 32B). Compared to free NU172 or RA-36 aptamers, aptamers conjugated with fibers exhibited prolonged retention in the bladder. Following kill-switch fiber administration, we observed rapid excretion likely due to reassociation of anti-thrombin and kill-switch fibers and concomitant generation of short DNA and RNA duplexes (Figure 32B).

No significant difference in whole-body imaging marking the biodistribution of anti-thrombin and kill-switch fibers was detected (Figure32B). At euthanasia, organs including liver, kidneys, heart, brain, spleen, and lungs were harvested and imaged ex vivo two hours post-injection (Figure 32C). Liver and kidney tissues displayed the highest level of fluorescence (Fig 32C). Lysate of liver and kidneys were obtained and their fluorescent intensity i.e., concentration of the constructs measured (Fig 32D). The concentrations of anti-thrombin fibers were significantly higher than those measured following free aptamer administration (Fig 32D). No difference was detected following the addition of kill-switch fibers possibly because of the renal excretion of the constructs throughout the duration of the experiments.

Next, the overtime fluorescence of the bladder of the treated mice was recorded and assessed as estimated concentrations (see Methods for details, Figure 32E). The three pairs of anti-thrombin and their kill-switch fibers all displayed similar bladder distribution over time. Around 30 minutes post injections, anti-thrombin fibers exhibited a peak accumulation in the bladder, and then the concentration was decreased. NU/RA fiber had a smoother reduction than NU and RA fibers. NU/RA fibers also showed the lowest concentration at the endpoint of this study (2 hours post injection) which indicated that they were excreted from the system the fastest. With the addition of the kill-switch fibers, NU/RA kill-switch fibers also showed a delayed accumulation in bladder around 60 minutes post injection compare to a slightly increase seen in other two kill-switch fibers. These observations suggest that aptamer excretion kinetics may be modulated depending on the aptamer combination used.

Finally, in a follow-up experiment, urine concentrations of NU fibers and anti-NU fibers were assessed over time (Figure 32F). The presence of kill-switch fibers increased the anti-thrombin fiber excretion rate, and this rate remained constant throughout the first 120 min.

3.4 Conclusion

In conclusion, we demonstrated control of thrombin activity by using antithrombin fibers and

their complementary kill-switch fibers while investigating their potential for immunostimulation and in vivo biodistribution. We showed efficient inhibition of thrombin functionality by antithrombin fibers which, in turn, yielded a prolonged coagulation time. On the other hand, kill-switch fibers successfully retrieve thrombin functionality. Also, we discovered that there was no significant complement activation observed, and cytokine activation was dependent on individual

Table 3. Blood coagulation of PT, APTT and TT results for all constructs used in this study. (Whole blood collected from donors in the United States)

Samples	Samples description	APTT (≤34.1s)		PT (≤ 13.4s)		TT (≤ 21s)	
		Mean (s)	SD	Mean (s)	SD	Mean (s)	SD
NU172 1+2	Both DNA have NU172 on 5' & 3' ends	92.28	16.68	21.60	15.49	55.98	6.08
NU172 L1+L2	NU172 on 5' of DNA1 and DNA2	86.54	28.44	15.68	2.13	56.76	7.24
NU172 L1 + R2	NU172 on 5' of DNA1 and 3' of DNA2	94.30	36.79	25.12	17.10	50.98	12.76
NU172 R1+R2 (NU fiber)	NU172 on 3' of DNA1 and 3' of DNA2	94.84	37.03	23.14	20.71	55.08	11.00
NU172 R1 + L2	NU172 on 3' of DNA1 and 5' of DNA2	97.96	31.41	20.04	4.89	60.00	0.00
RA36 1+2	Both DNA have RA36 on 5' & 3' ends	84.96	12.72	16.18	2.35	60.00	0.00
RA36 L1+L2	RA36 on 5' of DNA1 and DNA2	83.54	27.05	18.26	3.50	60.00	0.00
RA36 L1+R2	RA36 on 5' of DNA1 and 3' of DNA2	72.50	17.55	17.60	2.04	60.00	0.00
RA36 R1+R2	RA36 on 3' of DNA1 and 3' of DNA2	74.54	13.73	17.18	4.49	60.00	0.00
RA36 R1+L2 (RA fiber)	RA36 on 3' of DNA1 and 5' of DNA2	72.14	23.58	16.60	0.91	60.00	0.00
NU172 1 + RA36 2 (NU/RA fiber)	NU172 and RA36 on both ends of DNA1 & DNA2, respectively	89.04	18.81	16.42	4.16	60.00	0.00

RA36 R1	RA36 on 3' of the DNA1 and no aptamer on DNA2	75.50	6.26	20.50	5.53	60.00	0.00
DNA-RNA fiber	DNA-RNA fiber no aptamer	36.68	1.67	11.84	0.74	15.76	1.59
plasma	plasma	33.37	2.69	10.76	0.38	16.28	0.76
NU172 aptamer	NU172 aptamer	37.98	3.26	10.90	0.50	15.32	1.68
RA36 aptamer	RA36 aptamer	41.50	7.05	11.32	0.85	19.96	7.74

response. In vivo biodistribution indicated that fibers mostly accumulated in the liver and kidneys two hours post-injection. Short DNA and RNA duplexes resulting from the reassociation process between antithrombin fibers and their corresponding kill-switch fibers increased the rate of excretion in urine. Our data suggest that we were able to effectively lock and unlock thrombin functionality using nucleic acid nano-devices while successfully avoiding immunorecognition and fast excretion from circulation. In conclusion, this work demonstrated that nucleic acids complexed to antithrombin aptamers are effective, non- immunogenic and may pave the way towards an efficient and safe application as a novel and promising therapeutic platform.

3.5 Sequences used in this project

Anti-thrombin aptamer sequences:

NU172 Aptamer:

5' CGCCTAGGTTGGGTAGGGTGGTGGCG

NU172 Aptamer labeled with Fluor750:

5'- /5Alex750N/CGCCTAGGTTGGGTAGGGTGGTGGCG

RA-36 Aptamer:

5' GGTTGGTGTGGTTGGTGGTTGGTGTGGTTGG

RA-36 Aptamer labeled with Fluor750:

5' /5Alex750N/GGTTGGTGTGGTTGGTGGTTGGTGTGGTTGG

Anti-thrombin fiber:

To assemble anti-thrombin fibers, mix anti-thrombin aptamer DNA strand 1 with anti-thrombin aptamer DNA strand 2 with RNA antisense in 1 to 1 to 2 ratio.

NU172 1+2: NU172 aptamer on both right and left ends of the repeating unit of fiber

Fiber antisense DNA strand 1:

5'CGCCTAGGTTGGGTAGGGTGGTGGCGTTTTCCCTTTAGGGAATGACCCTGAAGTTC

ATCTGCACCACCGAGGGAAATCCCTT TTTCGCCTAGGTTGGGTAGGGTGGTGGCG

Fiber antisense DNA strand 2:

5' CGCCTAGGTTGGGTAGGGTGGTGGCGTTTTTCCCTAAAGGGATGACCCTGAAGTT

ATCTGCACCACCGAAGGGATTTCCCT TTTCGCCTAGGTTGGGTAGGGTGGTGGCG

RA36 1+2: RA36 aptamer on both right and left ends on repeating unit of the repeating unit of fiber

Fiber antisense DNA strand 1:

5'GGTTGGTGTGGTTGGTGGTTGGTGTGGTTGGTTTTCCCTTTAGGGAATGACCCTGAA
GTTCATCTGCACCACCGAGGGAAATCCCTTTTTGGTTGGTGTGGTTGGTGGTTGGTGT
GGTTGG

Fiber antisense DNA strand 2:

5'GGTTGGTGTGGTTGGTGGTTGGTGTGGTTGGTTTTTCCCTAAAGGGATGACCCTGA
AGTTCATCTGCACCACCGAAGGGATTTCCCTTTTGGTTGGTGTGGTTGGTGGTTGGTG
TGGTTGG

NU172 R1+R2 (NU fiber): Nu172 Aptamer on right side on repeating unit of fiber strand 1 and strand 2

Fiber antisense DNA strand 1:

5'TCCCTTTAGGGAATGACCCTGAAGTTCATCTGCACCACCGAGGGAAATCCCTTTTTC
GCCTAGGTTGGGTAGGGTGGTGGCG

Fiber antisense DNA strand 2:

5'TTCCCTAAAGGGATGACCCTGAAGTTCATCTGCACCACCGAAGGGATTTCCCTTTTC
GCCTAGGTTGGGTAGGGTGGTGGCG

NU172 L1 + R2: Nu172 Aptamer on left side on repeating unit of fiber strand 1 and right side on repeating unit of fiber 2

Fiber antisense DNA strand 1:

5'CGCCTAGGTTGGGTAGGGTGGTGGCGTTTTCCCTTTAGGGAATGACCCTGAAGTTC
ATCTGCACCACCGAGGGAAATCCCTT

Fiber antisense DNA strand 2:

5'TTCCCTAAAGGGATGACCCTGAAGTTCATCTGCACCACCGAAGGGATTTCCCTTTTC
GCCTAGGTTGGGTAGGGTGGTGGCG

NU172 R1 + L2: Nu172 Aptamer on right side of repeating unit of fiber strand 1 and left side of repeating unit of fiber 2

Fiber antisense DNA strand 1:

5'TCCCTTTAGGGAATGACCCTGAAGTTCATCTGCACCACCGAGGGAAATCCCTTTTTC
GCCTAGGTTGGGTAGGGTGGTGGCG

Fiber antisense DNA strand 2:

5'CGCCTAGGTTGGGTAGGGTGGTGGCGTTTTTCCCTAAAGGGATGACCCTGAAGTTC
ATCTGCACCACCGAAGGGATTTCCCT

NU172 L1+L2:Nu172 Aptamer on left side on repeating unit of fiber strand 1 and 2

Fiber antisense DNA strand 1:

5'CGCCTAGGTTGGGTAGGGTGGTGGCGTTTTCCCTTTAGGGAATGACCCTGAAGTTCATCTGCACCACCGAGGGAAATCCCTT

Fiber antisense DNA strand 2:

5'CGCCTAGGTTGGGTAGGGTGGTGGCGTTTTTCCCTAAAGGGATGACCCTGAAGTTCATCTGCACCACCGAAGGGATTTCCCT

RA36 R1+R2: RA-36 Aptamer on right side on repeating unit of fiber strand 1 and 2

Fiber antisense DNA strand 1:

5'TCCCTTTAGGGAATGACCCTGAAGTTCATCTGCACCACCGAGGGAAATCCCTTTTTGGTTGGTGTGGTTGGTGGTTGGTGTGGTTGG

Fiber antisense DNA strand 2:

5'TTCCCTAAAGGGATGACCCTGAAGTTCATCTGCACCACCGAAGGGATTTCCCTTTTGGTTGGTGTGGTTGGTGGTTGGTGTGGTTGG

RA36 L1+R2: RA-36 Aptamer on left side on repeating unit of fiber strand 1 and right side on repeating unit of fiber strand 2

Fiber antisense DNA strand 1:

5'GGTTGGTGTGGTTGGTGGTTGGTGTGGTTGGTTTTCCCTTTAGGGAATGACCCTGAAGTTCATCTGCACCACCGAGGGAAATCCCTT

Fiber antisense DNA strand 2:

5'TTCCCTAAAGGGATGACCCTGAAGTTCATCTGCACCACCGAAGGGATTTCCCTTTTGGTTGGTGTGGTTGGTGGTTGGTGTGGTTGG

RA36 R1+L2 (RA fiber): RA-36 aptamer on right side on repeating unit of fiber strand 1 and left side on repeating unit of fiber strand 2

Fiber antisense DNA strand 1:

5'TCCCTTTAGGGAATGACCCTGAAGTTCATCTGCACCACCGAGGGAAATCCCTTTTTGGTTGGTGTGGTTGGTGGTTGGTGTGGTTGG

Fiber antisense DNA strand 2:

5'GGTTGGTGTGGTTGGTGGTTGGTGTGGTTGGTTTTCCCTAAAGGGATGACCCTGAAGTTCATCTGCACCACCGAAGGGATTTCCCT

RA36 L1+L2: RA-36 aptamer on left side on repeating unit of fiber strand 1 and 2

Fiber antisense DNA strand 1:

5'GGTTGGTGTGGTTGGTGGTTGGTGTGGTTGGTTTTCCCTTTAGGGAATGACCCTGAAGTTCATCTGCACCACCGAGGGAAATCCCTT

Fiber antisense DNA strand 2:

5'GGTTGGTGTGGTTGGTGGTTGGTGTGGTTGGTTTTCCCTAAAGGGATGACCCTGAAGTTCATCTGCACCACCGAAGGGATTTCCCT

NU172 1 + RA36 2 (RA/NU fiber): Nu172 Aptamer on left and right sides on repeating unit of fiber strand 1 and RA36 aptamer on left and right sides on repeating unit of fiber strand 2

Fiber antisense DNA strand 1:

5'CGCCTAGGTTGGGTAGGGTGGTGGCGTTTTCCCTTTAGGGAATGACCCTGAAGTTC
ATCTGCACCACCGAGGGAAATCCCTTTTTCGCCTAGGTTGGGTAGGGTGGTGGCG

Fiber antisense DNA strand 2:

5'GGTTGGTGTGGTTGGTGGTTGGTGTGGTTGGTTTTTCCCTAAAGGGATGACCCTGAA
GTTCATCTGCACCACCGAAGGGATTTCCCTTTTGGTTGGTGTGGTTGGTGGTTGGTGT
GGTTGG

Antisense RNA:

5'CGGUGGUGCAGAUGAACUUCAGGGUCA

Antisense RNA labeled with Alexa 546:

5'Alexa 546-CGGUGGUGCAGAUGAACUUCAGGGUCA

Antisense RNA labeled with Alexa 750:

5'Alex750N/CGGUGGUGCAGAUGAACUUCAGGGUCA

Kill-switch of anti-thrombin fibers:

To assemble kill-switch fibers, mix anti fiber DNA strand 1 with anti- fiber DNA strand 2 with
RNA sense in 1 to 1 to 2 ratio

Anti NU172 R1 + Anti NU172 R2 (kill-swtitch fiber of NU fiber): Anti Nu172 Aptamer on right
side of repeating unit of fiber strand 1 and fiber strand 2

Fiber sense DNA strand 1:

5'CGCCACCACCCTACCCAACCTAGGCGAAAAAGGGATTTCCCTCGGTGGTGCAGATG
AACTTCAGGGTCATTCCCTAAAGGGA

Fiber sense DNA strand 2:

5'CGCCACCACCCTACCCAACCTAGGCGAAAAGGGAAATCCCTTCGGTGGTGCAGATG
AACTTCAGGGTCATCCCTTTAGGGAA

Anti RA36 R1 + Anti RA36 L2 (kill-swtitch fiber of NU fiber): Anti RA36 Aptamer on right side
on repeating unit of fiber strand 1 and left side on repeating unit of fiber strand 2

Fiber sense DNA strand 1:

5'CCAACCACACCAACCACCAACCACACCAACCAAAAAGGGATTTCCCTCGGTGGTGC
AGATGAACTTCAGGGTCATTCCCTAAAGGGA

Fiber sense DNA strand 2:

5'AGGGAAATCCCTTCGGTGGTGCAGATGAACTTCAGGGTCATCCCTTTAGGGAAAAA
CCAACCACACCAACCACCAACCACACCAACC

Anti NU172 1 + Anti RA36 2 (kill-swtitch fiber of NU/RA fiber): Anti NU172 Aptamer on left
and right sides on repeating unit of fiber strand 1 and RA36 aptamer on left and right sides on
repeating unit of fiber strand 2

Fiber sense DNA strand 1:

5'CGCCACCACCCTACCCAACCTAGGCGAAAAAGGGATTTCCCTCGGTGGTGCAGATG
AACTTCAGGGTCATTCCCTAAAGGGAAAACGCCACCACCCTACCCAACCTAGGCG

Fiber sense DNA strand 2:

5'CCAACCACACCAACCACCAACCACACCAACCAAAAGGGAAATCCCTTCGGTGGTG
CAGATGAACTTCAGGGTCATCCCTTTAGGGAAAAACCAACCACACCAACCACCAACC
ACACCAACC

Sense RNA:

5'ACCCUGAAGUUCAUCUGCACCACCG

Sense RNA labeled with Alexa 488:

5'Alex488N/ACCCUGAAGUUCAUCUGCACCACCG

3.6   References

1. Raber MN, W.H., Hall WD, Hurst JW *Coagulation Tests.* Clinical Methods: The History, Physical, and Laboratory Examinations. 3rd edition, 1990(Boston: Butterworths): p. Chapter 157.
2. Narayanan, S., *Multifunctional roles of thrombin.* Annals of Clinical and Laboratory Science, 1999. **29**(4): p. 275-280.
3. De Cristofaro, R. and E. De Candia, *Thrombin domains: Structure, function and interaction with platelet receptors.* Journal of Thrombosis and Thrombolysis, 2003. **15**(3): p. 151-163.
4. Di Cera, E., *Thrombin.* Mol Aspects Med, 2008. **29**(4): p. 203-54.
5. Girard, T.J., et al., *INHIBITION OF FACTOR-VIIA TISSUE FACTOR COAGULATION ACTIVITY BY A HYBRID PROTEIN.* Science, 1990. **248**(4961): p. 1421-1424.
6. Mann, K.G., *Thrombin formation.* Chest, 2003. **124**(3): p. 4S-10S.
7. Fennerty, A., *Venous thromboembolic disease and cancer.* Postgraduate Medical Journal, 2006. **82**(972): p. 642-648.
8. Cook, B.W., *Anticoagulation mangement* Semin Intervent Radiol 2010;27:360–367., 2010.
9. Nutescu, E.A., et al., *Pharmacology of anticoagulants used in the treatment of venous thromboembolism.* Journal of Thrombosis and Thrombolysis, 2016. **41**(1): p. 15-31.
10. *https://www.nhs.uk/conditions/anticoagulants/.*
11. Cai, S.D., et al., *Investigations on the interface of nucleic acid aptamers and binding targets.* Analyst, 2018. **143**(22): p. 5317-5338.
12. Ku, T.-H., et al., *Nucleic Acid Aptamers: An Emerging Tool for Biotechnology and Biomedical Sensing.* Sensors (Basel, Switzerland), 2015. **15**(7): p. 16281-16313.
13. Zavyalova, E., et al., *The Evaluation of Pharmacodynamics and Pharmacokinetics of Anti-thrombin DNA Aptamer RA-36.* Frontiers in Pharmacology, 2017. **8**.
14. Ke, W., et al., *RNA-DNA fibers and polygons with controlled immunorecognition activate RNAi, FRET and transcriptional regulation of NF-kappaB in human cells.* Nucleic Acids Res, 2019. **47**(3): p. 1350-1361.
15. Gatto, B.P., M.; Sissi, C., *Nucleic Acid Aptamers Based on the G-Quadruplex Structure: Therapeutic and Diagnostic Potential.* Current Medicinal Chemistry, 2009. **Volume 16, Number 10, 2009, pp. 1248-1265(18)**.
16. Viglasky, V. and T. Hianik, *Potential uses of G-quadruplex-forming aptamers.* Gen Physiol Biophys, 2013. **32**(2): p. 149-72.
17. Hotoda, H., et al., *Biologically active oligodeoxyribonucleotides. 5.(1) 5 '-end-substituted d(TGGGAG) possesses anti-human immunodeficiency virus type 1 activity by forming a G-quadruplex structure.* Journal of Medicinal Chemistry, 1998. **41**(19): p. 3655-3663.

18.   Dapic, V., et al., *Antiproliferative activity of G-quartet-forming oligonucleotides with backbone and sugar modifications.* Biochemistry, 2002. **41**(11): p. 3676-3685.

19.   Daei, P., et al., *Aptamer-based Targeted Delivery of miRNA let-7d to Gastric Cancer Cells as a Novel Anti-Tumor Therapeutic Agent.* Iranian Journal of Pharmaceutical Research, 2018. **17**(4): p. 1537-1549.

20.   Tasset, D.M., M.F. Kubik, and W. Steiner, *Oligonucleotide inhibitors of human thrombin that bind distinct epitopes.* Journal of Molecular Biology, 1997. **272**(5): p. 688-698.

21.   Griffin, L.C., et al., *INVIVO ANTICOAGULANT PROPERTIES OF A NOVEL NUCLEOTIDE-BASED THROMBIN INHIBITOR AND DEMONSTRATION OF REGIONAL ANTICOAGULATION IN EXTRACORPOREAL CIRCUITS.* Blood, 1993. **81**(12): p. 3271-3276.

22.   Macaya, R.F., et al., *THROMBIN-BINDING DNA APTAMER FORMS A UNIMOLECULAR QUADRUPLEX STRUCTURE IN SOLUTION.* Proceedings of the National Academy of Sciences of the United States of America, 1993. **90**(8): p. 3745-3749.

23.   Hwang, D.W., et al., *A Nucleolin-Targeted Multimodal Nanoparticle Imaging Probe for Tracking Cancer Cells Using an Aptamer.* Journal of Nuclear Medicine, 2010. **51**(1): p. 98-105.

24.   Wu, Y., B. Midinov, and R.J. White, *Electrochemical Aptamer-Based Sensor for Real-Time Monitoring of Insulin.* Acs Sensors, 2019. **4**(2): p. 498-503.

25.   Bonifacio, L., F.C. Church, and M.B. Jarstfer, *Effect of locked-nucleic acid on a biologically active G-quadruplex. A structure-activity relationship of the thrombin aptamer.* International Journal of Molecular Sciences, 2008. **9**(3): p. 422-433.

26.   Zavyalova, E., et al., *Module-Activity Relationship of G-quadruplex Based DNA Aptamers for Human Thrombin.* Current Medicinal Chemistry, 2013. **20**(38): p. 4836-4843.

27.   Padmanabhan, K., et al., *THE STRUCTURE OF ALPHA-THROMBIN INHIBITED BY A 15-MER SINGLE-STRANDED-DNA APTAMER.* Journal of Biological Chemistry, 1993. **268**(24): p. 17651-17654.

28.   Russo Krauss, I., et al., *Thrombin-aptamer recognition: a revealed ambiguity.* Nucleic Acids Research, 2011. **39**(17): p. 7858-7867.

29.   Esposito, V., et al., *A straightforward modification in the thrombin binding aptamer improving the stability, affinity to thrombin and nuclease resistance.* Organic & Biomolecular Chemistry, 2014. **12**(44): p. 8840-8843.

30.   Wermuth, C.G., et al., *Glossary of terms used in medicinal chemistry (IUPAC Recommendations 1998).* Pure and Applied Chemistry, 1998. **70**(5): p. 1129.

31.   Zavyalova, E., et al., *Evaluation of Antithrombotic Activity of Thrombin DNA Aptamers by a Murine Thrombosis Model.* Plos One, 2014. **9**(9): p. 7.

32.   Roxo, C., W. Kotkowiak, and A. Pasternak, *G-Quadruplex-Forming Aptamers-Characteristics, Applications, and Perspectives.* Molecules (Basel, Switzerland), 2019. **24**(20): p. 3781.

33.   Trapaidze, A., et al., *Investigation of the selectivity of thrombin-binding aptamers for thrombin titration in murine plasma.* Biosensors & Bioelectronics, 2016. **78**: p. 58-66.

34.   Ni, X., et al., *Nucleic Acid Aptamers: Clinical Applications and Promising New Horizons.* Current Medicinal Chemistry, 2011. **18**(27): p. 4206-4214.

35.   Keefe, A.D., S. Pai, and A. Ellington, *Aptamers as therapeutics.* Nature reviews. Drug discovery, 2010. **9**(7): p. 537-550.

36.   Zavyalova, E., et al., *The evaluation of pharmacodynamics and pharmacokinetics of anti-thrombin DNA aptamer RA-36.* Frontiers in pharmacology, 2017. **8**: p. 922.

37.   Woodruff, R.S. and B.A. Sullenger, *Modulation of the Coagulation Cascade Using Aptamers.* Arteriosclerosis Thrombosis and Vascular Biology, 2015. **35**(10): p. 2083-2091.

38.   Kalliolias, G.D. and L.B. Ivashkiv, *Overview of the biology of type I interferons.* Arthritis research & therapy, 2010. **12**(1): p. 1-9.

39.   Cardarelli, F., et al., *The intracellular trafficking mechanism of Lipofectamine-based transfection reagents and its implication for gene delivery.* Scientific reports, 2016. **6**: p. 25879.

40.   Ilinskaya, A.N., et al., *Nanoparticle physicochemical properties determine the activation of intracellular complement.* Nanomedicine: Nanotechnology, Biology and Medicine, 2019. **17**: p. 266-275.

41.   Ilinskaya, A.N., et al., *Nanoparticle physicochemical properties determine the activation of intracellular complement.* Nanomedicine-Nanotechnology Biology and Medicine, 2019. **17**: p. 266-275.

42.   Janeway Jr, C.A., et al., *The complement system and innate immunity*, in *Immunobiology: The Immune System in Health and Disease. 5th edition.* 2001, Garland Science.

43.   Vogel, C.W., et al., *Recombinant cobra venom factor.* Molecular Immunology, 2004. **41**(2-3): p. 191-199.

44.   Palta, S., R. Saroa, and A. Palta, *Overview of the coagulation system.* Indian journal of anaesthesia, 2014. **58**(5): p. 515-523.

4   Chapter 4: Exosome mediated delivery of functional nucleic acid nanoparticles (NANPs)

4.1   Introduction

Nucleic acid nanoparticles (NANPs) are modular nanoscaf- folds exclusively made of multiple oligonucleotides programmed to self-assemble into precise 3D structures with well-defined properties[1-4]. Rationally designed NANPs can be further decorated with cocktails of therapeutic nucleic acids (TNAs), which may differ in composition, secondary structure, and mechanism of action, allowing for synchronized targeting of multiple cellular pathways. This structural versatility–and ability to finely control the NANPs' sizes, shapes, composition, multivalences, and therapeutic payloads–makes this technology an attractive option for biomedical applications[5-7]. For example, a previously tested combinatorial RNAi strategy of NANPs functionalized with six different Dicer substrate (DS) RNAs[8] were effective in simultaneous targeting six distinct parts of the HIV-1 genome[1, 9]. These NANPs functionalized with DS RNAs relied on the assistance from the intracellular enzyme Dicer that initiated the nuclease-assisted release of siRNAs from the NANPs. Moreover, by simply extending either the 5′- or/and 3′- ends of each strand of the NANP's composition with its unique functionality, NANPs can be formulated to precisely package not only different TNAs but also fluorophores, targeting agents, small-molecule drugs, proteins, or other therapeutic cargoes[10-12].

A sophisticated approach to the conditional intracellular activation of RNAi was introduced through interdependent RNA/DNA NANPs in which the RNA (and/or DNA) functionalities were split into two inactive NANPs[13–15]. Driven by sequence complementarity, the inactive NANPs could recognize each other inside the cells and release the activated functionalities upon isothermal reassociation[2, 9,16]. Using the same approach, RNA/DNA fibers were recently designed for enhanced control of deliverable functionalities (e.g., DS RNAs targeting mutated $BRAF^{V600E}$ in melanoma cells) along with higher stability against enzymatic degradation in human blood and tunable rates of intracellular reassociation[17]. Another advantage of this user-friendly approach: the DNA part of

the RNA/DNA fibers contained split NF-κB (nuclear factor kappa-light-chain enhancer of activated B cells) decoy sequences, which activate upon intracellular fiber reassociation and restrain the immunostimulatory response. NF-κB is expressed in most mammalian cells and remains sequestered in an inactive state in the cytoplasm with the inhibitory protein IκB. Activation of NF-κB is initiated by a variety of stimuli, resulting in signal-induced degradation of IκB proteins by proteasomes. Subsequently, the NF-κB complex can enter the nucleus and initiate gene expression of pro-inflammatory cytokines. NF-κB decoys[18–20] mimic the κB consensus sequence and upon the decoy's binding to NF-κB its nuclear translocation becomes attenuated.

Since all NANPs are composed of negatively charged, hydrophilic biopolymers, they cannot easily penetrate through the hydrophobic biological membranes and thus, mainly rely on the use of different synthetic carriers for efficient intracellular delivery[17, 21–25]. Over the last few decades, extensive research efforts have been undertaken to improve the stability, efficacy, and specificity of TNA delivery systems, such as liposomes[26], micelles[27], nanoparticles[28], hydrogels[29], and viruses[30]. In spite of these massive attempts, most of these systems suffer from immunogenicity, cytotoxicity, rapid blood clearance, and poor biodistribution[31], hindering further clinical translation of therapeutic NANP platforms. Therefore, an urgent need to identify new endogenous sources for potential delivery systems that avoid the complications associated with synthetic materials is vital.

Extracellular vehicles (EVs) are membrane enclosed vesicles ranging from 30 nm to 1000 nm (or even larger) in size and secreted by cells into the extracellular space[32, 33]. EVs comprise of exosomes and microvesicles, which are differentiated by their biogenesis, content, size, release pathways, and function[34]. Exosomes have been widely investigated as emerging novel delivery vehicles for biological cargos. These structures range from 30 nm to 150 nm in size[35] and are released into most biological fluids. Biological molecules, such as proteins, lipids, and nucleic acids, undergo transport via exosomes from the cell of origin to recipient cells[36]. Exosomes form

by inward budding of the cell membrane, a process which generates early endosomes. After the endosomes mature into multivesicular bodies (MVB), they fuse with the cell membrane and exit from the cell; alternatively, they can fuse with a lysosome for degradation. (Figure 33 A)[37]. Reflective of the mechanism of biogenesis, exosomes are considered to be the "mini versions" of their parental cells in terms of the specially sorted "cargo" they carry[38]. The putative function of exosomes is to perform intercellular communication and trigger physiological responses. Interaction between exosomes and recipient cells is promoted via receptor-mediated endocytosis[39], micropinocytosis[40], or membrane fusion[41]. Once internalized, the exosomal contents are released into the cytosol directly or through back-fusion with the endosomal membrane, eliciting the effect on the recipient cell[42]. Such features of the exosomes highlight their potential as drug delivery systems to alter gene expression by delivering therapeutic genetic materials. Several studies have investigated their performance as therapeutic vehicles for exogenous genetic material delivery as well as their post-delivery functionality. The first published study showed that exosomes could efficiently deliver exogenous siRNAs to the brains of mice with successful knockdown of mRNA and BACE1 protein with negligible immune response[43]. Later, a myriad of studies reported using exosomes to deliver siRNAs and knockdown targeted genes in different diseases. For example, exosome-mediated delivery has shown promise in silencing specific genes, including VEGF, EGFR, AKT, MAPK, and KRAS[44]; inhibiting luciferase expression[45]; treating hepatitis C infection; causing massive cell death of recipient cells by RAD51 gene suppression[46]; and survivin siRNA suppression for the treatment of bladder cancer[47]. Recently, exosomes derived from normal fibroblast-like mesenchymal cells were engineered to carry shRNAs or siRNAs against the KrasG12D mutation known for triggering pancreatic cancer growth in multiple mouse models[48]. The use of exosomes as delivery vehicles demonstrates a plethora of advantages, including biocompatibility, efficacy, stability, and membrane permeation capability; as well as diminished toxicity; low immunogenicity; low off-target effect; and the ability to cross the blood-brain-barrier[31,49–53]. As a result, exosomes can significantly outperform other delivery methods.

In this work, we investigated the use of exosomes as carriers for delivering functional NANPs of different shapes, sizes, and compositions, among which were globular RNA cubes, planar RNA rings, and linear RNA/DNA fibers. We assessed, in vitro, the stability of exosome-loaded NANPs, in addition to their intracellular uptake, silencing efficiency, and immunostimulatory activity.

4.2   Methods

4.2.1   Cell culture

MDA-MB-231-GFP, MDA-MB-231 and HUVEC cells were used in this study. All oligonucleotides were purchased from Integrated DNA Technologies (IDTDNA.com, Coralville, IA, USA).

4.2.2   Assemblies of RNA/DNA fibers, RNA cubes and RNA rings targeting GFP and their analysis by native-PAGE

All individual strands were purified by an 8 M urea polyacrylamide gel (8% acrylamide, 19:1), gel extracted, eluted and dissolved in endotoxin-free water. All individual RNA strands for cube and rings were synthesized via in vitro run-off transcription (IVT) assay, purified by an 8 M urea polyacryl- amide gel (8% acrylamide, 19:1), gel extracted, eluted and dissolved in endotoxin-free water. RNA/DNA fibers, RNA cubes, and RNA rings were assembled in one-pot by combining individual monomers at equimolar concentrations in an assembly buffer. All NANPs were analyzed on 8% non-denaturing native polyacrylamide gel (19:1 for fibers, 37.5:1 for rings and cubes).

4.2.3   Atomic force microscopy (AFM) imaging of NANP

A freshly cleaved mica surface modified with APS (1-(3- aminopropyl) silatrane) was used for AFM imaging, which was performed on the MultiMode AFM NanoScope IV system (Bruker Instruments, Santa Barbara, CA, USA) in tapping mode.

4.2.4   Nuclease protection assay of DNA duplex

125 nM dsDNA labeled with Alexa Fluor 488 at the 5′ sense strand and an Iowa Black Quencher at the 3′ antisense strand was loaded into exosomes and then treated with RQ1 DNase I.

The fluorescence resulting from the digestion of the DNA duplex by RQ1 DNase was monitored at 37 °C for a total of 60 min with measurements at every 30 s. Free fluorescently quenched DNA duplex was used as the control.

4.2.5 Isolation of exosomes

Exosomes were isolated from MDA-MB-231 or HUVEC cells using ExoQuick-TC ULTRA (System Biosciences, Palo Alto, CA, USA) according to the manufacturer's manual. Protein concentration was measured by Qubit protein assay and all exosomes were stored at −20 °C.

4.2.6 Immunoblotting

5 μg of isolated exosomes was run on 4%-20% Mini- PROTEAN TGX gel, transferred to PVDF membrane and probed with primary antibodies overnight. Next day, the membranes were washed three times, probed with appropriate secondary antibody and imaged using Molecular Imager ChemiDOC XRS+ Imaging System (Bio-Rad, Hercules, CA, USA).

4.2.7 Nanoparticle tracking analysis and exosome labeling for f-NTA

Isolated exosomes were labeled with the ExoGlow-NTA fluorescent kit (System Biosciences, Palo Alto, CA, USA). Labeled exosomes were stored at −20 °C until the analysis. Unlabeled and labeled samples were analyzed by NTA and f- NTA using ZetaView.

4.2.8 TEM analysis

Isolated exosomes were fixed by addition of 4% paraformaldehyde; 5 μl of the sample was dropped on a carbon coated 400 mesh Cu/Rh grid (Ted Pella, Redding, CA, USA) and stained with5 μl of 1% uranyl acetate (Polysciences, Warrington, PA, USA) prepared in filtered distilled water. The grids were imaged with an FEI Talos L120C TEM with Gatan 4 k × 4 k OneView camera.

4.2.9 Loading of exosomes with NANPs

100 μg of isolated exosomes was loaded with 25 pmol NANPs using the Exo-Fect siRNA/miRNA transfection kit (System Biosciences, Palo Alto, CA, USA) according to the manufacturer's manual. The loaded exosomes were cleaned to remove any excess of free

NANPs/negative control siRNA, transfection reagent, or complexes. The cleaned NANP loaded exosomes were immediately added onto MDA-MB-231-GFP cells.

4.2.10 RNA purification and quantitative real time PCR (RT-qPCR) analysis

Total RNA was purified using RNeasy Plus Mini kit (Qiagen, Hilden, Germany) according to the manufacturer's manual. Purified total RNA was reverse transcribed using anchor Oligo $(dT)_{20}$ primer (Thermo Fisher Scientific, Wilmington, DE, USA) and Superscript III reverse transcriptase (Thermo Fisher Scientific, Wilmington, DE, USA). Real time qPCR was performed using TaqMan Fast Advanced Master Mix (Thermo Fisher Scientific, Wilmington, DE, USA) with TaqMan gene expression assay eGFP (Thermo Fisher Scientific, Wilmington, DE, USA, Mr04097229_mr) and with TaqMan gene expression assay Beta-2-microglobulin as a reference gene (Thermo Fisher Scientific, Hs00984230_m1, Wilmington, DE, USA) and the QuantStudio 6 FLEX (Applied Biosystems, Thermo Fisher Scientific, Wilmington, DE, USA).

4.2.11 Flow cytometry

MDA-MB-231-GFP treated cells were trypsinized with 0.25% trypsin–EDTA (Thermo Fisher Scientific, Waltham, MA, USA) for 2 min at 37 °C, quenched with DMEM supplemented with 10% FBS, and pelleted by centrifugation at 800 ×g for 2 min. The cell pellet was resuspended with 1× PBS supplemented with 1% FBS into a 12 × 75 mm test tube with a cell strainer cap (Falcon, Durham, NC, USA) and analyzed with the DxP FACScan (Cytek Biosciences, Fremont, CA, USA). The data were analyzed using FCS Express 5 (De Novo Software, Glendale, CA, USA).

4.2.12 Cell uptake imaging

Cells transfected with NANP loaded exosomes or negative control loaded exosomes were imaged 72 h post-transfection. For the cancer and primary cells transfected with exosomes loaded with DNA cube-Alexa 488, cells were imaged 24 h post- transfection. The images were captured using a Leica DMI3000 inverted microscope with a DFC360 FX digital camera (Leica Microsystems, Wetzlar, Germany).

4.2.13 Immunostimulation in vitro

HEK-Blue™ hTLR3 and 7 cells, and THP1-Dual™ cells (Invivogen, San Diego, CA, USA) were used for quantifying the activation of specific toll-like receptor (TLR) and intracellular signaling pathways, respectively. HEK-Blue™ hTLR 3 and 7 cells are HEK cells engineered to stably co-express human TLR and NF-κB-inducible SEAP (secreted embryonic alkaline phosphatase) reporter genes. The TLR activation results in downstream production of SEAP that can be detected and quantified using QUANTI-Blue™. THP1-Dual™ cells are engineered to express SEAP upon NF-kB stimulation, which can also be assessed by QUANTI-Blue™. In order to investigate the conditional activation of NF-kB decoys, Poly (I:C) (polyinosinic-polycytidylic acid, a synthetic analog of dsRNA) and Pam3CSK4 (a synthetic diacylated lipopeptide) were used to stimulate HEK-Blue™ hTLR3 and THP1-Dual™ cells, respectively. For the experiments with the HEK-Blue™ hTLR7 cells, R848 (resiquimod) was used as a positive control.

4.3   Results

4.3.1   Characterization of isolated exosomes

Extracellular vesicles are cell-derived membrane particles subdivided into microvesicles – ranging in size from 100 to 1000 nm – that are shed from the membrane and exosomes released by fusion of late endosomes with the cell membrane (30-150 nm size range) (Figure 33A)[33-35]. Although micro-vesicles and exosomes are structurally similar and overlap in size, their content and cell origins are different[32]. Exosomes secreted by MBA-MD-231(231) were isolated using ExoQuick-TC ULTRA. Prior to the addition of ExoQuick-TC reagent, centrifugation was used to remove cell debris and large particles, such as apoptotic bodies. The isolation method included two steps: (i) precipitation of exosomes with ExoQuick-TC and (ii) their purification with an affinity chromatography column, ULTRA. ExoQuick-TC ULTRA efficiently removes the major non-EV co-isolates, such as bovine albumin and bovine IgG, which usually are overrepresented in the tissue culture media[54]. Figure 33B shows high amounts of albumin and IgG after precipitation step and demonstrates significant reduction of the co-isolated after the second step of ULTRA purification. Thus, the use of ExoQuick-TC ULTRA was essential to achieve the higher purity of isolated

exosomes.

The ExoQuick-TC ULTRA isolation method yielded a particle concentration of 4.50E+11 ± 6.80E+10 particles/mL as measured by fluorescent NTA (fNTA) and 4.70E+11 ± 5.10E+10 particles/mL as measured by NTA (Figure 33C). Since NTA measures any particle in solution, including protein aggregates and buffer precipitates, we specifically labeled exosomes with a membrane sensor dye and measured the concentration of intact vesicles using fNTA[55, 56]. The mean diameter of the isolated exosomes was 103.5 ± 26.4 nm as fNTA and 123.1 ± 8.1 nm as measured by conventional NTA (Figure 33C). A size distribution curve showed a classical distribution of exosomes ranging in size from 30 to 150 nm. Common exosomal markers Hsp70, ALIX, and tetraspanin, CD63, were identified (Figure 33B). ALIX is an exosomal protein known for its involvement in the MVB biogenesis[32]. CD63 was enriched in exosomal membrane from different origins[57, 58]. Hsp70 was released into the extracellular space via exosomes as a membrane-bound protein[59]. Calnexin is an integral protein of the endoplasmic reticulum (ER) and was used in as a cellular marker. Absence of calnexin marker in the exosome prepartation indicated no cellular contamination was present. Transmission electron microscopy (TEM) images of isolated exosomes showed normal morphology without any distortion (Figure 33D)[60]. Altogether, we conclude that
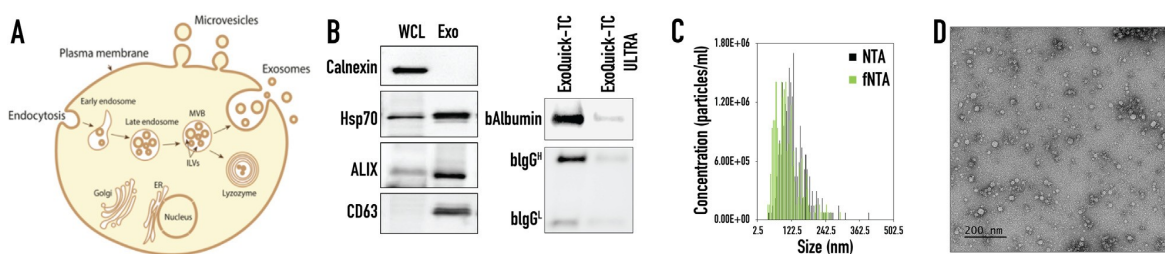
Figure 33. Characterization of exosomes isolated from MDA-MB-231 cells. (A) Schematic representation of exosome formation and release out to the extracellular space. (B) Western blot analysis of exosomal markers for CD63, ALIX and Hsp70, and cellular ER marker Calnexin in the whole cell lysate (WCL) and ExoQuick-TC ULTRA isolated exosomes (Exo). Western Blot analysis of the co-isolating proteins, bovine albumin (bAlbumin) and bovine immunoglobulin (bIgG) after one isolation step of precipitation step with ExoQuick-TC and after two steps of precipitation with ExoQuick-TC ULTRA. (C) The size distribution of isolated exosomes showing concentration in particles/mL. (D) TEM analysis of isolated exosomes.

the isolated sample was enriched in exosomes based on our results.

4.3.2   Characterization of NANP loaded exosomes and nuclease protection assay

The NANPs used in this study have distinct, strategic designs that confer different compositions, connectivities, shapes, and sizes[61]. Both cube and ring RNA scaffolds are assembled from six individual RNAs; cubes are globular (3D), whereas rings are planar (2D). The hydrodynamic radii (based on DLS results) of cubes and rings functionalized with six anti-GFP DS RNAs were estimated to be ~12 and ~15 nm, respectively[16,62]. DNA/ RNA fibers are linear (1D) and composed of both DNA and RNA strands. While RNA cubes and RNA/DNA fibers are assembled only via intermolecular Watson–Crick base pairing, assembly of RNA rings initially requires intramolecular Watson–Crick base pairing to further facilitate magnesium-dependent intermolecular kissing loop interactions[63]. Although each of these structures has distinct properties, all of them can be functionalized with DS RNAs that upon intracellular dicing release siRNAs designed to silence intended gene through sequence specific mRNA targeting. In addition, DNA/RNA fibers are functionalized with NF-κB decoys, inhibiting immune responses through the NF-κB pathway. All NANPs were analyzed by native-PAGE and AFM, as shown in Figure 32A, to confirm the correct assembly.

To load NANPs into isolated exosomes, Exo-Fect siRNA/ miRNA Transfection Kit was used. The Exo-Fect transfection reagent formed a complex with the NANPs and assisted with exosome insertion. Following the transfection, all samples were run through a clean-up column to remove excess Exo-Fect reagent, as well as free NANPs and their complexes. TEM images showed exosomes loaded with functionalized RNA rings, RNA cubes, and RNA/DNA fibers possessed morphology similar to free exosomes (Figure 33D and Figure 34B) with no associated structural changes. To verify the integrity of loaded exosomes, the presence of common exosomal markers (Hsp70, ALIX, and tetraspanin, CD63) was confirmed (Figure 34C). Interestingly, NTA analysis indicated that exosomes originally with mean diameter of ~102-103 nm became larger by ~20-30
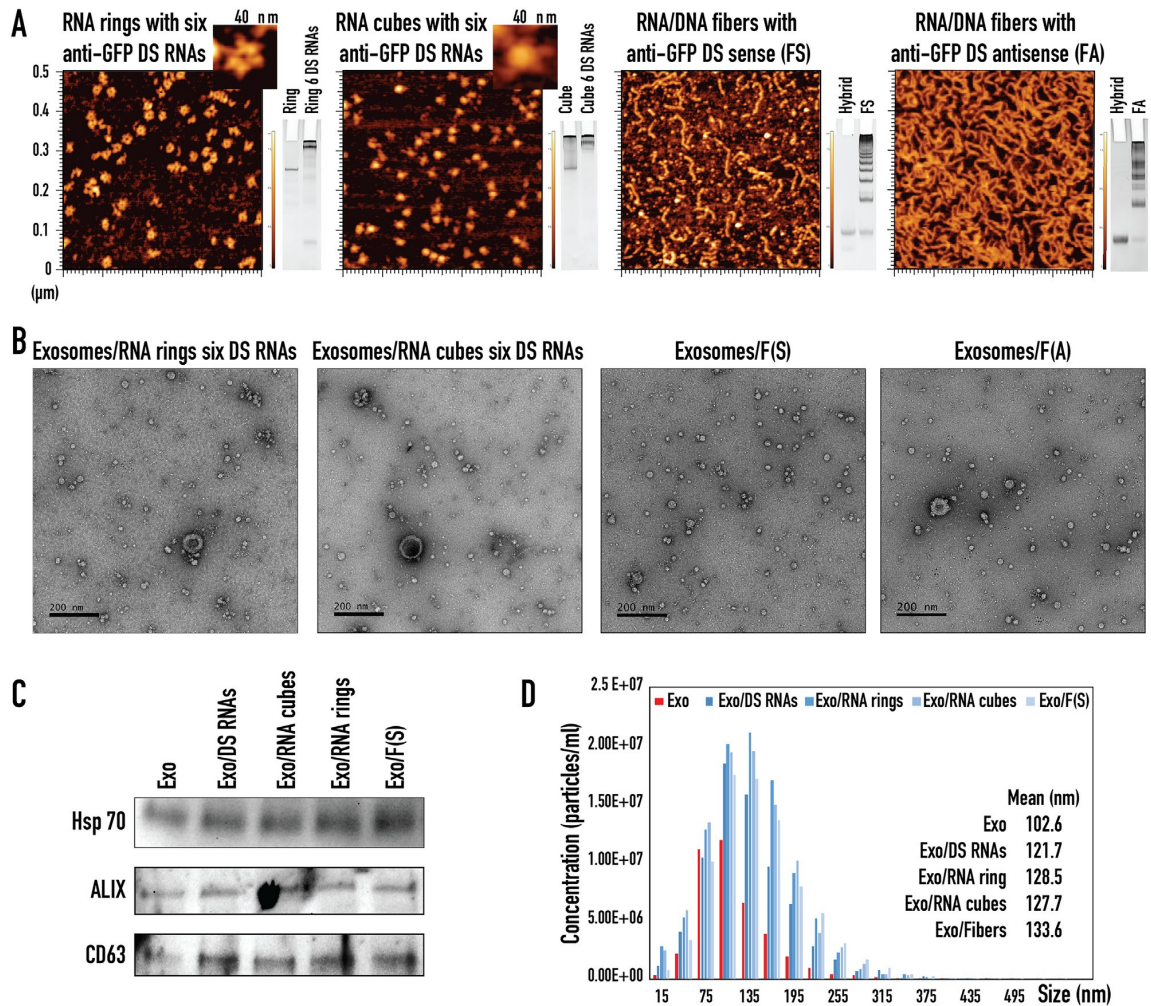
Figure 34. Characterization of various functionalized NANPs and NANP loaded exosomes. (A) Representative AFM images and native-PAGE results of RNA rings with six anti-GFP Dicer substrate (DS) RNAs, RNA cubes with six anti-GFP DS RNAs, RNA/DNA fibers with anti-GFP DS sense, and RNA/DNA fibers with anti-GFP DS antisense. (B) TEM images of exosomes loaded with RNA rings with six anti-GFP DS RNAs, RNA cubes with six anti-GFP DS RNAs, RNA/ DNA fibers with anti-GFP DS sense, and RNA/DNA fibers with anti-GFP DS antisense. (C) Western blot analysis of exosomal markers for CD63, ALIX, and Hsp70 in ExoQuick-TC ULTRA isolated exosomes (Exo) taken through the loading steps as negative control and exosomes loaded with anti-GFP DS RNAs (Exo/DS RNAs), RNA cubes with six anti-GFP DS RNAs (Exo/RNA cubes), RNA rings with six anti-GFP DS RNAs (Exo/RNA rings), and RNA/DNA fibers with anti-GFP DS sense (Exo/Fibers). (D) NTA analysis of ExoQuick-TC ULTRA isolated exosomes (Exo) taken through the loading steps as negative control and exosomes loaded with anti-GFP DS RNAs (Exo/DS RNAs), RNA cubes with six anti-GFP DS RNAs (Exo/RNA cubes), RNA rings with six anti-GFP DS RNAs (Exo/RNA rings), and RNA/DNA fibers with anti-GFP DS sense (Exo/Fibers).

nm after loading with NANPs (Figure 34D).

Next, the exosomes' ability to protect a loaded nucleic acid cargo from nuclease degradation were analyzed using a nuclease protection assay (Figure 35A) developed from previous

works[19, 22, 64]. As a model system, exosomes loaded with DNA duplexes labeled with Alexa 488 at

the 5′-end and Iowa Black quencher at the complementary 3′-end were used. Due to the quencher's

proximity to the fluorophore, the fluorescent signal from the DNA duplex was quenched. However,

after RQ1 DNase treatment and subsequent DNA degradation, the fluorophore escaped from the

quencher, leading to a progressively increasing fluorescent signal. At the same time, exosome-

encapsulated DNA duplexes were protected from DNase digestion and yielded no changes in the

fluorescent signal. Indeed, the miniscule increase in fluorescence proves that exosomes can

effectively protect nucleic acid cargo from nuclease digestion. Free exosomes were used as controls

to show that little to no signal appears in these samples. Results of this experiment suggest that

exosomes were able to completely shield their nucleic acid cargos from degradation by enzymatic
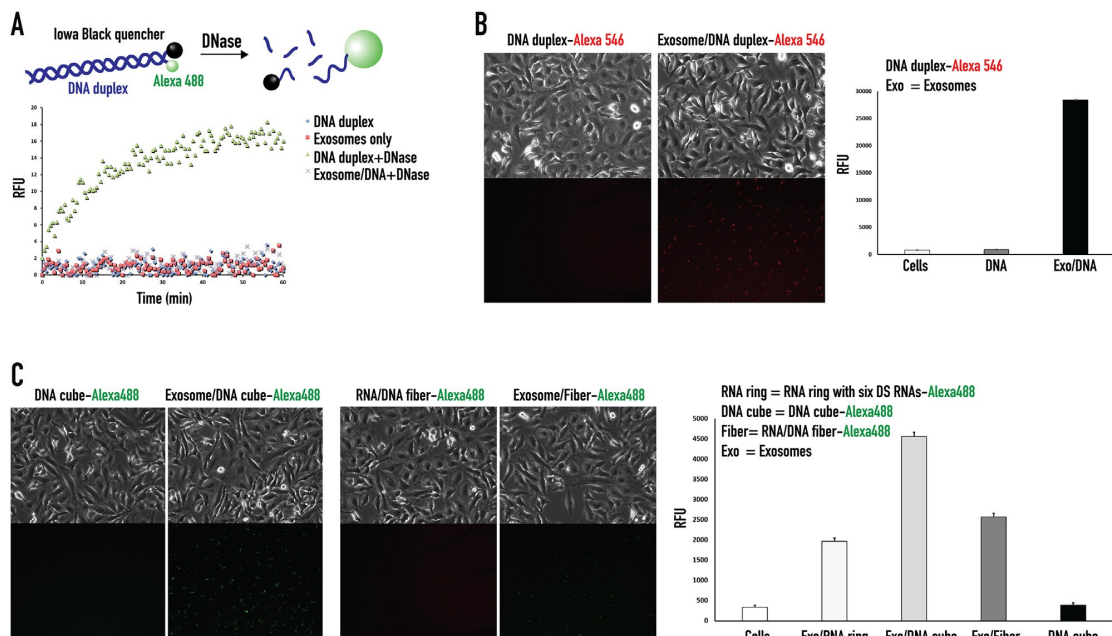
activity for at least 60 min.

Figure 35. Exosomes protect nucleic acids cargo from enzymatic degradation and promote its cellular uptake. (A) Schematic diagram of nuclease digestion assay and assay results for DNA duplexes loaded exosomes after incubation with RQ1 DNase. (B-C) Fluorescent microscope images of human breast cancer MDA- MB-231 show cell uptake of fluorescently labeled DNA duplexes (B) and NANPs (C) and the corresponding flow cytometry analysis.

4.3.3   Cellular uptake of exosomes loaded with NANPs

To confirm effective delivery of loaded NANPs, exosomes isolated from human breast

cancer MDA-MB-231 (231) cells were loaded with either Alexa 488- or Alexa 546-labeled NANPs and added to 231 cells. Fluorescence microscopy images captured 24 h post-transfection validated the internalization of loaded exosomes into cells (Figure 35 B-C). Flow cytometry and microscopy results demonstrated that exosomes loaded with Alexa 546-labeled DNA duplex internalized into the cells and, with no exosomes present, no significant cellular uptake occurred (Figure 35B). Interestingly, flow cytometry results show different transfection efficiencies of exosome-encapsulated Alexa 488-labeled NANPs, indicating that NANP polyplex shapes may potentially affect cellular uptake efficiency (Figure 35C). Overall, data confirmed that NANP-loaded exosomes can be internalized by human cells with visible effects on transfection efficiency. Interestingly, we noticed that the uptake efficiency for the same number of NANP loaded exosomes is significantly lower for primary cell lines when compared to cancer cells (Figure 36). This may offer additional advantages for exosome mediated delivery of NANP, due to the potential reduction in undesired off-target effects in healthy tissues.

4.3.4   GFP gene silencing with functionalized NANP loaded exosomes

We achieved successful transfection of labeled NANPs into cells using exosomes as delivery vesicles. To confirm retention of the NANPs' intended function upon delivery, NANPs decorated with DS RNA against GFP[1, 6, 16, 65] were used. Human breast cancer cells MDA-MB-231-
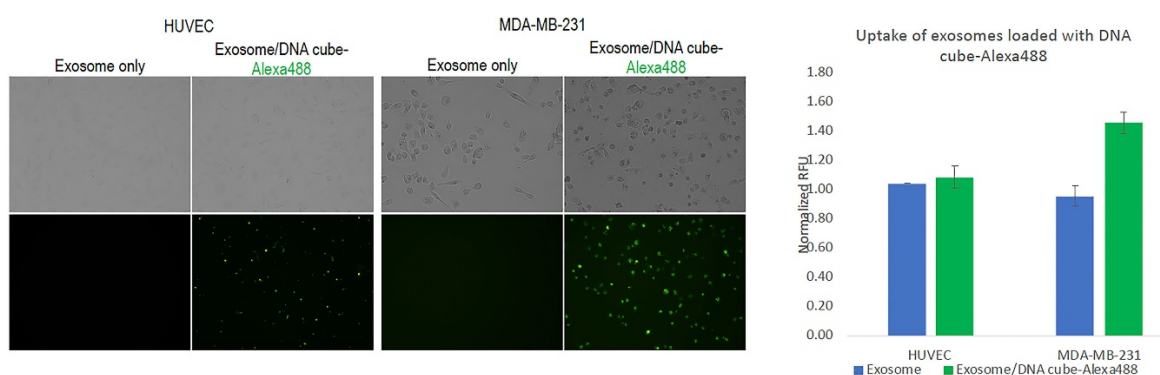

Figure 36. Cellular uptake of exosomes loaded with NANPs. Fluorescent microscope images of human breast cancer MDA-MB-231 or human umbilical vein endothelial primary cells HUVEC taken 72 hours post treatment show cell uptake of exosomes only or exosomes loaded with fluorescently labeled DNA cubes (Exosomes/DNA cube-Alexa488) and the corresponding Alexa488 fluorescence intensity reading normalized to number of cells.

GFP express- ing GFP (231-GFP) were treated with a panel of exosomes loaded with anti-GFP-functionalized NANP polyplexes (Figure 35A-B). Based on microscopy, flow cytometry, and RT-qPCR results, we found that 231-GFP cells treated with RNA ring- and RNA cube-loaded exosomes demonstrated a marked decrease in GFP expression. Exosomes loaded with sense (FS) or antisense (FA) RNA/DNA fibers did not change GFP expression individually; however, when both exosomes were added onto the same cell, there was a significant decrease in GFP expression. Therefore, fibers can re-associate and release DS RNAs only upon internalization with exosomes. Despite differences in shape, functional RNA cubes, RNA rings, and RNA/DNA fibers performed similarly in GFP silencing experiments (Figure 37A-B), while no cytotoxicity was observed (Figure 38).

4.3.5   Inhibition of NF-κB pathway

To further verify the intact dual functionality of DNA/RNA fibers that carry NF-κB response specificity and GFP silencing, we conducted a follow-up study using the reporter cell line HEK-Blue™ hTLR3. These cells are designed for the study of human TLR3 stimulation through assessment of NF-κB activation. The latter process induces production of secreted embryonic alkaline phosphatase (SEAP). Poly (I:C), a synthetic mimetic of viral dsRNA, can be used to trigger NF-κB activation and, ultimately, SEAP production (Figure 35C and Figure 37). In this experiment, cognate RNA/ DNA fibers (FS and FA) were separately pre-loaded into exosomes which were then mixed together for co-delivery (see FS/Exo + FA/Exo). Individual FS- and FA-loaded exosomes were used as controls (see FS/Exo and FA/Exo). On the same day that the complexes were added to the HEK-Blue™ hTLR3 cells, the cells were challenged with Poly (I:C). Supernatants were then collected and analyzed for presence of secreted alkaline phosphatase (SEAP), which can be easily detected and quantified using QUANTI-Blue™ reagent. Cells treated with poly (I:C) produced significant SEAP signal, and when FS and FA were delivered separately, no inhibition in SEAP production was observed. However, co-delivered of FS and FA significantly reduced SEAP synthesis. To show the generality, another reporter cell line – THP1-Dual™ – that also expressed
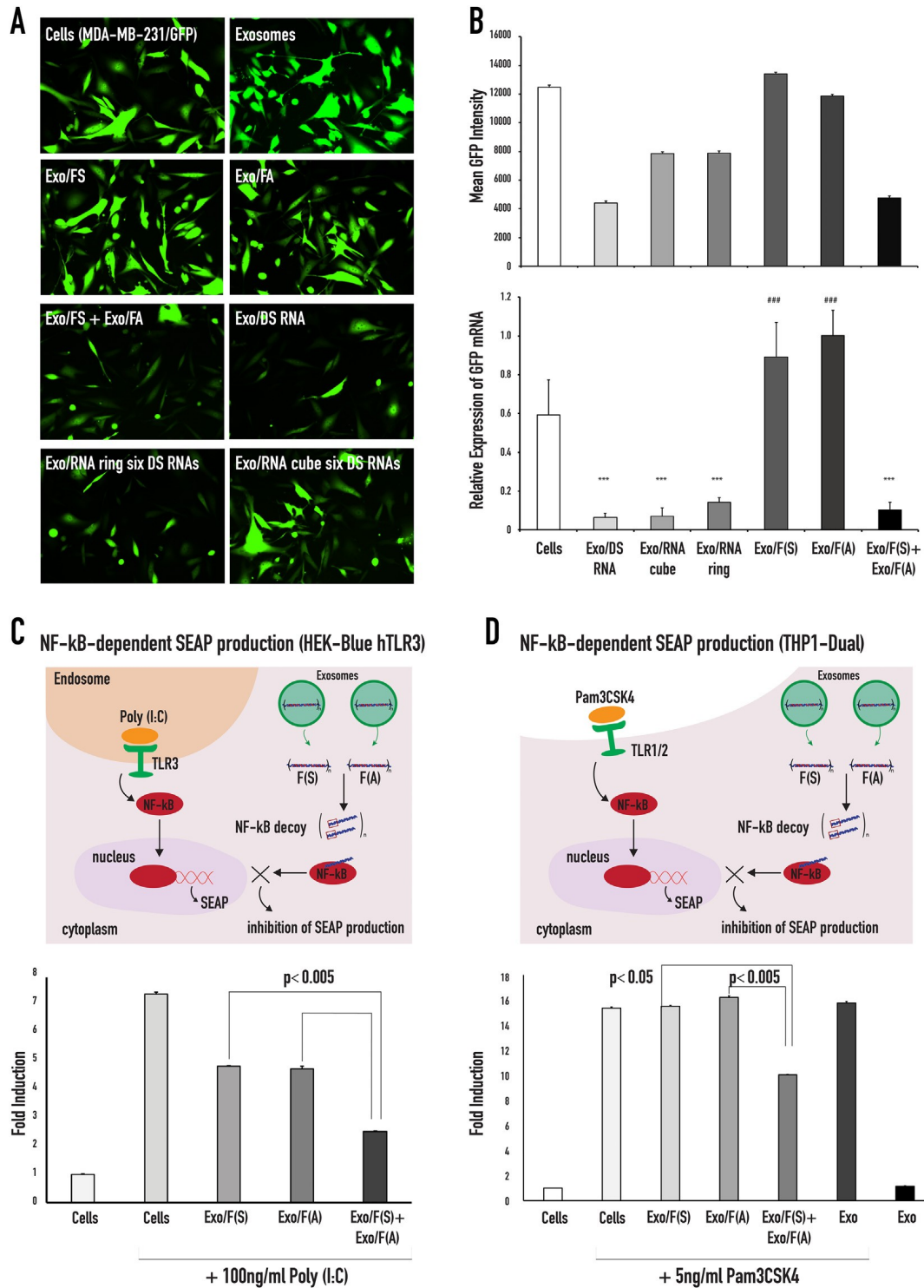
Figure 37. GFP silencing in MDA-MB-231/GFP cells treated with functionalized anti-GFP NANPs loaded into exosomes and inhibition of NF-κB function in HEK-Blue™ hTLR3 and THP1-Dual™ cells. (A) Fluorescent microscope images of MDA-MB-231-GFPs taken 72 h post treatment with exosomes and exosomes loaded with either NANPs. (B) Flow cytometry data of the mean GFP fluorescence and RT-qPCR analysis of the relative GFP

expression of MDA-MB-231-GFP cells after 72 h of incubation with NANPs loaded exosomes. Statistical significance for the samples compared to the negative control is denoted by * (*** P < 0.001). Statistical significance of Exo/FS, Exo/FA compared to Exo/FS + Exo/FA is denoted by # (### P < 0.001). (C) Schematic demonstration of the TLR3 signaling that activates the NF-κB pathway and the assembly of the NF-κB decoys (upon re-association of the RNA/DNA fibers) that inhibits the nuclear translocation of the activated NF-κB. Poly (I:C) is used to activate the TLR3 ligand, the TLR3 signal resulted in the activation of NF-κB and subsequently NF-κB entered the nucleus, where it will bind to specific sequences of DNA to promote the downstream transcription and translation of secreted embryonic alkaline phosphatase (SEAP). The reporter cell line HEK-Blue™ hTLR3 was transfected with fibers and stimulated with Poly (I:C). The cells were incubated for 24 h, and the levels of NF-κB-dependent SEAP were measured in the supernatants. (D) Schematic demonstration of the TLR1/2 signaling that activates the NF-κB pathway that can be inhibited with the NF-κB decoys assembled upon re-association of RNA/DNA fibers (F(S) and F(A)).

SEAP under the NF-κB promoter was tested (Figure 37D). To induce the activation of the NF-κB

pathway, THP1-Dual™ cells were challenged with a TLR agonist (PAM3CSK4). On the same day,

exosomes loaded with fibers were added to PAM3CSK4 treated cells and the supernatants were

collected and analyzed for the presence of SEAP. The cells treated with Pam3CSK4 induced

significant SEAP production, and when FS and FA were delivered separately, no inhibition of

SEAP was observed. However, co-delivered FS and FA reduced SEAP production. These results

were consistent with Lipofectamine 2000's actions as a transfection reagent, as described

previously[65]. When the cells were treated with Poly (I:C) for 24 h prior to addition of RNA/DNA

fibers and then incubated for an additional 24 h, the extent of SEAP inhibition was decreased

(Figure 39). All of these results support intracellular release of NANPs without any loss of their

intended function.

4.3.6 Immunostimultion by exosome loaded NANPs

Another nucleic acid-specific TLR was investigated using HEK-Blue™ hTLR7 cells.

Both HEK-Blue™ hTLR 3 and 7 cells were obtained by co-transfection of the hTLR gene into

HEK293 cells and engineered to express a single Toll-like receptor. Stimulation of TLR7 with

R848, an imidazoquinoline and agonist of TLR7, led to production of SEAP whose levels can be

determined using HEK-Blue™ detection reagent in real time. Here, we used these cells to evaluate

the potential immunostimulation by the NANP/exosome complexes (Figure 39). Both TLR3 and

TLR7 are responsible for RNA detection, while TLR3 activated by dsRNA and TLR7 detects

ssRNA[66]. Our data confirmed stimulation from both TLR3 and TLR7 cells to be negligible.
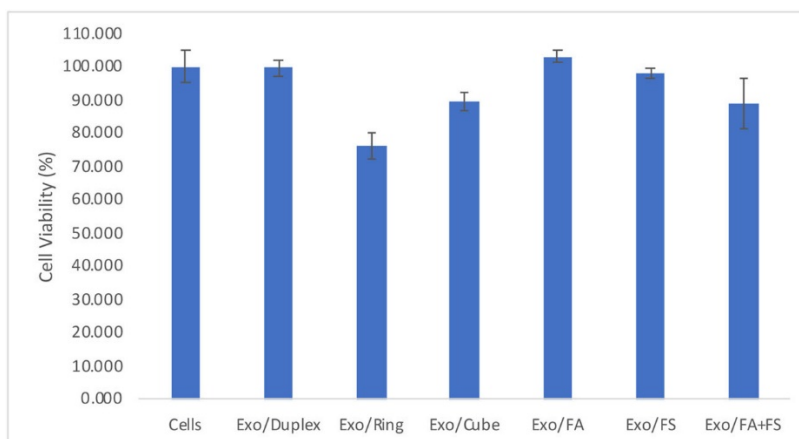

Figure 38. Cell viability of MDA-MB 231 cells treated with exosomes loaded with NANPs. Viability was measured 72hrs post treatment with isolated exosomes (Exo) and exosomes loaded with anti-GFP DS RNAs (Exo/Duplex), RNA rings with six anti-GFP DS RNAs (Exo/Ring), RNA cubes with six anti-GFP DS RNAs (Exo/Cube), RNA–DNA fibers with anti-GFP DS antisense (Exo/FA), RNA–DNA fibers with anti-GFP DS sense (Exo/FS), and their combination (Exo/FA+FS).

4.4   Discussion

Here, we demonstrated exosome-mediated delivery of different NANPs exhibiting various

shapes and structures and investigated their intracellular uptake, post-delivery gene silencing

efficiency, and immunostimulation potential. Exosome loading with NANPs of various sizes can

be challenging and numerous methods have been developed to efficiently facilitate the transfection.

One technique is chemical transfection, which shows promising results for direct cargo loading.

Exo-Fect™ siRNA/miRNA transfection kit (System Biosciences, Palo Alto, CA, USA) has shown

positive results for nucleic acid transfection into exosomes (unpublished results). In order to load

the cube, ring, and fiber NANPs into exosomes, Exo-Fect reagent forms a complex with the nucleic

acids. We showed that exosomes remain intact post packaging and retain the common exosomal

marker such as CD63. Interestingly, we noticed that the exosomes become slightly bigger upon

NANPs loading. We demonstrated that NANPs loaded into exosomes with intact shape reassumed
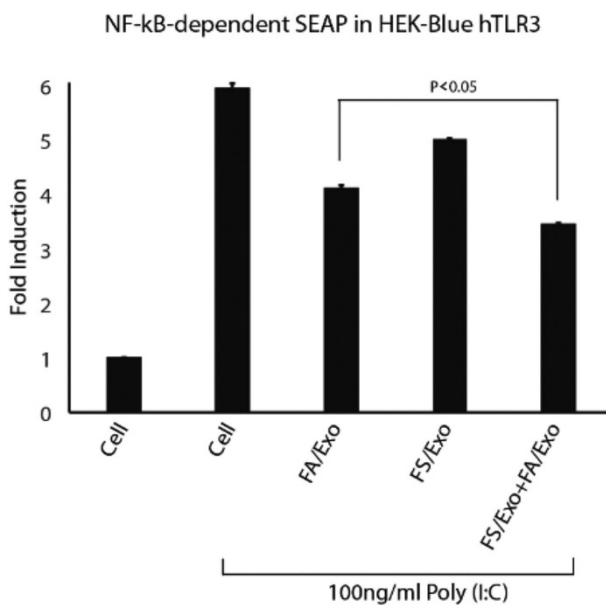
Figure 39. NF-κB-dependent SEAP production in HEK-Blue-hTLR3. Reporter cell line HEK-Blue hTLR3 was transfected with fibers and stimulated with Poly (I:C). After 24 hours, the cells were treated with NANPs and incubated for additional 24 hours, and the levels of NF-κB-dependent SEAP were measured in supernatants.

their original functionalities upon delivery (Figure 40) and effectively silenced GFP in the cells that constitutively express GFP. In our earlier studies using HEK 293 cells that overexpress human TLR7 and the SEAP genes, we showed that the RNA cubes delivered by L2K and PgP induced SEAP production when placed under the control of an NF-kB and AP-1-inducible promoter[61, 67]. In contrast, even for the RNA cubes (known for displaying the greatest immunostimulatory properties) we observed negligible immune response after using exosomes to deliver these structures. Our data suggest that exosome-mediated NANP delivery can potentially "stealth- coat" exosome contents from certain pattern recognition receptors, but further studies are required. In summary, this work

may pave the way towards the efficient and safe application of NANPs in personalized medicine by implementing patient-derived exosomes as a novel and promising therapeutic platform.
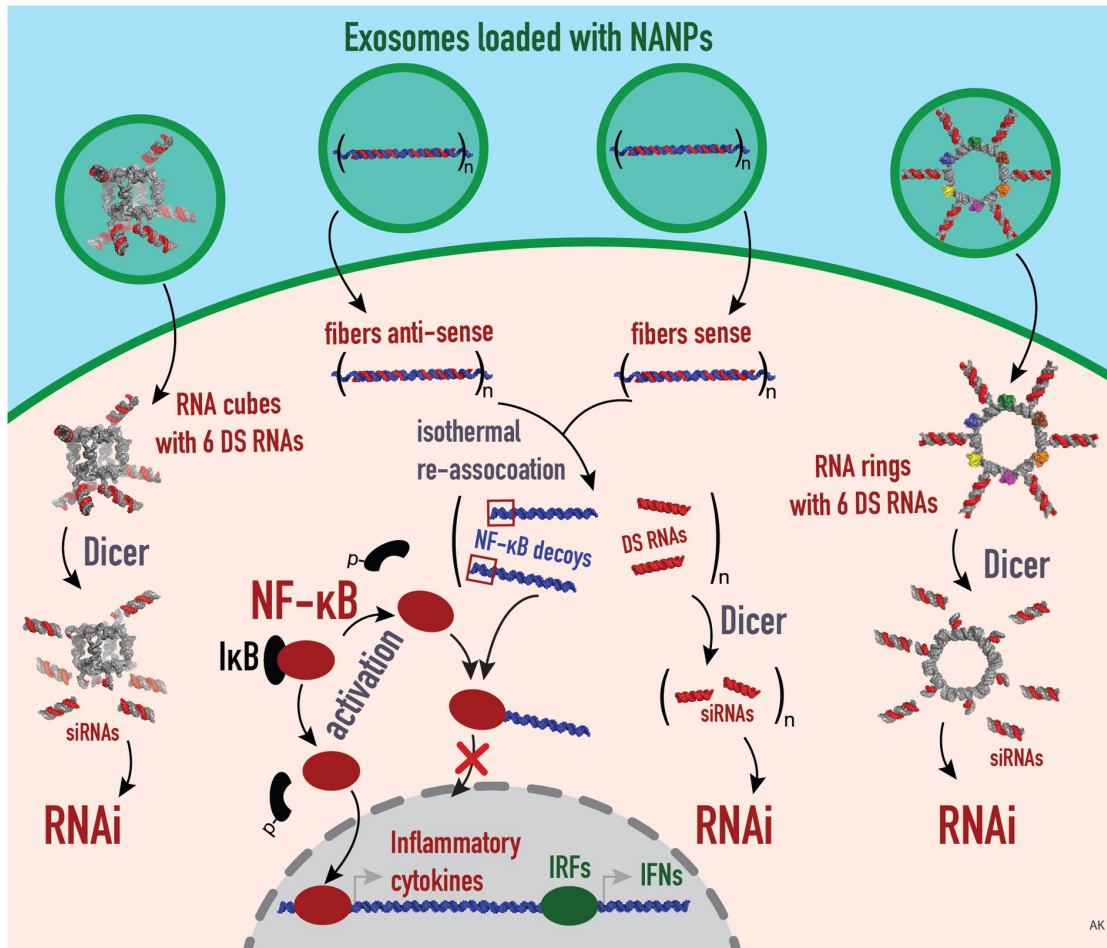
Figure 40. Schematic summary of the proposed mechanism of exosome-mediated delivery of different functionalized NANPs. Exosomes are loaded with NANPs, such as RNA cubes and RNA rings, that are functionalized with 6 DSRNAs, and fiber antisense and fiber sense that carry n numbers of DS RNAs and NF-κB decoys. Those NANPs are delivered by exosomes and released inside the target cells. In the cytosol, the DS RNAs will be further diced by Dicer to result in the generation of siRNAs, by which the RNAi pathway is activated. Meanwhile, the NF-κB decoys are released from the fibers, which in turn bind to NF-κB in order to prevent its nuclear translocation, thus inhibiting the downstream production of IRF and IFNs.

4.5 Sequences used in this project

GFP fiber sense DNA strand 1:

5' – AAGGGATTTCCCTCGGTGGTGCAGATGAACTTCAGGGTcaTTCCCTAAAGGGA

GFP fiber sense DNA strand 2:

5' – AGGGAAATCCCTTCGGTGGTGCAGATGAACTTCAGGGTcaTCCCTTTAGGGAA

GFP fiber antisense DNA strand 1:

5' –TCCCTTTAGGGAATGACCCTGAAGTTCATCTGCACCACCGAGGGAAATCCCTT

GFP fiber antisense DNA strand 2:

5' – TTCCCTAAAGGGATGACCCTGAAGTTCATCTGCACCACCGAAGGGATTTCCCT

DS RNA sense against GFP:

5' –ACCCUGAAGUUCAUCUGCACCACCG

DS RNA antisense against GFP:

5' –CGGUGGUGCAGAUGAACUUCAGGGUCA

DS RNA sense labeled with Alexa 488:

5' –ACCCUGAAGUUCAUCUGCACCACCG-Alexa488

DS RNA antisense labeled with Alexa 546:

5' –Alexa 546-CGGUGGUGCAGAUGAACUUCAGGGUCA

Six-stranded RNA ring functionalized with six DS RNAs against GFP:

Strand A

5' –CGGUGGUGCAGAUGAACUUCAGGGUCGGGAACCGUCCACUGGUUCCCGCUACG
AGAGCCUGCCUCGUAGCUUCGGUGGUGCAGAUGAACUUCAGGGUCA

Strand B

5' –GGGAACCGCAGGCUGGUUCCCGCUACGAGAGAACGCCUCGUAGCUUCGGUGGU
GCAGAUGAACUUCAGGGUCA

Strand C

5' –GGGAACCGCGUUCUGGUUCCCGCUACGAGACGUCUCCUCGUAGCUUCGGUGGU
GCAGAUGAACUUCAGGGUCA

Strand D

5' –GGGAACCGAGACGUGGUUCCCGCUACGAGUCGUGGUCUCGUAGCUUCGGUGGU
GCAGAUGAACUUCAGGGUCA

Strand E

5' –GGGAACCACCACGAGGUUCCCGCUACGAGAACCAUCCUCGUAGCUUCGGUGGU
GCAGAUGAACUUCAGGGUCA

Strand F

5' –GGGAACCGAUGGUUGGUUCCCGCUACGAGAGUGGACCUCGUAGCUUCGGUGGU
GCAGAUGAACUUCAGGGUCA

Six-stranded RNA cube functionalized with six DS RNAs against GFP:

Strand A

5' –CGGUGGUGCAGAUGAACUUCAGGGUCGGGAACCGUCCACUGGUUCCCGCUACG
AGAGCCUGCCUCGUAGCUUCGGUGGUGCAGAUGAACUUCAGGGUCA

Strand B

5' –GGGAAAUUUCGUGGUAGGUUUUGUUGCCCGUGUUUCUACGAUUACUUUGGUC

UUCGGUGGUGCAGAUGAACUUCAGGGUCA

Strand C

5' –
GGACAUUUUCGAGACAGCAUUUUUUCCCGACCUUUGCGGAUUGUAUUUUAGGU

UCGGUGGUGCAGAUGAACUUCAGGGUCA

Strand D

5' –GGCGCUUUUGACCUUCUGCUUUAUGUCCCCUAUUUCUUAAUGACUUUUGGCCU

UCGGUGGUGCAGAUGAACUUCAGGGUCA

Strand E

5' –GGGAGAUUUAGUCAUUAAGUUUUACAAUCCGCUUUGUAAUCGUAGUUUGUGU

UUCGGUGGUGCAGAUGAACUUCAGGGUCA

Strand F

5' –GGGAUCUUUACCUACCACGUUUUGCUGUCUCGUUUGCAGAAGGUCUUUCCGAU
UCGGUGGUGCAGAUGAACUUCAGGGUCA

DNA-Sense-Al488:

5' –GGAGACCGTGACCGGTGGTGCAGATGAACTTCAGGGTCATT-Alexa488

DNA-Anti-Sense-Iowa Black:

Iowa Black Quencher-TGACCCTGAAGTTCATCTGCACCACCGGTCACGGTCTCC

4.6 References

1.	Afonin KA, Viard M, Koyfman AY, Martins AN, Kasprzak WK, Panigaj M, et al. Multifunctional RNA nanoparticles. *Nano Lett* **2014**; 14 (10):5662-71.
2.	Afonin Kirill A, Lindsay B, Shapiro Bruce A. Engineered RNA nanodesigns for applications in RNA nanotechnology. *DNA and RNA Nanotechnology* **2013**; 1:1-15.
3.	Grabow WW, Jaeger L. RNA self-assembly and RNA nanotechnology.*Acc Chem Res* **2014**; 47(6):1871-80.
4.	Lee H, Lytton-Jean AKR, Chen Y, Love KT, Park AI, Karagiannis ED, and et al. Molecularly self-assembled nucleic acid nanoparticles for targeted in vivo siRNA delivery. *Nat Nanotechnol* **2012**; 7(6):389-93.
5.	Afonin KA, Bindewald E, Yaghoubian AJ, Voss N, Jacovetty E, Shapiro BA, et al. In vitro assembly of cubic RNA-based scaffolds designed in silico. *Nat Nanotechnol* **2010**; 5(9):676-82
6.	Rackley L, Stewart JM, Salotti J, Krokhotin A, Shah A, Halman JR, et al. RNA fibers as optimized nanoscaffolds for siRNA coordination and reduced immunological recognition. **2018**; 28(48):1805959.
7.	Bui MN, Johnson MB, Viard M, Satterwhite E, Martins AN, Li Z, et al. Versatile RNA tetra-U helix linking motif as a toolkit for nucleic acid nanotechnology. **2017**;13(3):1137-46
8.	Rose SD, Kim DH, Amarzguioui M, Heidel JD, Collingwood MA, Davis ME, et al. Functional polarity is introduced by Dicer processing of short substrate RNAs. *Nucleic Acids Res* **2005**; 33(13):4140-56.
9.	Afonin KA, Viard M, Kagiampakis I, Case CL, Dobrovolskaia MA, Hofmann J, et al. Triggering of RNA interference with RNA-RNA, RNA-DNA, and DNA-RNA nanoparticles.

ACS Nano **2015**; 9(1):251-9.

10.	Chandler M, Panigaj M, Rolband LA, Afonin KA. Challenges to optimizing RNA nanostructures for large scale production and controlled therapeutic properties. *Nanomedicine (Lond)* **2020**; 15(13):1331-40.

11.	Panigaj M, Johnson MB, Ke W, McMillan J, Goncharova EA, Chandler M, et al. Aptamers as modular components of therapeutic nucleic acid nanotechnology. *ACS Nano* **2019**; 13(11):12301-21.

12.	Afonin KA, Dobrovolskaia MA, Church G, Bathe M. Opportunities, barriers, and a strategy for overcoming translational challenges to therapeutic nucleic acid nanotechnology. *ACS Nano* **2020**; 14 (8):9221-7.

13.	Afonin KA, Viard M, Martins AN, Lockett SJ, Maciag AE, Freed EO, et al. Activation of different split functionalities on re-association of RNA- DNA hybrids. *Nat Nanotechnol* **2013**; 8(4):296-304.

14.	Halman JR, Satterwhite E, Roark B, Chandler M, Viard M, Ivanina A, et al. Functionally-interdependent shape-switching nanoparticles with controllable properties. *Nucleic Acids Res* **2017**; 45(4):2210-20.

15.	Chandler M, Afonin KA. Smart-responsive nucleic acid nanoparticles (NANPs) with the potential to modulate immune behavior. *Nanomaterials* (Basel) **2019**; 9(4).

16.	Afonin KA, Desai R, Viard M, Kireeva ML, Bindewald E, Case CL, et al. Co-transcriptional production of RNA-DNA hybrids for simultaneous release of multiple split functionalities. *Nucleic Acids Res* **2014**; 42 (3):2085-97.

17.	Ke W, Hong E, Saito RF, Rangel MC, Wang J, Viard M, et al. RNA- DNA fibers and polygons with controlled immunorecognition activate RNAi, FRET and transcriptional regulation of NF-kappaB in human cells. *Nucleic Acids Res* **2019**; 47(3):1350-61.

18.	Porciani D, Tedeschi L, Marchetti L, Citti L, Piazza V, Beltram F, et al. Aptamer-mediated codelivery of doxorubicin and NF-kappaB decoy enhances chemosensitivity of pancreatic tumor cells. *Mol Ther Nucleic Acids* **2015**; 4e235.

19.	Kim KH, Lee ES, Cha SH, Park JH, Park JS, Chang YC, et al. Transcriptional regulation of NF-kappaB by ring type decoy oligodeoxynucleotide in an animal model of nephropathy. *Exp Mol Pathol* **2009**; 86(2):114-20.

20.	Griesenbach U, Scheid P, Hillery E, de Martin R, Huang L, Geddes DM, et al. Anti-inflammatory gene therapy directed at the airway epithelium. *Gene Ther* **2000**; 7(4):306-13.

21.	Parlea L, Puri A, Kasprzak W, Bindewald E, Zakrevsky P, Satterwhite E, et al. Cellular delivery of RNA nanoparticles. *ACS Comb Sci* **2016**; 18(9):527-47.

22.	Halman JR, Kim KT, Gwak SJ, Pace R, Johnson MB, Chandler MR, et al. A cationic amphiphilic co-polymer as a carrier of nucleic acid nanoparticles (Nanps) for controlled gene silencing, immunostimulation, and biodistribution. *Nanomedicine* **2020**; 23:102094.

23.	Gupta K, Mattingly SJ, Knipp RJ, Afonin KA, Viard M, Bergman JT, et al. Oxime ether lipids containing hydroxylated head groups are more superior siRNA delivery agents than their nonhydroxylated counterparts. *Nanomedicine (Lond)* **2015**; 10(18):2805-18.

24.	Gupta K, Afonin KA, Viard M, Herrero V, Kasprzak W, Kagiampakis I, et al. Bolaamphiphiles as carriers for siRNA delivery: from chemical syntheses to practical applications. *J Control Release* **2015**; 213:142-51.

25.	Cruz-Acuna M, Halman JR, Afonin KA, Dobson J, Rinaldi C. Magnetic nanoparticles loaded with functional RNA nanoparticles. *Nanoscale* **2018**; 10(37):17761-70.

26.	Tiwari G, Tiwari R, Sriwastawa B, Bhati L, Pandey S, Pandey P, et al. Drug delivery systems: an updated review. *Int J Pharm Investig* **2012**; 2(1):2-11.

27.	Makhmalzade BS, Chavoshy F. Polymeric micelles as cutaneous drug delivery system in normal skin and dermatological disorders. *J Adv Pharm Technol Res* **2018**; 9(1):2-8.

28.	Bhaskar S, Tian F, Stoeger T, Kreyling W, de la Fuente JM, Grazú V, et al. Multifunctional Nanocarriers for diagnostics, drug delivery and targeted treatment across blood-

brain barrier: perspectives on tracking and neuroimaging. *Part Fibre Toxicol* **2010**; 7:3.

29.   Yan JF, Zhu JH, Cui MF, Zhang J, Ma F, Su YP, et al. Multifunctional mineral hydrogels: potential in artificially intelligent skins and drug delivery. *Acs Omega* **2019**; 4(21):19145-52.

30.   Czapar AE, Steinmetz NF. Plant viruses and bacteriophages for drug delivery in medicine and biotechnology. *Curr Opin Chem Biol* **2017**; 38:108-16.

31.   Das CK, Jena BC, Banerjee I, Das S, Parekh A, Bhutia SK, et al. Exosome as a novel shuttle for delivery of therapeutics across biological barriers. *Mol Pharm* **2019**; 16(1):24-40.

32.   Raposo G, Stoorvogel W. Extracellular vesicles: exosomes, micro- vesicles, and friends. *J Cell Biol* **2013**; 200(4):373-83.

33.   Lo Cicero A, Stahl PD, Raposo G. Extracellular vesicles shuffling intercellular messages: for good or for bad. *Curr Opin Cell Biol* **2015**; 35:69-77.

34.   Abels ER, Breakefield XO. Introduction to extracellular vesicles: biogenesis, RNA cargo selection, content, release, and uptake. *Cell Mol Neurobiol* **2016**; 36(3):301-12.

35.   Simons M, Raposo G. Exosomes—vesicular carriers for intercellular communication. *Curr Opin Cell Biol* **2009**; 21(4):575-81.

36.   Ha D, Yang N, Nadithe V. Exosomes as therapeutic drug carriers and delivery vehicles across biological membranes: current perspectives and future challenges. *Acta Pharmaceutica Sinica B* **2016**; 6(4):287-96.

37.   Van Niel G, Porto-Carreiro I, Simoes S, Raposo G. Exosomes: a common pathway for a specialized function. *J Biochem* **2006**; 140(1):13-21.

38.   Zhang Y, Liu Y, Liu H, Tang WH. Exosomes: biogenesis, biologic function and clinical potential. *Cell Biosci* **2019**; 9(1):19.

39.   Tian T, Wang Y, Wang H, Zhu Z, Xiao Z. Visualizing of the cellular uptake and intracellular trafficking of exosomes by live-cell microscopy. *J Cell Biochem* **2010**; 111(2):488-96.

40.   Saeedi S, Israel S, Nagy C, Turecki G. The emerging role of exosomes in mental disorders. *Transl Psychiatry* **2019**; 9(1):1-11.

41.   Parolini I, Federici C, Raggi C, Lugini L, Palleschi S, De Milito A, et al. Microenvironmental pH is a key factor for exosome traffic in tumor cells. *J Biol Chem***2009**; 284(49):34211-22.

42.   Marcus ME, Leonard JN. FedExosomes: engineering therapeutic biological nanoparticles that truly deliver. *Pharmaceuticals (Basel)* **2013**; 6(5):659-80.

43.   Valadi H, Ekström K, Bossios A, Sjöstrand M, Lee JJ, Lötvall JO. Exosome-mediated transfer of mRNAs and microRNAs is a novel mechanism of genetic exchange between cells. *Nat Cell Biol* **2007**; 9 (6):654-9.

44.   Aqil F, Munagala R, Jeyabalan J, Agrawal AK, Kyakulaga AH, Wilcher SA, et al. Milk exosomes — natural nanoparticles for siRNA delivery. *Cancer Lett* **2019**; 449:186-95.

45.   Banizs AB, Huang T, Dryden K, Berr SS, Stone JR, Nakamoto RK, et al. In vitro evaluation of endothelial exosomes as carriers for small interfering ribonucleic acid delivery. Int J Nanomedicine 2014; 9:4223-30.

46.   Shtam TA, Kovalev RA, Varfolomeeva EY, Makarov EM, Kil YV, Filatov MV. Exosomes are natural carriers of exogenous siRNA to human cells in vitro. *Cell Commun Signal* **2013**; 11:10.

47.   Yang R, Yan X, Zhang S, Guo HJTJoU. MP88-16 targeted exosome- mediated delivery of survivin sirna for the treatment of bladder cancer. **2017**.

48.   Kamerkar S, LeBleu VS, Sugimoto H, Yang S, Ruivo CF, Melo SA, et al. Exosomes facilitate therapeutic targeting of oncogenic KRAS in pancreatic cancer. *Nature* **2017**; 546(7659):498-503.

49.   Barile L, Vassalli G. Exosomes: therapy delivery tools and biomarkers of diseases. *Pharmacol Ther* **2017**; 174:63-78.

50.   Ha D, Yang N, VJAPSB Nadithe. Exosomes as therapeutic drug carriers and delivery vehicles across biological membranes: current perspectives and future challenges. **2016**; 6(4):287-96.

51.   Kibria G, Ramos EK, Wan Y, Gius DR, Liu H. Exosomes as a drug delivery system in cancer therapy: potential and challenges. *Mol Pharm* **2018**; 15(9):3625-33.

52.   Murphy DE, de Jong OG, Brouwer M, Wood MJ, Lavieu G, Schiffelers RM, et al. Extracellular vesicle-based therapeutics: natural versus engineered targeting and trafficking. *Exp Mol Med* **2019**; 51(3):1-12.

53.   Zhang Y, Liu Y, Liu H, Tang WHJC. Exosomes: biogenesis, biologic function and clinical potential. **2019**; 9(1):19.

54.   Thery C, Witwer KW, Aikawa E, Alcaraz MJ, Anderson JD, Andriantsitohaina R, et al. Minimal information for studies of extracellular vesicles 2018 (MISEV2018): a position statement of the International Society for Extracellular Vesicles and update of the MISEV2014 guidelines. *J Extracell Vesicles* **2018**; 7(1):1535750.

55.   Andrew Malloy DG, Hole Patrick, Carr Bob. Counting and sizing of viral vector particles and aggregates by nanoparticle tracking analysis (NTA). *MUSCULO-SKELETAL GENE & CELL THERAPY IIIIIIII* **2010**; 18(S223).

56.   McNicholas K, Li JY, Michael MZ, Gleadle JM. Albuminuria is not associated with elevated urinary vesicle concentration but can confound nanoparticle tracking analysis. *Nephrology (Carlton)* **2017**; 22 (11):854-63.

57.   Escola JM, Kleijmeer MJ, Stoorvogel W, Griffith JM, Yoshie O, Geuze HJ. Selective enrichment of tetraspan proteins on the internal vesicles of multivesicular endosomes and on exosomes secreted by human B- lymphocytes. *J Biol Chem* **1998**; 273(32):20121-7.

58.   Zoller M. Tetraspanins: push and pull in suppressing and promoting metastasis. *Nat Rev Cancer* **2009**; 9(1):40-55.

59.   Chanteloup G, Cordonnier M, Isambert N, Bertaut A, Marcion G, Garrido C, et al. Membrane-bound exosomal HSP70 as a biomarker for detection and monitoring of malignant solid tumours: a pilot study. *Pilot Feasibility Stud* **2020**; 6:35.

60.   Wu Y, Deng W, Klinke 2nd DJ. Exosomes: improved methods to characterize their morphology, RNA content, and surface protein biomarkers. *Analyst* **2015**; 140(19):6631-42.

61.   Hong EP, Halman JR, Shah AB, Khisamutdinov EF, Dobrovolskaia MA, Afonin KA. Structure and composition define immunorecognition of nucleic acid nanoparticles. *Nano Lett* **2018**; 18(7):4309-21.

62.   Afonin KA, Grabow WW, Walker FM, Bindewald E, Dobrovolskaia MA, Shapiro BA, et al. Design and self-assembly of siRNA- functionalized RNA nanoparticles for use in automated nanomedicine. *Nat Protoc* **2011**; 6(12):2022-34.

63.   Grabow WW, Zakrevsky P, Afonin KA, Chworos A, Shapiro BA, Jaeger L. Self-assembling RNA nanorings based on RNAI/II inverse kissing complexes. *Nano Lett* **2011**; 11(2):878-87.

64.   Kim T, Viard M, Afonin KA, Gupta K, Popov M, Salotti J, et al. Characterization of cationic bolaamphiphile vesicles for siRNA delivery into tumors and brain. *Mol Ther Nucleic Acids* **2020**; 20:359-72.

65.   Ke W, Hong E, Saito RF, Rangel MC, Wang J, Viard M, et al. RNA– DNA fibers and polygons with controlled immunorecognition activate RNAi, FRET and transcriptional regulation of NF-κB in human cells. *Nucleic Acids Res* **2018**; 47(3):1350-61.

66.   Ohto U, Shimizu T. Structural aspects of nucleic acid-sensing Toll-like receptors. *Biophys Rev* **2016**; 8(1):33-43.

67.   Halman JR, Kim K-T, Gwak S-J, Pace R, Johnson MB, Chandler MR, et al. A cationic amphiphilic co-polymer as a carrier of nucleic acid nanoparticles (Nanps) for controlled gene silencing, immunostimulation, and biodistribution. Nanomedicine: Nanotechnology. *Biology and Medicine* **2020**; 23:102094.

5 Chapter 5: Conclusions

Over the past few decades, artificial, rationally designed and self-assembled nucleic acid nanoparticles have emerged as a powerful platform with broad biomedical applications. The unique features of nucleic acid nanoparticles enable them to carry numerous functionalities in a single fabrication. With the advancement of nucleic acid nanotechnology, more and more nucleic acid-based therapeutics are on the verge of clinical approval. However, nucleic acids' natural negative charges, vulnerability to nuclease degration and potential immunostimulation are major drawbacks that hinder their progress. This dissertation presented three articles that discussed the design of nucleic acid nanoparticles with defined physiochemical and immunostimulatory properties that ultimately perform desired functions. Furthermore, an endogenous natural carrier was investigated as a safe, efficient and stable vehicle for nucleic acid intracellular delivery.

In the first study, a strand-displacement strategy led to reassociation of two cognate nonfunctional RNA-DNA hybrid mononers via mutual intracellular interactions of complementary toeholds. This process, in turn, released a large quantity of DS RNAs as well as longer DNA duplexes. In order to offset DNA duplex immunogenicity, NF-κB decoy sequences were embedded into the DNA sequences. A simple rotation of one sequence by 180° promoted formation of either fibers or polygon structures with different physiochemical properties that were subsequently characterized with electrophoresis and AFM. DS RNAs against GFP have been shown to possess silencing efficiency at sub-nanomolar concentration, while DS RNAs against mutated *BRAF* genes displayed cellular responses comparable to the FDA-approved drug vemurafenib, but without activation of the NF-κB pathway. Release of the functional NF-κB decoy hijacked the NF-κB dimer entering the nucleus, reducing the amount of NF-κB-dependent cytokine production. This approach allows for activation of desired functionalities only when two cognate NANPs are present in proximity; this controlled strategy limited the risk of RNAi pathway activation in unwanted cells, providing an opportunity for specific-targeted, conditionally activated therapeutics.

The second study continued exploring possibilities for RNA-DNA fiber utilization in blood coagulation. Use of RNA-DNA fibers self-assembled with thrombin-binding aptamers NU172 and/or RA-36 that possess G-quadruplex structures results in binding at thrombin exosite-I rather than the active site, allowing for inhibition of both free- and clot-bound thrombin. Conjugation of RNA-DNA fiber and anti-thrombin aptamers in one assembly enabled stabilization of the construct against nuclease degradation in human serum and prolonged its blood retention time in vitro and in vivo due to its increased molecular weight. Thrombin's inhibitory effect has been assessed by PT, APTT, TT in human plasma and the anti-thrombin fiber's duration of action was effectively reversed by a kill-switch fiber which restored thrombin coagulation activity and promoted its rapid excretion. In vivo biodistribution was performed to monitor anti-thrombin and kill-switch fibers' cellular locations and concentrations over time. This approach demonstrated a highly effective stategy for controlled regulation of blood coagulation with very low immunogenicity and the potential to directly benefit medical specializations such as hematology and cardiovascular biology.

Finally, the third study described the delivery of NANPs with different shapes, sizes, and compositions, among which were globular RNA cubes, planar RNA rings, and linear RNA-DNA fibers. Exosomes are a natural endogenous source of nanovesicles, making them useful for this study. A nuclease protection assay confirmed the stability of exosome-loaded NANPs in the blood. Thanks to exosomes' inborn cellular communication properties, RNA-DNA fibers released into the target cells possessed intact structures. RNA-DNA fibers functionalized with NF-κB decoy, which prevented NF-κB nuclear translocation, as well as DS RNAs against GFP were assessed for their desired functions in the target cells. Their conditional activation of gene silencing and cytokine inhibition effects were confirmed in vitro. As a result, this approach demonstrated the successful use of exosomes as safe, efficient and stable delivery vehicles for different types of NANPs.

Programmable, rationally-designed and self-assembled NANPs with controlled immunorecognition capacity can be used for a variety of functions. Because of these features,

stable, effective, biocompatible, and customizable nucleic acid-based nanostructures will likely become a clinical reality. Since 2016, the FDA has approved eight ODN-based medications including: Defitelio, Exondys 51, Heplisav-B, Tegsedi, Onpattro, Givlaari and Vyondys 53 to treat a variety of diseases. There are still more in clinical trials or in laboratories owing to the lack of appropriate carriers. This dissertation introduced a novel concept for programming NANPs with desired therapeutic motifs that are conditionally activated only in target cells. Also, it examined the use of exosomes as delivery vehicle for shuttling functional NANPs. We anticipate this work will be utilized and developed further for a broader range of applications in therapeutic NANP nanotechnology.